THE ROLE OF HYPOXIA IN NEUROINFLAMMATORY DISEASE

Roshni Anil Desai

UCL Institute of Neurology

A thesis submitted for the degree of

Doctor of Philosophy (Ph.D)

I, Roshni Anil Desai confirm that the research presented in this thesis is my own, unless stated otherwise.

Studies on EAE (experimental autoimmune encephalomyelitis) and the LPS (lipopolysaccharide) dorsal column model were carried out in collaboration with Dr Andrew Davies, Ph.D.

Resin sections were processed and prepared by Dr Daniel Morrison, Ph.D.

ACKNOWLEDGEMENTS

I would like to express my sincerest gratitude to my supervisors Professor Ken Smith and Dr Martin Smith, for their continuous support, patience and guidance throughout my Ph.D. I would also like to further express my gratitude to Ken for giving me the opportunity to work in his laboratory, his encouragement and advice has been invaluable. Ken has been an inspiration, and this project would not have been possible without him.

I would also like to thank my colleagues and peers in the lab, in particular Dr Andrew Davies. He has been a pillar of strength during my Ph.D, with his continuous support advice, and words of encouragement when it all got too much. Many thanks also to Dr Daniel Morrison, Diogo Trigo and Peter Bloomfield, for their friendship and encouragement. I would also like to express my thanks to Dr Peter McIntosh for mentoring me when I first started in the lab.

I would like to express my utmost thanks to my family and friends, but in particular my parents, and my brothers Kunal and Krish for their undeniable support and for instilling a belief in me that I am capable of anything I set my mind to. Finally I would like to thank Amish for all his encouragement and support during the write-up stage of my Ph.D.

ABSTRACT

Multiple sclerosis (MS) is an inflammatory demyelinating and degenerating disease of the central nervous system (CNS) that typically starts with a relapsing-remitting course of neurological deficits. Among the enigmas in the disease are 1) the cause of the neurological deficits, 2) the cause of the demyelination, 3) the cause of the degeneration, and 4) the cause of the disease itself. This thesis examines the novel hypothesis that tissue hypoxia might illuminate at least some of these enigmas. Tissue hypoxia can easily account for loss of function in a tissue as heavily dependent on oxidative phosphorylation as the CNS, and it can similarly selectively kill cells such as oligodendrocytes and neurons/axons if they are reliant on oxidative metabolism. Hypoxia can also promote inflammation in tissues and thereby reduce the threshold for the initiation of inflammatory disease. Three experimental models have been examined, namely experimental autoimmune encephalomyelilits (EAE, a common model of MS), an experimental model of the demyelinating Pattern III MS lesion, and animals rendered temporarily hypoxic due to placement in an atmosphere of 10% oxygen. We provide chemical, physical and therapeutic evidence that tissue hypoxia is, in part, responsible for 1) neurological dysfunction in EAE, 2) the demyelination in the model Pattern III lesion, in association with nitric oxide and superoxide, 3) by extension, perhaps neurodegeneration, and 4) a sensitization of the CNS to pro-inflammatory conditions, including evidence of the special sensitivity of oligodendrocytes to hypoxia. We conclude that true tissue hypoxia is a hitherto-unrecognised, but potentially important, factor in several of the cardinal characteristics of MS.

HYPOTHESES

1. Hypoxia mediates neurological dysfunction in rMOG EAE and in the development of demyelination in the experimental Pattern III Lesion.

2. Intrinsic regional and cellular vulnerabilities of the normal spinal cord to hypoxia render it susceptible to hypoxia-mediated damage.

TABLE OF CONTENTS

LIST OF FIGURES

Page

LIST OF TABLES

ABBREVIATIONS

ANOVA	Analysis of Variance
ADP	Adenosine Diphosphate
ATP	Adenosine Triphosphate
BBB	Blood Brain Barrier
bpp	bits per pixel
CA2	Carbonic Anhydrase 2
CAD	C-terminal Transactivation Domain
CBF	Cerebral Blood Flow
CBP	CREB-binding protein
CBV	Cerebral Blood Volume
CNPase	Cyclic Nucleotide Phosphodiesterase
CNS	Central Nervous System
CO_2	Carbon Dioxide
CSF	Cerebrospinal Fluid
DA	Dark Agouti
DAB	Diaminobenzidine
DHE	Dihydroethidium
EAE	Experimental Autoimmune Encephalomyelitis
EBV	Epstein - Barr virus
EBNA	EBV Nuclear Antigen
EEG	Electroencephalography
FAD	Flavin Adenine Dinucleotide
FIH	Factor Inhibiting HIF
GABA	γ-aminobutyric acid
Gd-DTPA	Gadolinium-Diethylene Triamine Pentacetic Acid
GFAP	Glial Fibrillary Acidic Protein
GLUT-1	Glucose Transporter-1
GTP	Guanosine triphosphate
Hb	Haemoglobin
H_2O_2	Hydrogen Peroxide
HIF-1α	Hypoxia Inducible Factor-1 alpha
HRE	Hypoxia Responsive Element
IFA	Incomplete Freund's adjuvant
IF-γ	Interferon-γ
IL-10	Interleukin-10
LFB	Luxol Fast Blue
LPS	Lipopolysaccharide
MAG	Myelin Associated Glycoprotein
MBP	Myelin Basic Protein
MHC	Major Histocompatibility Complex
MOG	Myelin Oligodendrocyte Glyocoprotein
MRI	Magnetic Resonance Imaging
MRS	Magnetic Resonance Spectroscopy
MS	Multiple Sclerosis
$NaBH_4$	Sodium Borohydride
NAD	Nicotinamide Adenine Dinucleotide
NADPH	Nicotinamide Adenine Dinucleotide Phosphate
Na+/K+	Sodium/potassium
NAWM	Normal Appearing White Matter
NCX	Sodium-calcium exchanger
NO	Nitric Oxide
NOS	Nitric Oxide Synthase
OCT	Optimum Cutting Temperature
OPCs	Oligodendrocyte Precursor Cells

PAS	Periodic Acid Schiff	RT	Room Temperature
PBS	Phosphate Buffered Saline	SaO_2	Saturation Arterial Oxygen
PFA	Paraformaldehyde	S.D.	Standard Deviation
PHD	Prolyl Hydroxylate	S.E.M	Standard Error of Mean
PLP	Proteolipid Protein	SPMS	Secondary Progressive MS
pO_2	Partial Pressure of Oxygen	Th-1	T-helper 1
PPMS	Primary Progressive MS	TNF-α	Tumour Necrosis Factor-alpha
RECA-1	Rat Endothelial Cell Antigen-1	VEGF	Vascular Endothelial Growth
rMOG	Recombinant Myelin		Factor
	Oligodendrocyte Glycoprotein	VHL	von Hippel-Lindau
RNS	Reactive Nitrogen Species	WPBs	Weibel-Palade bodies
ROS	Reactive Oxygen Species	3-NT	3-Nitrotyrosine
RRMS	Relapsing Remitting MS	8-Oxo-dG	8-Oxo-2'-deoxyguanosine

CHAPTER ONE

INTRODUCTION

1.1.0.0 Multiple Sclerosis

Multiple sclerosis (MS) was first described by Charcot in the 1860s, and, more than a hundred years later, it remains the prototypical immune-associated, demyelinating disease of the central nervous system (CNS). Although largely idiopathic in nature, an interplay between viral infection (Cook et al., 1995; Herndon, 1996), genetics (Compston, 1997) and the environment (Weinshenker et al., 1989) has been implicated in the aetiology of MS. This enigmatic disease, traditionally considered a white matter phenomenon, is now realised also to affect the grey matter. The pathology is characterised by multifocal, perivascular inflammation and focal destruction of myelin, resulting in a typically relapsing, but ultimately progressive, degenerative disorder. The majority of MS patients initially follow a relapsing/remitting disease course (relapse/remitting MS; RRMS), associated with periodic relapses of neurological dysfunction, which are often related to a site of observable pathology (Compston and Coles 2008). This relapsing phase begins early in adulthood, but is extremely variable with regard to its nature and duration, and it is often subsequently followed by a progressive (secondary progressive MS; SPMS) disease course. In a small proportion of patients (10-20%), a progressive disease is exhibited from the onset in the absence of relapses (primary progressive MS; PPMS). Inflammatory demyelinating, focal white matter lesions appear to dominate the pathology in RRMS, whereas the progressive phase is associated with diffuse atrophy of the white and grey matter (Miller et al.,

2002), in addition to subtle pathological changes in the normal appearing white matter (NAWM) (Allen and McKeown, 1979; De Groot et al., 2001). Anti-inflammatory, immunomodulatory and immunosuppressive therapies are regarded as only being effective during the early, relapsing stage of the disease (Leary and Thompson, 2003).

Clinical manifestations of MS are heterogeneous, but are thought primarily to be a consequence of aberrant electrical properties of axons due to demyelination. However, increasing evidence suggests that inflammation, in the absence of demyelination, can also cause neurological dysfunction, (Moreau et al., 1994; Bitsch et al., 1999). The mechanisms responsible are not, however, understood, and form the basis of some of this thesis. The type of deficit exhibited is largely determined by the anatomical location of the lesion. Initial symptoms usually include, but not restricted to, limb weakness, sensory disturbances, visual problems, gait instability, and ataxia (Hauser and Oksenberg, 2006). As the disease progresses, bladder dysfunction, fatigue and heat insensitivity are common (Hauser and Oksenberg, 2006). In advanced disease, cognitive deficits have also been reported. Nevertheless, the variability of the neurological disease course, and the fact that much of the disease is clinically silent, has massive implications for therapy.

Despite numerous histopathological studies and recent advances in magnetic resonance (MR) technology, the MS lesion is not well understood. The mechanism(s) responsible for the initiation and evolution of an MS lesion, and its correlation with the expression of a neurological deficit, are largely unknown, and will be a focus of this thesis.

1.2.0.0 Pathology of MS lesions

The pathological hallmark of MS is the presence of large demyelinated lesions at any site in the CNS (Charcot, 1868), however, there is a predilection for the optic nerves, spinal cord, brain stem, periventricular areas (Stadelmann et al., 2011), and subpial grey matter (Bo et al., 2003). Characteristic features of white matter lesions include demyelination, oligodendrocyte loss (Lucchinetti et al., 1999; Barnett and Prineas, 2004), preferential loss of small calibre axons (Evangelou et al., 2001), impaired remyelination (Chang et al., 2002) and astroglyosis. However, different molecular events take place in different regions of a given lesion, thereby making it difficult to unravel the molecular mechanisms involved in the pathogenesis of MS. Thus, the mechanisms involved in plaque formation are still unclear. Some researchers propose that the spectrum of lesion pathologies indicates pathogenic heterogeneity (Lucchinetti et al., 2000), whereas others have proposed that an initial homogeneous pathogenic mechanism is involved in the formation of a new lesion (Barnett and Prineas, 2004). Barnett and Prineas reported the presence of two different types of lesions within the same patient, and thus propose that a stage-dependent sequence of pathology occurs whereby a lesion may progress from the first stage (oligodendrocyte apoptosis) to the second stage (T-cell mediated inflammation) (Barnett et al., 2009).

Traditionally, MS was considered as a disease predominantly affecting the white matter, but it is now clear that grey matter damage is a fundamental component of the disease that is affected from the earliest stages in both RRMS and PPMS, becoming more prominent in the secondary progressive stage (Kutzelnigg et al., 2005; Fisniku et al., 2008; Fisher et al., 2008). Indeed, the presence of grey matter pathology is not

surprising given that the cell bodies of axons in white matter tracts reside within the grey matter. It is easy to appreciate how damage to the white matter may affect the grey matter and vice versa. Unlike demyelination in the white matter, cortical demyelination is thought to affect not only motor function but also cognitive function (de Stefano et al., 2003; Deloire et al., 2011). Moreover, cortical pathology not only plays a key role in clinical progression (Calabrese et al 2010), but its accumulation is thought to represent the transition from RRMS to SPMS (Stadelmann, 2011).

It has previously been shown that cortical lesions may form secondary to white matter damage, due to Wallerian degeneration (Cifelli et al., 2002). However, more recent studies have shown that cortical demyelination not only occurs distal to white matter pathology (Bo et al., 2007; Antulov et al., 2011), but can also evolve faster than white matter pathology (Geurts and Barkhof, 2008; Calabrese et al., 2010). In contrast to white matter lesions, evidence of significant lymphocyte infiltration, BBB disruption and complement deposition has not yet been found in grey matter lesions (Bo et al., 2003; Brink et al., 2005; van Horssen et al., 2007). Meningeal inflammation is often associated with cortical demyelination, particularly in the progressive stages of disease (Magliozzi et al., 2007, 2010; Howell et al., 2012), but it has more recently been described to additionally occur in the acute stages of disease (Lucchinetti et al., 2011).

1.2.1.0 Heterogeneity of Lesions

Lucchinetti et al., (2000) classified MS lesions into four lesion subtypes; patterns I-IV, based on differences in immunological parameters among patients. Moreover, the pathology of all the lesions in a given individual was found to conform to one pattern (Lucchinetti et al., 2000; Konig et al., 2008). The lesion subtypes are described to differ

with regard to their morphological characteristics (Lucchinetti *et al*., 2000) and the mechanisms of tissue injury (Lassmann *et al*., 2001). Patterns I and II exhibit perivascular inflammation, with associated demyelination and evidence of remyelination. Deposition of immunoglobulin and complement are specific to Pattern II lesions. Pattern III lesions also contain an inflammatory infiltrate, but have ill-defined lesion boundary, selective loss of myelin associated glycoprotein (MAG), apoptosis of oligodendrocytic cells, and often a preserved rim of myelinated axons surrounding an inflamed blood vessel. Pattern IV lesions have well-defined boundaries comprising an inflammatory infiltrate dominated by T-lymphocytes and macrophages, with oligodendrocyte apoptosis confined to a rim of periplaque white matter adjacent to an area of active myelin destruction (Lucchinetti *et al*., 2000).

1.2.2.0 Lesion Evolution in the white matter

Classical active MS lesions are primarily found in patients with acute or relapsing disease, and initially exhibit an acute phenotype which develops to a more chronic form. Acute plaques are comprised of macrophages containing similar stages of myelin degradation, dispersed throughout the entire lesion (Lassmann, 2011). Chronic active plaques, are comprised of macrophages with early stages of myelin degradation concentrated at the lesion edge, whilst in the core, macrophages with later stages of myelin debris are observed, or they may have disappeared (Lassmann, 2011). The classical active lesions evolve in a concentric manner, whereby different stages of plaque formation are found in close vicinity. Four distinct zones of the lesion are recognised; the periplaque white matter, the initial ‘pre-phagocytic’ lesion, the early

active lesion and the late active lesion. These zones may vary in size, thus reflecting the speed of lesion development or their stage of evolution (Lassmann, 2011).

1.2.2.1 Preactive lesion

The white matter can appear to be normal upon superficial examination, by eye, or by MRI, but in reality the NAWM is often highly abnormal, showing biochemical and histological abnormalities (Allen and McKeown, 1979). One interesting feature is the presence of clusters or nodules of activated microglial cells, characterised by the expression of major histocompatability (MHC) class II molecules (De Groot et al., 2001). These microglial nodules have also been found to be closely associated with stressed oligodendrocytes (van Noort et al., 2010), and express the inflammatory cytokines tumor necrosis factor-α (TNF-α) and interleukin-10 (IL-10) (van Horssen et al., 2012). No evidence of leukocyte infiltration, demyelination, or axonal damage is evident in such areas (Allen and McKeown, 1979; De Groot et al., 2001; van Horssen et al., 2012). These lesions can be found in the CNS of MS patients irrespective of disease subtype and duration, although they tend to occur more frequently in the vicinity of active lesions (van Horssen et al., 2012). Due to the frequency, and characteristics of these lesions, it is believed that not all preactive lesions develop into demyelinating lesions, but rather spontaneously resolve. Thus, this lesion is thought to represent the earliest, and potentially reversible, stage of the formation of an MS plaque.

1.2.2.2 Periplaque white matter

In a more established lesion, the periplaque white matter is the region of tissue adjacent to the lesion. Although myelin and oligodendrocytes remain intact, diffuse, perivascular inflammatory infiltrates are present, with only few lymphocytes scattered throughout the parenchyma in addition to generalised microglial activation, characterised by the expression of CD68 (Marik et al., 2007). Occasionally, dystrophic axons are seen, and may represent either initial axonal injury that precedes demyelination, or secondary, Wallerian degeneration (Evangelou et al., 2000).

1.2.2.3 Initial 'pre-phagocytic' lesion

Adjacent to the periplaque white matter, is the initial (Marik et al., 2007) or pre-phagocytic (Barnett and Prineas, 2004) zone of the active lesion. Here, the largely intact myelinated tissue exhibits extensive oligodendrocyte apoptosis, with early microglial activation (Barnett and Prineas, 2004; Henderson et al., 2009), microglial NADPH oxidase activity (Fischer et al., 2012), and oxidised DNA and lipids (Haider et al., 2011). This zone contains an increased number of axonal spheroids and end bulbs (Marik et al., 2007), that are surrounded by normal myelin sheaths. Astrocytes show an up-regulation of glial fibrillary acidic protein (GFAP), and appear to have, in part, lost their polarity (Sharma et al., 2010). In Pattern III lesions, there is a profound loss of the most distal myelin proteins of the oligodendrocytes; myelin-associated glycoprotein (MAG) and cyclic nucleotide phoshodiesterase (CNPase) (Lucchinetti et al., 2000).

1.2.2.4 Early active lesion

The early active demyelinating lesion comprises large numbers of microglia/macrophages which contain myelin degradation products with immunoreactivity for all the major and minor myelin proteins (Bruck et al., 1995). This zone contains the highest density of axonal spheroids or end bulbs (Ferguson et al., 1997; Trapp et al., 1998; Kornek et al., 2000), with some oligodendrocte loss. Large protoplasmic astrocytes are present, many of them having lost their polarity and expression of α-synuclein at the astrocytic end feet (Sharma et al., 2011).

1.2.2.5 Late active lesion

The late active lesion is the zone closest to the centre of the plaque. Here, the density of macrophages is decreased compared to that seen in early active lesions. Myelin is completely lost, and any remaining macrophages contain later stages of myelin degradation (myelin basic protein; MBP and proteolipid protein (PLP), or contain oil red O-reactive lipids (Bruck et al., 1995). Axonal density is reduced, and only a few axonal spheroids or end bulbs remain (Lassmann, 2011). A subset of lesions, have been reported to contain a considerable number of oligodendrocytes (Raine et al., 1981; Prineas et al., 1989), which are thought to be recruited from the pool of progenitor cells, and is associated with the early stages of remyelination (Patrikios et al., 2006; Bramow et al., 2010).

1.2.3.0 Cortical lesions

To date, three types of cortical lesion have been described; leukocortical lesions, which extend out from the white matter into the cortex, intracortical lesions, which radiate from microvessels, and subpial lesions, which project from the pia into the cortex (Bo et al., 2003a,b). In early stage MS, leukocortical lesions appear to be most common (Lucchinetti et al., 2011), whereas in later stage disease, subpial lesions are the most abundant form of cortical demyelination (Bo et al., 2003a). During the early stages of MS, myelin-laden macrophages are present to different extents, depending on the lesion subtype; leukocortical lesions contain the largest numbers, and subpial lesions, the lowest (Lucchinetti et al., 2011). Inflammation is also associated with cortical lesions in early disease (Lucchinetti et al., 2011). Leukocortical and subpial lesions, in particular, predominantly show severe to moderate T-cell inflammation. Occasionally, neuritic swelling, oligodendrocyte loss and focal neuronal injury are also evident (Lucchinetti et al., 2011). Cortical lesions in progressive disease are somewhat different. No T-cells or B-cells are evident in intracortical and subpial cortical lesions, but there can be profound microglial activation (Bo et al., 2003b). Actively demyelinating plaques are rare (Peterson et al., 2001; Bo et al., 2003a, b), however, transected neurites and apoptotic neurons within the demyelinated cortex have been reported (Peterson et al., 2001).

1.2.4.0 Slowly expanding lesions of progressive disease

Classical active MS plaques are rare in progressive disease, although some focal demyelinated white matter lesions are still present (Lassmann et al., 2007). Some of these pre-existing plaques show a slow, gradual expansion of the lesions at their

margins (Prineas et al., 2001). Unlike classical active lesions, slowly expanding lesions containing macrophages with all stages of myelin degradation are rare or absent. Rather, these lesions are characterised by a rim of activated microglia at the lesion edge. T-cells, if present, are primarily found perivascularly. Ongoing myelin destruction occurs in the absence of any significant inflammation, but it is found in close concert with activated microglia and complement deposition (Prineas et al., 2001). BBB damage, assessed by the leakage of serum proteins, is not evident (Hochmeister et al., 2006). The centre of the plaque is characterised by a dense astrocytic scar accompanied by demyelination, which is associated with a complete loss of oligodendrocytes and a substantial decrease in axonal density (Mews et al., 1998).

1.3.0.0 The pathogenesis of MS: 'outside-in' or 'inside-out'?

The classical pathological spectrum associated with MS includes BBB breakdown, inflammation, demyelination and degeneration. Due to the overwhelming inflammatory nature of the disease, it was traditionally assumed that some abnormality in the adaptive immune repertoire, against a CNS antigen(s), was the primary trigger for the infiltration of peripheral immune cells and their subsequent 'attack' on myelinated axons, thereby initiating the formation of the infamous inflammatory demyelinating MS lesion (McFarland and Martin, 2007). Consequently, a substantial amount of research was conducted, over the past several decades, to deduce the immunological mechanism(s) that may be involved. It was proposed that interferon-γ (IFN-γ) secreting, myelin-reactive T-helper 1 (Th1) cells initiate the macrophage-mediated destruction of normal myelin. Indeed, both the Th1 cytokine profile of MS patients with active disease (Imam

et al., 2007), and the similarities to the T-cell mediated experimental animal model of the disease, uphold and support such a hypothesis. A great deal of knowledge has been gained from studies focusing on this 'outside-in' hypothesis of MS (Stys et al., 2012), including, but not restricted to, the elucidation that a strong genetic association with immune regulation exists (Sawcer et al., 2011), the illumination of mechanisms of immune-mediated damage to CNS components (Hertz et al., 2010), and the development of immune-modulating pharmacological agents (Menge et al., 2008). However, inconsistencies exist, and with recent observations raising a number of questions with regard to the exact sequence of events, the 'outside-in' hypothesis has been challenged by some. The earliest changes in the myelin begin peri-axonally, involving a uniform widening of the inner myelin lamellae, often in areas distant to inflammatory foci (Rodriguez and Scheithauer, 1994) with the outer myelin wraps still intact. Histological studies on early MS lesions are consistent with these observations, showing that the innermost myelin protein, MAG, is preferentially lost (Aboul-Enein et al., 2003). If damage was primarily mediated by immune cells, it is suspected that the outermost myelin regions would be affected first. The lack of T-cell or B-cell infiltration in early areas of active demyelination and oligodendrocyte loss (Barnett and Prineas, 2004; Henderson et al., 2009), also raises the question of whether MS is in fact an autoimmune disease. Neuropathalogical studies have shown that the NAWM of MS patients commonly exhibits pathological abnormalities, such as microglial activation (De Groot et al., 2001; Barnett and Prineas, 2004), oligodendrocytic stress (van Noort et al., 2010), myelin pallor and oligodendrocytic apoptosis (Barnett and Prineas, 2004), and even axonal changes (Trapp et al., 1998), in the absence of an adaptive immune response. These studies, therefore propose a putative 'inside-out' hypothesis (Stys et al., 2012), whereby an unknown trigger initiates oligodendrocytic damage, which in turn

activates the innate immune system, and elicits the involvement of the adaptive immune system. Indeed, stressed oligodendrocytes have been found to co-cluster with, and activate, microglia, within preactive lesions, the supposed earliest stage of MS lesion formation (van Noort et al., 2010), corroborating such a hypothesis. However, the primary trigger that may induce oligodendrocyte damage has yet to be discovered. These studies clearly raise important questions regarding the aetiology of MS, and have significant implications for the treatment of the disease. Nevertheless, the cause of MS currently remains an enigma.

1.4.0.0 Mediators of dysfunction and tissue damage

1.4.1.0 Nitric Oxide

The inflammatory process results in the release of a number of toxic mediators, some of which have been found directly to affect axonal conduction and induce structural damage. One such mediator, nitric oxide (NO), is synthesised by the enzyme nitric oxide synthase (NOS), which catalyses the reaction of arginine with one molecular oxygen to produce citrulline and NO (Bredt, 1999). To date, three isoforms of NOS have been identified, the constitutively-expressed endothelial NOS and neuronal NOS, and the transcriptionally regulated iNOS. The former two are normally present in the CNS and account for nanomolar concentrations of NO in a calcium dependent manner, whereas the latter inducible isoform is responsible for the high concentrations of NO seen at sites of inflammation. Indeed, increased iNOS mRNA expression is evident in MS plaques (Bö et al., 1994). *In vivo*, NO is rapidly degraded into its metabolites nitrate and nitrite, and their concentrations can be a direct indication of NO levels in body fluids. Increased NO metabolite levels have been found in the cerebrospinal fluid (CSF)

of MS patients (Yamashita et al., 1997; Cross et al., 1998; Giovannoni et al., 1998), and appear to correlate with disease activity and course (Svenningsson et al., 1999; Rejdak et al., 2004). Increased iNOS and NO levels have also been found in experimental autoimmune encephalomyelitis (EAE) (Lin et al., 1993; Hooper et al., 1995), an experimental model of MS, with the former also correlating with disease severity (Okuda et al., 1995). The levels of iNOS have been found to be most pronounced during the peak of the disease, corresponding with complete hind limb paralysis, whereas they are absent during the recovery phase of the disease (Okuda et al., 1995).

NO has been proven to mediate a reversible conduction block, not only in normal axons (Redford et al., 1997; Shrager et al., 1998), but also in demyelinated axons, which are particularly vulnerable (Redford et al., 1997). Thus, low levels of NO would selectively mediate conduction block in demyelinated axons (Smith and Lassmann, 2002). Although the exact mechanism of NO-mediated conduction block is unclear, it is thought to involve the modulation of ion channels, including sodium (Li et al., 1998) and potassium (Kurenny et al., 1994) channels, which would affect conduction. Although calcium channels are not prominently expressed along myelinated axons, they are present at sites of demyelination (Kornek et al., 2001). These too can be affected by NO (Kurenny et al., 1994), resulting in impaired conduction. Direct modulation of the sodium-potassium (Na^+/K^+) ATPase by NO (Guzman et al., 1995) may result in axonal depolarisation, and a subsequent conduction block. Alternatively, NO may impair mitochondrial energy metabolism (Bolanos et al., 1994, 1997; Brown et al., 1995), and ultimately cause conduction block. Besides NO, numerous cytokines are also present in the inflammatory milieu. Some of these cytokines, for example tumour necrosis factor-α (TNF-α) and IFN-γ, exert some of their actions through the induction

of iNOS expression (Goodwin et al., 1995; Hu et al., 1995; Goureau et al., 1997), and thus NO.

Besides its ability to induce dysfunction, NO has also been implicated in structural damage, arguably due to NO-mediated mitochondrial dysfunction. As will be described below, mitochondrial dysfunction can have a significant impact on physiological function. Oligodendrocytes and axons are particularly vulnerable to NO exposure (Smith et al., 1999; Smith and Lassmann, 2002). Although NO induces conduction block in demyelinated axons (Redford et al., 1997), demyelinated axons that are exposed to both, NO and metabolic stress, degenerate (Smith et al., 2001). Several lines of evidence suggest that NO directly affects mitochondrial function (Bolanos et al., 1994; Brown and Cooper, 1994; Mitrovic et al., 1994; Erevinska et al., 1995). NO has been shown to irreversibly damage mitochondrial respiratory chain complexes II through to IV (Bolanos et al., 1994) and succinate dehydrogenase (Mitrovic et al., 1994), *in vitro*. Moreover, NO competitively inhibits the consumption of molecular oxygen, at the level of complex IV (Brown and Cooper, 1994), resulting in a decrease in oxygen consumption and the ATP/ADP ratio (Erecinska et al., 1995). Consequently, an energy insufficiency ensues, the consequence of which will be discussed in further detail below. Thus, vulnerable cell types, such as oligodendrocytes and neurons, are presumably unable to withstand such an insult, and therefore respond by initiating a cascade of events resulting in cell death. Consistent with this notion, oligodendrocytes have been found to be particularly vulnerable to NO exposure *in vitro* (Mitrovic et al., 1994). Accordingly, the tissue damage in the ‘hypoxia-like’ Pattern III MS lesion has been attributed to NO-mediated mitochondrial damage (Aboul-Enein et al., 2005) in vulnerable cell types.

1.4.2.0 Reactive oxygen and nitrogen species

Under physiological conditions, basal levels of reactive oxygen species (ROS) and reactive nitrogen species (RNS) are routinely generated by various tissues; but although inherently toxic they pose very little threat owing to a highly developed set of defence and repair mechanisms present in cells. Nevertheless, during certain events, such as inflammation, there is an overproduction of these toxic mediators, or a failure in the antioxidant mechanisms, and then damage to lipids, proteins and nucleic acids may ensue, ultimately leading to cell death.

ROS/RNS include superoxide, peroxynitrite and the hydroxyl radical, all of which are produced as part of the inflammatory response. Superoxide is produced by a one-electron reduction of oxygen, and it is the precursor of most other forms of ROS. Aberrant superoxide production occurs under adverse conditions, particularly when mitochondria are damaged (Murphy, 2009), a well-recognized feature of MS lesions (Mahad et al., 2008). Dismutation of superoxide produces hydrogen peroxide (H_2O_2), which in turn can be fully reduced to water, or partially reduced to the notorious hydroxyl radical. Superoxide can also react with NO, in a reaction that is limited by the rate of diffusion of both radicals, to produce peroxynitrite. Superoxide can be formed *in vivo* in a number of ways, one of which is the mitochondrial respiratory chain. Some components of the respiratory chain e.g. ubiquinone, leak electrons directly to molecular oxygen. As oxygen accepts one electron at a time, superoxide is released (Halliwell and Gutteridge, 1985). The rate of electron leakage, and superoxide production, increases with the oxygen concentration (Turrens et al., 1982). Paradoxically, mitochondrial superoxide production is also reported to increase in response to low oxygen concentrations (Chandel et al., 1998; Guzy and Schumacker, 2006). Besides the

mitochondrial respiratory transport chain, another abundant source of superoxide is the respiratory burst system of activated microglia and macrophages, whereby copious amounts of the free radical are generated on the microglial outer membrane during oxygen dependent destruction of pathogens, and released into the surroundings (Gilgun Sherki et al., 2004).

Superoxide itself is relatively harmless; it is in fact its reaction products such as peroxynitrite and hydroxyl radical that are potent mediators of damage. Peroxynitrite initiates DNA strand breaks, and subsequent activation of poly (ADP-ribose) synthetase (Szabó, 1996). This enzyme depletes local ATP stores in an attempt to repair the damaged DNA, which results in cell death due to metabolic failure (Szabó, 2003). Peroxynitrite is also thought to induce axonal damage, with characteristics similar to acute axonopathy (Smith et al., 1999).

Oxidative damage has been detected biochemically (Vladimirova et al., 1998; Bizzozero et al., 2005; Qin et al., 2007) and immunohistochemically (Haider et al., 2011), in the tissue of patients with MS, suggesting an important role for ROS/RNS in MS. Furthermore, a recent study has reported a role for free radical-mediated mitochondrial damage, which is followed by axonal damage prior to any demyelination, in murine EAE (Nikić et al., 2011). Furthermore, elevated concentrations of 3-nitrotyrosine (3-NT), a marker of peroxynitrite-mediated damage, has also been found in MS (Cross et al., 1998; Liu et al., 2001) and EAE lesions (Cross et al., 1997). In acute lesions, cells of mononuclear/macrophage lineage and hypertrophied astrocytes express 3-NT, whereas no such expression was detected in chronic lesions (Oleszac et al., 1998). Due to these findings, and others, oxidative/nitrative stress is increasingly

recognised to play an important role in the pathogenesis of demyelination and neurodegeneration in MS.

1.5.0.0 Energy insufficiency as a mechanism of neurological dysfunction and tissue damage

Understanding the mechanisms responsible for the expression of a neurological deficit and tissue injury in MS represents a challenging yet active area of research. Increasing evidence suggests that ultimately an energy insufficiency may represent a key event in MS (Smith et al., 2001; Aboul-Enein et al., 2005; Mahad et al., 2008). Indeed, the selective vulnerability of small diameter axons in MS (Evangelou et al., 2001), supports such a hypothesis as smaller axons have a large surface to cytoplasmic volume ratio, rendering them more susceptible to damage (Aboul-Enein et al., 2005).

ATP is a vital substrate required for a number of physiological cellular processes, including signal transduction, ionic balance and macromolecule synthesis and transport. It is therefore not surprising that ATP depletion can have devastating consequences on cellular function and survival. Although energy insufficiency currently represents one of many hypotheses of axonal degeneration in chronically demyelinated axons (Bechtold and Smith, 2005; Trapp and Stys, 2009), it can also account for the loss of function, and structural damage to vulnerable cell types. The maintenance of sodium ion homeostasis is paramount to ensure physiological functioning, thus a disruption to the ionic gradients can have a considerable impact. Essentially a decrease in the intracellular ATP pool results in the failure of the Na+/K+ ATPase. This ionic pump is exceptionally ATP consuming (Ames, 2000), and is responsible for the maintenance of the ionic membrane gradient. Failure of the pump therefore prevents extrusion of

sodium ions, resulting in sodium loading within the cell. Presumably, vulnerable cell types, such as oligodendrocytes and neurons, would be particularly affected by such an energy insufficiency.

Sodium loading is further promoted in axons, following demyelination, due to the redistribution of sodium channels along the axolemma (Bostock and Sears, 1978; Felts et al., 1997). Once the intracellular sodium increases above its nominal concentration (Stys et al., 1997), the sodium-calcium exchanger (NCX), responsible for exchanging extracellular sodium for intracellular calcium, operates in reverse. Consequently, calcium accumulates within the axons, and calcium-mediated degenerative pathways are initiated (Trapp and Stys, 2009). Indeed, demyelinated axons in patients with chronic MS show signs of calcium-activated protease activity, e.g. fragmented neurofilaments, depolymerised microtubules, and fewer organelles (Dutta et al., 2006).The energy deficit needs to be quite severe before calcium-mediated degenerative pathways are activated, but it seems reasonable to predict that an energy deficit of a smaller magnitude may result in more subtle deficits, such as aberrant axonal conduction and, thereby, neurological dysfunction. However, the ability of an energy deficit to induce neurological dysfunction remains to be proven.

Essentially, any mechanism that impairs ATP production during inflammatory demyelination is likely to result in energy insufficiency. It has been proposed that a number of factors conspire to compromise ATP production in MS (Aboul-Enein et al., 2005; Mahad et al., 2008), including NO, ROS/RNS, and hypoxia/ischaemia, however they most likely exert their toxic effects on mitochondria, as will be described in further detail below.

1.5.1.0 Mitochondrial dysfunction

Mitochondrial dysfunction is increasingly recognised as an important mediator of damage in both acute (Mahad et al., 2008) and chronic (Lu et al., 2000; Dutta et al., 2006; Mahad et al., 2009; Witte et al., 2009) MS lesions. Functional defects in the mitochondrial respiratory chain complex IV, in addition to COX-I, its catalytic component, have been described in acute, Pattern III MS lesions (Mahad et al., 2008). Mitochondrial complex I activity is substantially reduced in chronic MS lesions (Mahad et al., 2009), whilst complex I and III activity is decreased in non-lesional motor cortex of MS patients (Dutta et al., 2006). The decrease in complex I and III activity in non-lesional motor cortex is accompanied by a decrease in γ-aminobutyric acid (GABA) mediated inhibitory input (Dutta et al., 2006). Thus, it has been proposed that the energy demand of demyelinated axons increases, not only due to the diffuse distribution of sodium channels (Craner et al., 2004; Waxman et al., 2004), but also increased firing due to the loss of inhibitory inputs from interneurons. The ensuing failure of the Na+/K+ ATPase, following inevitable sodium loading, has been attributed to a population of dysfunctional mitochondria that are supplied by the upper motor neuron, by some researchers (Dutta and Trapp, 2011).

As mentioned briefly above, a number of different mediators are capable of provoking mitochondrial dysfunction in inflammatory lesions, including, but not limited to, NO (Bolanos et al., 1997; Brorson et al., 1999; Heales et al., 1999; Beltran et al., 2000) and ROS/RNS (Lu et al., 2000). Despite its ability to directly affect mitochondrial function, NO is also a precursor for a number of ROS/RNS, one of which is particularly deleterious to mitochondria. As described above, the reaction between NO and superoxide, results in the formation of peroxynitrite. Besides its detrimental effects on DNA, peroxynitrite can also irreversibly damage mitochondrial respiratory

complexes II to IV (Bolaños et al., 1994, 1995), an event that is thought to precede cell death (Bolaños et al., 1995). Thus, irreversible damage mediated by peroxynitrite may lead to neurotoxicity, ATP depletion and ultimately cell death (Bolanos et al., 1995, 1996).

Evidently, unravelling the exact mechanisms of energy failure in MS during the different stages of disease is important and may provide the basis for the development of novel therapeutic strategies.

1.6.0.0 Animal models of MS

1.6.1.0 Experimental Autoimmune Encephalomyelitis

EAE is an animal model of MS that dates back to the 1900s, with the discovery that rabbits inoculated with human spinal cord homogenate develop spinal cord inflammation and paralysis (Koritschoner and Schweinburg, 1925; Gold *et al*., 2006; Stromnes and Goverman, 2006). Since then, there has been much progress in inducing EAE, particularly through the development of a mineral oil-based adjuvant by Jules Freund which results in disease after a single injection of a CNS encephalitogen emulsified in the adjuvant (Freund *et al*., 1947). Encephalitogens used for the induction of EAE can be purified myelin proteins, recombinant proteins, synthesised peptides, or whole brain and spinal cord homogenates (Wallström and Olsson, 2008). Although no animal model can reflect the entire pathological spectrum of this insidious disease, EAE shows neurological signs, immunological and histopathological similarities with MS (Hohlfeld and Wekerle, 2001), and the disease can be induced in a number of different

species, through either active or passive immunisation. The former type of immunisation refers to the co-injection, with adjuvant, of myelin antigens, such as MBP, PLP and MOG, whereas the latter involves the adoptive transfer of encephalitogenic T-cells. Various factors, including genetic susceptibility, species, age, sex, the type and preparation of antigen employed, and the dose and administration route, influence the pathogenesis, sensitivity, clinical course of the disease, and the pathology of EAE (Teixeira *et al*., 2005). Thus, in essence, each animal species and type of EAE, potentially allows the study of one or more aspects of MS. Nevertheless, differences in the nature, size and the distribution of lesions throughout the CNS exist, between EAE models and the human disease (Storch *et al*., 1998). Furthermore, EAE is essentially an autoimmune disease principally mediated by T-cells (Ben Nun et al., 1981) that enter the CNS, recruit circulating monocytes and activate resident microglia. These effector cells are central to the induction of inflammatory damage in EAE (Berger et al., 1997), but whether this is an accurate model of MS remains uncertain. In the majority of susceptible rodent strains, the disease presents as an ascending flaccid paralysis, beginning with a limp tail, followed by unilateral and subsequent bilateral hind limb paralysis, progressing to the forelimbs, and ultimately death. This pattern is entirely unlike MS, a point which is often ignored and not understood (Simmons et al., 1984).

In the last three decades, rats and mice have become the preferred choice of animal model for EAE studies (Teixeira *et al*., 2005; Stromnes and Goverman, 2006). Although it is possible to induce EAE in mice, producing a chronic-progressive or relapsing-remitting disease with demyelination, they are relatively resistant to EAE, with highly variable degrees of incidence and time of attack, and the need for an ancillary adjuvant to induce disease (Teixeira *et al*., 2005). Furthermore, in comparison

with susceptible rat strains, multiple injections of high doses of antigen are required, with the additional use of pertussis toxin as an adjuvant supplement. However, the discovery that MOG (or MOG peptides), a minor myelin component, can induce chronic paralytic EAE in mice, including the previously resistant C57BL/6 mice (Amor et al., 1994; Slavin et al., 1998), has facilitated the generation of numerous transgenic mice. MOG is a myelin encephalitogen in that it not only elicits an encephalitic T-cell response, but also widespread antibody-mediated CNS demyelination (Johns *et al*., 1995; Gold *et al*., 2006), resulting in a chronic relapsing or progressive disease in both a homogeneous and relatively predictable manner (Storch *et al*., 1998). In C57BL/6 mice, the transgenic introduction of either myelin-specific MHC class I CD8+ antigen, or MHC class II CD4+ antigen, T cell receptors, into all T cells results in spontaneous disease (Bettelli, 2007; Johnson et al., 2010). Similarly, the introduction of myelin-specific human T cell receptors and human MHC antigens also yields spontaneous disease in mice (Ellmerich et al., 2005; Friese et al., 2006). Although the humanised models have been suggested to provide significant improvements over the conventional models (Friese et al., 2006), the mice rapidly develop a monophasic, chronic disease course, with poor recovery (Jones et al., 2008; Soulika et al., 2009).

MOG induced EAE in the female dark agouti (DA) rat, yields a relatively predictable and reliable disease course that more fully represents the pathology and clinical course of MS (Storch *et al*., 1998). At lower doses of MOG (50μg), an acute progressive disease course with increasing neurological deficit is observed, whereas at higher doses (200μg), a progressive relapsing disease course develops, with relapses superimposed upon a slowly increasing neurological deficit, beginning approximately 12-14 days post injection (Papadoupoulos *et al*., 2006a,b). The pathology of MOG induced EAE in the DA rat, has been found to resemble the pathological spectrum of

MS, more so than the other EAE models available (Storch *et al*., 1998), and thus it can represent one of the better EAE models in which to study factors related to MS.

1.6.2.0 LPS dorsal column model of the MS Pattern III lesion

The direct intraspinal injection of the pro-inflammatory agent lipopolysaccharide (LPS) into the dorsal column of Sprague Dawley rats induces a focal demyelinating lesion that exhibits characteristics of the human Pattern III lesion (Felts et al., 2005; Marik et al., 2007). Within 8 hours, an inflammatory response is elicited in the dorsal columns, but the myelin sheaths remain intact at this time (Felts et al., 2005). Following initial microglial activation, a functional disturbance begins in astrocytes, namely retraction of foot processes, and loss of aquaporin IV and connexin proteins (Sharma et al., 2010). The early stages of this lesion are associated with massive precipitation of fibrin, particularly on the surface of activated macrophages and microglia (Marik et al., 2007). Preferential loss of MAG begins between 5 and 7 days, with demyelinated lesions persisting between 9 and 14 days once formed (Felts et al., 2005), and is accompanied by profound axonal degeneration (Marik et al., 2007). Interestingly, the lesions form at the base of the dorsal columns, rather than at the site of the injection of LPS (Felts et al., 2005). The lesion persists indefinitely, even if is properties may change (e.g. remyelination), and encompasses more than 50% of the cross-sectional area of the dorsal columns (Felts et al., 2005). By 28 days, the lesions are largely remyelinated, primarily by Schwann cells (Felts et al., 2005).

The development of tissue injury in the LPS lesion resembles that of the human Pattern III lesion, thus a common mechanism of damage is thought to exist (Marik et al., 2007). However, the exact sequence of events that leads to the formation of

'hypoxia-like' demyelination remains unclear. It is clear that focal microglial activation results in the production of a number of toxic mediators, including NO, that are capable of inducing mitochondrial dysfunction, thereby promoting 'hypoxia-like' injury of the axons and supporting cells (Marik et al., 2007). Thus the tissue injury, is currently attributed largely to mitochondrial dysfunction as a consequence of oxygen and nitrogen radicals, such as NO (Marik et al., 2007). However, administration of the broad-spectrum anti-inflammatory agent dexamethasone, did not reduce the extent of LPS-induced demyelination, despite significantly reducing the number of cells expressing iNOS (Felts et al., 2005). Therefore, although NO likely plays an important role in the development of 'hypoxia-like' demyelination, it may not be the only factor involved.

1.7.0.0 Cerebral Blood Flow, Oxygenation and Metabolism

The brain is a highly oxidative organ that relies on an efficient supply of nutrients to maintain normal function and tissue viability. The dependence of cells on a constant and plentiful supply of ATP requires an adequate provision of oxygen, which essentially depends on the vasculature. Values for cerebral blood flow (CBF) and oxygen consumption (CMRO2) are species-specific, with larger values being associated with smaller animals (Siesjo, 1978). In rat, the CBF has been reported to be 0.8–1.1 ml/min per gram wet weight of tissue, and the reported whole brain CMRO2 rate 3.4–4.6 μmol/min per gram wet weight (Erecińska and Silver, 2001).

Increases in CBF have been reported to occur in areas that are expected to be activated by a specific stimulus, for example, in the visual cortex in response to a visual input (Ances et al., 1999; Colebatch et al., 1991; Lassen and Friberg, 1988; Lu et al.,

2004), or in the motor cortex during finger movement (Allison et al., 2001). Although it is relatively established that under basal conditions in the rodent brain, oxygen and glucose consumption, and blood flow are coupled to local brain function (Yarowski and Ingvar, 1981; Fox and Raichle, 1986; Fox et al., 1988 Clarke and Sokoloff, 1999), there were controversies as to whether such a coupling exists between these parameters during physiological activation. Some groups reported a good correlation between CBF, and oxygen uptake and glucose utilisation (Yarowski and Ingvar, 1981; Di Rocco et al., 1989; Clarke and Sokoloff, 1999), whereas others reported that, during activation, the CBF and glucose utilisation increased by 53–55%, while oxygen consumption increased only by 5% (Fox and Raichle, 1986; Fox et al., 1988). Fox and colleagues proposed that this uncoupling of CBF and CMRO2 suggested that the metabolic needs of the tissue are met, in part, by non-oxidative metabolism (i.e. glycolysis). Indeed, such a notion was supported years later by studies showing activity-induced increases in lactate concentration in different brain areas (Figley and Stroman, 2011). It is now generally accepted that following physiological activation, (1) CBF increases with metabolic demand, (2) CBF and glucose utilisation increase more than oxygen utilisation, and (3) oxidative and glycolytic pathways are involved in satisfying the increased metabolic demand (Figley and Stroman, 2011).

More than 90% of the oxygen consumed by the brain is used by mitochondria during the oxidation of glucose, to produce energy in the form of ATP (Schiamanna and Lee, 1993). The consumption of oxygen and glucose is adjusted to meet regional metabolic demand (Sokoloff, 1981; Yarowski and Ingvar, 1981; Fox and Raichle, 1986; Fox et al., 1988; Clarke and Sokoloff, 1999). Since glycogen stores are limited in the brain, a permanent supply of glucose is essential to maintain brain function.

Accordingly, a cessation of oxygen and glucose supply leads to unconsciousness and coma within less than 10 sec (Clarke and Sokoloff, 1999).

Metabolism in the brain is highly compartmentalized, in that, within a given cell, there is more than one pool of a given metabolite (Siegel et al., 2006). This compartmentalisation is due to the specialised cellular and subcellular localisation of transporters, enzymes and metabolic pathways, allowing brain cells to carry out specific functions and remain independent (Siegel et al., 2006). Cerebral metabolism is thus a complex process, where continuous interactions between neurons and glial cells are crucial for correct functioning of the brain (Hertz et al., 1999).

The traditional view of cerebral energy metabolism was that aerobic respiration of glucose was solely responsible for yielding energy in neurons and glia. However, each cell type preferentially uses different metabolic substrates and pathways for the production of ATP under physiological conditions. Besides glucose, neurons and glial cells can additionally utilise lactate, pyruvate, glutamate and glutamine as metabolic substrates (Zielke et al., 2009). Among these substrates, lactate is increasingly emerging as an important energy source for the brain (Schurr et al., 1999; Gallagher et al., 2009; Smith et al., 2003; Boumezbeur et al., 2010; Belanger et al., 2011). Recent evidence also suggests that lactate is an important product of glycolysis, in addition to pyruvate (Schurr and Payne, 2007). Moreover, a putative mitochondrial lactate oxidation complex, which allows entry and oxidation within mitochondria, has been described to exist in neurons (Hashimoto et al., 2008). Interestingly, growing evidence suggests that neurons can use lactate as an energy source (Schurr et al., 1997; Bouzier et al., 2000; Qu et al., 2000; Serres et al., 2005; Boumezbeur et al., 2010; Bellanger et al., 2011), and even show a preference for lactate, over glucose when both are available (Itoh et al.,

2003; Bouzier-Sore et al., 2006; Bellanger et al.. 2011). Accordingly, increasing evidence suggests that neurons and astrocytes may share some sort of "coupled lactate metabolism", a mechanism by which astrocytes glycolytically convert glucose to lactate, and release it into the extracellular space, where it can be taken up into neighbouring neurons to be utilised as a metabolic substrate for oxidative phosphorylation (Vibulsreth et al., 1987; Walz and Mukerji, 1988; Magistretti et al., 1999). More recently, oligodendrocytes have been found to be vital suppliers of lactate to axons (Fünfschilling et al., 2012; Lee et al., 2012), via the lactate transporter MCT-1 (Lee et al., 2012).The process of oxidative phosphorylation yields 38 moles of ATP from just one mole of glucose compared to a meagre two moles of ATP for every mole of glucose via glycolysis. Therefore, it is understandable why oxygen is essential to ensure an efficient rate of energy metabolism, particularly in metabolically demanding cells such as neurons and oligodendrocytes.

Most of the energy consumed by the brain is used for the restoration of the membrane resting potential, following neuronal depolarisation, which is accomplished by the Na^+/K^+ ATPase (Attwell and Laughlin, 2001). Neuronal activity is reported to account for almost 80% of the energy consumed by the brain (Sibson et al. 1998; Rothman et al. 1999), whereas, neurotransmitter recycling utilises 3–5% of the total energy used by the brain (Magistretti and Pellerin, 1996; Sibson et al., 1998; Magistretti, 1999; Ames, 2000; Attwell and Laughlin, 2001). Therefore, an impairment of energy metabolism can have significant consequences on CNS function.

1.8.0.0 Hypoxia and the CNS

1.8.1.0 The inherent vulnerability of the CNS to hypoxia

The structural organisation and intrinsic characteristics of the CNS render it particularly vulnerable to hypoxia/ischaemia-induced damage. The brain's substantial energy requirements, its limited capacity to store excess glucose, and its poor vascular supply, all contribute to the process of hypoxic tissue damage.

The brain and spinal cord rely on a continuous, rich blood supply to sustain ongoing activity. If blood flow is arrested, unconsciousness ensues within 6-7s (Kabat and Anderson, 1943; Hansen et al., 1985) and irreversible brain damage occurs within minutes. Although the brain comprises only 2% of the body weight, it is estimated to receive 15% of the cardiac output, and, 20% and 10% of the oxygen (Afifi and Bergman, 2005) and glucose (McKenna et al., 2006) consumed by the entire body, respectively. Thus, the brain is a very metabolically expensive organ. This high demand for metabolic energy has important implications for the evolution of the brain and its function. In fact, the availability of energy essentially limits brain size (Aiello and Wheeler, 1995), and determines the circuitry and activity patterns (Mitchison, 1992; Koulakov and Chklovskii, 2001) and neural codes (Levy and Baxter, 1996; Baddeley et al., 1997; Balasubramanian et al., 2001). Moreover, the energy supplied to the CNS is in the form of oxygen and glucose, and the rate of their consumption and utilisation, respectively, is high. Despite the considerable reliance on these substrates for energy, the CNS has very little in the form of glycogen stores to sustain energy metabolism at times of high demand, compared with other tissues such as liver and muscle.. Astrocytes are the principal storage sites of glycogen in the CNS (Cataldo and Broadwell, 1986), although it is not known whether all astrocytes store glycogen, and if

they store glycogen at the same concentration. Indeed, the greatest accumulation of glycogen occurs in areas of high synaptic density (Phelps, 1972; Brown and Ransom, 2007), and the utilization of such stores has been found to sustain neuronal activity during periods of hypoglycaemia (Suh et al., 2007). Nevertheless, during periods of ischaemia *in vivo*, the glycogen stores are rapidly depleted, concurrently with ATP (Swanson et al., 1989). Thus, despite the presence of these stores, and their role in providing energy substrates when the blood-borne glucose is insufficient to meet the demand (Brown et al., 2003; Choi et al., 2003), they are relatively inadequate. The stores are essentially there to supplement the glucose available to maintain energy metabolism, not to be the main or sole source of substrate. Therefore, during hypoxic/ischaemic insults, it is not surprising that the glycogen stores are unable to maintain substrate delivery.

Through evolution, the brain has developed a thick parenchyma, which is disproportional to its vasculature. The major arteries that enter at the cranial vault at the base of the brain are distributed to bifurcate and anastomose on the cortical surface, giving off smaller nutrient arteries that penetrate the parenchyma. These small diameter penetrating arteries only have a capillary network to provide collateral flow (Moody et al., 1990), with each penetrating artery supplying the given surrounding area of tissue (Nishimura et al., 2007). Particular areas of the brain, including the cortex, centrum, basal ganglia, and thalamus, are supplied by a single penetrating artery (Moody et al., 1990), rendering them particularly vulnerable to hypoperfusion. Similarly areas that lie between two major arterial supplies, known as watershed zones, are also vulnerable to hypoperfusion. The best known watershed zones in the brain lie between the anterior and middle cerebral circulations, and the middle and posterior cerebral circulations. Another watershed zone also exists in the tegmentum of the brain stem.

Similar to the brain, the spinal cord also has a vascular architecture which renders it vulnerable to hypoxia, whereby major arteries, the ventral and the two dorsal spinal arteries supply the cord, promoting segmental vulnerabilities. The ventral spinal artery, supplying the ventral and central portions, and the grey matter core, gives off smaller end-arteries that penetrate the ventral spinal cord parenchyma. The dorsal spinal arteries, however, descend on the dorsal surface of the spinal cord, and are fed by dorsal feeding arteries. The dorsal spinal arteries supply the periphery through the circumferential pial network, a rich anastamotic network on the surface of the spinal cord that sends penetrating branches into the white matter at all levels of the spinal cord (Tveten, 1976; Hayashi et al., 1983). Both the ventral spinal artery and the dorsal spinal arteries are dependent on segmental contributions from feeding arteries, along the length of the cord. The number of feeding vessels that contribute to each, however, has been found to be variable; the average number of arteries contributing to the ventral spinal artery is 7, whereas the average number of arteries contributing to the dorsal spinal arteries is 25 (Tveten, 1976). For the ventral spinal artery, these feeding arteries were more frequent at C5 and C6, and from T11 to L1, and less frequent at C1-C3, T1-T3 and caudal to L2 (Tveten, 1976). The presence of one dominant feeding vessel of the lumbar segment has been previously reported in the rat (Tveten, 1976), similar to the human artery of Adamkeiwicz. However, later studies have suggested that there are in fact three to five such vessels between T11 and L4 vertebral segments (Schievink et al., 1988). The vascular architecture of the brain and spinal cord does not appear to be optimal, with particular intrinsic characteristics rendering the CNS vulnerable to hypoxic damage, rather than preventing it.

1.8.2.0 Effects of hypoxia on the CNS

Multiple intrinsic and extrinsic mechanisms exist within the CNS to maintain a suitable level of oxygen availability. Hypoxia refers to a decrease in the availability of oxygen, or a decrease in the partial pressure of oxygen (pO_2; LaManna, 2007). At physiological partial pressures, haemoglobin is saturated with oxygen, and even a slight decrease in the ambient oxygen does not influence the haemoglobin saturation, and tissue oxygen availability remains the same (LaManna, 2007). When the arterial pO_2 falls below 12 kPa, a condition known as hypoxaemia (lower blood oxygen) ensues. Successful long-term adaptation is possible when the hypoxic exposure is mild (below 12 kPa but above 6 kPa), and it is these adaptations that allow mammals to live at high altitudes (LaManna et al., 2004). Mild hypoxia does not usually lead to any tissue damage; therefore, there are no problems for humans up to an altitude of 3000 m (LaManna, 2007). However, between 4 and 6 kPa, there is a good chance of permanent damage and with longer exposure below 4 kPa, the hypoxia is severe and results in loss of consciousness and neurodegeneration (LaManna, 2007). Indeed, mountain climbers often ascend to higher altitudes than 3000 m, and although high altitude illness is the most common disturbance reported, neurological conditions such as mental disturbances (Ryn, 1988), focal neurological deficits (Song et al., 1986) and transient global amnesia (Litch and Bishop, 2000) have also been reported. Cortical atrophy has been found on MRI in 92% of Everest (8848 m) climbers, and subcortical lesions were found on MRI of inexperienced climbers who were not adequately acclimatized (Fayed et al., 2006). Furthermore, such high altitude exposures have been found to provoke subtle white and grey matter changes that mainly affect the brain regions that are associated with motor activity (Paola et al., 2008).

Systemic compensatory changes that occur in response to mild hypoxia include increased ventilation, increased haematocrit, decreased core temperature, weight loss and bicarbonate ion excretion (LaManna et al., 2004). For instance, exposure of rats to hypobaric hypoxia for a week or more, more than doubles their ventilatory rates (LaManna et al., 2004). This increased ventilation results in a decrease in the arterial partial pressure of carbon dioxide and subsequent bicarbonate ion excretion by the kidney to reduce the blood alkalosis. A fall in core body temperature has also been described following exposure to mild hypoxia (Wood, 1991; Mortola, 1993; Mortola et al., 1994; Wood and Gonzales, 1996). The drop in temperature is a transient phenomenon, lasting only for a few days before returning to basal levels, and may suggest decreased metabolism. Furthermore, studies in humans have reported appetite suppression and subsequent body weight loss at high altitudes due to hypoxic conditions (Westerterp et al., 1994; Westerterp et al., 1999; Shulka et al., 2005).

In contrast to the systemic changes, organ specific adaptations are primarily found in the capillary bed and the components involved in metabolism (LaManna et al., 2004), and the brain is no different. Physiologically, the tissue pO_2 varies spatially and temporally, with the mean tissue pO_2 lower than the venous pO_2, and there are many low values (Sick et al., 1982; LaManna et al., 2004). The CNS undergoes significant adaptations in order to preserve tissue oxygen and the energy supply required to support cellular functions. One such adaptation is an increase in CBF. An increase in CBF in response to hypoxia was previously described, when Kety and Schmidt (1948) recorded an average CBF increase of 137 ± 9% in seven young men, whilst breathing 10% oxygen. Similarly, Severinghaus and colleagues (1966) reported a mean CBF increase from 42 ± 2 ml/100g of brain tissue per minute to 51 ± 4 ml/100g of brain tissue per minute after 6-12 hours at altitude, and a subsequent decrease to 47 ± 3 ml/100g of

brain tissue per minute. A possible reason as to why the CBF re-normalises could be due to the increase in haematocrit, or packed red blood cell volume (Lefant and Sullivan, 1971; Xu and LaManna, 2006), by day 3 of exposure to mild hypoxia (Xu et al., 2004). Increase in haematocrit level allows an increase in the oxygen content of the circulating blood, and restoration of oxygen delivery at the pre-hypoxic rate of blood flow rate. An increase in cerebral blood volume, which also occurs in response to acute hypoxia (Shockley and LaManna, 1988; Julien-Dolbec et al., 2002), is associated with an increase in the capillary mean transit time (Shockley and LaManna, 1988), that is the average time it takes for any unit of blood to travel from the arterial end of the capillary to the venous end (Xu and LaManna, 2006). An increase in capillary transit time increases the time available for the unloading of vital nutrients such as oxygen and glucose. This increase in glucose influx across the BBB is seen as an adaptation to chronic exposure to mild hypoxia (Harik et al., 1994). There is also an increase in capillary density, by week 1 of exposure to prolonged hypoxia, which results in a decrease in the inter-capillary distance, and thus decreased diffusion distance (LaManna et al., 2004). In the rat brain, the capillary density almost doubles, thereby decreasing the inter-capillary distance from approximately 50 to 40 μm (Lauro and LaManna, 1997). Not only is there an increase in capillary density, there is also an increase in glucose transporter 1 (GLUT-1), as measured by molecules per milligram of microvessel (Xu and LaManna, 2006). Interestingly, endothelial cell activation was reported in response to prolonged hypobaric hypoxia (Dore-Duffy et al., 1999). Exposure to hypoxia resulted in the expression of specific markers associated with endothelial cell activation, such as cell surface adhesion molecules, whose expression increased in a time dependent manner from 0 to 2 weeks. Induction of endothelial MHC class II molecules in addition to increased constitutive expression of GLUT-1 was

observed within 24 hours of exposure, and an increase in constitutive expression of MHC class I by 48 hours (Dore-Duffy et al., 1999). By 3 weeks of exposure to hypoxia, the endothelial cells returned to their quiescent state (Dore-Duffy et al., 1999).

1.8.0.0 Hypoxia and MS

Increasing evidence from neuropathological, microarray and imaging studies suggest that hypoxic conditions may exist within MS lesions. Firstly, the demyelination in Pattern III MS lesions has been described to occur by a 'hypoxia-like' mechanism, due to the pathological similarities this lesion shares with acute white matter stroke lesions (Aboul-Enein et al., 2003). As described above, the characteristic feature of Pattern III lesions is the striking, preferential loss of MAG (Lucchinetti et al., 2000), a myelin protein concentrated in periaxonal regions of the myelin sheath, most distal to the oligodendrocyte cell body (Trapp and Quarles, 1984), and a common feature of acute white matter stroke lesions. Other myelin proteins, PLP and MBP, which are located in compact myelin, and MOG, which is expressed on the surface of oligodendrocytes and their processes, initially remain well preserved in this lesion subtype (Lucchinetti et al., 2000; Lassmann, 2003). In these lesions, areas of MAG loss are associated with increased expression of hypoxia-inducible transcription factor-1α (HIF-1α), predominantly in oligodendrocytes, astrocytes and some endothelial cells (Aboul-Enein et al., 2003). Although the expression of HIF-1α can be induced by hypoxia-independent factors, its presence in the 'hypoxia-like' MS lesion is suggestive that oxygen concentrations within the lesion may actually be low. Secondly, microarray studies of the NAWM have revealed an up-regulation of a number of genes involved in hypoxic pre-conditioning (Graumann et al., 2003). However, these studies have

attributed the findings to an energy insufficiency, consequent to NO-mediated mitochondrial dysfunction, rather than to hypoxia *per se*.

Vascular disturbances could easily lead to tissue hypoxia, and indeed such abnormalities have been described in MS patients. Cerebral hypoperfusion has been reported in MS patients since 1983 (Swank *et al*., 1983; Brooks *et al*., 1984; Lycke *et al*., 1993; Sun *et al*., 1998), however, it was not until the development of dynamic susceptibility MRI that this phenomenon regained interest (Law *et al*., 2004; Adhya *et al*., 2006). Law et al (2004), described a decrease in CBF and an increase in mean transit time throughout the NAWM of patients with RRMS, compared with that of control subjects. Similarly, Adhya et al (2006) found a significant reduction in both the CBF and CBV in patients with RRMS and patients with PPMS in comparison to controls. Interestingly, more recently, a profound decrease in CBF in the NAWM was found in patients with early RRMS, precisely within the first five years of symptoms (Varga et al., 2009), suggesting that perfusion abnormalities are present, even in the very early stages of disease. It seems reasonable that these perfusion abnormalities have a considerable effect on tissue oxygenation, particularly given that atrophy would not be expected at this stage of the disease, and would therefore not account for the decrease in CBF. However, increases in CBF and CBV have also been described in a longitudinal study, as early as three weeks prior to, and at the time of Gd-DTPA enhancement in patients with early RRMS, and mean disease duration of 30.9 months (Wuerfel et al., 2004). Besides this pattern of perfusion, Wuerfel and colleagues (2004) also described decreases in CBF and CBV, and an increase in the mean transit time, in the T1-hypointense region of lesions that developed ring enhancements, which is consistent with previous studies (Haselhorst et al., 2000). Such lesions, are typically focal, and exhibit a hyperintense ring at the lesion margin on un-enhanced T1-weighted images,

and are thought to persist for long periods of time (Guttmann et al., 1995). The perfusion changes associated with the T1-hypointense region has therefore been proposed to play a part in the development of a subcategory of focal MS lesions (D'haeseleer et al., 2011).

More recently, MS has controversially been associated with a reduced CNS venous blood drainage, referred to as chronic cerebrospinal venous insufficiency (CCSVI) (Zamboni et al., 2009; Al-Omari and Rousan, 2010; Simka et al., 2010). CCSVI is characterised by obstruction at different levels of the internal jugular veins, vertebral veins, azygous system, and the lumbar venous plexus (Zamboni et al., 2009). It is hypothesised that CCSVI stretches the venous walls, which leads to the extravasation and degradation of erythrocytes, and subsequent peri-venular iron deposits (Singh and Zamboni, 2009). These iron deposits in turn initiate inflammation and plaque generation. Indeed, such an abnormality would also be expected to have a considerable effect on tissue oxygenation. However, CCSVI remains a particularly controversial topic among the MS community, with other groups unable to reproduce the original findings (Doepp et al., 2010; Baracchini et al., 2011; Mayer et al., 2011).

1.9.0.0 Detection of Tissue hypoxia

Hypoxia is a feature of a number of pathological conditions, yet it represents a phenomenon that has not been routinely measured *in vivo*. This, in part, could be due to the limitations associated with traditional invasive methods, such as oxygen microelectrodes, and non-specific extrinsic hypoxia markers. However, there have been significant improvements in the techniques available to measure CNS oxygen tension *in vivo*. Such techniques exploit the chemical and physical properties of oxygen in order

to acquire a relatively accurate measurement. Such methods include polarography, optical probes, electron paramagnetic resonance, nuclear magnetic resonance, positron emission tomography and mass spectrometry (Ndubuiza and LaManna, 2007). Alternatively, indirect measurements of oxygen concentration, such as haemoglobin saturation, cytochrome oxidase redox state, and NADH redox state, also give an indication of tissue oxygen concentration. Although, these techniques may differ with regard to their sensitivity, accuracy, and ability to measure repetitively (Swartz, 2007), no one technique is able to map the oxygen distribution of the brain *in vivo.*

The expression of a number of genes is altered in response to hypoxia (Leonard et al., 2003; Manalo et al., 2005; Xia et al., 2009). This response to hypoxia is mediated by the transcription factor HIF-1α, and, therefore, its presence within tissue is often used as an indicator of hypoxia. Pimonidazole, a chemically stable, water soluble drug that can cross the BBB and is routinely used in tumour studies, represents another means to detect tissue hypoxia. This drug is thought to facilitate the measurement of oxygen gradients at the cell level. The mechanisms of action of HIF-1α, pimonidazole, and fibre-optic oxygen probes, will be discussed in further detail below.

1.9.1.0 Hypoxia inducible factor (HIF-1α)

HIF is a heterodimer comprising a constitutively expressed stable β-subunit and an oxygen-sensitive α-subunit (Wang et al., 1995; Semenza, 2000). Both HIF-α and HIF-β are continuously transcribed and translated, however the HIF-α subunit is subject to oxygen-dependent post-translational modifications. Under normoxic conditions, conserved proline residues in the oxygen degradation domain, Pro^{402} and Pro^{564} in HIF-1α (Schofield and Ratcliffe, 2004; Coleman and Ratcliffe, 2007), are hydroxylated by

prolyl hydroxylate enzymes (PHDs) (Bruick and McKnight, 2001). In order to hydroxylate proline residues on HIF-1α, the PHDs require iron and 2-oxoglutarate as substrates in addition to oxygen (Schofield and Zhang, 1999). The hydroxylation of either proline residue creates a recognition and binding site for an E3 ubiquitin ligase, von Hippel-Lindau protein (VHL), which rapidly targets HIF-1α for proteasomal degradation (Maxwell et al., 1999; Ivan et al., 2001; Jaakkola et al., 2001; Kilmova and Chandel, 2008). A second oxygen-sensitive control of HIF activity is mediated by the c-terminus, which contains the c-terminal transactivation domain (CAD; Coleman and Ratcliffe, 2007). The HIF-1α CAD is responsible for recruiting the transcriptional co-activators p300 and CREB-binding protein (CBP; Coleman and Ratcliffe, 2007; Kilmova and Chandel, 2008). Under normoxic conditions, HIF-1α CAD activity is suppressed by the hydroxylation of a conserved asparagine residue, Asn^{803}, by factor inhibiting HIF (FIH), which, like the PHDs, requires iron and 2-oxoglutarate as substrates in addition to oxygen (Schofield and Ratcliffe, 2004).

Under hypoxic conditions, HIF-α is not hydroxylated by either PHDs or FIH, allowing it to translocate into the nucleus, dimerise with HIF-β and bind to specific hypoxia-responsive elements (HRE) in promoter regions of its target genes (Kilmaova and Chandel, 2008). It has been estimated, at least *in vitro*, that more than 50% of the genes that respond to hypoxia are regulated directly or indirectly by HIF (Elvidge et al., 2006).

The cellular responses mediated by hypoxic stabilisation of HIF-α include changes in energy metabolism, cell growth, survival and migration (Coleman and Ratcliffe, 2007). For instance, HIF promotes the delivery of oxygen to hypoxic areas via the up-regulation of growth factors involved in angiogenesis, such as vascular endothelial growth factor (VEGF), and can promote the delivery of glucose via the up-

regulation of glucose transporters, such as GLUT-1. Thus, it is no wonder that HIF is sometimes considered the master regulator of hypoxia.

1.9.2.0 Pimonidazole

Pimonidazole is a chemical compound that allows the detection of hypoxia during life. It is often used as a marker of hypoxia in tumour studies (Raleigh et al., 1998; Wykoff et al., 2000; Janssen et al., 2002; Airley et al., 2003; Hoskin et al., 2003; Hutchison et al., 2004; van Laarhoven et al., 2006), and currently represents one of the best ways in which to detect cellular hypoxia. Following administration, pimonidazole is metabolised as depicted in Figure 1.9.2.0. Briefly, in the presence of adequate oxygen, pimonidazole is subject to oxidative metabolism to an amine oxide, or conjugation to sulfotransferase or glucuronyl transferase all of which are readily excreted (Arteel at al., 1998). Pimonidazole is also subject to a series of reduction steps, whereby nitroreductases such as NADPH and NADH transfer electrons to the parent compound. Oxygen, is the rate limiting factor, and competes for the transfer of the first electron to pimonidazole, reoxidising the nitro-intermediate pimonidazole, thereby preventing further reduction of pimonidazole by nitroreductases (Arteel et al., 1998). In the absence of oxygen, the nitro-intermediate pimonidazole is further reduced, and can bind to thiol containing molecules such as glutathione and proteins to form pimonidazole adducts. The location of these adducts can then be determined by immunohistochemistry using antibodies directed against the bound pimonidazole.

In addition to hypoxic labelling, pimonidazole has been found to label normoxic tissues, raising the suspicion that its ability to bind may not be oxygen dependent in all cases, and may in fact also depend on the presence of specialised nitroreductases (Cobb

et al., 1990). However, neither the distribution of nitroreductases (Arteel et al., 1995), nor the redox state of nitroreductases (Arteel et al., 1998), influences the binding ability of pimonidazole.

Correlations between pimonidazole binding and other endogenous hypoxia markers have been carried out in a number of tumour studies (Raleigh et al., 1998; Wykoff et al., 2000; Janssen et al., 2002; Airley et al., 2003; Hoskin et al., 2003; Hutchinson et al., 2004; van Laarhoven et al., 2006)). In cervical carcinomas, a mild, yet statistically significant correlation between pimonidazole binding and HIF-α, and GLUT-1 was found (Airley et al., 2003; Hutchinson et al., 2004), whereas no correlation between pimonidazole labelling and VEGF was found (Raleigh et al., 1998). Pimonidazole binding was found to correlate with GLUT-1 in bladder carcinoma (Wykoff et al., 2000; Hoskin et al., 2000). It appears that the correlation between pimonidazole binding and other endogenous markers, is not absolute, and may sometimes depend on the model being examined. Nevertheless, pimonidazole represents an alternative yet novel way of labelling the CNS for hypoxia during life.

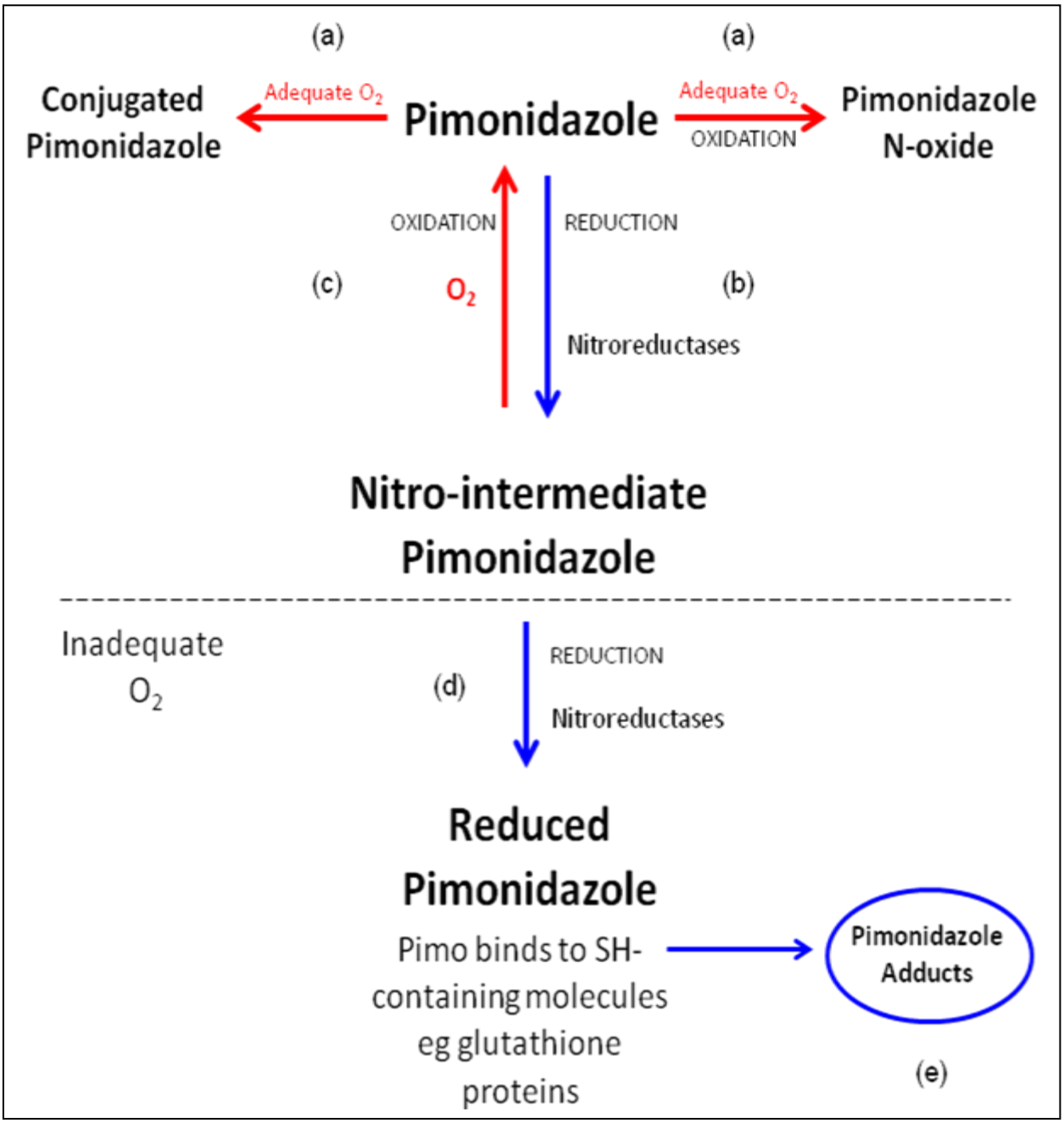

Figure 1.9.2.0: Metabolism of pimonidazole *in vivo*

(a) *In vivo***,** under normoxic conditions, pimonidazole is rapidly metabolised and eliminated from the body, by oxidation or conjugation. (b) In the absence of oxygen pimonidazole is reduced by nitroreductases to a nitro-intermediate; however, oxygen is the rate limiting factor at this point, and can oxidise the nitro-intermediate back to pimonidazole (c). In hypoxic cells, the nitro intermediate is subject to a series of reductions (d), until reduced pimonidazole can bind to thiol (SH-) containing molecules resulting in the formation of pimonidazole adducts (e). Adapted from Arteel et al., 1998.

1.9.3.0 Fibre optic oxygen sensitive probes

Optical oxygen probes are based on the ability of oxygen to act as a fluorescence quencher, thereby decreasing the lifetime of an excited, immobilised lumniphore (Kautsky, 1939; Klimant et al., 1995). Specially formulated dyes, designed for their highly efficient oxygen quenching capabilities, have facilitated oxygen measurement *in vivo*. In essence, collision between the lumniphore and molecular oxygen results in a change in energy state, and thus, deactivation of the luminescent indicator molecule. Accordingly, an inverse relationship between the oxygen concentration and luminescent decay time exists, whereby a low oxygen concentration is associated with a long decay time. The advantage these probes provide over traditional electrodes is that they do not consume oxygen and so reach equilibrium. Moreover, they offer relatively high spatial and temporal resolution.

CHAPTER TWO

HYPOXIA AND DYSFUNCTION

2.1.0.0 INTRODUCTION

The mechanisms through which neuroinflammation can cause neurological dysfunction remain unclear. Traditionally, neurological dysfunction in MS has been attributed to demyelination, and axonal degeneration. However, increasing evidence suggests that inflammation, in the absence of demyelination, is also capable of causing significant clinical deficits (Youl et al., 1991; Moreau et al., 1996; Bitsch et al., 1999). Alterations in the conduction properties of axons are thought to underlie a number of symptoms, particularly during the relapse-remitting stage of the disease (Smith and McDonald, 1999). Negative symptoms during relapse (e.g. blindness, numbness, paralysis), have been attributed to conduction block, whereas axonal hyperexcitability is thought to cause positive symptoms (e.g. tingling sensations). Demyelinated axons are particularly susceptible to such changes in electrical activity; however, myelinated axons can also be affected. NO, a toxic mediator found to be elevated in MS (Bo et al., 1994), has emerged as a key mediator of such electrical disturbances. NO can induce reversible conduction block in normal axons (Redford et al., 1997; Shrager et al., 1998), through mechanisms such as ion channel modulation (Kurenny et al., 1994; Li et al., 1998; Smith and Lassmann, 2002), inhibition of mitochondrial energy metabolism (Bolanos et al., 1994; Brown et al., 1995), and the disruption of synaptic transmission (Kilbinger et al., 1996; Holscher et al., 1997; Kara and Friedlander, 1998; Smith and McDonald, 1999). However, besides the release of toxic mediators, inflammation might also promote a hypoxic environment within the tissue. Indeed, a ‘hypoxia-like’ mechanism

of tissue injury is suggested to occur in Pattern III MS lesions (Aboul-Enein et al., 2003), and genes associated with hypoxic pre-conditioning have been found to be up-regulated in NAWM (Graumann et al., 2003). Hypoxia can directly impair neuronal function, and therefore, if present in MS, may not only induce tissue damage, but may also play a role in the expression and progression of a neurological deficit. We therefore examined the rMOG EAE model of MS for evidence of hypoxia.

2.1.1.0 Aims

1. To determine whether the spinal cord inflamed by EAE is hypoxic
2. To determine the role of hypoxia in causing neurological deficits rMOG EAE.
3. To determine the efficacy of acute normobaric hyperoxia on function in rMOG EAE
4. To establish the effects of combination therapy (iNOS inhibition, antioxidant, and oxygen) on the disease course of rMOG EAE

2.1.2.0 Hypothesis

Hypoxia mediates neurological dysfunction in the first peak of rMOG EAE.

2.2.0.0 MATERIALS AND METHODS

2.2.1.0 Induction of rMOG-EAE

All animals were randomized into cages and treatment groups, prior to the experiments, and left to acclimatise for at least 7 days. The N-terminal sequence (aa 1-125) of rat recombinant MOG (rMOG; a gift from C. Linington, University of Aberdeen, UK) was used to induce EAE in adult female DA rats (Harlan, UK; 150g- 190g). Animals (n = 191) were injected subcutaneously in the rear flank near the base of the tail, with 0.2 ml of a hard emulsion comprising 0.100 ml rMOG in 0.100 ml incomplete Freund's adjuvant (IFA; Sigma-Aldrich, USA), under general anaesthesia (2% isoflurane in room air). Control animals received 0.2 ml injections of an emulsion of IFA and saline (n = 19), or saline (n = 19) alone.

2.2.2.0 Neurological Evaluation

Rats were daily weighed and examined blindly throughout the course of the experiments to determine the degree of neurological deficit using a 10-point scoring system (Table 2.2.2.0). Briefly, neurological scores were assigned on a scale of 0 to 10, whereby the final score represented the total of all the individual scores. The neurological assessment comprised examination of tail and bilateral hind limb muscle strength (normal, weak, paralysed). The scores corresponded to the following clinical

deficit: 0 = normal muscle strength; 1 = muscle weakness; 2 = complete muscle paralysis.

Neurological Deficit
Tail tip weakness
Tail weakness
Tail paralysis
Abnormal gait
Abnormal toe spreading
Unilateral hind limb weakness
Bilateral hind limb weakness
Unilateral hind limb paralysis
Bilateral hind limb paralysis
Moribund

Table 2.2.2.0: Conventional scoring scale for evaluating neurological deficit

Table showing the criteria used to evaluate the extent of neurological deficit in animals immunised with rMOG. A score of one was given for each of the deficits outlined in the table to give a total score out of ten.

2.2.3.0 Selection of animals

2.2.3.1 rMOG EAE disease time course

During various stages of the disease (asymptomatic (prior to deficit), first peak (within 3 days of onset of deficit), remission (at least two days of functional improvement following an initial deficit), and relapse (at least two days of increasing severity of deficit following the remission period)), animals were grouped into cohorts of eight animals comprised of an IFA control (n=15 in total), a saline control (n=15 in total), and 6 animals displaying a range of neurological deficit scores (n=75 in total).

2.2.3.2 One hour oxygen therapy in rMOG EAE

At the onset of neurological deficit, rMOG animals were placed in pairs based on the similarity and timing of their neurological deficit as dictated by their 10-point neurological score, and each animal of the pair was randomly assigned to receive either room air (n=12) or normobaric hyperoxia (~98%, n=12). IFA (n=2 per treatment) and saline (n=2 per treatment) controls were also included. Animals were housed in a purpose-built chamber (BioSpherix, USA), for the duration of the treatment (1 hour), and temperature, oxygen concentration, and carbon dioxide concentration were monitored and controlled throughout. Prior to, and following treatment, animals were subjected to a more rigorous neurological assessment using a 25-point scale (Table 2.2.3.2). Thus each hind limb was assessed for stretch withdrawal, pinch withdrawal, toe spreading, spasticity, and plantar placement with a maximum of two points awarded for each measure (ten points per hind limb), with a score of zero indicating normal

function. Tail function (0-3 points) and hip flexion (0-2 points) were also assessed, for a total maximum score of 25 points.

Neurological Deficit			Score
Hind limbs			
	Stretch Withdrawal		
		Delayed, Weak, Partial	1
		No Response	1
	Pinch Withdrawal		
		Delayed, Weak, Partial	1
		No Response	1
	Toe Spreading		
		Incomplete, Asymmetrical Foot Splaying or Toe Spreading	1
		No Response	1
	Spasticity		
		Partial rigidity or immobilization, some residual movement	1
		Complete rigid spasticity	1
	Plantar Placement		
		Attempted but unsuccessful or incomplete plantar placement during walking	1
		No attempted plantar placement during walking	1
Tail			
		Tail tip weakness	1
		Tail weakness	1
		Complete tail paralysis	1
Hip			
		Asymmetrical, some flexion	1
		Complete Absence of flexion, or dragging	1

Table 2.2.3.2: Enhanced scoring scale for the evaluation of neurological deficit

Table outlining the criteria used to evaluate the extent of neurological dysfunction in animals immunised with rMOG, prior to and following treatment with one hour of oxygen. A score of one was given for each deficit, resulting in a total score out of 25.

2.2.3.3 7-day combination therapy

To assess the relative contributions of oxygen, NO and superoxide to functional impairment in EAE, the effects of prolonged normobaric hyperoxia (~75% oxygen), iNOS inhibition (1400W; Enzo Life Sciences Ltd, UK), mitochondrially targeted antioxidant therapy (MitoQ, a kind gift from M. Murphy), and a combination of all the therapies, was investigated. Animals (n = 85) were randomly assigned to one of five treatment groups; oxygen (n=17), 1400W (iNOS inhibitor; n = 17), MitoQ (antioxidant; n = 17), All (n = 17) and controls (n = 17), at least 7 days prior to immunisation. Oral administration of MitoQ (500 μM), via the drinking water, began on the day of immunisation, and was monitored daily. All other treatments began on the day of disease onset. 1400W (10 mg/ml in sterile saline) was administered daily intraperitoneally, to animals in the 1400W and All, treatment groups, from disease onset. The remaining animals were daily administered intraperitoneal injections of saline alone, from disease onset. Treatment was continued for 7 days post-disease onset. Daily monitoring and assessment of neurological deficit was performed by a blind assessor.

2.2.4.0 Intravenous and tissue probes

Four hours prior to perfusion, intravenous injections of pimonidazole (60mg/kg in sterile saline; HPI Inc, USA), and dihydroethidium (DHE) (1μg/ml in DMSO, Sigma Aldrich, UK) were administered into each of the saphenous veins, under light anaesthesia (2% isoflurane in room air, or oxygen, as appropriate). Animals that were part of the acute oxygen therapy study were maintained in their respective treatment condition, from the beginning of treatment, until perfusion. Prior to perfusion, a laminectomy was performed at the T13/L1 vertebral level, under general anaesthesia

(2% isoflurane in room air, or oxygen, as appropriate), so as to expose the cord. A small hole was made in the dura, approximately 700 μm lateral to the midline, and the neighbouring dorsal spinous process stabilised using a secure haemostat. A tapered-tip (<50 μm) oxygen-sensitive optical probe (OxyMicro, WPI inc, USA) was then inserted at an angle of 12 degrees from vertical into the grey matter, through the hole in the dura, to a depth of 1100 μm and then retracted 100 μm. Subsequent oxygen and temperature measurements were recorded continuously (1 Hz) using OxyMicro software (WPI inc, USA) for at least five minutes following stabilization of the recording. The oxygen probe was calibrated prior to use on a daily basis.

All protocols for animal research were carried out in accordance with UK Home Office scientific procedures act and an appropriate project license.

2.2.5.0 Tissue Processing

Animals were perfused transcardially with phosphate-buffered saline (PBS; Sigma-Aldrich, USA), followed by 4% paraformaldehyde (PFA) for fixation, under general anaesthesia (2% isoflurane in room air, or oxygen, as appropriate). Spinal cord tissue was harvested and post-fixed in 4% PFA overnight, with subsequent cryoprotection in 30% sucrose (BDH International, UK) in PBS. The spinal cords were cut into 5 segments comprising the sacral, lumbar, upper lumbar, lower thoracic and mid-thoracic regions of cord, and embedded in cryomoulds containing OCT medium (Leica, UK). The tissue was frozen by immersion in pre-cooled isopentane (VWR International, UK) in liquid nitrogen. Sections were cut to a thickness of 12 μm with a cryostat (Leica Microsystems, Germany) at -20^{0}C, and thaw-mounted onto glass slides. The sections were stored frozen at -20^{0}C until use.

2.2.6.0 Histology

2.2.6.1 Immunohistochemistry/Immunofluorescence (IHC/IF)

The cryosections were air dried for at least two hours prior to any histology. First, sections were washed in 0.1M PBS and pretreated with 0.3% hydrogen peroxide (Sigma Aldrich) in neat methanol (VWR International, UK), or methanol alone, for immunofluorescence, for 15 minutes, to quench endogenous peroxidase activity, followed by PBS washes. Where necessary, sections were additionally pre-treated with 1mg/ml sodium borohydride ($NaBH_4$; Sigma Aldrich) in PBS, twice, for 5 minutes each (Table 2.2.6.1). For 8-hydroxydeoxyguanosine immunohistochemistry, tissue was additionally pre-treated with a buffer containing 100µg/ml RNase A (Sigma Aldrich), 150mM sodium chloride and 15mM sodium citrate, for 1 hour at 37^{o}C, followed by 2N hydrochloric acid, and 1M Tris-base, for 5 minutes each. Non-specific binding was blocked with the appropriate blocking buffer (Table 2.2.6.1), for 30 minutes. Tissue was then incubated overnight at 4^{o}C with the primary antibody. Negative controls were incubated with blocking buffer alone.

Primary antibodies were detected with either, horse anti-mouse, or goat anti-rabbit biotinylated secondary antibodies (1:200, Vector Laboratories Inc, UK), followed by visualisation using an avidin-biotin complex horseradish peroxidise kit (Vectastain Elite ABC kit, Vector Laboratories), with diaminobenzidine (DAB) (Vector Laboratories) as the chromogen. Sections were finally dehydrated in graded alcohol to xylene, and coversliped in DPX mounting medium (BDH). PBS washes were carried out between all steps.

For immunofluorescence, mouse primary antibodies were detected with a horse anti-mouse biotinylated secondary antibody (1:200, Vector), followed by a streptavidin-

FITC (Fluorescein isothiocyanate) conjugated antibody (1:200, Invitrogen, UK), and rabbit primary antibodies were detected with a goat anti-rabbit Cy3 conjugated secondary antibody (1:200, Invitrogen). Sections were then coversliped with vectashield aqueous mounting medium (Vector). PBS washes were carried out between all steps.

Table 2.2.6.1: Antibody details for IHC/IF

Antibody	Target	Isotype	Pre-Treatment	Blocking Buffer	Dilution	Source
Mouse Anti-Rat ED1	Activated macrophages/ microglia	Mouse IgG_1	None	5% horse serum (NHS; Vector Labs) in 0.01% PBS-triton	1:200	AbD Serotec
Mouse Anti-P47^{phox}	NADPH oxidase subunit	Mouse IgG_1	None	5% NHS in 0.01% PBS-triton	1:50	Santa Cruz Biotechnology
Mouse Hydroxyprobe-1-Mab anti-pimonidazole	Pimonidazole adducts	Mouse IgG_1	1mg/ml $NaBH_4$	0.25% casein (VWR) in 0.1% PBS-triton	1:500	HPI Inc
Mouse Anti-RECA-1	Rat endothelial cells	Mouse IgG_1	None	5% NHS in 0.01% PBS-triton	1:200	Abcam
Mouse Anti-8-oxo-dG	Oxidative DNA damage	Mouse IgG_{2b}	RNase buffer, 2N HCl, 1M Tris base	5% NHS in 0.01% PBS-triton	1:500	Trevigen
Mouse Anti-B-tubulin III	Neurons	Mouse IgG_{2b}	1mg/ml $NaBH_4$	5% NHS in 0.01% PBS-triton	1:200	Sigma
Rabbit Anti-Pimonidazole	Pimonidazole adducts	Rabbit IgG	1mg/ml $NaBH_4$	5% goat serum (NGS; Vector Labs) in 0.01% PBS-triton	1:200	HPI Inc
Rabbit Anti-iNOS	Inducible nitric oxide synthase	Rabbit IgG	None	5% NGS in 0.01% PBS-triton	1:200	BD Transductions Ltd
Rabbit Anti-GFAP	Astrocytes	Rabbit IgG	1mg/ml $NaBH_4$	5% NGS in 0.01% PBS-triton	1:500	Dako
Rabbit Anti-HIF-1α	Hypoxia inducible factor-1 α	Rabbit IgG	1mg/ml $NaBH_4$	5% NGS in 0.01% PBS-triton	1:500	Millipore
Rabbit Anti-IBA	Macrophages/microglia	Rabbit IgG	1mg/ml $NaBH_4$	5% NGS in 0.01% PBS-triton	1:200	Wako Chemicals
Rabbit Anti-P22^{phox}	NADPH oxidase subunit	Rabbit IgG	None	5% NGS in 0.01% PBS-triton	1:100	Santa Cruz Biotechnology

2.2.6.2 Myelin chemical stain

Sections were stained with luxol fast blue (LFB)/periodic acid Schiff (PAS)/haematoxylin to assess demyelination. Sections were taken to 100% ethanol (VWR) with gentle shaking in 70% ethanol, followed by 90% ethanol for 5 minutes each. The sections were then incubated overnight at 50^0C with LFB solution: 0.1% LFB (BDH) in acidified 95% ethanol (1.0g LFB, 1000ml 95% ethanol, 0.5ml glacial acetic acid). The following day the sections were removed from the LFB solution, and washed well in running tap water. Subsequently, the sections were differentiated by cycling through saturated lithium carbonate (Merck, Germany) for 30 seconds, followed by 70% ethanol, washing with running tap water in between each step. This was continued until the stain was removed from non-myelinated tissue. Next, the sections were initially oxidised in 1% periodic acid (VWR) for 20 minutes at room temperature (RT), and then incubated in neat Schiff's reagent (VWR) for 20 minutes at RT, once again washing in running tap water after each step. Finally, the sections were counterstained in neat Harris haematoxylin (VWR) for 2 minutes, washed in running tap water, differentiated until clear in 1% acid alcohol, and then washed well in running tap water. Dehydration through graded alcohol was performed by 5 minute incubations in 70% and 90%, followed by two x2 minute incubations in 100% ethanol, and then two incubations in 100% xylene for more than 2 minutes. The slides were then mounted using DPX mounting medium (VWR).

2.2.7.0 Microscopy

2.2.7.1 Light Microscopy and Quantification

Tissue developed using the peroxidase development system (DAB) was viewed with an Axiophot light microscope (Zeiss, Germany), and photographed with a Nikon D300 camera (Nikon, USA). The illumination was kept consistent throughout image acquisition. Captured images were imported into Image J (NIH, Bethesda, MD) and converted from RGB 24 bits per pixel (bpp) to grey scale 8 bpp images. Analysis of the intensity of the labelling with pimonidazole was carried out by manually demarcating the spinal white and grey matter, and measuring the pixel intensity above a set threshold. Quantification of ED1 and iNOS immunoreactivity was performed by counting the number of pixels above a set threshold, and expressed as the percentage of cross-sectional area coverage. Quantification of vessel count and size was performed using the automated 'analyse particles' tool, on binary images, and subsequently filtered for size and circularity. All the quantification was performed blind.

2.2.7.2 Confocal Laser Microscopy

Fluorescent images were obtained using a Zeiss LSM5 Pascal confocal microscope, with a x40 objective. Excitation wavelengths of 488 nm and 543 nm were provided by argon and helium-neon gas lasers, respectively. Emission filters BP505-570, BP505-530, and LP560 were used to obtain the images.

2.2.8.0 Disease parameters

The change in neurological deficit score on the last day, the total cumulative score, and the score on the day of perfusion, were used to indicate disease severity. Thus, these

parameters were taken into consideration when assessing the contribution of various pathological markers to the expression of a neurological deficit.

2.2.9.0 Statistical Analysis

Pearson correlation coefficients were used to assess association between variables where indicated.

A one-way analysis of variance (ANOVA) with a Bonferroni correction was used to compare pimonidazole labelling, oxygen probe measurements, blood vessel diameter, and blood vessel number between groups as indicated. A single sample t-test was used to assess the difference between one hour of treatment with oxygen, or room air, using the difference in score change between paired animals. An independent t-test was used to assess differences in neurological deficit score between the control group and each treatment group respectively (1400W, MitoQ, oxygen, and ALL). A one-tailed significance is stated for the acute oxygen and long term therapy studies, based on the *a priori* hypothesis that treatment would reduce the observed neurological deficit. Q-Q plots were used to assess whether the data were normally distributed.

2.3.0.0 RESULTS

2.3.1.0 Clinical course of rMOG EAE

Subcutaneous injection of 100 μg rMOG in female DA rats induced a relapsing disease (Figure: 2.3.1.0 A), characterised by ascending motor paralysis, with a typical disease onset of 9 days post-induction (PI) and an incidence of 96%. The onset of disease was coupled with a loss in body weight. Within this first peak of disease, disease severity varied from tail weakness to a complete flaccid paralysis of the lower limb extremities. The first peak of the disease was characterised histopathologically by the infiltration of large numbers of inflammatory cells, particularly near the root entry zones and subpial white matter, in the absence of any obvious demyelination (Figure: 2.3.1.0 B). This first peak of disease was followed by a remission phase (13-17 days PI), at which point some evidence of demyelination, indicated by the loss of LFB staining, was observed. The remission phase was followed by an aggressive relapse phase (18 days PI), during which the demyelination was extensive (Figure: 2.3.1.0 B), and a spastic, rather than flaccid, paralysis was dominant. Neither asymptomatic nor control animals displayed any evidence of neurological disability, or a loss in body weight.

A

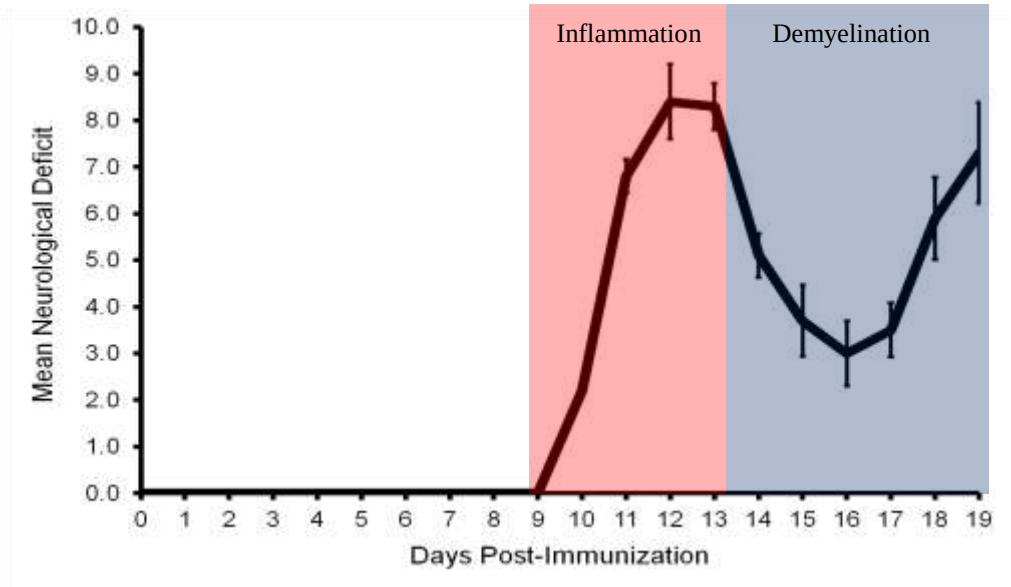
Inflammation
Demyelination
Mean Neurological Deficit
10.0
9.0
8.0
7.0
6.0
5.0
4.0
3.0
2.0
1.0
0.0
0 1 2 3 4 5 6 7 8 9 10 11 12 13 14 15 16 17 18 19
Days Post-Immunization

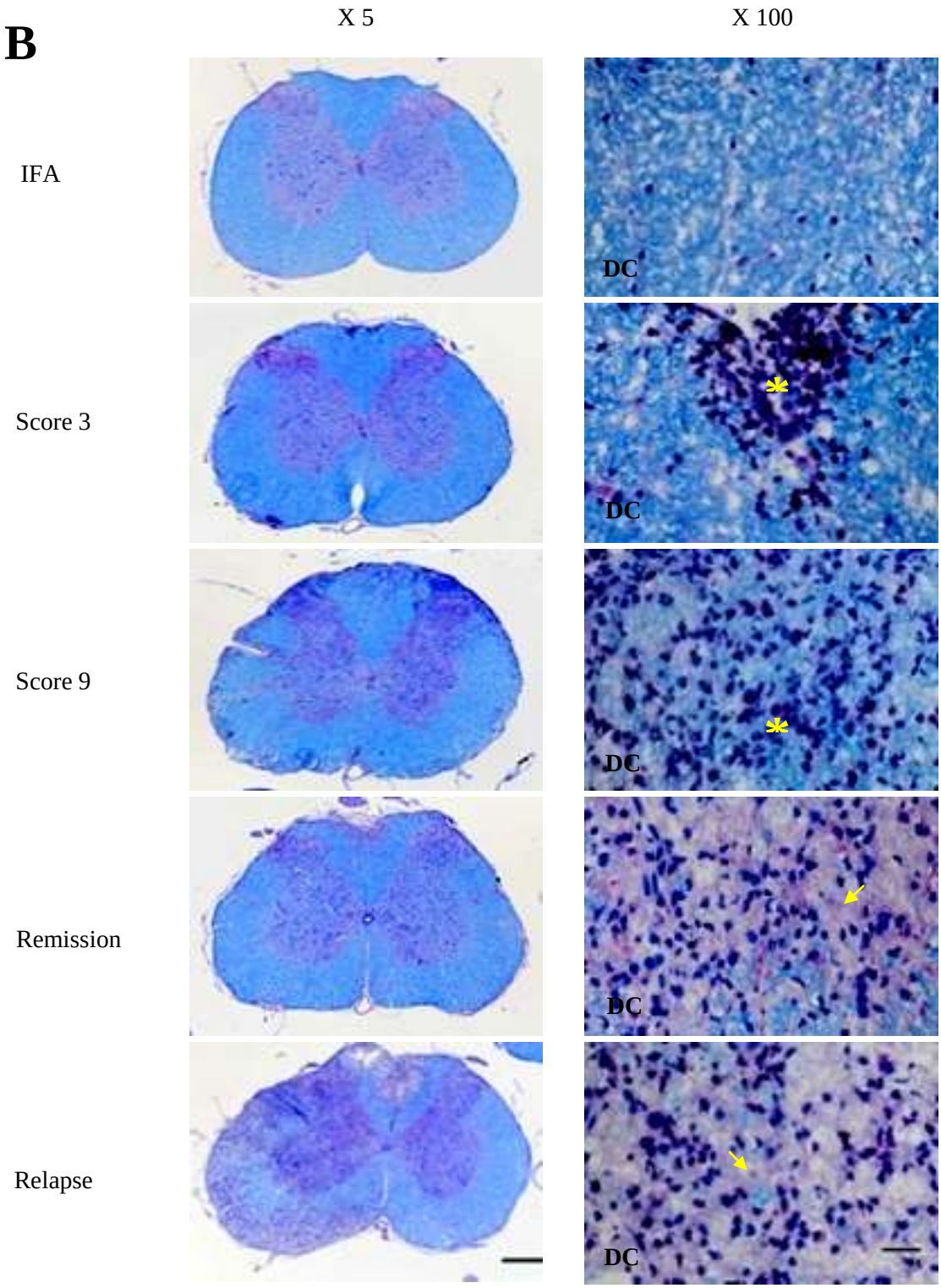

Figure 2.3.1.0: EAE time course: Inflammatory and demyelinating aspects
(A) Graph showing the average scores for neurological deficit over the course of rMOG EAE in DA rats. Values are mean ± S.D. The two peaks in neurological deficit appear to be caused by different mechanisms. Dysfunction in the first peak is thought, partly from current observations, to occur via a mechanism that arises primarily from inflammation, whereas dysfunction in relapse (second peak) appears to be due primarily to demyelination. (B) Transverse spinal cord sections stained with LFB/PAS, and counterstained with hematoxylin (B-top, scale bar 500 µm), and high magnification of the top of the

dorsal column (DC) (B-bottom, scale bar 25 μm). Demyelination, revealed by the loss of LFB staining (blue) is absent during the first peak, which is characterised by massive infiltration of inflammatory cells (*). Loss of LBF staining is particularly visible in the spinal cord of animals in relapse (arrow), and remission (arrow), although to a lesser extent. All micrographs are representative.

2.3.2.0 Inflammation over the time course of rMOG EAE

2.3.2.1 ED1 labelling as a correlate of disease severity

Microscopically, symptomatic rMOG animals exhibited varying amounts of spinal inflammation, characterised by ED1 immunoreactivity, which was largely absent from asymptomatic, and control animals (Figure: 2.3.2.1). At the early stages of disease (neurological deficit score 3), ED1 positive cells were predominantly found near the root entry zones, and subpial areas in the white matter (Figure: 2.3.2.1 Ai), however, as the disease progressed towards the peak of neurological deficit (neurological deficit score 7-9) the inflammatory cells were found to penetrate deeper into the parenchyma. At this stage of disease, perivascular cuffing was common. The extent of inflammation eased during remission, however, ED1 immunoreactivity during relapse was profound (Figure: 2.3.2.1 Ai). At this stage of disease, the inflammation was not restricted to the subpial white matter, but, rather involved the entire white matter, and grey matter, although to a much lesser extent. These areas in which ED1 immunoreactivity was profound commonly appeared oedematous.

Throughout the time course of rMOG EAE, there was a notable change in ED1 cell morphology. At first peak, the cells displayed the characteristic activated, amoeboid morphology, however during remission and relapse stages of disease, the cells displayed a 'foamy' debris-engulfing morphology (Figure: 2.3.2.1 Aii).

The extent of inflammation progressively increased within the first three days of disease, but varied considerably thereafter (Figure: 2.3.2.1 Bi). The extent of inflammation was directly related to the neurological deficit score at perfusion ($p< 0.001$, $r^2=0.792$, n=71, Figure: 2.3.2.1 Bii). Thus, the spinal cords of animals with a higher neurological deficit score were more inflamed than those of animals with a lower neurological deficit score. During the first peak of disease, the inflammation followed

the ascending nature of the disease: most extensive in the caudal portions of spinal cord, and decreasing more rostrally (Figure: 2.3.2.1 Biii). Similarly, in remission and relapse stages of disease, the extent of inflammation was largest most caudally, but decreased in the lumbar cord, before increasing in the rostral portions of the cord (Figure: 2.3.2.1 Biii). No such labelling was evident in control animals.

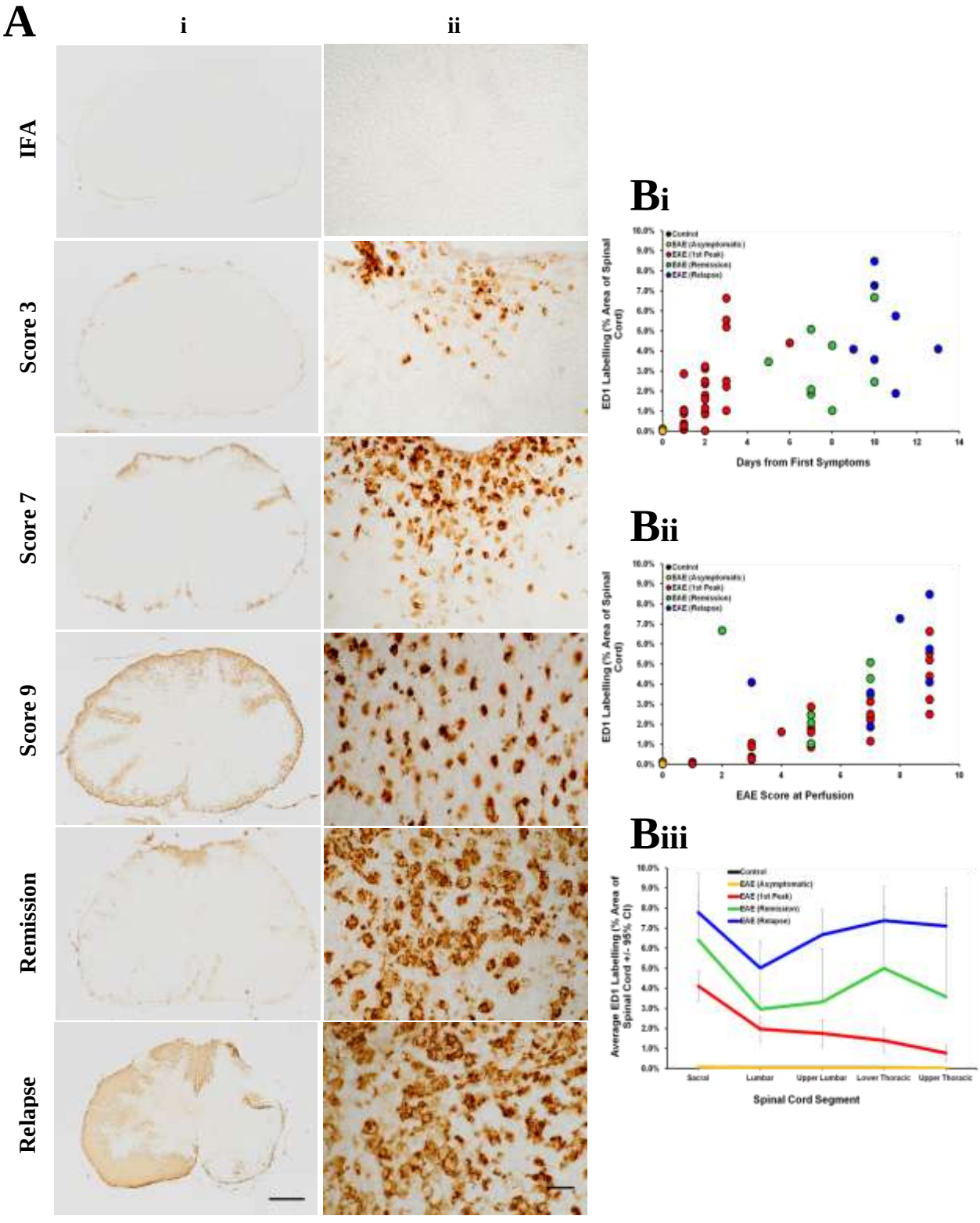
A
i
ii
IFA
Score 3
Score 7
Score 9
Remission
Relapse
Bi
ED1 Labelling (% Area of Spinal Cord)
Days from First Symptoms
Bii
ED1 Labelling (% Area of Spinal Cord)
EAE Score at Perfusion
Biii
Average ED1 Labelling (% Area of Spinal Cord +/- 95% CI)
Sacral
Lumbar
Upper Lumbar
Lower Thoracic
Upper Thoracic
Spinal Cord Segment

Figure 2.3.2.1: ED1 labelling in rMOG EAE

(Ai) Transverse spinal cord sections labelled with ED1, a marker of activated macrophages/microglia, at different stages of rMOG EAE. At the early stages of the disease, during the first peak (score 3), activated macrophages/microglia are present sub-pially, however, as the disease progresses (scores 7 and 9), activated cells begin to penetrate deeper into the parenchyma, and numerous perivascular cuffs can be seen (arrows). Scale bar 500 µm. Examination of these ED1 cells at high magnification (Aii) shows a change in morphology from an amoeboid phenotype, in the first peak, to a foamy debris-engulfing macrophage phenotype, during remission and relapse. Scale bar 25 µm. (Bi) Scatter plot showing the relationship between the extent of ED1 labelling and the number of days from first symptoms. (Bii) Scatter plot showing that ED1 labelling increases with the severity of the disease. (Biii) Graph showing the rostro-caudal extent of ED1 labelling at different stages of the disease (mean ± S.E.M). All micrographs are representative (Contols n=20; asymptomatics n=7; first symptoms n=29; remission n=7; relapse n=7).

2.3.2.2 iNOS expression occurs in the first 3 days following onset of the disease

In rMOG EAE, iNOS expression, although negligible, was only evident in symptomatic animals during the first peak of disease (Figure: 2.3.2.2). iNOS immunoreactivity was largely found in the root entry and exit zones, at the early stages of disease (neurological deficit score 3), but was also found in perivascular cuffs at the peak of disease (Figure: 2.3.2.2 A). iNOS was largely expressed in the first three days following disease onset (Figure: 2.3.2.2 Bi), and therefore, did not correlate well with the neurological deficit score at perfusion (Figure: 2.3.2.2 Bii). Thus, an animal terminated with a neurological deficit score of 9 on day 5 following the onset of disease, would generally have less iNOS than an animal terminated with a neurological deficit score of 7 on day 3 following the onset of disease. The rostro-caudal gradient of labelling was similar to ED1, with iNOS expression greatest most caudally (Figure: 2.3.2.2 Biii). iNOS was absent from asymptomatic animals, and those that were in remission or relapse, and control animals.

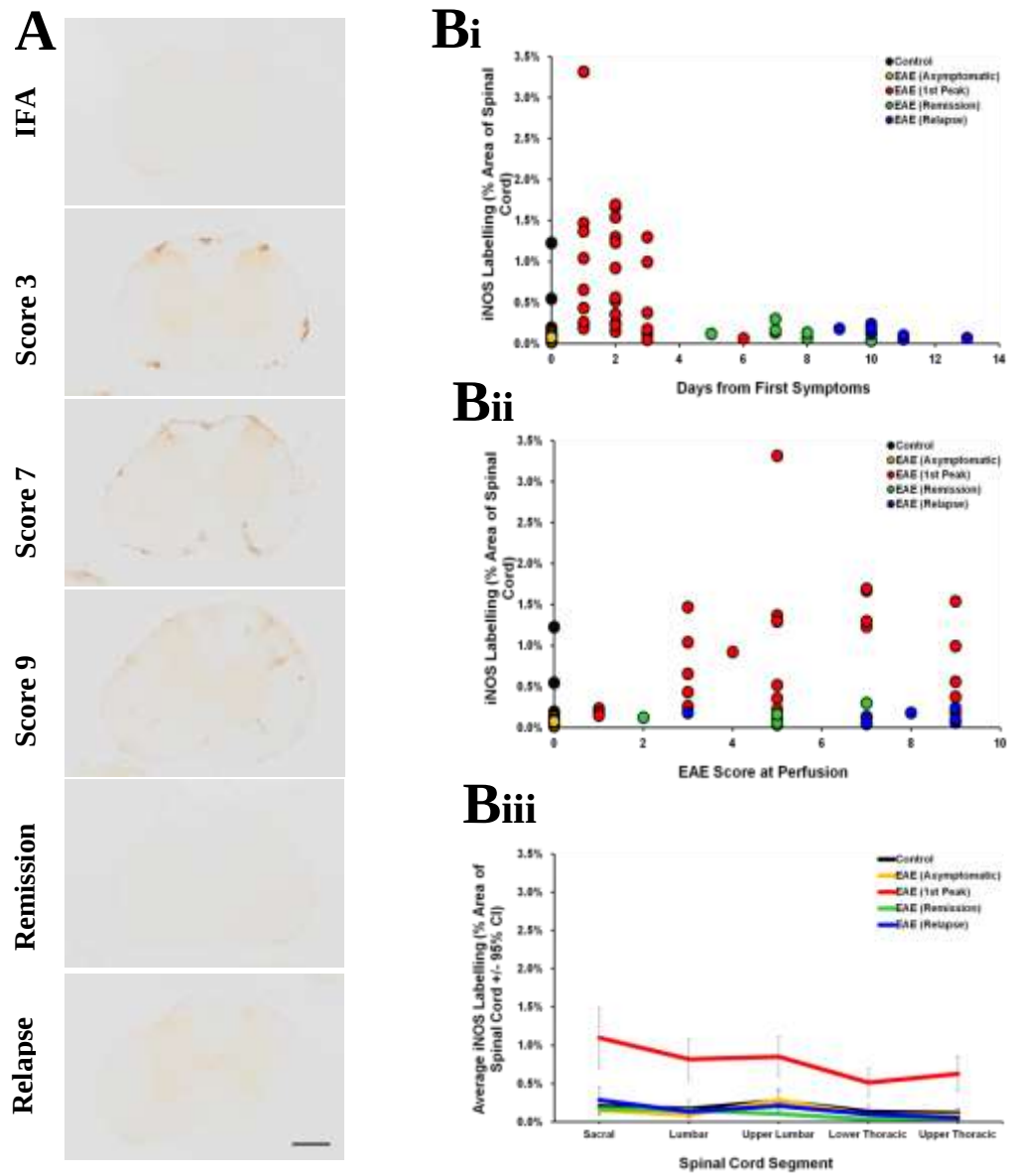

Figure 2.3.2.2: iNOS expression in rMOG EAE

(A) Transverse spinal cord sections labelled with an anti-iNOS antibody. iNOS expression is only evident in the first peak of disease, specifically in the first three days following onset in rMOG animals (n=29) (A; Bi). Scale bar 500 µm. Labelling for iNOS is absent in IFA controls (n=20), asymptomatic controls (n=7) and rMOG animals in remission (n=7) and relapse (n=7) (A; B). (Bii) Scatter plot showing the correlation between the extent of iNOS labelling and the score at perfusion. Although iNOS expression is increased in symptomatic animals, there does not appear to be any obvious correlation with disease severity. (Biii) Graph showing labelling for iNOS along the length of the spinal cord, at different stages of disease (mean ± S.E.M). All micrographs are representative.

2.3.3.0 Hypoxia is a feature of rMOG EAE

2.3.3.1 rMOG EAE Spinal tissue labels positive for hypoxia

Pimonidazole, an intravenous probe that allows the detection of low tissue oxygen concentrations during wakefulness, ostensibly, was administered to all animals prior to perfusion, and the bound drug subsequently detected immunohistochemically. During the first peak of disease, spinal tissue from symptomatic rMOG animals labelled positive for pimonidaozle (Figure: 2.3.3.1). The labelling was most obvious in the spinal grey matter, although punctuate cellular labelling was also observed in the white matter, particularly in perivascular cuffs, extending out of the grey matter (Figure: 2.3.3.1 Ai, Aii). Immunohistochemistry with an antibody against HIF-1α, an alternative marker of hypoxia, yielded a similar pattern of labelling within the grey and white matter. Neuronal labelling for pimonidazole and HIF-1α was especially prominent, with the intensity of labelling increasing with neurological deficit (Figure: 2.3.3.1 Aii, Aiii). At remission, the grey matter labelling for both pimonidazole and HIF-1α disappeared, however, by relapse, some grey matter labelling returned, but intense pimonidazole labelling of foci in the white matter was also observed (Figure: 2.3.3.1 A). No such labelling was evident in asymptomatic, or control animals.

The grey matter pimonidazole labelling correlated temporally with the onset of neurological deficit (Figure: 2.3.3.1 Bi). That is, labelling for pimonidazole was most prominent in the first three days following disease onset, and thus, during the first peak of disease expression. Similarly, the extent of grey matter pimonidazole labelling increased with the magnitude of the neurological deficit ($p = 0.029$, $r^2 = 0.405$, n = 29, Figure: 2.3.3.1 Bii). Spatially, labelling for pimonidazole precisely followed the ascending nature of the disease (Figure: 2.3.3.1 Biii). The labelling was most intense in the most caudal regions of the cord (lumbar $p < 0.001$, n = 70; sacral p = 0.043, n = 67,

serving the paralysed hind limbs and tail respectively), and decreased rostrally. Pimonidazole labelling positively correlated with HIF-1α labelling ($p = 0.05$, $r2 = 0.343$, $n = 65$).

To determine whether this tissue hypoxia was cell specific, or a general phenomenon, double label immunofluorescence was conducted with a range of cell specific markers. Interestingly, astrocytes, neurons and in particular oligodendrocytes, labelled positive for pimonidazole (Figure: 2.3.3.1 C). Macrophages/microglia generally did not label positively for pimonidazole, although there were a few exceptions (Figure: 2.3.3.1 C).

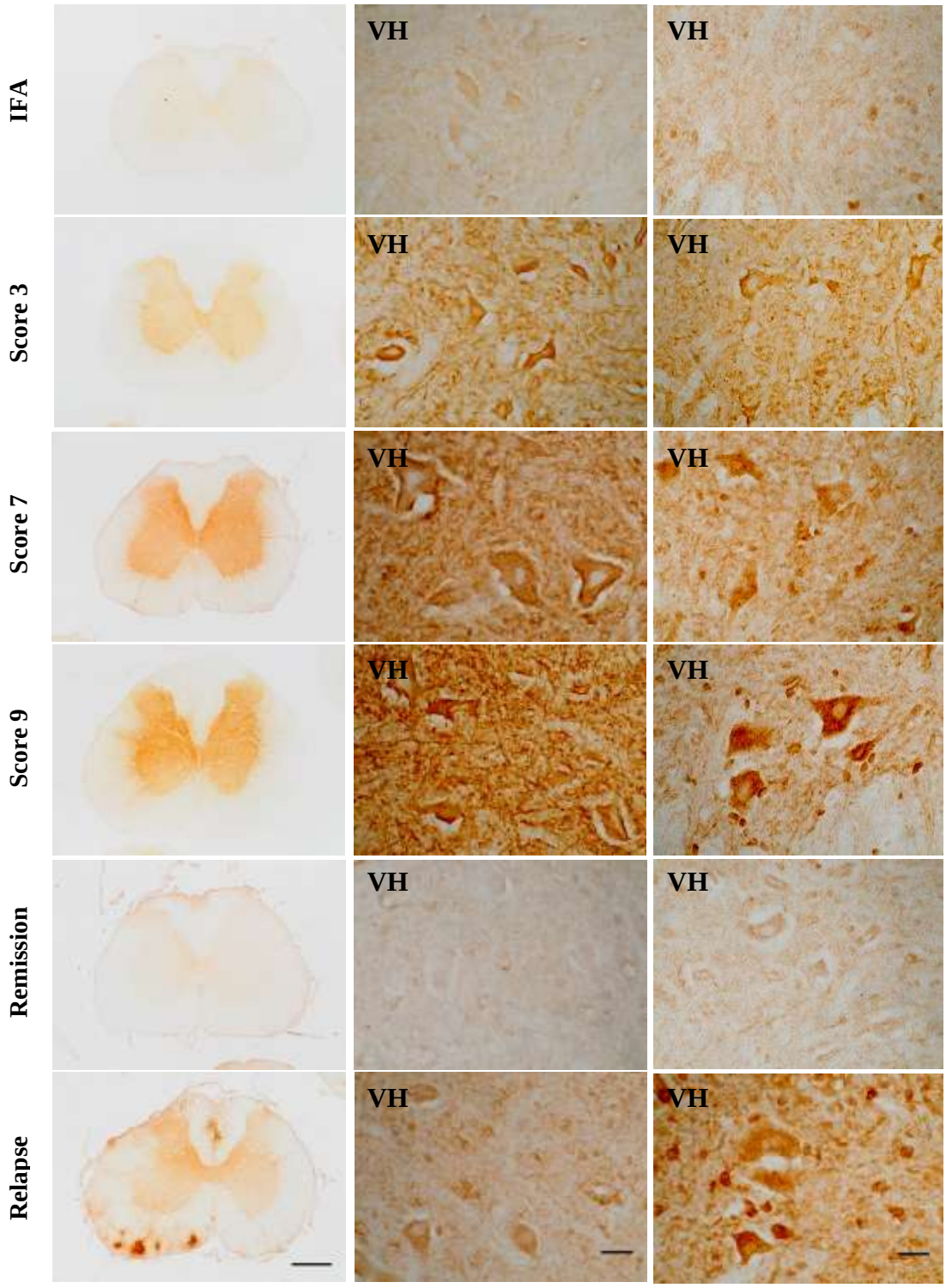
A
i
ii
iii
Pimonidazole
Pimonidazole
HIF-1α
IFA
Score 3
Score 7
Score 9
Remission
Relapse
VH

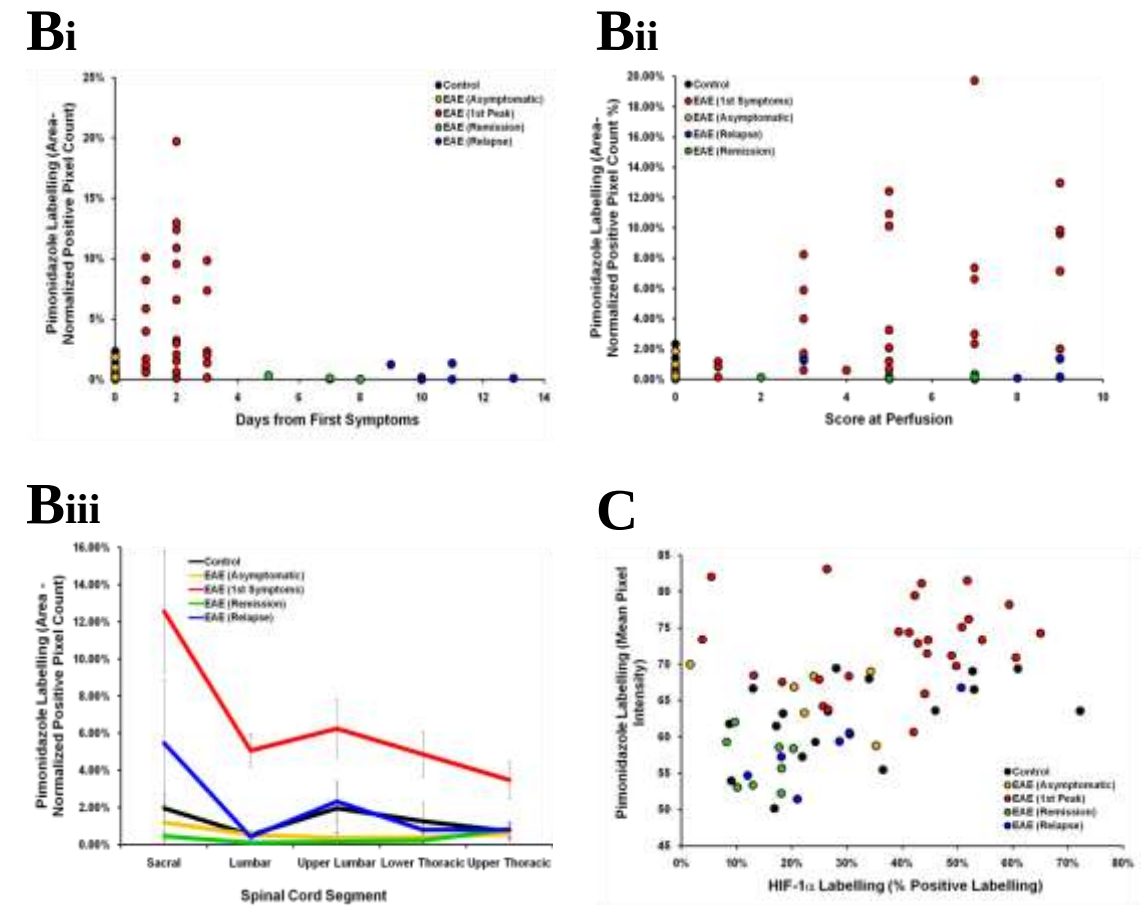

Figure 2.3.3.1: Labelling for tissue hypoxia in rMOG EAE

(A) Transverse lumbar spinal cord sections labelled with anti-pimonidazole, at different stages of disease progression. Positive pimonidazole labelling is virtually absent in IFA control animals, but is increased in the grey matter of first peak (scores 3-9) rMOG EAE animals (Ai, scale bar 500 μm; Aii, scale bar 25

μm). Similarly, labelling for HIFα, an independent marker of hypoxia, is increased in the ventral motor neurons of symptomatic animals (Aiii, scale bar 25 μm). The pimonidazole grey matter labelling is increased during the first three days of disease (Bi), and also increases with disease severity (Bii). Although, animals in remission and relapse showed decreased grey matter labelling (A; Bi), animals in the relapse had intense foci of pimonidazole labelling in the white matter (Ai). (Biii) Graph showing the intensity of pimonidazole labelling along the length of the cord, for animals with differing severity of neurological deficit (Mean ± S.E.M), showing a gradient of labelling which follows the ascending nature of the disease (contols n=20; asymptomatics n=7; first symptoms n=29; remission n=7; relapse n=7). (C) Scatter plot showing the correlation between pimonidazole and HIF-1α labelling. (D) Confocal laser microscopy of transverse spinal cord sections labelled with anti-pimonidazole, and anti-IBA (microglia), anti-GFAP (astrocytes), anti-β-tubulin (neurons), and anti-CA2 (oligodendrocytes) antibodies. Co-localisation of these cell specific markers (arrows) with pimonidazole suggests a generalised tissue hypoxia. Scale bar =100 μm. All micrographs are representative.

2.3.3.2 The oxygen concentration of spinal cord tissue is low in rMOG EAE

Measurements of spinal oxygen concentration, taken using an oxygen-sensitive probe revealed that rMOG animals expressing a neurological deficit consistently had lower spinal oxygen concentrations than control animals (first peak $p = 0.007$, relapse $p = 0.029$, Figure: 2.3.3.2 A). The average spinal cord oxygen concentration of control animals was 34.99 ± 2.7 mmHg (mean ± S.E.M), whereas for rMOG animals with a neurological deficit score of nine was 20.06 ± 3.9 mmHg (mean ± S.E.M). Moreover, the oxygen concentration varied inversely with the magnitude of the deficit ($p< 0.001$, $r^2 = 0.619$, n = 71, Figure: 2.3.3.2 A, B) and with the severity of the disease represented by the change in neurological deficit score on the day of perfusion (Figure: 2.3.3.2 C). The spinal oxygen concentration was found to only mildly correlate inversely with the pimonidazole labelling ($p = 0.06$, $r^2 = -0.331$, n = 68, Figure: 2.3.3.2 D).

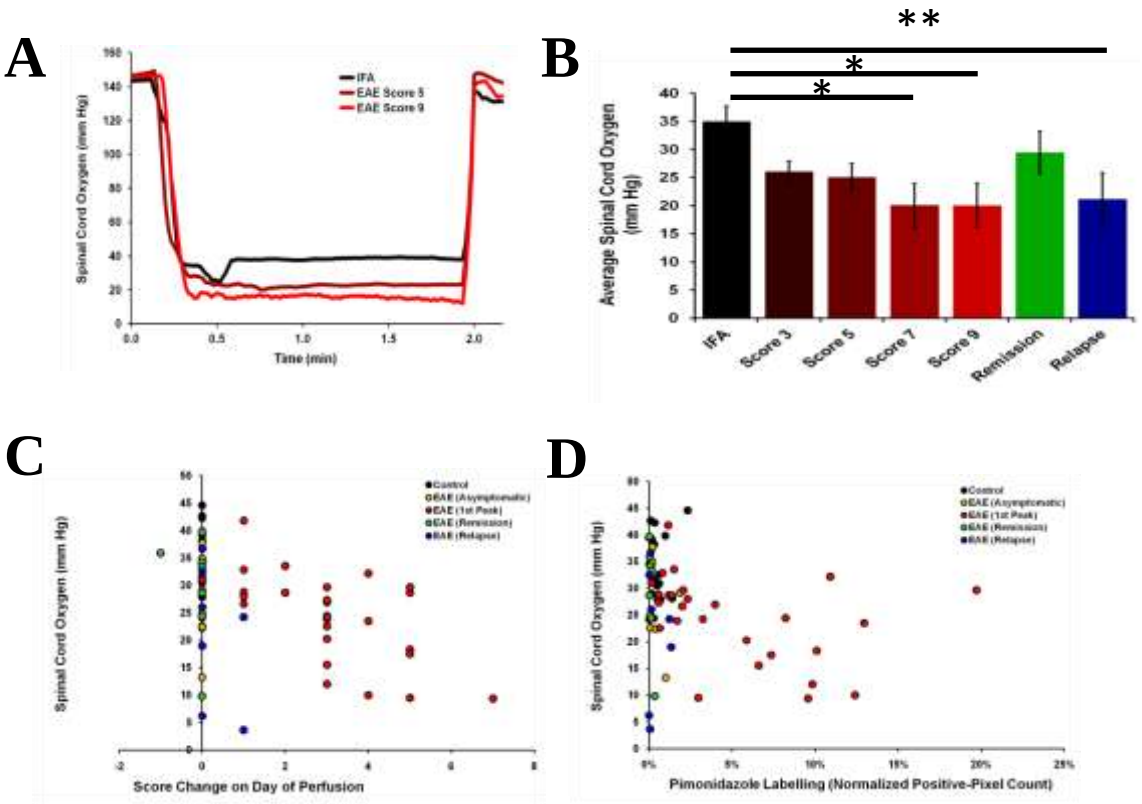

Figure 2.3.3.2: Spinal oxygen probe measurements in rMOG EAE

(A) Representative records from animals during different stages of rMOG EAE. The records show readings at first in air, then the lower oxygen concentration when the probe is inserted into the spinal grey matter, and finally the reading in air upon withdrawal. The spinal oxygen concentration is lower in rMOG animals compared to IFA controls. Furthermore, the animals in the first peak of disease exhibiting a more severe neurological deficit, and animals with relapse disease, had significantly lower (*$p<0.05$, ANOVA with Bonferoni correction) spinal oxygen concentrations than IFA controls (B; mean ± S.E.M). (C) A scatter plot showing the correlation between the spinal oxygen concentration and the score change on the day of perfusion. Animals with increasing severity of disease at the time of termination (first peak animals), generally had lower spinal oxygen concentrations. (D) A scatter plot showing the correlation between pimonidazole (immunohistochemical marker) labelling, and spinal tissue oxygen concentration (contols n=20; asymptomatics n=7; first symptoms n=29; remission n=7; relapse n=7).

2.3.4.0 Vascular changes over the time course of rMOG EAE

Hypoxia is known to induce many downstream changes, one of which is alterations in the vascular architecture. Therefore, evidence of such changes was sought over the time course of rMOG EAE. During the first peak of disease, increases in vessel size probably representing vasodilation, were observed in asymptomatic and symptomatic rMOG animals (p = 0.001) along the length of the cord (Figure: 2.3.4.0 A, Bi), compared to those of control animals. The average vessel size in the spinal cord of animals in remission and relapse was smaller than controls (Figure: 2.3.4.0 Bi). However, at these later stages of disease (relapse), the total number of vessels was increased in the caudal segments of the spinal cord, but particularly in the lumbar and sacral segments (Figure: 2.3.4.0 Bii), compared to control animals (p=0.003). Furthermore, many of these vessels had a fenestrated appearance, particularly in the white matter. Symptomatic animals at the first peak of disease also displayed a moderate increase in vascular density compared to control animals. The longer term vascular changes were associated with a concomitant increase in cross-sectional area of the whole spinal cord, a measure of oedema (Figure: 2.3.4.0 Biii).

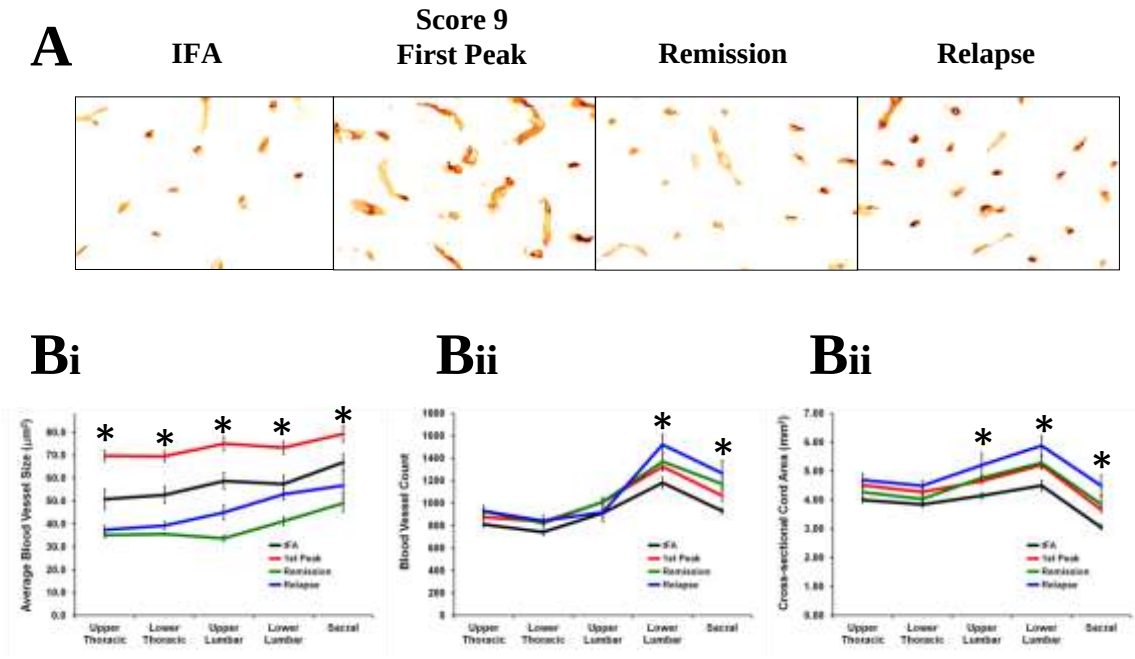

Figure 2.3.4.0: Vascular changes during the course of rMOG EAE

(A) Spinal grey matter labelling with anti-RECA1. At the acute stage of the disease (first peak), vessel size is increased, relative to IFA controls, and rMOG animals in remission and relapse. As the disease progresses, the vascular density increases, particularly in animals in relapse. (Bi) Graph showing the average vessel size along the length of the cord in animals at the different stages of disease (mean ± SEM. (Bii) Graph showing the vascular density, along the length of the cord in animals at different stages of disease (mean ± S.E.M). (Biii) Graph showing that the cross-sectional area of the whole spinal cord (a measure of oedema) was greater over time in animals with EAE when compared with controls (mean ± S.E.M) (contols n=20; asymptomatics n=7; first symptoms n=29; remission n=7; relapse n=7).

2.3.5.0 NADPH oxidase subunit expression during the first peak of disease

NADPH oxidase is a major consumer of molecular oxygen during the respiratory burst, generating large amounts of superoxide. Thus multi-label immunofluorescence using antibodies against NADPH oxidase subunits $p22^{phox}$ and $p47^{phox}$ was performed. In control animals, labelling for $p22^{phox}$ was observed, however no labelling for $p47^{phox}$ was evident (Figure 2.3.5.0). In the first peak of disease, animals with moderate neurological deficit (neurological deficit score of five) displayed increases in $p22^{phox}$ and $p47^{phox}$ labelling, particularly surrounding inflamed vessels (Figure: 2.3.5.0). As the magnitude of the deficit increased, the extent of labelling and co-expression of these markers also increased (Figure: 2.3.5.0).

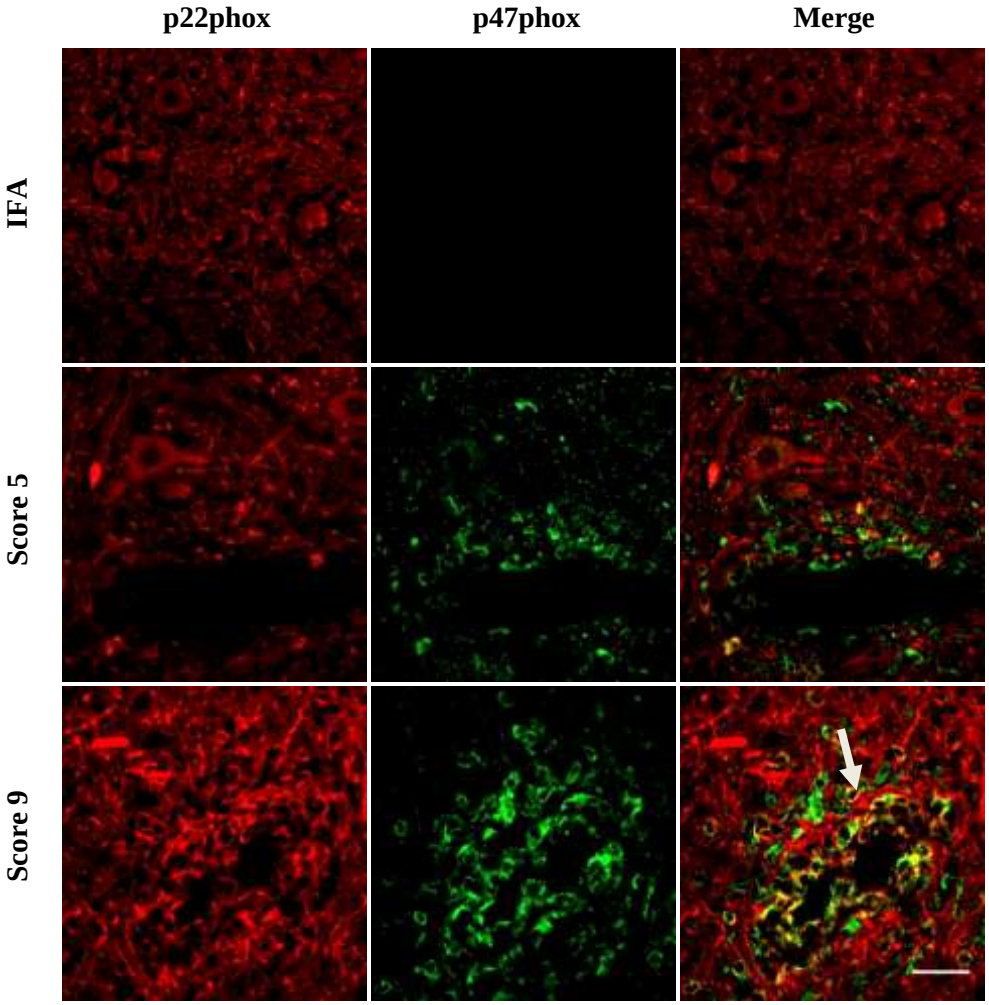

Figure 2.3.5.0: NADPH Oxidase subunit labelling in first peak EAE

Confocal laser microscopy of transverse spinal cord sections labelled with NADPH oxidase subunits p22phox (red) and p47phox (green). Labelling for p22phox is evident in the spinal cord of all animals, but the extent of labelling is increased in rMOG animals exhibiting a neurological deficit. Labelling for P47phox is absent in IFA control animals, however perivascular expression of p47phox is observed in rMOG animals expressing a neurological deficit. In animals with more severe disease (score 9), perivascular co-expression of the subunits is evident (arrow).

2.3.6.0 Histopathology of the white matter foci of pimonidazole labelling in relapse animals

As mentioned previously, intense foci of pimonidazole labelling were observed in the white matter of animals in relapse (Figure 2.3.6.0 A). These foci were found at various places in the white matter, but predominantly in the oedematous region of the spinal cord. At high magnification, reactive swollen astrocytes, was seen amongst phagocytosing inflammatory cells (Figure 2.3.6.0 Aii). These regions were commonly found to be sparse in vasculature, abundant in ED1 positive cells, and largely demyelinated (Figure 2.3.6.0 B).

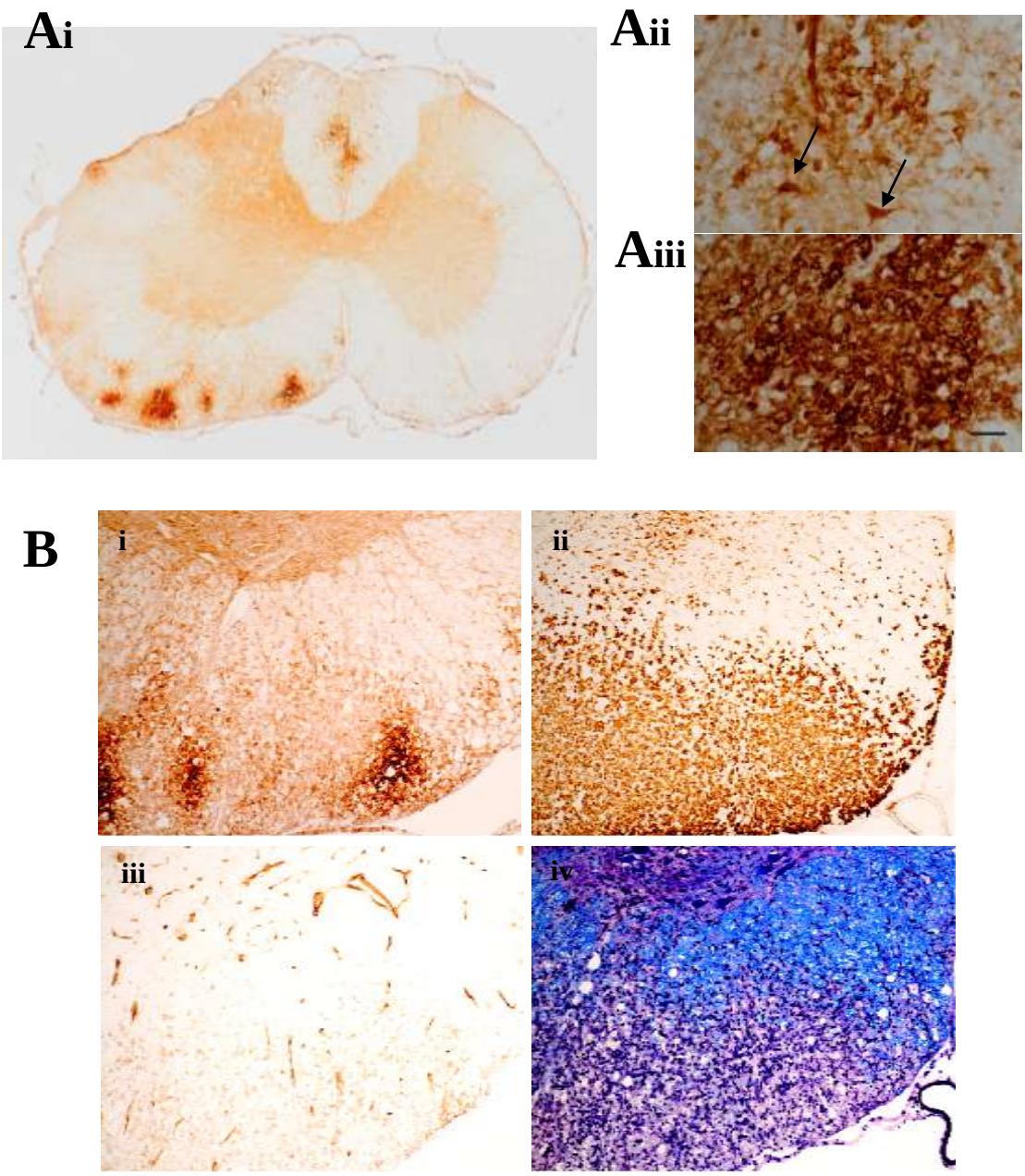

Figure 2.3.6.0: Intense pimonidazole foci in the white matter of relapse animals

(Ai) Light micrograph of a lumbar spinal cord section from an rMOG animal in relapse, labelled for pimonidazole. Intense pimonidazole-positive foci are evident in the white matter of relapse animals. Scale bar 500 µm. (Aii) High magnification of pimonidazole-positive foci, showing labelling of cells tentatively identified as hypertrophied astrocytes (arrow), in addition to other cells. Scale bar 25 µm. (B) Adjacent sections labelled for pimonidazole (i), ED1 (ii), and RECA-1 (iii), or stained with LFB (iv). The observed foci of intense pimonidazole labelling correspond with areas of extensive ED1-positive cell infiltration, comparatively sparse vascular supply, and demyelination. Scale bars 100 µm. All micrographs are representative.

2.3.7.0 Normobaric oxygen therapy in rMOG EAE

2.3.7.1 One hour of normobaric hyperoxia partially restores function

Given that hypoxia is an early feature of rMOG EAE that correlates quantitatively, temporally and spatially with the first peak of disease, pairs of rMOG symptomatic animals (matched for neurological deficit) were treated with one hour of normobaric hyperoxia, or room air as a control, to determine whether acute oxygen therapy could restore lost function. Treatment with only one hour of 100% oxygen resulted in partial restoration of function, with increased sensation and restoration of the hindlimb stretch and pinch withdrawal reflexes being the most common changes observed.

Most rMOG animals exposed to 100% oxygen showed an improvement in neurological deficit score on the 25-point scale following treatment, relative to their counterparts treated with room air (Figure: 2.3.7.1 A). In some instances, there was no change, or a worsening, in neurological deficit score, following hyperoxic treatment, compared to the room air counterpart. However, on average, the cohort of animals exposed to 100% oxygen showed a statistically significant improvement in score (p = 0.014, n = 24), compared to the cohort of animals exposed to one hour of room air (Figure: 2.3.7.1 B).

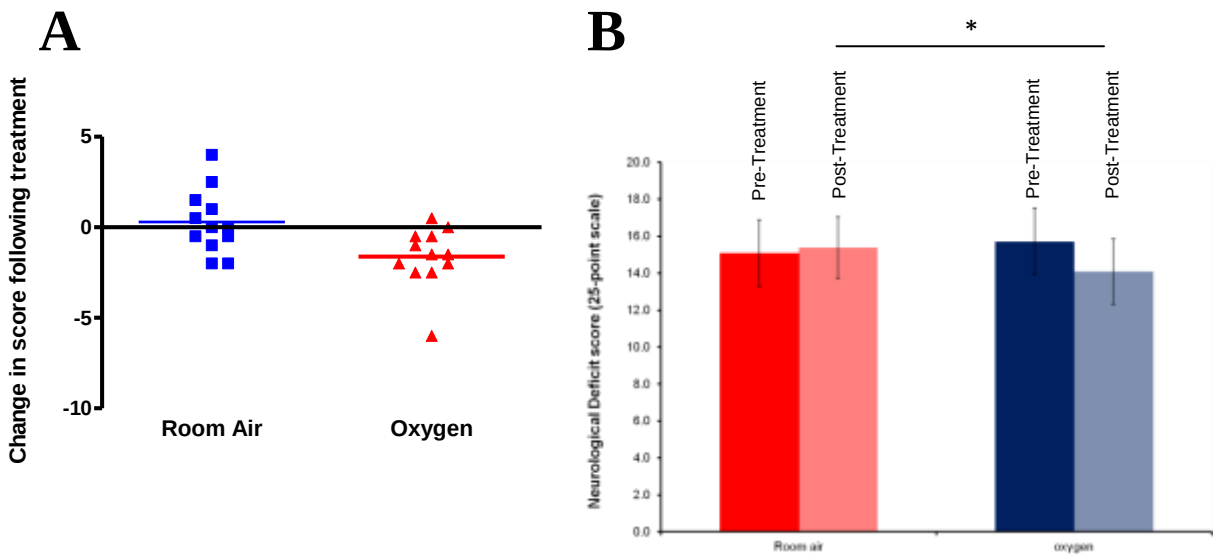

Figure 2.3.7.1: The effects of one hour of normobaric oxygen therapy on rMOG EAE

(A) Plot showing the change in score rMOG EAE animals, following one hour of therapy (normobaric 100% oxygen n=12, or room air n=12), using the 25-point scale. A negative change in score indicates a functional improvement. (B) Bar graph showing the average (+/- S.E.M.) neurological deficit score, before and after breathing room air (control) or 100% oxygen. (*$p<0.05$, repeated measures ANOVA, n=24).

2.3.7.2 Labelling for hypoxia decreases following one hour of oxygen therapy

Histological evaluation of spinal cord tissue from animals exposed to one hour of normobaric oxygen, revealed a decrease in labelling for hypoxia (Figure: 2.3.7.2). The extent of pimonidazole labelling in IFA control animals did not change following exposure to 100% oxygen, with some faint neuronal, and grey matter labelling still evident at high magnification (Figure: 2.3.7.2 A). Spinal cord tissue from rMOG animals exposed to room air, labelled positive for hypoxia, indicated by the intense pimonidazole immunoreativity. However the spinal cords from animals exposed to 100% oxygen showed no evidence of pimonidazole labelling, and thus hypoxia. Rather, the labelling was less than that observed in IFA control animals. The lack of neuronal labelling, in particular, was surprising (Figure: 2.3.7.2 A). Similarly, in IFA control animals, labelling for HIF-1α did not change following 100% oxygen therapy, but neuronal HIF-1α was completely lost in rMOG animals exposed to 100% oxygen (Figure: 2.3.7.2 B).

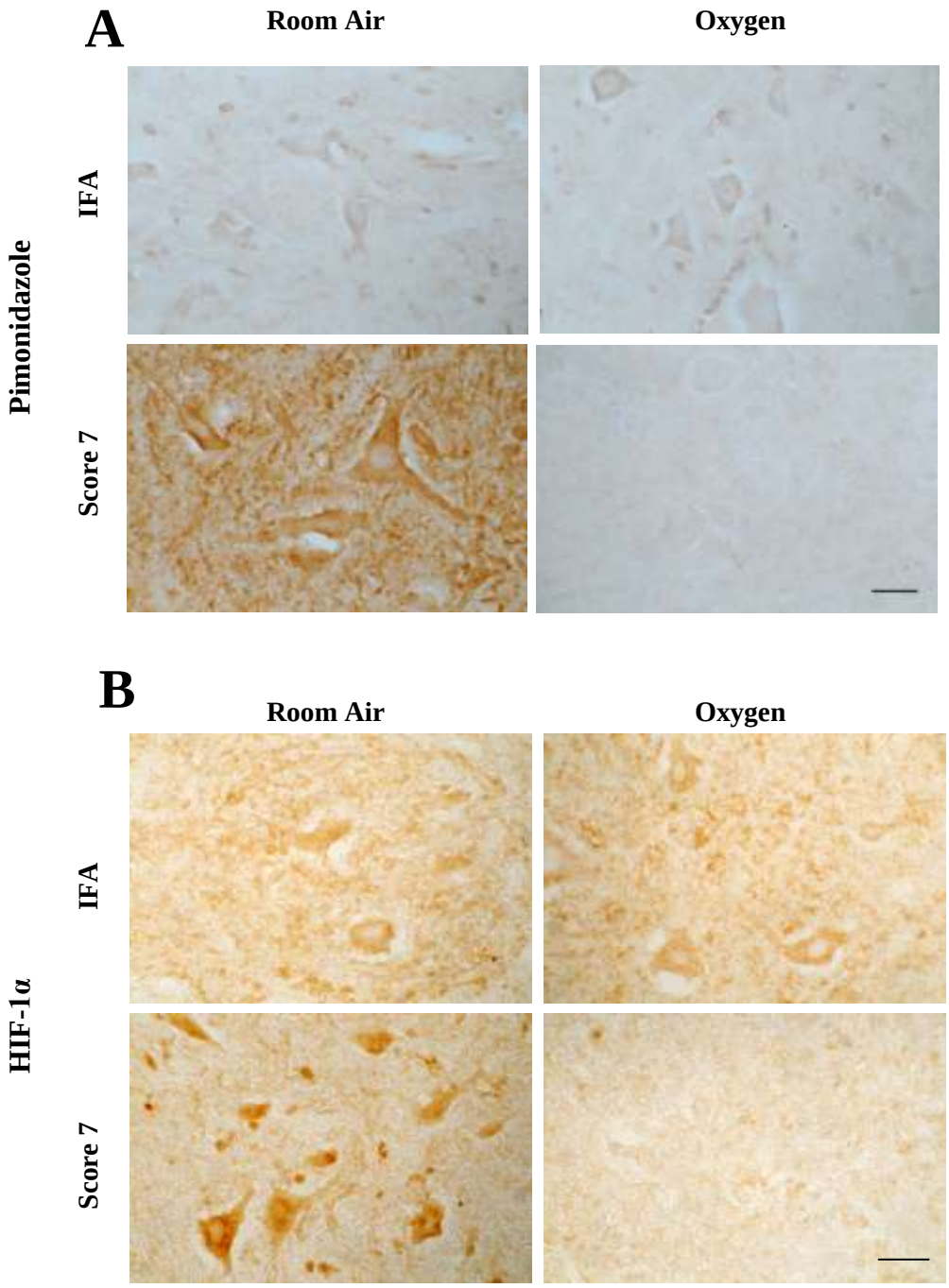

Figure 2.3.7.2: Labelling for hypoxia following acute normobaric oxygen therapy

Micrographs of the spinal ventral grey matter of animals from the acute oxygen therapy study, showing labelling for pimonidazole (A) and HIF-1α (B). In IFA controls, pimonidazole labelling does not appear to change following exposure to 100% oxygen, however, in symptomatic rMOG animals, pimonidazole labelling is decreased substantially (A). Exposure to 100% oxygen does not affect the extent of HIF-1α labelling in IFA controls, however, in symptomatic rMOG animals, the extent of labelling is decreased considerably (B). The lack of any neuronal pimonidazole or HIF-1α labelling, following 100% oxygen in symptomatic animals is striking. Scale bar 25 μm. All micrographs are representative.

2.3.7.3 One hour hyperoxia does not increase oxidative damage

Oxygen therapy can be associated with increased oxidative damage, so the tissue was examined to determine the magnitude of such damage. Oxidative DNA damage, as indicated by 8-Oxo-2'-deoxyguanosine (8-Oxo-dG) labelling, was not a common feature of rMOG EAE. Clusters of 8-Oxo-dG positive cells, when observed, were located predominantly surrounding vessels in the white matter, co-localising with DHE (Figure: 2.3.7.3 A). Animals treated with 100% oxygen generally displayed a decrease in the size, and fluorescent intensity of these white matter clusters (Figure: 2.3.7.3 A). The uncanny co-localisation of 8-Oxo-dG and DHE raised the potential problem of fluorescence bleed through, however, these clusters were also observed in DAB labelled tissue (Figure: 2.3.7.3 B), and sections with DHE-induced fluorescence alone, thereby ruling out fluorescence bleed through.

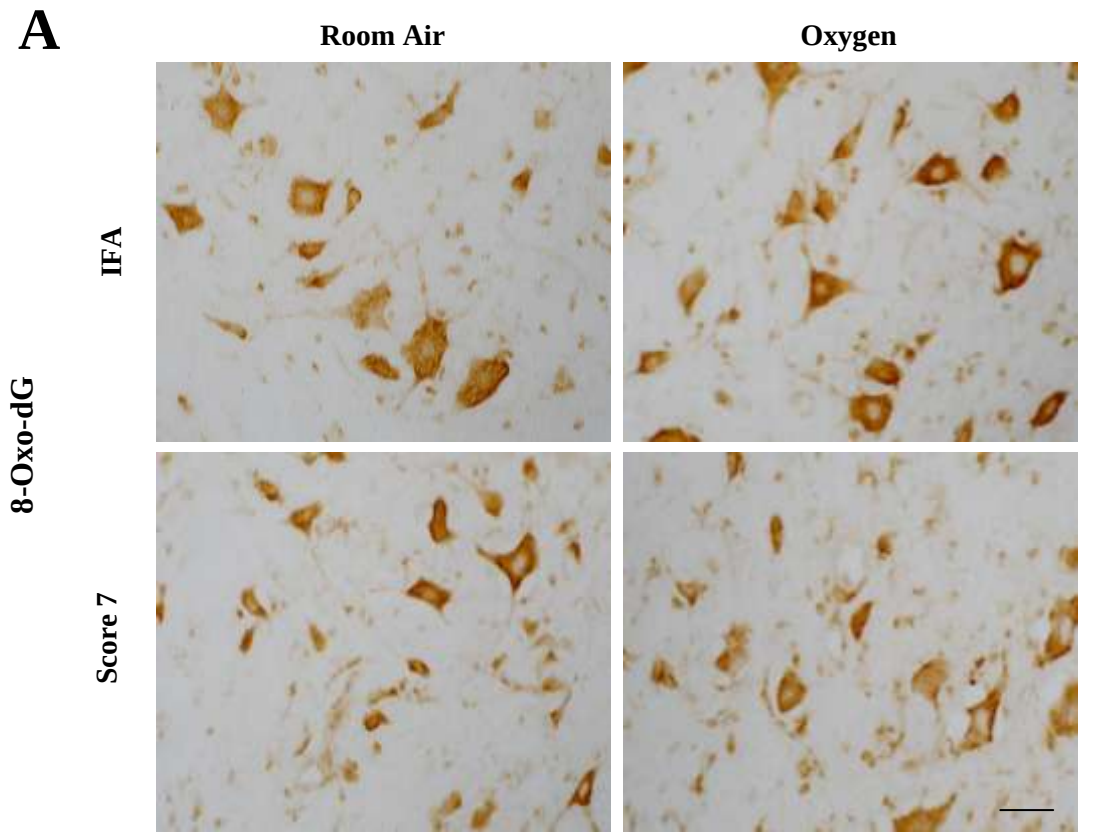
A
Room Air
Oxygen
8-Oxo-dG
IFA
Score 7

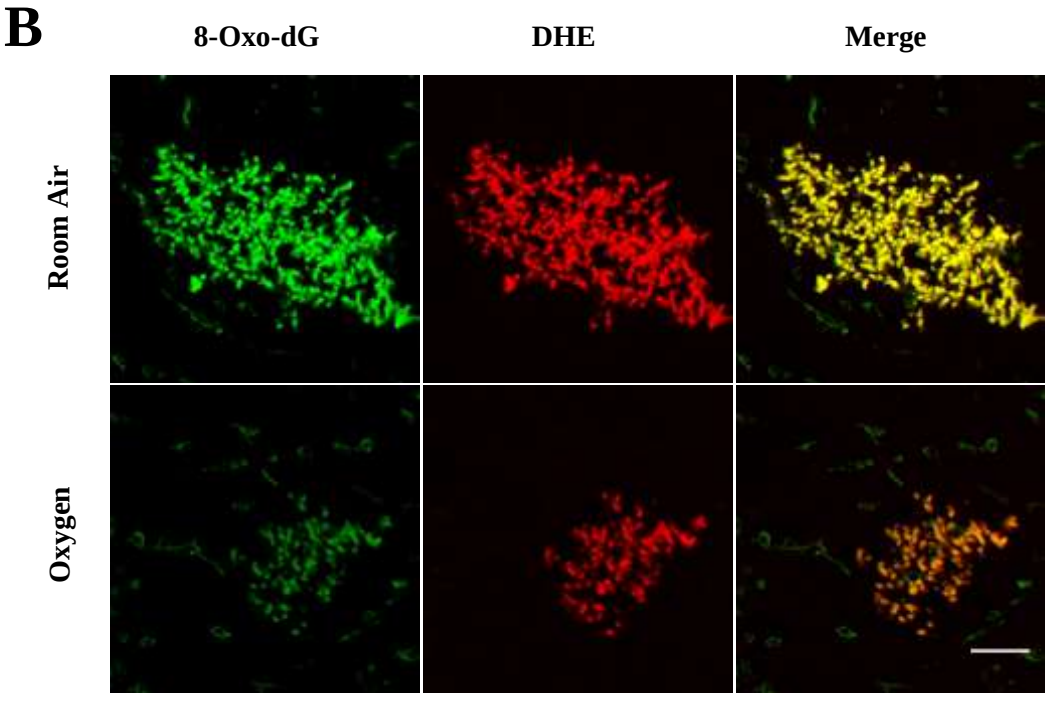
B
8-Oxo-dG
DHE
Merge
Room Air
Oxygen

C

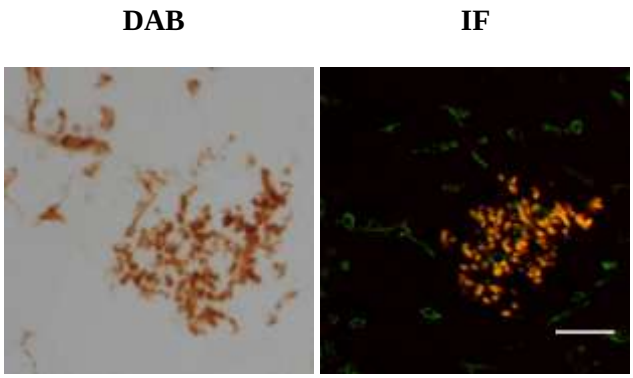

Figure 2.3.7.3: ROS labelling following acute normobaric oxygen therapy

(A) Light micrographs of ventral horn grey matter in lumbar spinal cord cross-sections labelled with antibodies to 8-Oxo-dG. No difference in the extent of labelling is evident between IFA controls and animals with EAE during the first peak of disease, or animals treated with room air and animals treated with normobaric oxygen. Scale bar 25 μm. (B) Fluorescence microscopy images of sections through the lumbar spinal cord white matter from animals with EAE during the first peak of disease, labelled with DHE *in vivo* and antibodies to 8-Oxo-dG obtained with a confocal microscope reveal co-localization of 8-Oxo-dG-positive cells and DHE-induced fluorescence. No increase in 8-Oxo-dG or DHE-induced labelling is evident following treatment with normobaric oxygen as compared to room air, in fact a tendency to reduced labelling is observed. Scale bar 200 μm. (C) Spinal cord section labelled for 8-Oxo-dG with the DAB detection method, and an adjacent section labelled for 8-Oxo-dG and DHE-induced fluorescence, The pattern of labelling observed when tissue is labelled with antibodies against 8-Oxo-dG using DAB as the chromogen, is the same as when tissue is labelled fluorescently in conjunction with DHE-induced fluorescence, confirming co-localisation of DHE and 8-Oxo-dG is real and not bleed through. Scale bar 25 μm. All micrographs are representative.

2.3.8.0 7-day combination therapy in rMOG EAE

Inflammation, hypoxia, and oxidative damage (although minimal in this model), have been shown to be features of rMOG EAE. Therefore, their relative contributions to functional impairment in EAE were assessed by treating these pathopysiological aspects of the disease, individually, and collectively. Five, 7-day treatment regimes, commencing on the onset of neurological deficit, comprised of groups designated as controls, an iNOS inhibitor (1400W), 75% normobaric oxygen, a mitochondrially targeted antioxidant (MitoQ), and a combination of the three (ALL) (Table 2.3.8.0).

Control rMOG animals followed the standard course of EAE, with an average peak neurological deficit score of 6.6 ± 0.5 (mean ± SEM), within three days of the onset of disease (Figure: 2.3.8.0). By five days following the onset of disease, animals in the control group entered the remission stage of the disease, with an average neurological deficit score of 5.3 ± 0.6 (mean ± SEM), and they remained in this stage until termination (n=14) (Figure: 2.3.8.0). It is worth noting that the 10-point scale used to evaluate the neurological deficit is by no means linear. Thus an animal with a neurological deficit score of 7 displays complete bilateral hindlimb weakness with absent or incomplete plantar placement, and is therefore unable to walk. An animal with a neurological deficit score of 5 displays complete tail paralysis, with an abnormal, wobbly gait, but is able to walk.

Administration of 1400W, oxygen, MitoQ, and ALL treatment regimes resulted in amelioration of the disease severity, compared with controls, respectively (Figure: 2.3.8.0). Animals treated with 1400W followed an attenuated disease course, with an average peak neurological deficit score of 6.0 ± 0.5 (mean ± SEM), and a termination end score of 5.0 ± 0.5 (Figure: 2.3.8.0). The average neurological deficit score was significantly lower than the control group only on day one of treatment with 1400W

(p=0.015, n = 15). Animals treated with MitoQ, also followed an attenuated disease course, with an average peak neurological deficit score of 5.8 ± 0.7, and a terminal neurological deficit score of 5.1 ± 0.9 (Figure: 2.3.8.0). The average neurological deficit score on the first day of treatment with MitoQ was significantly lower than controls (p= 0.047, n=17). However, the average neurological deficit was not significantly lower than control animals on any other day of treatment. Animals treated with 75% oxygen had an average peak neurological deficit score of 5.4 ± 0.6, and a terminal neurological deficit score of 3.6 ± 0.5 (Figure: 2.3.8.0). Treatment with 75% oxygen resulted in a statistically significant improvement after one day (p=0.028, n=15), and a significantly reduced neurological deficit at day 7, when compared with control animals breathing room air (p=0.019, n=15). Animals treated with a combination of the three treatments (ALL), followed a particularly attenuated disease course, with an average peak neurological deficit score of 4.9 ± 0.8, and a terminal score of 3.3 ± 0.8 (Figure: 2.3.8.0). This group had a significantly lower average neurological deficit score than control animals, at all time points after day 1 (p< 0.05, n = 15), with the exception of days 4 and 5.

The variation in neurological deficit score observed in the oxygen and ALL treatment groups represented a decreased efficacy of these treatments in animals that were recruited when neurological deficit score at disease onset was 3 or more. Oxygen and combination therapy was particularly effective in animals that displayed a neurological deficit score of 1, at onset of disease. In these treatment groups, reversal of tail paralysis was frequently observed. Moreover, function was completely restored in some animals. Differences in the final numbers represented morbidity, or animals that had to be culled for ethical reasons, and were therefore omitted from the study.

A

Table 2.3.8.0: 7-day combination therapy treatment regime

Therapy	Onset of Therapy	Route of Administration	Days from Onset of Symptoms/Days of therapy						
			1	2	3	4	5	6	7
CONTROL	n/a	n/a	n=17	n=17	n=17	n=17	n=17	n=15	n=15
1400W	Onset of symptoms	Intraperitoneal	n=17*	n=17	n=17	n=17	n=17	n=17	n=17
OXYGEN	Onset of symptoms	Inhalation (purpose-built chamber/tent)	n=17*	n=17	n=15	n=15	n=15	n=15*	n=15*
MITOQ	Day of immunisation	Oral (in drinking water)	n=17*	n=17	n=17	n=16	n=16	n=16	n=16
ALL	MitoQ treatment began on the day of immunization. Oxygen and 1400W additionally administered at the onset of symptoms	Oral, intraperitoneal, inhalation	n=17*	n=17*	n=16*	n=16	n=16	n=15*	n=15*

B

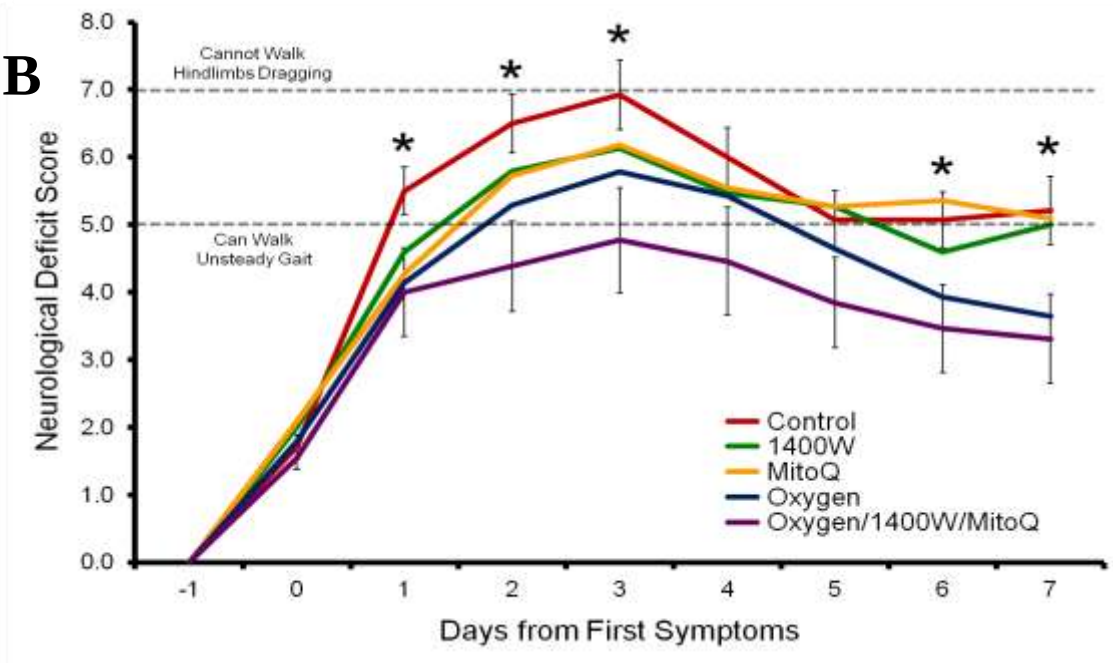

Figure 2.3.8.0: Combination therapy in rMOG EAE

(A) Table showing the different treatment regimes employed and numbers of animals throughout the study and statistical significance (* $p<0.05$). (B) Graph showing the average changes in neurological deficit (non-linear 10 point scale) over the course of rMOG EAE following five treatment regimens; control, MitoQ, 1400W, 75% normobaric oxygen, and ALL. Treatment began at the onset of neurological deficit, and was maintained for the next 7 days. The graph shows that the ALL group had a significantly (* $p<0.05$) lower neurological deficit score than controls at all time points after day 1, with the exception of days 4 and 5. Notably, animals receiving the ALL treatment regimen were able to walk throughout the course of disease, and were significantly less affected at trial termination than control animals. Values are means ± S.E.M.

2.4.0.0 DISCUSSION

The present study reveals that tissue hypoxia is quantitatively, spatially and temporally related to neurological dysfunction in rMOG-induced EAE, and perhaps causally related. Furthermore, the study provides evidence that acute and chronic treatment with normobaric hyperoxia partially restores lost function, and attenuates the disease severity, respectively. Thus, hypoxia plays a crucial role in the development and progression of neurological dysfunction in rMOG EAE, a model of MS

2.4.1.0 Inflammation mediates neurological dysfunction during the first peak of disease in rMOG EAE

Inflammation, demyelination and axonal degeneration are the cardinal features of MS, however, the relationship of these pathological events to the onset, and progression of neurological disability is yet to be fully elucidated. Inflammation has been implicated in the induction of clinical deficits in MS, in the absence of demyelination (Bitsch et al., 1999), and the current results suggest that the neurological deficit, during the first peak of rMOG EAE, is also mediated by inflammation alone. In the current study, the extent of inflammation, characterised by the presence of activated macrophages/microglia, correlated well with the severity of the disease. Activated macrophages and microglia were found most extensively at the midline and lateral borders of the dorsal columns, and at the superficial lamina of the dorsal grey matter, and they were present more diffusely in the rest of the grey matter. These sites are eloquent areas of the nervous system, and damage would be expected to cause neurological deficits. Neurons of the motor cortex, associated with hind limb movement, project to the spinal lumbar enlargement (Li et al., 1990), with a somatotopic arrangement of hind limb nerves in the mediolateral compartments of the dorsal horns (Molander and Grant, 1985; Woolf and

Fitzgerald, 1986; Rivero-Melián and Grant, 1991; Paxinos, 1995). Similarly, the ascending collaterals of primary afferent fibres are somatotopically arranged in the dorsal column, with fibres from the tail found close to the midline, and fibres from the hind limbs at the lateral borders more rostrally (Paxinos, 1995). Therefore, inflammation affecting these specific areas provides a possible explanation for the motor deficits observed in this study.

Activated macrophages/microglia were present at all stages of the disease, but a change in cell morphology was observed during remission and relapse. A typical amoeboid, activated phenotype was found during the first peak of disease, whereas a 'foamy', phagocytic phenotype was prevalent during remission and relapse stages of disease, accompanied by extensive demyelination. The morphological changes associated with the demyelination in addition to the absence of iNOS during the remission and relapse stages of disease, conform to the notion that the dysfunction during first peak of rMOG EAE is inflammation-mediated, whereas relapse is largely driven by demyelination. The levels of the anti-inflammatory interleukin, IL-10, known to inhibit cytokine release from macrophages (Fiorentino et al., 1991), are drastically increased during remission (Kennedy et al., 1992), explaining the alleviation of neurological deficit during this stage of disease. During relapse, the widespread demyelination is known to be elicited by anti-MOG antibodies (Linington and Lassmann, 1987; Linington et al., 1988). However, despite these findings, the question as to how inflammation causes dysfunction still remains.

2.4.2.0 Hypoxia- a mediator of neuroinflammation-induced neurological dysfunction

The mechanisms through which neuroinflammation cause neurological dysfunction remain unclear. In the last few decades, NO has emerged as a likely culprit. Indeed,

moderate levels of iNOS were expressed by the activated macrophages/microglia, in the current study, with expression occurring primarily during the first three days following the onset of neurological deficit. Such a temporal pattern of expression implicates NO in the onset of neurological deficits. Indeed, the inhibition of iNOS has been found to decrease the clinical deficits and inflammation in EAE by some researchers (Cross et al., 1994; Zhao et al., 1996; Brenner et al., 1997). However, in the current study iNOS-positive cells were restricted to the subpial white matter and perivascularly, not in the grey matter where motor neurons reside. Thus NO may only account for a part of the neurological dysfunction in rMOG, indicating that other factors may also play a role.

Inflamed tissue undergoes drastic shifts in tissue metabolism. Changes include nutrient depletion, increased oxygen consumption, and ROS/RNS production (Taylor and Colgan, 2007; Kominsky et al., 2010). A common downstream consequence of such changes is tissue hypoxia (Kokura et al., 2002; Saadi et al., 2002; Karhausen et al., 2004). Our findings suggest that the rat spinal cord also becomes hypoxic, during the inflammatory phase of rMOG EAE, confirmed by two independent methods immunohistochemically, using the biochemical marker pimonidazole, and an anti-HIF-1α antibody, and optically, using an oxygen-sensitive optrode. Although different in principle, both methods yielded similar results in that the spinal grey matter of symptomatic rMOG animals had lower oxygen concentrations than that of control animals. However, the poor correlation between the intensity of pimonidazole labelling and spinal oxygen concentrations can possibly be explained by a number of factors. Firstly, pimonidazole is administered to the animals during a dynamic stage of the disease, a period when their neurological deficit is rapidly progressing, and can therefore change within the span of a few hours. Thus an animal with a neurological deficit score of 3 at the time of intravenous administration of pimonidazole may have

progressed to a neurological deficit score of 4 by the time of probe insertion and spinal oxygen measurement. Secondly, immunohistochemical detection of tissue hypoxia using pimonidazole, does not give an absolute oxygen value, as does the oxygen-sensitive probe. Rather, the output is merely an arbitrary value. DAB does not follow Beer-Lamberts law therefore the intensity does not relate to the amount of pimonidazole bound.

The hypoxia appeared to be a global epiphenomenon, affecting all cell types within the spinal cord, however, the grey matter labelled particularly obviously for hypoxia. Given that the grey matter requires greater vascular perfusion and oxygen delivery than the white matter (Leenders et al., 1990; Helenius et al., 2003), the fact that the spinal grey matter labels for hypoxia in rMOG EAE is not surprising. In line with the current data, the spinal cord grey matter has been found to be especially susceptible to ischemic insults (DeGirolami and Zivin, 1982). In the current study, neurons and surrounding grey matter in the lumbo-sacral cord showed a tendency to label more intensely for hypoxia than other segments. Interestingly, motor neurons that innervate the tail (Grossmann et al., 1982) and hind limbs (Mong, 1990) are most concentrated within this segment of the spinal cord. Thus suggesting that hypoxia may directly affect spinal motor neurons, resulting in dysfunction. Indeed, synaptic transmission in the dorsal horn has been shown to be particularly vulnerable to hypoxia (Fukuda et al., 2006). Hypoxia can also induce metabolic depression via the downregulation of particular mitochondrial genes (Benita et al., 2009). Interestingly, a downregulation of mitochondrial genes has been observed in the normal appearing grey matter in rMOG EAE (Zeiss et al., 2008). Perhaps, in the case of EAE, metabolic depression may be detrimental rather than protective, or protective at the expense of function.

The hypoxia was found to be associated temporally, spatially and quantitatively with the neurological deficit. Thus, the hypoxia was prevalent during the first three days following onset of the neurological deficit, with a descending gradient along the rostro-caudal axis. Furthermore, the hypoxia increased with increasing neurological deficit. These findings suggest that tissue hypoxia may contribute to the expression, and progression, of a functional deficit in rMOG EAE.

The transcription factor HIF-1α, an important mediator of hypoxia-induced responses, is prominently expressed within glia, macrophages and some endothelial cells in active MS lesions (Aboul-Enein et al., 2003). The current study reports the additional presence of HIF-1α in neurons and inflammatory cells of symptomatic rMOG animals. The intensity of the HIF-1α labelling correlated well with the intensity of the pimonidazole labelling, thus further strengthening the finding that the spinal cord in hypoxic in rMOG EAE. In cancer research the correlation between HIF-1α and pimonidazole has been somewhat varied. Some studies report a significant correlation between the labels (Goethals et al., 2006), whereas others report a poor, insignificant correlation (Janssen et al., 2002; Begg, 2003). These discrepancies have been attributed to differences in the biology of individual tumours. HIF-1α is the principal regulator of the adaptative response to hypoxia, and perhaps inflammation.

2.4.3.0 Hypoxia-induced vascular changes

HIF-1α has been estimated, at least *in vitro,* to regulate more than 50% of the genes that respond to hypoxia (Elvidge et al., 2006). One such gene is VEGF, a crucial mediator of angiogenesis. The present study reports increased vascular density at relapse and remission in rMOG EAE, compared to controls. Moreover these vessels had a fenestrated, abnormal appearance, and this is in line with previous findings in EAE

(Seabrook et al., 2010). Although angiogenesis is a common compensatory response following inflammation (Cramer et al., 2003; Walmsley et al., 2005), and hypoxia (LaManna et al., 1992), there is a difference between physiological and pathological angiogensis. Physiological angiogenesis is a tightly regulated process, mediated by a number of growth factors, and pro-angiogenic cytokines, as well as angiogenic inhibitors. A disruption in the balance of these mediators leads to aberrant angiogenesis. Although a pro-angiogenic environment has been reported to exist in MS lesions (Holley et al., 2010; Seabrook et al., 2010), and EAE (Seabrook et al., 2010), the fenestrated and abnormal appearance of the vessels during the angiogenic relapse stage of EAE, in the current study, suggests that the angiogenesis may be pathological, thereby propagating the disease process. This hypothesis is supported by the fact that the infusion of VEGF exacerbates the neurological deficit in EAE (Proescholdt et al., 2002), whereas treatment with a VEGFR-2 receptor antagonist ameliorates neurological deficit (Roscoe et al., 2009).

2.4.4.0 Potential causes of hypoxia during neuroinflammation

Under inflammatory conditions, tissue hypoxia will ensue when the oxygen demand of the cells outweighs the supply. Increases in metabolic demand may result from the recruitment and activation of inflammatory cells such as myeloid cells, and lymphocytes, whereas alterations in the supply of nutrients may result from the vascular disturbances, such as thrombosis, or endothelial cell damage/dysfunction.

Inflammatory cells of different lineage have significantly different metabolic and oxygen demands. Whereas cells of myeloid lineage, such as neutrophils and macrophages, rely almost exclusively on glycolysis for energy, lymphocytes

predominantly use oxidative phosphorylation (Fox et al., 2005; van Raam et al., 2008). These differences in energy metabolism are thought to influence the nature of the immune response. Neutrophils are primarily glycolytic, have few mitochondria, and therefore produce very little energy from respiration (Borregaard and Herlin, 1982). This unique phenotype is thought to ensure that myeloid cells can function at the very low oxygen concentrations that are associated with inflammatory lesions. Up-regulation of HIF-1α in these cells is essential to survival, and function (Cramer et al., 2003; Kong et al., 2004; Kong et al., 2007). T-lymphocytes, in comparison, rely heavily on oxidative phosphorylation, and therefore utilise glucose, amino acids and lipids as energy sources (Kominsky et al., 2010). Cell migration during the recruitment of inflammatory cells, requires large amounts of actin turnover, and is therefore metabolically expensive (Pollard and Borisy, 2003; Kominsky et al., 2010). In addition, proliferation of inflammatory cells can also be very metabolically demanding (Greiner et al., 1994). Once at the site of inflammation, the nutrient, energy and oxygen demands increase, for processes such as phagocytosis.

During phagocytosis, neutrophils and macrophages increase their oxygen consumption by as much as fifty fold in the generation of ROS (Gabig et al., 1979; Baboir et al., 1984). This process known as the respiratory burst, is mediated by the oxygen-dependent enzyme NADPH oxidase. The core enzyme itself is comprised of five phagocytic oxidase (phox) subunits; $p40^{phox}$, $p47^{phox}$, $p67^{phox}$, $p22^{phox}$ and $p91^{phox}$. In resting leukocytes, the enzyme is kept inactive through differential distribution of these subunits between the plasma membrane and cytosol. The cytosolic complex consists of $p40^{phox}$, $p47^{phox}$, $p67^{phox}$ subunits. Upon exposure to a variety of stimuli, the p47phox is hyperphosphorylated, resulting in the translocation of the complex to the plasma membrane where it associates with the remaining two subunits, to form the

active oxidase (Baboir, 1999). The current study provides evidence that the expression of NADPH oxidase subunits p22phox and p47phox is increased in rMOG animals expressing a neurological deficit, compared to control animals. Furthermore, co-expression of the two subunits, indicative of functional enzyme complex, was more prevalent in animals with a high neurological deficit score and predominantly localised perivascularly. NADPH oxidase expression has recently been described in MS lesions (Fischer et al., 2012). In line with the present findings, Fischer et al described increased expression of p22phox and p47phox in 'pre-phagocytic' lesions. Furthermore, they show that NADPH oxidase subunit expression is decreased in macrophages that have taken up myelin debris (Fischer et al., 2012). Besides increased oxygen consumption, an increased affinity of glucose transporters for glucose, and thus glucose uptake, has been reported, during activation of the respiratory burst (Ahmed et al., 1997). Indeed, energy needed to fuel NADPH oxidase is primarily derived from extracellular glucose, which is quickly metabolised by the hexose monophosphate shunt to produce NADPH (Kiyotaki et al., 1984; Rist et al., 1991; Ahmed et al., 1997). Thus, the presence, and activity of NADPH oxidase in rMOG EAE, may account for some of the metabolic changes that would eventually lead to tissue hypoxia. Certainly, the perivascular localisation of the functional enzyme complex, in the present study, ensures a continuous supply of essential nutrients required for the respiratory burst. Consequent to the perivascular distribution of inflammatory cells, the distance between the blood vessel and the surrounding tissue will be increased, and the available oxygen and glucose, for the remaining tissue will be decreased. Cells must be within 100-200μm from a vessel to prevent detrimental effects (Carmeliet and Jain, 2000; Kirk et al., 2004), thus this increased distance and decreased nutrient availability may pose a threat to the survival of the surrounding tissue. Despite this, polymorphisms in the p47phox subunit that

increase its expression have been shown to ameliorate the disease and pathology in EAE (Becanovic et al., 2006). This finding suggests that, independent of tissue damage, ROS may play a role in modulating the immune response (Lassmann and van Horssen, 2011).

Blood vessels can become damaged during the inflammatory process, resulting in the disruption of supply and thereby tissue hypoxia. Endothelial damage or an inflammatory reaction at the vessel wall may result in the activation of haemostasis, followed by thrombotic occlusion and microcirculatory disruptions (Lassmann, 2003). The perivascular nature of functionally active NADPH oxidase complexes, as reported in the current study, represents a potent source of ROS which could easily initiate such a cascade of events. Alternatively, the reaction could be the result of either an antibody mediated response, whereby recognition of an antigen within the vessel wall, or a cytokine mediated response (Lassmann, 2003), can result in endothelial activation and the subsequent upregulation of adhesion molecules (Millan et al., 1997; Lassmann, 2003).

CD8+ T-cells auto-reactive for MBP have also been suggested to play a role to play in vascular damage in EAE (Huseby et al., 2001). Huseby and colleagues induced EAE by the passive transfer of MHC class I restricted T cells directed against MBP. The animals developed widespread CNS inflammation, with inflammatory lesions characterized by perivascular tissue damage (Huseby et al., 2001). It is thought that myelin basic protein liberated from demyelinating lesions diffuses to nearby vessels, where it is presented to cytotoxic T-cells, resulting in the initiation of an inflammatory response (Lassmann, 2003).

2.4.5.0 Hypoxia during relapse

Besides evidence of global tissue hypoxia during the first peak of disease, intense foci of pimonidazole labelling, were found in the white matter of animals in the relapse stage of disease. Indeed, these areas of hypoxia were found to be largely demyelinated, packed full of 'foamy' macrophages, positive for NADPH oxidase and relatively sparse in vasculature, probably as a result of dispersion due to oedema. It is reasonable to propose that a combination of the factors described above may result in local ischaemia, and thus foci of pimonidazole labelling. Alternatively, these areas may represent glial scars, as reactive astrocytes were evident in the foci. Astrocytes are thought to contribute to the pathogenesis of MS by inhibiting remyelination (Nair et al., 2008). They might achieve this through the formation of a glial scar, which can act as a physical barrier around demyelinated lesions. The scars are composed of interwoven astrocytic processes, held together by tight junctions (Eng et al., 1987; Reier and Houle, 1988). Glial scars have been reported in MS (Holley et al., 2003), and EAE (Matsumoto et al., 1992).

2.4.6.0 Oxygen therapy in rMOG EAE

2.4.6.1 One hour oxygen therapy

Given the current finding that hypoxia correlates quantitatively, spatially and temporally with the neurological deficit in rMOG EAE, it seemed reasonable to explore the effect of increasing tissue oxygenation on the neurological dysfunction in this model of MS. The current study shows that the loss of function in rMOG EAE animals was partially restored following acute administration of normobaric oxygen (NBO), in the current study. The promptness of this restoration of function supports the suggestion that the neurological deficit in rMOG EAE is at least partly due to hypoxia. Indeed, hypoxia

may explain the occurrence of some symptoms such as fatigue, often observed in MS patients (Freal et al., 1984; Krupp et al., 1988; Bakshi et al., 2000), although fatigue in MS is complex and may be attributable to a number of factors. These findings are consistent with the historical observations that vasodilators such as histamine, can improve symptoms in patients with MS (Brickner, 1955; Brickner, 1958). In these studies, patients frequently displayed drastic functional improvements within only an hour of a histamine injection. This acute improvement became known as "relief by flush", due to the flushing of the skin in response to the vasodilation (Brickner, 1955). Interestingly, the therapy was only efficacious in patients in which symptoms had been present for only a few weeks (Brickner, 1995). Consistent with this historical observation, the present data suggest that the oxygen-sensitive period in EAE only persists for the first few days following the onset of neurological deficit, implying that the therapeutic window is narrow and the timing of therapy crucial, for an observable functional benefit.

The promptness of the restoration of function following NBO was surprising, given that the arterial haemoglobin (Hb) oxygen saturation (S_aO_2) is normally 97% whilst breathing room air. However, inspiring 100% oxygen at 1 atmosphere (ATM) increases the S_aO_2 to 100% and the total oxygen content of the blood by approximately 20 ml/L (Beynon et al., 2012). This increase is accounted for by an increase in the amount of oxygen dissolved in plasma (Beynon et al., 2012). Furthermore, oxygen delivery from capillaries has been described to occur radially, with each capillary supplying a cylindrical volume of tissue surrounding it (Krogh, 1919). This area of supply has been proposed to increase if the oxygen tension is increased (Krogh, 1919), as with therapeutic hypoxia. Therefore, it is understandable how an increased tissue oxygenation can be achieved with NBO therapy.

Re-oxygenation of hypoxic tissue, particularly at high atmospheric pressures, has previously been associated with an increase in oxidative stress and damage (Clark, 2008). However, the current preliminary histological examination of ROS and oxidised DNA did not reveal evidence of such damage. This finding is consistent with previous studies that also show no detectable increase in oxidative damage, following NBO (Singhal et al., 2002). However, the safety of prolonged oxygen administration remains unclear and requires further investigation.

2.4.6.2 One hour oxygen therapy reverses labelling for hypoxia

Given that NBO can partially restore function in rMOG EAE, it was of interest to determine whether it could also reverse the labelling for hypoxia. Indeed, a decrease in the labelling for markers of hypoxia was observed in control and symptomatic animals. Furthermore, the labelling in rMOG animals that exhibited a neurological deficit and were treated with NBO, was lower than that in IFA control animals exposed to NBO. Although this observation is difficult to interpret, it may represent differences in the physiological properties of the tissue in the respective groups. It seems reasonable to propose that the inflammation and subsequent oxygen debt in the spinal cords of rMOG animals creates a steep oxygen diffusion gradient, resulting in more oxygen being extracted from the blood. Conversely, there is no such inflammation or oxygen debt in the spinal cords of control animals, thus a smaller diffusion gradient would exist, resulting in less oxygen to be extracted from the blood. Increased oxygen concentrations in the tissue will lead to rapid metabolism and excretion of pimonidazole (Arteel et al., 1998), and rapid degredation of HIF-1α (Maxwell et al., 1999; Ivan et al., 2001; Jaakkola et al., 2001; Kilmova and Chandel, 2008). Therefore, if more oxygen is

available in spinal cord tissue of rMOG animals, there will be a decrease in the immunoreactivity of these markers.

2.4.6.3 7-day combination therapy

Due to its ability to impair axonal conduction (Redford et al., 1997; Shrager et al., 1998) and mitochondrial energy metabolism (Bolanos et al., 1994; Brown et al., 1995), NO has been viewed as a key inflammatory mediator of neurological dysfunction. More recently, a role for ROS/RNS has also emerged (Qi et al., 2006; Nikić et al., 2011). Accordingly, the present study set out to identify the relative contributions of each of these factors, in addition to hypoxia, to the development and progression of neurological dysfunction in rMOG EAE. The present results describe a transient improvement of animals treated with 1400W, an iNOS inhibitor, and MitoQ, a mitochodrially targeted antioxidant, compared with non-treated controls, thereby suggesting a role for NO and superoxide in the production of neurological deficits. Although the administration of these agents individually did not result in a statistically significant improvement in the neurological deficit score, when the agents were administered together with oxygen a significant, and biologically important, improvement in walking ability was achieved. The improvement was evident in the first few days following the onset of disease, when iNOS is expressed within the tissue. During this period, NO likely promotes mitochondrial dysfunction (Bolanos et al., 1994; Brown et al., 1995), thereby exacerbating an energy deficit resulting from inadequate oxygenation.

The decreased efficacy of 1400W and MitoQ, when administered alone was somewhat surprising. We have found the expression of iNOS to be very variable between different EAE trials, suggesting that although NO can be an important cause of

neurological dysfunction it may not be the only factor involved. Previous studies have reported conflicting results with iNOS inhibition in EAE, with some reporting a functional benefit (Zhao et al., 1996; Brenner et al., 1997), whilst others report a worsening of neurological dysfunction (Willenborg et al., 1999). These discrepancies may either reflect the heterogeneous nature of different EAE models, differences in the type of inhibitor employed, or differences in the timing of the therapy. Mitochondrial membrane potential drives MitoQ uptake and accumulation into the mitochondrial matrix (Liberman and Skulachev, 1970; Ross et al., 2005). Therefore, although the administration of MitoQ had some effects on the disease course, its therapeutic efficacy may have been attenuated by the loss of mitochondrial membrane potential. Indeed, mitochondrial pathology and loss of membrane potential has been described in EAE (Qi et al., 2006; Nikic et al., 2011).

The present results suggest an important role for hypoxia in the production of neurological deficits in rMOG EAE, and that the therapeutic window is narrow. This finding may explain why many of the hyperbaric oxygen (HBO) trials failed, 30 years ago (Bennett and Heard, 2010). Many of the trials were designed to detect an effect of daily, short exposures to HBO on disease course over the course of a few months, rather than an acute effect on symptoms. Thus, the trials did not aim to recruit patients with early disease, or during relapses. Such factors have been highlighted as key determinants of therapeutic benefit in the current study; we therefore believe that the HBO trial data are not relevant in this context.

2.4.7.0 Conclusion

The current study provides chemical, physical and therapeutic evidence that neurological deficits in rMOG EAE can arise from tissue hypoxia. Moreover, the

hypoxia is quantitatively, spatially and temporally associated with the onset and distribution of neurological dysfunction. Early treatment with NBO not only alleviates the hypoxia, but is also effective in reducing the severity of the neurological deficit. Although further studies are necessary to investigate the best therapeutic regimen, these novel findings provide further insight into the pathogenesis and pathophysiology of EAE, and perhaps also MS.

CHAPTER THREE

THE DORSAL COLUMN LPS LESION

3.1.0.0 INTRODUCTION

Demyelination is a cardinal feature of MS, but the mechanism(s) by which it occurs remain uncertain. Many favour an autoimmune mechanism, but examination of the early forming lesion indicates roles for innate immunity (Barnett and Prineas, 2004) and 'hypoxia-like' (Aboul-Enein et al., 2003) mechanisms. The intraspinal injection of LPS into the rat dorsal column induces a focal, inflammatory demyelinating lesion (Felts et al., 2005) and has been demonstrated to be an accurate model of the MS Pattern III lesion (Marik et al., 2007). Pattern III lesions are characterised by the preferential loss of MAG, which is associated with nuclear condensation and fragmentation in oligodendrocytes (Lucchinettti et al., 2000). HIF-1α positive oligodendrocytes, astrocytes and endothelial cells are also found within areas of MAG loss in Pattern III lesions (Aboul-Enein et al., 2003). These pathological findings are similar to that seen in white matter stroke, thereby leading to the suggestion that a common mechanism of injury exists, that is, a 'hypoxia-like' metabolic tissue injury (Aboul-Enein et al., 2003). Indeed, loss of the mitochondrial proteins of COX-I and COX-IV of respiratory complex IV, and general reduction of mitochondrial density, has also been found in Pattern III lesions (Mahad et al., 2008). In agreement with this, microarray studies on the NAWM of MS patients have revealed an up-regulation of a number of genes consistent with an energy deficit (Graumann et al., 2003). To date, however, the data have been interpreted as a hypoxic pre-conditioning, rather than hypoxia *per se*. Thus, the demyelination in the Pattern III MS lesion has been attributed to an energy deficit

arising from NO-mediated mitochondrial inhibition (Aboul-Enein et al., 2003). Indeed NO is capable of interfering with mitochondrial function in the brain, through the inhibition of respiratory chain complex II, III and especially IV activity (Bolanos et al., 1994), and reversibly inhibiting oxygen consumption (Schweizer and Richter, 1994). Despite this, NO may not be sufficient to induce structural damage acting alone. Indeed, treatment with dexamethasone was found to suppress iNOS activity, but did not affect the extent of demyelination (Felts et al., 2005). Besides NO, increases in ROS and hypoxia (Taylor and Colgan, 2007) are also evident within the inflammatory milieu. NO itself can promote mitochondrial superoxide production via NO-mediated mitochondrial damage, and subsequent ATP depletion (Murphy, 2009), and can increase the vulnerability of cells, such as oligodendrocytes, to hypoxia, by raising the apparent Km of mitochondrial complex IV for oxygen (Brown and Cooper, 1994). Thus we propose an alternative mechanism for causing demyelination involving hypoxia, NO and superoxide, and have therefore, examined the animal model of the human lesion for evidence of these pathological features.

3.1.1.0 Aims

1. To determine whether the DC LPS lesion labels for hypoxia.
2. To identify whether superoxide production is increased within the lesion.
3. To investigate the pathological factors that may contribute to the 'hypoxia-like' demyelination.

3.1.2.0 Hypothesis

Hypoxia precedes demyelination in the experimental Pattern III lesion.

3.2.0.0 MATERIALS AND METHODS

3.2.1.0 Surgery

A laminectomy was performed between T12 and T13 vertebral levels in adult male Sprague Dawley rats (312g ± 31.9, mean ± S.D.). A small hole was made in the dura, a drawn glass micropipette inserted into the right dorsal column, and 0.5µl of LPS (*Salmonella enteric* serotype abortus equi, Sigma-Aldrich) (100ng/µl saline) injected at depths of 0.7 and 0.4 mm, respectively (n = 3 rats per time point). The location of the injection site was marked with charcoal. Control animals received injections of saline alone (n = 2 per time point).

3.2.2.0 Tissue Processing

Pimonidazole (60 mg/kg in sterile saline), and DHE (1µg/ml in DMSO) were administered intravenously into the saphenous veins of all animals, under light anaesthesia (2% isofluorane), with recovery, 4 hours prior to perfusion. Animals were perfused trans-cardially with PBS, followed by 4% PFA, at 0.5, 1, 2, 3, 7 and 14 days post-LPS injection and the spinal cord harvested. Spinal cords were transected at the site of the injection and the rostral portion processed for resin sections and the caudal portion processed for cryosections. Tissue was post-fixed overnight in 4% PFA prior to either post-fixation in 4% glutaraldehyde in 0.15M phosphate buffer, or cryoprotection in 30% sucrose in PBS, for resin processing or immunohistochemical analysis, respectively. Frozen tissue used for immunohistochemistry was processed as described previously (section 2.2.5).

3.2.3.0 Histology

3.2.3.1 IHC/IF

Spinal cord sections were air dried for a few hours prior to any histology. Spinal cord tissue from the site of the injection of LPS was examined immunohistochemically using a range of markers for inflammation, hypoxia, and ROS (Table 3.2.3.1). Briefly, sections were washed with PBS, prior to incubation with either 0.3% H_2O_2 in neat methanol, or neat methanol alone for IHC and IF, respectively. Sections were blocked in the appropriate blocking buffer for 30 minutes, before incubation in primary antibody overnight at 4^{o}C. Primary antibodies were visualised either using the DAB/peroxidase or fluorescent reporter systems. For the detection of superoxide production, spinal cord sections were washed in PBS and mounted in Vectashield medium, prior to confocal microscopy.

Table 3.2.3.1: Antibody Details for IHC/IF

Antibody	Target	Isotype	Pre-Treatment	Blocker	Dilution	Supplier
Rabbit Anti-iNOS	Inducible Nitric Oxide Synthase		N/A	5% goat serum mixed in PBS containing 0.1% Triton X-100	1/200	BD Transductions Laboratories Franklin Lakes, NJ
Mouse Hydroxyprobe-1-Mab anti-pimonidazole	Pimonidazole adducts		$NaBH_4$	0.25% casein mixed in PBS containing 0.1% Triton X-100 (for IHC) 5% goat serum mixed in PBS containing 0.1% Triton X-100 (for IF)	1:500 1:200	HPI Inc
Rabbit Hydroxyprobe-1-Mab anti-pimonidazole	Pimonidazole adducts		$NaBH_4$	5% goat serum mixed in PBS containing 0.1% Triton X-100	1/200	HPI Inc
Rabbit Anti-HIF-1α	Active Hypoxia Inducible Factor-1α		$NaBH_4$	5% goat serum mixed in PBS containing 0.1% Triton X-100	1/500	Milipore Inc Billerica, MA
Rabbit Anti-GLUT-1	Glucose transporter		N/A	5% goat serum mixed in PBS containing 0.1% Triton X-100	1/200	Abcam
Mouse Anti-VEGF	Vascular endothelial growth factor		N/A	5% horse mixed in PBS containing 0.1% Triton X-100	1/500	Abcam
Mouse Anti-GFAP	Astrocytes		$NaBH_4$	5% goat serum mixed in PBS containing 0.1% Triton X-100	1/400	Sigma
Rabbit Carbonic anhydrase 2 (CA2)	Oligodendrocytes		$NaBH_4$	5% goat serum mixed in PBS containing 0.1% Triton X-100	1/200	Kindly provided by Dr N. Gregson

3.2.3.2 Resin Sections

Spinal cord tissue was cut into 0.5 mm thick segments and post-fixed in 1.5% osmium tetroxide in 0.15 M phosphate buffer, with subsequent dehydration in graded alcohols, passed through propylene oxide and embedded in resin (Taab Laboratories, Aldermaston, UK). Sections were cut to a thickness of 1 µm on an ultramicrotome (Leica Microsystems, UK), and stained with 0.1% thionin acetate and 1% aqueous basic acridine orange. Stained sections were then mounted in DPX mounting medium and examined with light microscopy.

3.2.4.0 Microscopy

3.2.4.1 Light Microscopy and Quantification

Tissue developed using the peroxidase detection system was viewed using an Axiophot light microscope (Zeiss, Germany) and pictures taken with a Nikon D300 camera (Nikon, USA). All analysis and quantification was performed blind. Analysis of the intensity of the labelling with pimonidazole was performed by tracing around the spinal cord sections (white and grey matter, and grey matter alone), and measuring the pixel intensity using Image J (National institute of health, USA). Quantification of iNOS and HIF-1α positive cells was carried out using Image J. Briefly, the images were made binary, and then the dorsal columns of each spinal cord section were delineated using the freehand selection tool, before using the 'analyze particles' tool to count the number of positive cells. The same criteria were used for each image, and area measurements were carried out concurrently.

3.2.4.2 Confocal Laser Microscopy

Fluorescent images were obtained using a Zeiss LSM5 pascal confocal microscope, with a 40x objective. Excitation wavelengths of 488 nm and 543 nm were provided by argon and helium-neon gas lasers, respectively. Emission filters BP505-530, BP505-570, and LP560 were used for obtaining the images.

3.2.5.0 Statistical Analysis

All data were tested for normality using either the Kolmogorov-Smirnov or the Shapiro-Wilk test, depending on the size of the data set, and for stability of variances using the Levene's test. Data that were not normally distributed were evaluated using non-parametric statistics as indicated. P-values of 0.05 (*), 0.01 (**) and 0.001 (***), were considered as statistically significant. All statistical analyses were carried out using SPSS version 14.0 (USA).

3.2.5.1 Statistical Analysis of Pimonidazole Intensity

The pixel intensity of the pimonidazole labelling was normally distributed in all spinal cord sections examined. Therefore, the percentage of pixels labelled with an intensity greater than the control mean plus one standard deviation were counted and compared to the appropriate vertebral segment-matched control using a two-way ANOVA; the room air treatment group and saline-injected group served as controls in each of the respective experiments.

2.3.6.2 Statistical Analysis of Other Labels

A linear regression model was used to compare the iNOS, HIF-1α and RECA-1 cell densities between LPS-injected animals and saline-injected controls. This was

followed by a pairwise comparison at the different time points using an independent t-test.

3.3.0.0 RESULTS

3.3.1.0 Intraspinal injection of LPS induces a focal demyelinating lesion

The intraspinal injection of LPS into the dorsal columns induced a focal demyelinating lesion commencing around 3 days post injection (Figure 3.3.1.0). At the early time points (0.5, 1 and 2 days), tissue integrity was largely maintained although evidence of inflammation was observed in the dorsal white matter. At 3 days post injection, the tissue was largely oedematous and there was evidence of demyelination, particularly at the base of the dorsal columns. By 7 days, post injection, the demyelination was more extensive, and was localised to the ventral half of the dorsal column, with some evidence of tissue oedema (Figure 3.3.1.0). Debris-filled macrophages were also observed within the lesion at 7 days. At 14 days post injection, the lesions were comprised of demyelinated axons, axons associated with cells (Felts et al., 2005), and debris-filled macrophages (Figure 3.3.1.0).

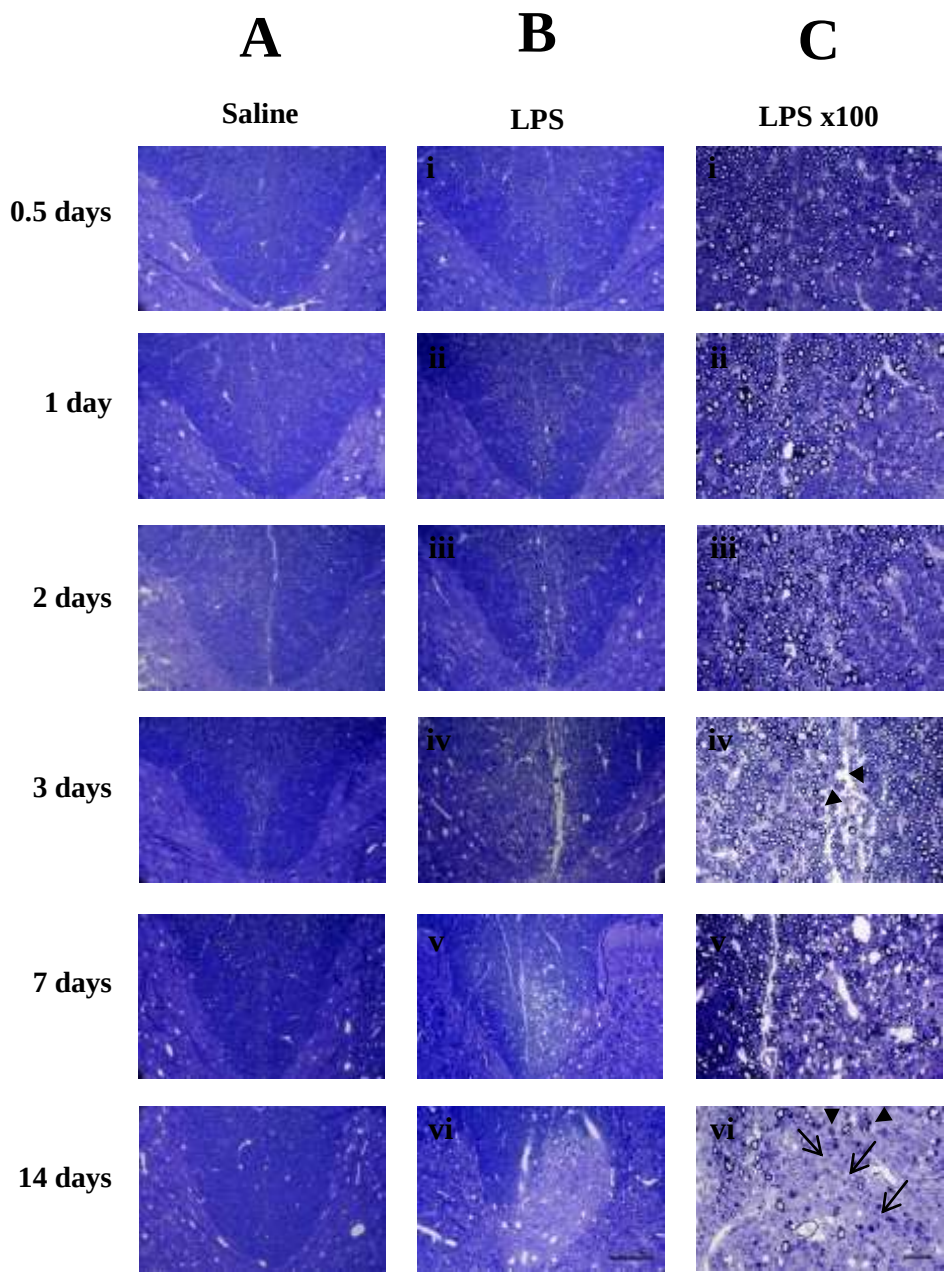

Figure 3.3.1.0: Formation of a demyelinating lesion following intraspinal LPS injection

(A-C) Light micrographs of transverse spinal cord sections at the level of the injection of saline (A) or LPS (B, C). (A) In saline-injected control animals, tissue appears to be relatively normal, with no apparent pathology. (B, C) Following the intraspinal injection of LPS, a focal demyelinating lesion appears to form between 3 and 7 days post-injection. In the acute lesion (0.5-2 days post-injection), little or no demyelination is present. At 3 days post-injection, several debris-filled macrophages are evident in the dorsal columns of LPS-injected animals (C iv, arrowheads). (C v) At 7 days post-injection the lesion is oedematous, with some evidence of demyelination. (C vi) By 14 days, the lesion contains demyelinated axons, several debris filled macrophages (arrowheads) and axons in association with cells (arrows). Scale bars 200µm (A, B), and 100µm (C). All Micrographs are representative.

3.3.2.0 The acute DC LPS lesion labels positive for hypoxia

3.3.2.1 Acute transient pimonidazole labelling in the DC LPS lesion

The intravenous probe pimonidazole was used to detect tissue hypoxia in the DC LPS lesion. Pimonidazole immunoreactivity was evident in the grey matter and dorsal columns of LPS-injected animals at all the time points examined (Figure 3.3.2.1 A, B). However, labelling for pimonidazole was only statistically significantly increased in the grey matter of LPS-injected animals at 1 day ($p< 0.001$) and 2 days (independent t-test, $p = 0.014$) post injection, compared with saline-injected controls. In the acute lesion, before any demyelination was evident, labelling for pimonidazole was prominent, particularly at 1 day post injection, with a band of intense labelling visible in the adjacent grey matter 'cradling' the base of the dorsal column (Figure 3.3.2.1 A). The grey matter labelling was specific to neuronal cell bodies and the surrounding extracellular matrix. Of all the time points examined, labelling for hypoxia was most intense at 1 day post LPS injection (Figure 3.3.2.1 A, B). By 2 days, the intensity of pimonidazole labelling decreased in the grey matter, although this still remained increased in comparison with saline-injected controls. The Spearman's Rank order correlation test identified that the intensity of pimonidazole labelling in the acute DC LPS lesion strongly correlated with the iNOS cell density ($p = 0.08$, $r^2 = 0.701$, $n = 9$), suggesting that the intensity of pimonidazole labelling increases concomitantly with the iNOS cell density.

Although pimonidazole does not label myelin, leading to the less obvious labelling of the white matter, some punctate, cell-specific labelling was observed in the dorsal columns of LPS injected animals, particularly evident at 1 day post injection (Figure 3.3.2.1 A). Morphological analysis of these cells suggested that they may be

composed of oligodendrocytes and astrocytes, therefore double label IF was carried out to confirm their identity. This revealed that pimonidazole-positive cells co-labelled with CA2, a marker of oligodendrocytes (Ghandour et al., 1980), and GFAP, a marker of astrocytes (Figure 3.3.2.1 C). No such labelling was present in saline-injected controls.

A

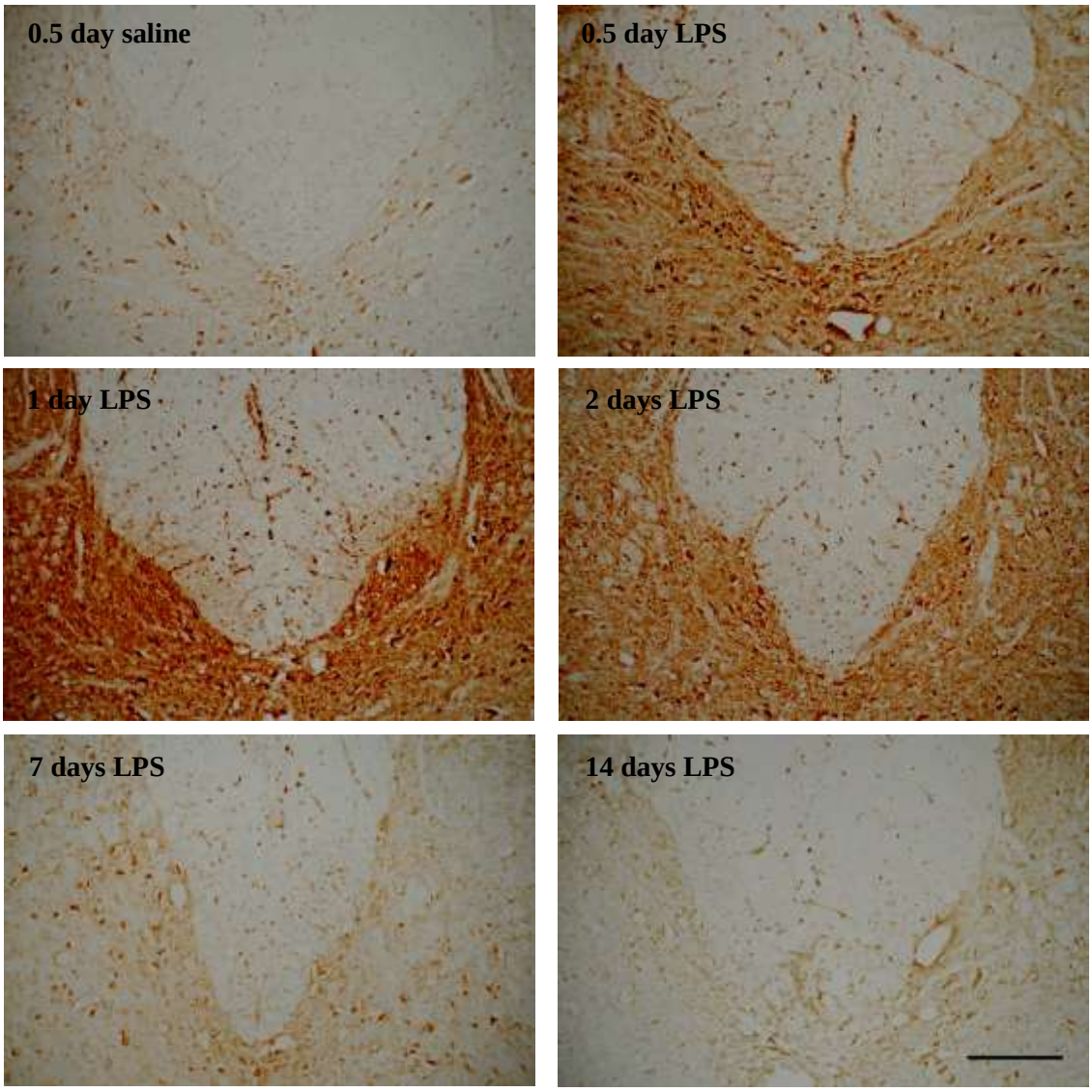
0.5 day saline
0.5 day LPS
1 day LPS
2 days LPS
7 days LPS
14 days LPS

B

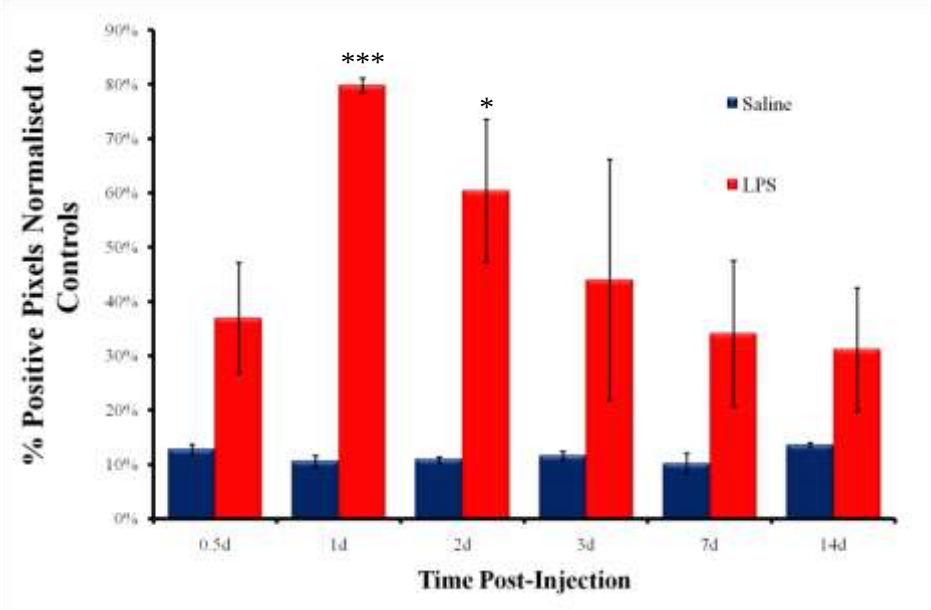
% Positive Pixels Normalised to Controls
90%
80%
70%
60%
50%
40%
30%
20%
10%
0%
***
*
Saline
LPS
0.5d
1d
2d
3d
7d
14d
Time Post-Injection

C

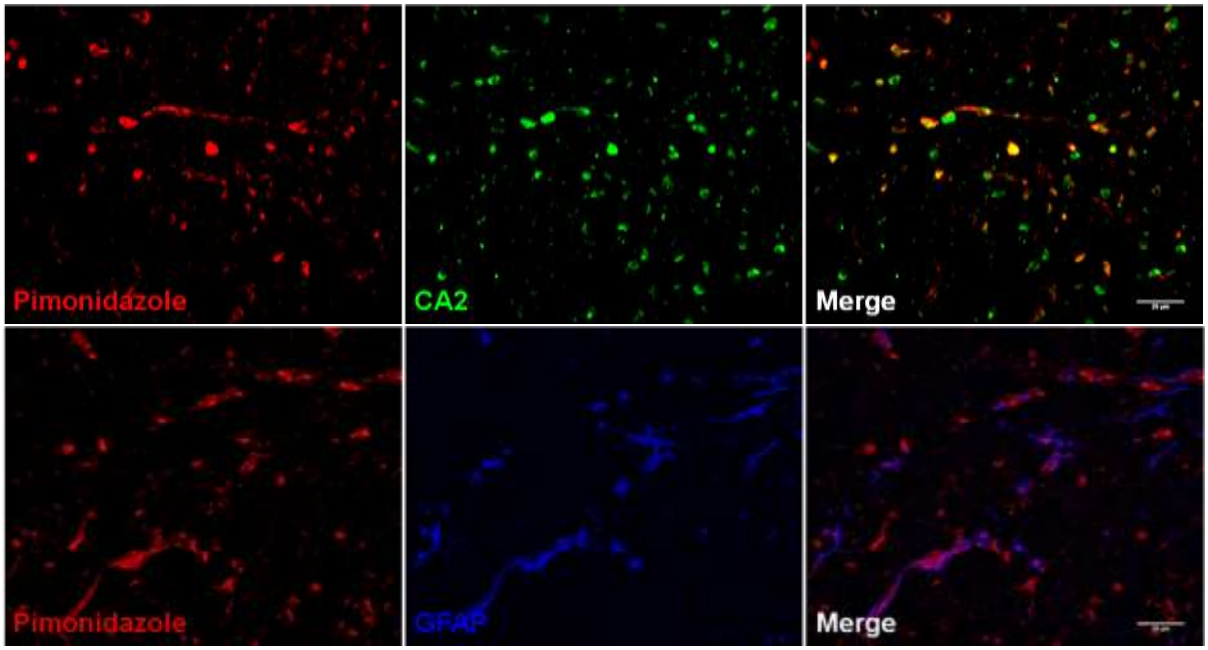

Figure 3.3.2.1: Pimonidazole immunohistochemistry in the LPS dorsal column lesion

(A) Spinal cord sections at the level of the injection of saline (0.5 days post-injection) or LPS, at 0.5, 1, 2, 7 and 14 days post-injection labelled with an antibody against bound pimonidazole adducts. Labelling for pimonidazole is substantially increased in the grey matter and the dorsal columns of animals injected with LPS, compared with saline-injected controls, particularly in the acute lesion (0.5-2 days post-injection). Scale bar 200µm. (B) Graphical representation of the intensity of pimonidazole labelling over the time course of the LPS dorsal column lesion (control n=2 per time point; LPS n=3 per time point). Labelling for pimonidazole is most intense at 1 day post-LPS injection, but decreases thereafter. Statistical significance was determined by an independent t-test, comparing saline-injected and LPS-injected animals at each time point, * $p<0.05$, *** $p<0.001$. Values are mean ± SD. (C-top) Double label immunofluorescence with antibodies against pimonidazole (false-coloured red) and CA2 (green) showing that a subset of oligodendrocytes label positively for pimonidazole. (C-bottom) Double label immunofluorescence with antibodies against pimonidazole (false-coloured red) and GFAP (blue), showing that a subset astrocytes also label for pimonidazole. Scale bar 100 µm. All micrographs are representative.

3.3.2.2 HIF-1α expression in increased in LPS-injected animals

HIF-1α is expressed in some MS lesions, therefore immunohistochemistry was used to identify whether HIF-1α is expressed in the dorsal columns of LPS-injected animals, to corroborate our findings with pimonidazole. HIF-1α expression was increased in the dorsal columns of LPS-injected animals, compared with saline-injected controls (Figure 3.3.2.2 A, B). Labelling for HIF-1α was statistically significantly increased at 0.5 days ($p = 0.022$) and 2 days ($p = 0.004$), post injection. Although extensive labelling was also observed at 1 day post-injection, this did not reach statistical significance in our sample ($p = 0.059$). Cytoplasmic and nuclear HIF-1α labelling was seen as early as 0.5 days post injection, in the dorsal columns of LPS-injected animals, and at all other time points examined (Figure 3.3.2.2 A). Up to, and including, 2 days post injection, these HIF-1α-expressing cells, identified as glial cells based on their morphology, were found scattered throughout the dorsal columns and did not show a preference for the injection side. Moreover, labelling for HIF-1α was also increased in the adjacent grey matter in these animals. However, at the subsequent time points the expression of HIF-1α was primarily localised to the injection side of the dorsal white matter. The labelling for HIF-1α was particularly impressive at 3 days post-LPS injection, where it seemed to be expressed by activated macrophages/microglia, within the demyelinating lesions and surrounding vessels. At 14 days post LPS injection, endothelial expression of HIF-1α was also evident, in addition to the glial expression observed at the earlier time points. Saline-injected controls only displayed basal levels of HIF-1α expression within the dorsal white matter: very little HIF-1α was observed in the adjacent grey matter (Figure 3.3.2.2 A, B).

A

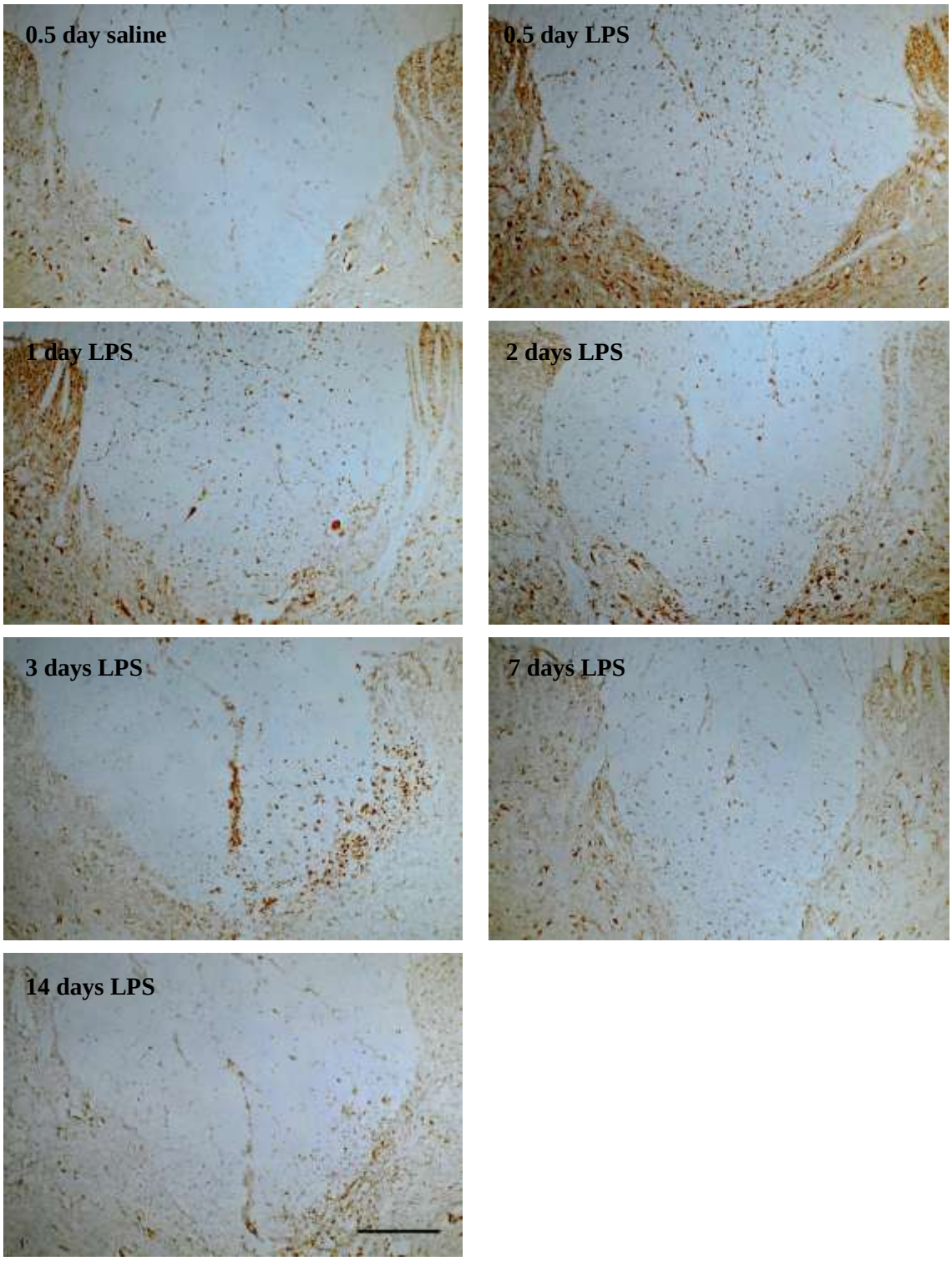
0.5 day saline
0.5 day LPS
1 day LPS
2 days LPS
3 days LPS
7 days LPS
14 days LPS

B

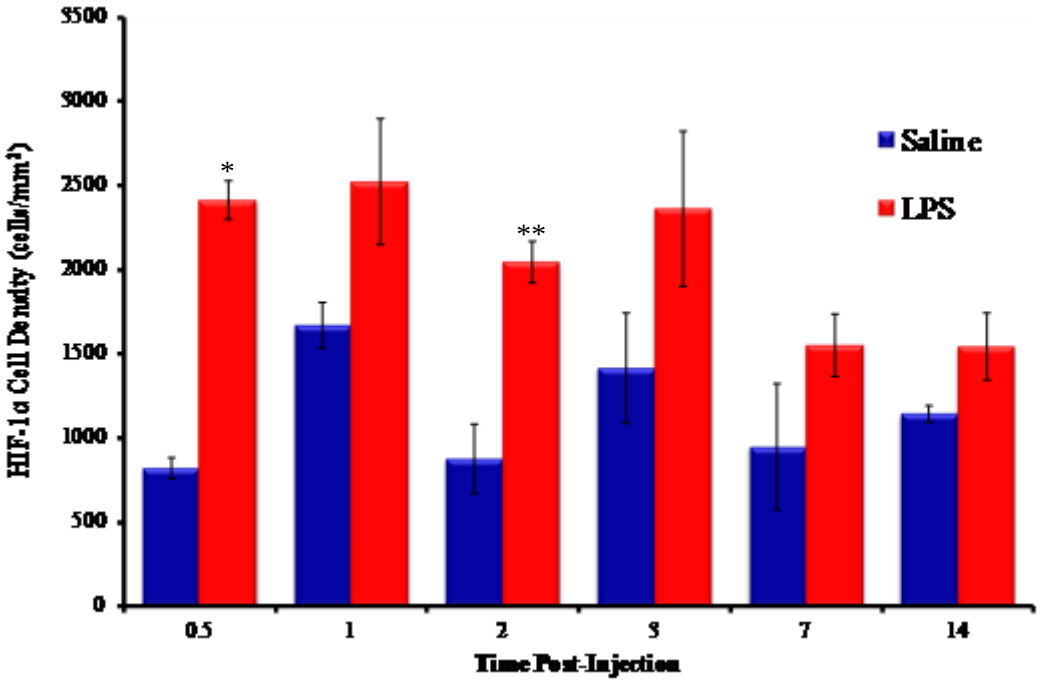

Figure 3.3.2.2: HIF-1α immunohistochemistry in the LPS dorsal column lesion
(A) Spinal cord sections at the level of the injection of saline (0.5 day post-injection), and LPS at 0.5, 1, 2, 3, 7 and 14 days post-injection, labelled with an antibody against HIF-1α. HIF-1α immunoreactivity is increased in LPS-injected animals compared with saline-injected control animals. HIF-1α positive cells are evident in the dorsal column, and adjacent grey matter, of LPS-injected animals. Scale bar 200 µm. All micrographs are representative. (B) Graphical representation comparing the HIF-1α cell density between saline-injected and LPS-injected animals at all the time points examined. Values are mean ± S.D. (n=2 for controls, per time point; n=3 for LPS, per time point). Statistical significance determined by an independent t-test comparing the mean cell density between LPS-injected and saline-injected animals, at each time point, * $p<0.05$, ** $p<0.01$.

3.3.2.3 The expression of Hypoxia inducible proteins is increased following LPS injection

HIF-1α regulates the transcription of a number of genes. GLUT-1 and VEGF are two such genes, and their increased expression in response to hypoxia is well established. GLUT-1, expressed on both endothelial cells and glia within the CNS, was increased in the dorsal columns of LPS-injected compared with saline-injected controls (Figure 3.3.2.3 A), particularly at 0.5 days post injection. In the dorsal columns of saline-injected animals, GLUT-1 was primarily expressed on endothelial cells (Figure 3.3.2.3 A), however, at the early time points (0.5 and 1 day post LPS-injection), GLUT-1 expression was seen on endothelial and glial cells. This change in pattern of expression probably contributed to the increase in GLUT-1 labelling observed at these early time points. By 2 days, the expression of GLUT-1 decreased to that observed in saline-injected controls (Figure 3.3.2.3 A), with expression restricted to endothelial cells. Similarly at the subsequent time points, the extent of GLUT-1 labelling in LPS-injected animals was comparable to that seen in saline-injected controls.

VEGF, a key signal protein responsible for the stimulation of neovascularisation and angiogenesis, was clearly expressed in the dorsal columns of LPS-injected animals, at all time points examined (Figure 3.3.2.3 A). In the acute lesion, particularly at 0.5 and 1 day post injection, VEGF was diffusely distributed throughout the dorsal columns, with no preference for the injection side (Figure 3.3.2.3 A). However, at the subsequent time points, the labelling was observed on endothelial cells. Saline-injected controls did not show any evidence of such labelling.

Despite the expression of VEGF, there was no apparent increase in vascular density within the dorsal columns of LPS injected animals, at any of the time points

examined, compared with saline-injected controls. Rather, the vascular density of the dorsal white matter in LPS-injected animals was decreased, if not comparable to that of control animals (Figure 3.3.2.3 B). However, a considerable degree of variation in the vascular density was observed in the control group at different time points (Figure 3.3.2.3 B).

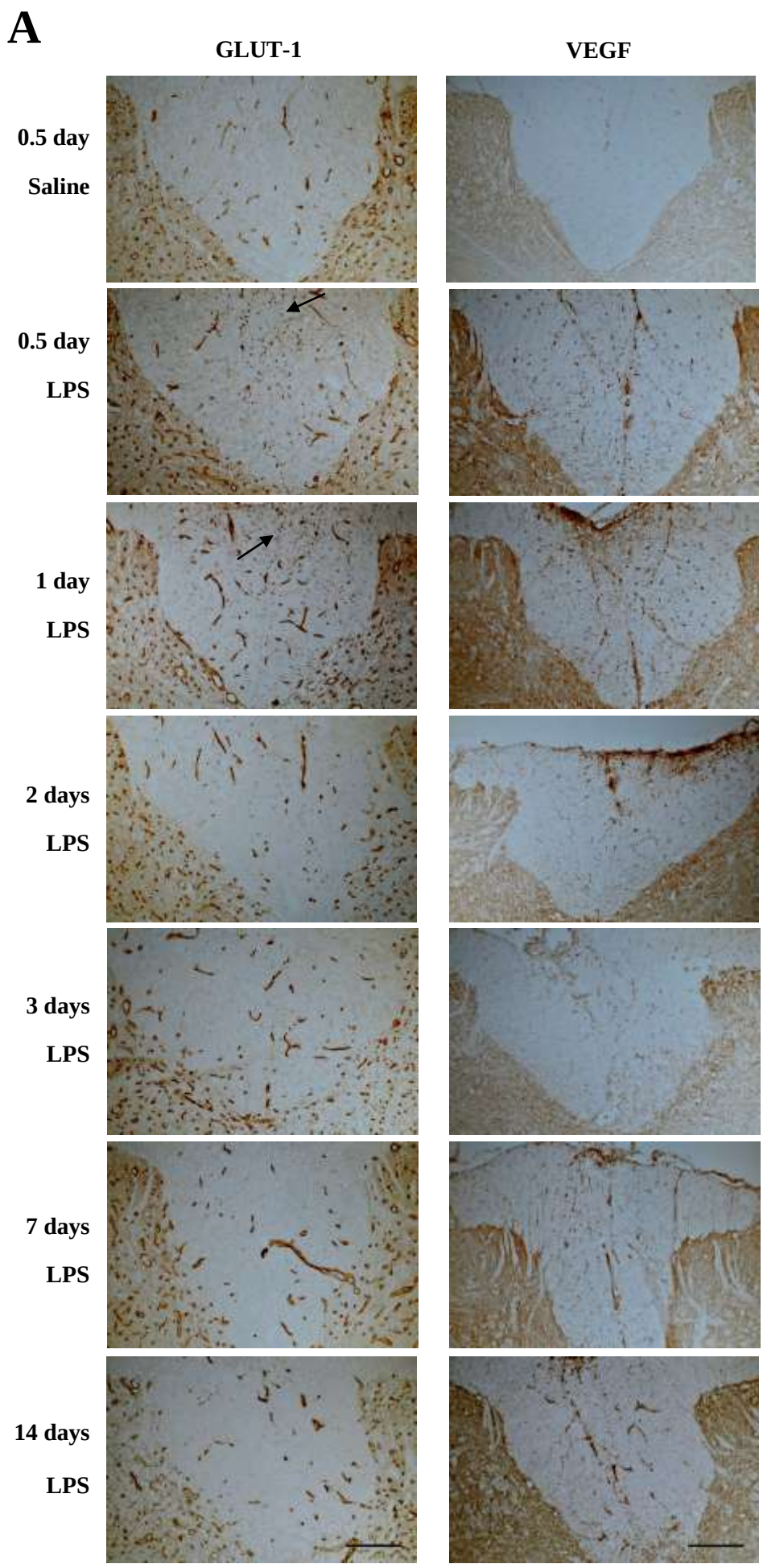
A
GLUT-1
VEGF
0.5 day
Saline
0.5 day
LPS
1 day
LPS
2 days
LPS
3 days
LPS
7 days
LPS
14 days
LPS

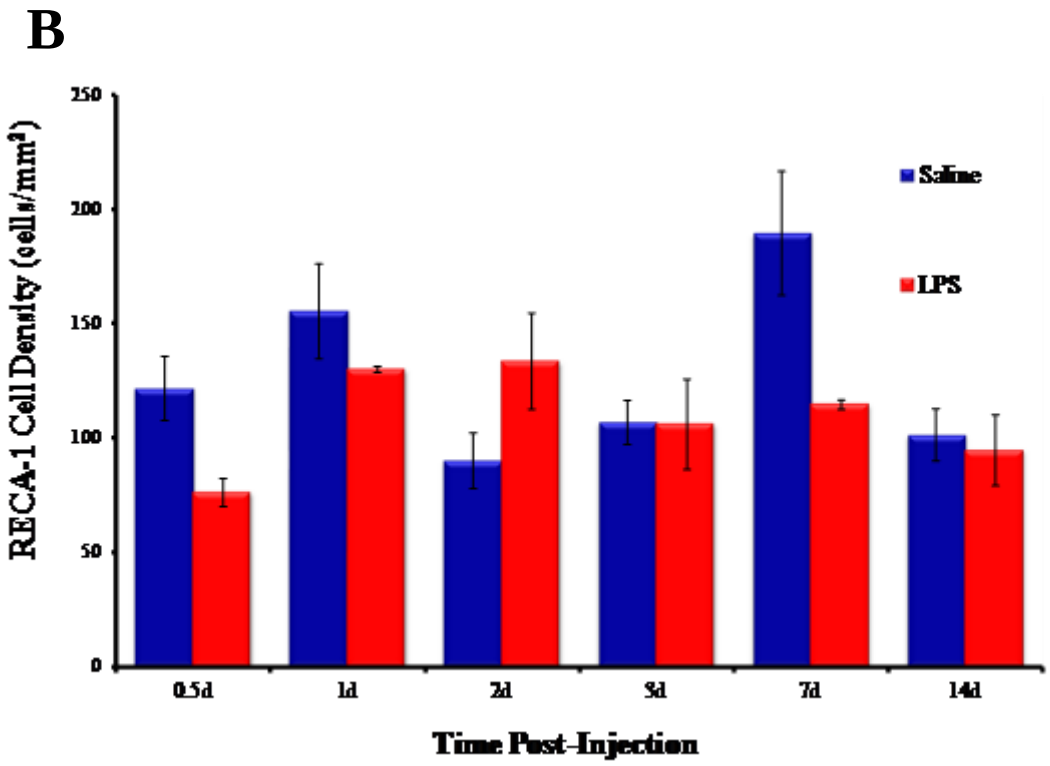

Figure 3.3.2.3: Expression of HIF-1α regulated genes in the LPS dorsal column lesion

(A, left) Spinal cord sections at the level of the injection of saline (0.5 days post-injection), and LPS at 0.5, 1, 2, 3, 7 and 14 days post-injection, labelled with an antibody against GLUT-1. GLUT-1 immunoreactivity is increased in the dorsal columns of LPS-injected animals compared with saline-injected control animals. The increase in immunoreactivity is particularly evident in the acute lesion (0.5-1 day post-injection), due to the additional expression of GLUT-1 in glia (arrow). (A, right) Spinal cord sections at the level of the injection of saline (0.5 days post-injection), and LPS at 0.5, 1, 2, 3, 7 and 14 days post-injection, labelled with an antibody against VEGF. VEGF immunoreactivity is evident in the dorsal columns of animals injected with LPS, at all time points examined. In the acute lesion (0.5-2 days post-injection), VEGF immunoreactivity is dispersed throughout the dorsal white matter, however, at the subsequent time points, VEGF immunoreactivity is largely restricted to endothelial cells No such labelling is evident in the spinal cords of saline-injected controls. Scale bar 200µm. All micrographs are representative. (B) Graphical representation of the vascular density within the dorsal columns of animals injected with saline or LPS at 0.5, 1, 2, 3, 7, and 14 days post-injection (control n=2 per time point; LPS n=3 per time point). Vascular density was relatively comparable between the two groups at all the time points examined, with the exception of day 7 post-injection. Values are means ± S.E.M.

3.3.3.0 Reactive oxygen and nitrogen species

3.3.3.1 Lateralisation of superoxide production in the acute DC LPS lesion

Superoxide production was assessed using the intravenous fluorescent probe DHE, and was present at basal levels in the spinal cords of saline-injected animals (Figure 3.3.3.1). In these animals, uniform superoxide production was typically observed within the dorsal columns and grey matter, with particularly prominent neuronal labelling. Following the intraspinal injection of LPS, superoxide production appeared to be elevated in the dorsal columns and/or grey matter, at most, if not all, the time points examined, compared with saline-injected controls (Figure 3.3.3.1). Interestingly, at 1 day post-injection, there was a lateralisation of superoxide production in the adjacent grey matter, on the side of the injection (Figure 3.3.3.1).

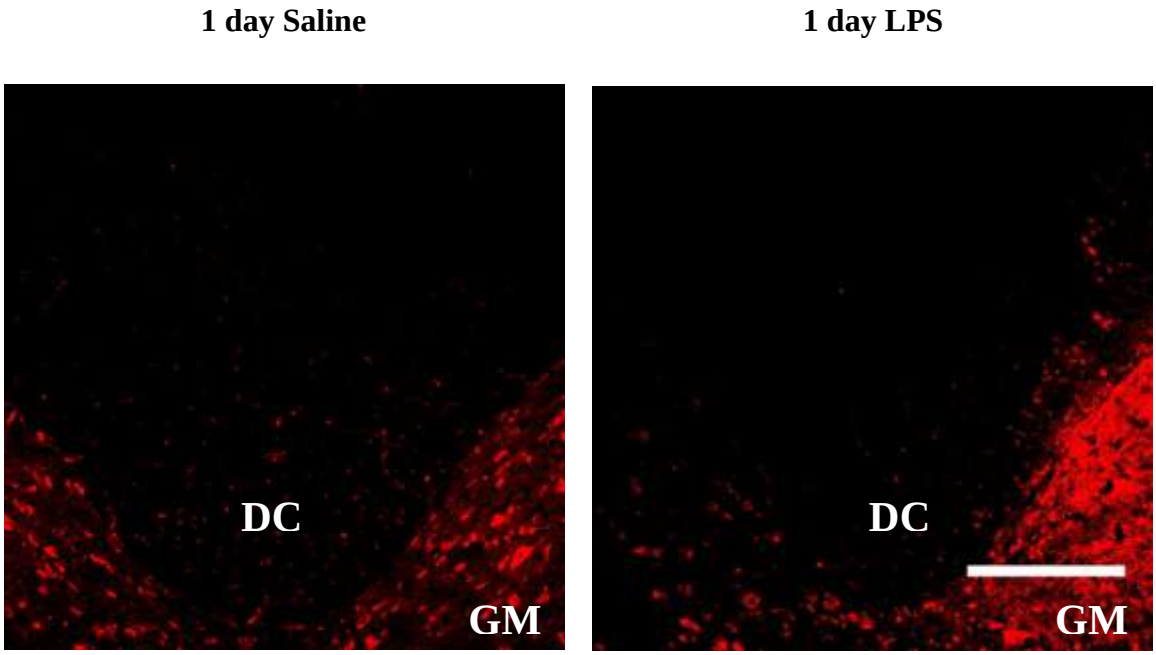

Figure 3.3.3.1: Lateralisation of superoxide production following LPS-injection
Confocal laser micrographs of spinal cord sections at the level of the injection of saline (left) and LPS (right) at 1 day post-injection, examined for DHE-induced fluorescence. DHE-induced fluorescence is evident in saline-injected controls in the grey matter (GM) and dorsal white matter (DC). Following the injection of LPS, there is a complete lateralisation of DHE-induced fluorescence in the adjacent grey matter, on the side of the injection. Scale bar 200µm. All micrographs are representative.

3.3.3.2 Acute iNOS expression following intrapinal LPS injection

The expression of iNOS is a well documented feature of MS lesions, and its expression was acutely increased in the dorsal columns following the intrapinal injection of LPS. The expression of iNOS was observed at the earliest time point examined, 0.5 day post LPS injection ($p< 0.001$), but the iNOS-positive cell density was greatest at 1 day ($p< 0.001$), before decreasing considerably by 2 days ($p = 0.011$) post-injection (Figure 3.3.3.2 A, B). iNOS positive cells were primarily found dispersed diffusely throughout the dorsal columns of LPS-injected animals, with no clear preference for the side injected. However, some positive cells were also found in the adjacent grey matter, with a dense cluster localised in the grey matter at the base of the dorsal columns (Figure 3.3.3.2 A). This pattern of labelling was particularly obvious at 1 day following the injection of LPS. No such labelling was present in saline-injected controls, or in LPS-injected animals after 2 days post-injection (Figure 3.3.3.2 A, B).

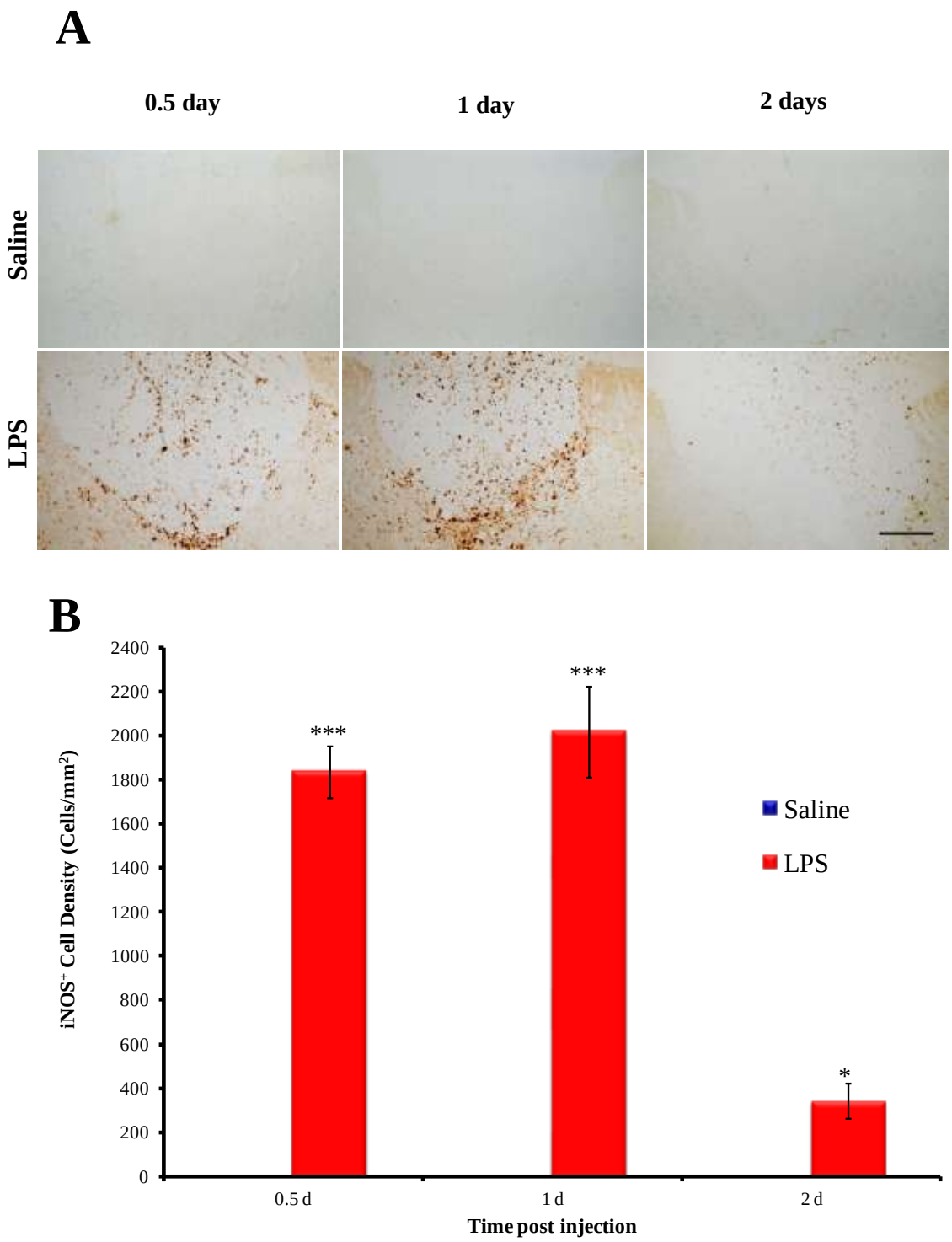

Figure 3.3.3.2: iNOS immunoreactivity in the LPS dorsal column lesion
(A) Spinal cord sections from saline-injected and LPS-injected animals, 0.5, 1 and 2 days post-injection, at the site of the injection. iNOS positive cells are prominently expressed at 0.5 and 1 day following LPS injection. Positive cells can be seen scattered throughout the dorsal columns, with large clusters in the adjacent grey matter. The expression of iNOS is considerably decreased by 2 days post-injection. No such labelling is evident in saline-injected controls. Scale bar 200µm. Micrographs are representative. (B) Graphical representation comparing the iNOS cell density between saline-injected and LPS-injected animals at 0.5, 1 and 2 days post-injection. Values are mean ± S.D. (n=2 for controls, per time point; n=3 for LPS, per time point). Statistical differences were determined by an independent t-test, * $p<0.05$, *** $p<0.001$.

3.3.3.3 Labelling for nitrotyrosine residues follows the spatio- temporal pattern of iNOS

Nitrotyrosine is the molecular footprint of peroxynitrite, and its transient expression was observed in the dorsal columns of LPS-injected animals (Figure 3.3.3.3). The labelling followed the spatio-temporal pattern of labelling seen with iNOS. Accordingly, nitrotyrosine was present as early as 0.5 days post LPS injection, but most prominent at 1 day, before decreasing by 2 days post-injection (Figure 3.3.3.3). Nitrotyrosine-positive cells were observed diffusely dispersed throughout the dorsal columns, with aggregates of nitrotyrosine-positive cells at the base of the dorsal column. As with other labels, there was no apparent lateralisation of labelling for nitrotyrosine on the side of the injection. No such labelling was evident in saline-injected controls (Figure 3.3.3.3) or in LPS-injected animals after 2 days post-injection.

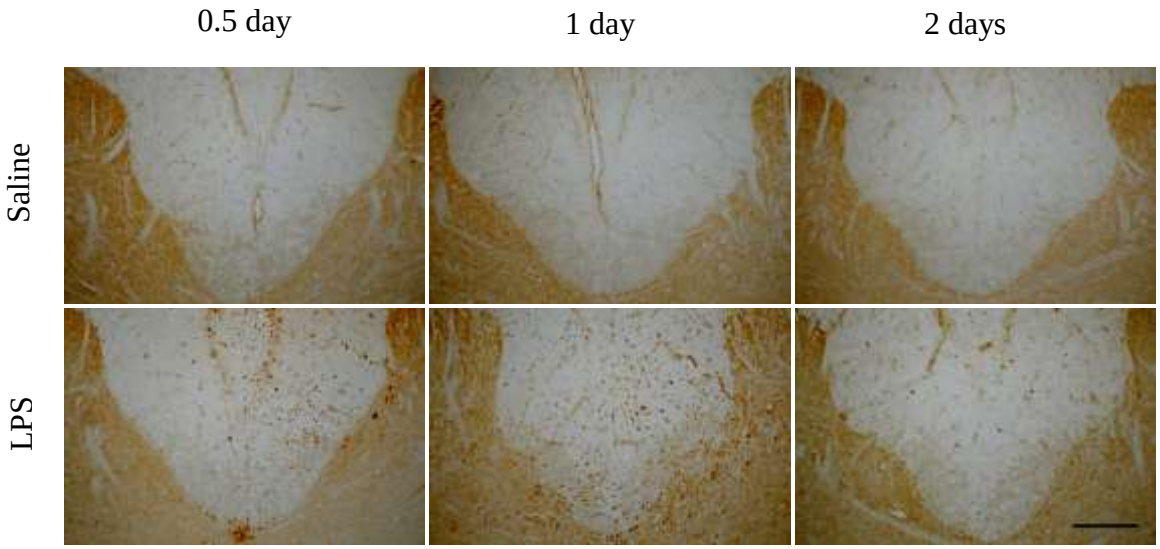

Figure 3.3.3.3: Nitrotyrosine immunoreactivity in the acute lesion
Micrographs of spinal cord sections at the level of the injection of saline (top row) or LPS (bottom row), labelled with an antibody against 3-NT. In the acute lesion (0.5-2 days), immunoreactivity for 3-NT is evident in the dorsal columns of LPS-injected animals, but is absent in saline-injected controls. NT-positive cells can be seen dispersed throughout the dorsal white matter, however clusters of NT-positive cells are also observed in the adjacent grey matter and at the base of the dorsal columns. By 2 days post-injection, immunoreactivity for NT is decreased considerably. Scale bar 200µm. Micrographs are representative.

3.4.0.0 DISCUSSION

The results show that the direct intraspinal injection of LPS into the rat spinal cord results in acute, transient tissue hypoxia, with a concomitant increase in NO and superoxide production, prior to the onset of demyelination. Moreover this 'toxic trio' appears to influence the exact topographical location of the demyelinated lesion that forms two weeks later.

3.4.1.0 Hypoxia is an early feature of the DC LPS lesion

LPS is a common inflammagen that is frequently used to induce an innate immune response in the CNS (Andersson et al., 1992; Bell and Perry, 1995; Stern et al., 2000). In the CNS this endotoxin exerts its actions via Toll-like receptor 4 (TLR4) (Hoshino et al., 1999) on resident microglia (Lehnardt et al., 2003), initiating a cascade of events that can ultimately lead to neurodegeneration. Sites of inflammation are often hypoxic, due to the altered metabolism of the tissue and vascular disturbances. Accordingly, the current study demonstrates that prior to the occurrence of demyelination, the rat spinal grey and white matter labels positive for pimonidazole, a marker of hypoxia, with the extent of labelling greatest at 1 day post LPS injection. The labelling of the grey matter for hypoxia was not surprising given that it represents a highly metabolic compartment of the CNS that is dominated primarily by excitatory synapses (Abeles, 1991; Braitenberg and Schuz, 1998). These synaptic terminals are rich in mitochondria, highlighting synapses as major consumers of metabolic energy (Wong-Riley, 1989; Wong-Riley et al., 1998). Considering that the majority of the energy used by the grey matter goes on signalling processes (Attwell and Laughlin, 2001), one can assume that

although the grey matter is well vascularised, the demand for oxygen simply outweighs its supply, rendering it vulnerable to becoming hypoxic.

Besides, the grey matter labelling, the current study reports that oligodendrocytes and astrocytes, within the dorsal white matter label positive for pimonidazole, 1 day post LPS injection. These results suggest that oligodendrocytes and astrocytes that reside in the base of the dorsal column are vulnerable to hypoxia following the intraspinal injection of LPS. This is in line with previous studies that have shown that chronic hypoperfusion of the rat forebrain causes preferential death of oligodendrocytes, *in vivo* (Masumura et al., 2001). The vulnerability of oligodendrocytes to hypoxia/ischemia is increasingly being recognised, and is largely attributed to a number of their intrinsic properties. During myelination, oligodendrocytes synthesise approximately three times their weight in membrane per day, and eventually support this membrane which accounts for up to a hundred times the weight of the cell body (McLaurin and Yong, 1995; Connor and Menzies, 1996; Ludwin, 1997; McTigue and Tripathi, 2008; Bradl and Lassmann, 2010). Thus, oligodendrocytes are particularly metabolically demanding cells that need to consume large amounts of ATP and oxygen (McTigue and Tripathi, 2008) to support and maintain their extensive membrane. This high metabolic rate inevitably leads to the production of the toxic by-products H_2O_2 and ROS. Furthermore, the enzymes required to synthesise the myelin require iron as a co-factor, resulting in extremely high intracellular concentrations of ROS and iron. Indeed, oligodendrocytes contain the largest intracellular stores of iron in the brain (Cheepsunthorn et al., 1998; Thorburne and Juurlink, 1996), which can predispose them to ROS-mediated damage by evoking free radical formation and lipid peroxidation (Braughler et al., 1986; Juurlink, 1997) via the fenton reaction. Despite their high ROS-generating potential, oligodendrocytes have

a limited capacity to scavenge ROS, containing very low levels of glutathione (Thorburne and Juurlink, 1996). Under inflammatory conditions, where the metabolic demands of the tissue are higher than the supply of oxygen, it is not surprising that oligodendrocytes were found to be hypoxic in the current study.

The study also found that some astrocytes become hypoxic following LPS-injection. Astrocytes, unlike oligodendrocytes, have inherent hypoxia-inducible and anti-oxidant (Eftekharpour et al., 2000) responses. Moreover, astrocytes are the principal site for glycogen storage in the CNS (Phelps, 1972), and they are able to up-regulate anaerobic isoforms of glycolytic enzymes in response to hypoxia (Marrif and Juurlink, 1999). Nevertheless, functional disturbance of astrocytes, defined by the retraction of astrocytic foot processes at the glia limitans, loss of aquaporin IV (AQ-4), and the loss of connexins, which are of fundamental importance for the formation of gap junction between astrocytes and oligodendrocytes, has been recently described in the LPS dorsal column lesion (Sharma et al., 2010). Although astrocytes can adapt to hypoxic conditions by glycolytic ATP production alone (Swanson, 1992), they are particularly vulnerable to the resultant acidosis (Giffard et al., 1990; Swanson et al., 1997). This sensitivity has been attributed to the fact that astrocytes express an electrogenic sodium bicarbonate co-transporter that mediates an inward sodium current (Chen and Swanson, 2003), and is thought to explain astrocytic death following prolonged hypoxia (Giffard et al., 2000). Therefore, perhaps hypoxia precedes and potentially acts as a precursor to the functional disturbances noted in astrocytes following the injection of LPS into the dorsal column.

The transcription factor HIF-1α, an important mediator of hypoxia-induced responses, has been found to be prominently expressed within glia, macrophages and some endothelial cells, in active MS pattern III lesions (Aboul-Enein et al., 2003). The

current study reports the presence of HIF-1α positive cells in the dorsal column of animals injected with LPS, at all time points examined. Evidence of HIF-1α expression was observed as early as 0.5 days post-injection, with the number of HIF-1α positive cells greatest at 1 day post-injection. Moreover, genes, whose expression is under the transcriptional control of HIF-1α, were also increased in the dorsal columns following LPS injection. This finding is consistent with previous studies that show HIF-1α expression in oligodendrocytes, astrocytes and some endothelial cells within Pattern III lesions (Aboul-Enein et al., 2003).

At first glance, one might assume that the stabilisation and accumulation of HIF-1α confirms that the cells within the dorsal columns of LPS-injected animals are hypoxic. However, the interpretation of HIF-1α expression is more complex owing to the fact that this transcription factor is not only stabilised under hypoxic conditions via stabilisation of oxygen-sensitive enzymes involved in its degradation (Semenza, 2007), but is also stabilised by a variety of other mechanisms, including the action of NO adducts (Mateo et al., 2003; Kasuno et al., 2004; Peyssonnaux et al., 2005) and ROS (Brunelle et al., 2005; Guzy et al., 2005; Mansfield et al., 2005). Therefore, determining the exact trigger of HIF-1α stabilisation in an environment where both inflammation and hypoxia are present is complicated. Indeed, the expression of HIF-1α occurring simultaneously with pimonidazole labelling, particularly at the early time points, makes one more inclined to believe that it is the declining concentration of oxygen itself that leads to stabilisation of the transcription factor in this model.

Different cell types would be expected to react differently to low oxygen concentrations depending on their capacity to adapt to such an environment. Indeed, the stabilisation and subsequent nuclear translocation of HIF-1α in macrophages under inflammatory conditions can occur in an oxygen-dependent and oxygen-independent

manner (Peyssonnaux et al., 2005). However, hypoxic activation is important, potentiating the bactericidal activities of these inflammatory cells (Cramer et al., 2003; Peyssonnaux et al., 2005). Active immune cells are adapted to survive in a hypoxic milieu, and one such adaptation is a switch to glycolysis (Oda et al., 2006), which is facilitated by the expression of HIF-1α. This is consistent with the finding that macrophage-like appearing cells label positive for HIF-1α at 3 days post LPS injection in the current study.

HIF-1α supports glycolysis in a number of ways, one of which is the up-regulation of glucose transporters, namely GLUT-1, a glucose transporter expressed by endothelial cells and glial cells. The present study found an increase in expression of GLUT-1 in the dorsal columns of LPS-injected animals, which is consistent with previous findings that hypoxia induces an up-regulation of this glucose transporter (Boardo and Pardridge, 2002), in what appeared morphologically to be endothelial cells and glia. Curiously, glial expression of GLUT-1 was only evident in animals injected with LPS, and in saline-injected controls GLUT-1 expression was restricted to endothelial cells. This shift in the pattern of expression implies that glial cells within the dorsal columns may have switched to glycolysis, in response to HIF-1α signalling, and additional glucose is required to fuel this process to prevent ATP depletion and subsequent cell death. Indeed, astrocytes are capable of switching to glycolytic ATP production under hypoxic conditions (Swanson, 1992), and are the primary glial cell that express GLUT-1 transporters. Perhaps the astrocytes that up-regulate their expression of GLUT-1 are also the ones that do not label for hypoxia.

A major function of HIF-1α under inflammatory conditions is the promotion of angiogenesis (Cramer et al., 2003; Walmsley et al., 2005). VEGF is crucial for angiogenesis, and its expression is controlled by HIF-1α. VEGF initiates angiogenesis,

allowing the tissue to increase its oxygen supply. We report evidence of VEGF expression in the LPS dorsal column lesion at all the time points examined. The expression of VEGF in the lesion was initially suspected to represent a compensatory response to increase the delivery of oxygen and other metabolic substrates by increasing vascularisation (Shweiki et al., 1992; Marti and Risau, 1999). However, an increase in the vascular density was not observed following the injection of LPS in the current study. This finding may be explained by the pattern of expression of VEGF throughout the time course of lesion development. At the early time points, labelling was predominantly cellular, whereas at the later time points labelling progressively became restricted to endothelial cells. This perhaps suggests that VEGF may exert a pathological effect in the LPS DC lesion. VEGF is a known mediator of vascular permeability (Dobrogowska et al., 1998; Rosenstein et al., 1998; Proescholdt et al., 1999; Croll et al., 2004), and recent evidence shows that glial-derived VEGF drives BBB disruption and subsequent neuroinflammation in mice (Argaw et al., 2012). Moreover, hypoxia-induced VEGF expression has also been reported to cause vascular leakage (Schoch et al., 2002). Given that the early expression of VEGF appears to coincide with tissue hypoxia in the LPS DC lesion, BBB disruption and vascular leakage may represent functions of VEGF during the early stages of neuroinflammation. Croll et al (2004) showed that low doses of VEGF infused directly into the neocortex of rats does not result in any significant vascular proliferation, even following 7 days of infusion. Furthermore, VEGF-mediated changes in vascular permeability have been found to precede the angiogenic response *in vivo* (Croll et al., 2004). Perhaps, a similar situation exists in the LPS DC lesion, and angiogenesis may be evident if searched for at subsequent time points.

3.4.2.0 NO, superoxide and nitrotyrosine are present in the acute DC LPS lesion

NO is a messenger molecule, which has been studied extensively for its physiological and pathophysiological functions. The inducible isoform of NOS, iNOS, is expressed in a number of tissues including the CNS, and is regarded as a key source of ROS/RNS (Licinio et al., 1999). Pattern III MS lesions show profound up-regulation of iNOS (Marik et al., 2007). As described previously (Felts et al., 2005), the intraspinal injection of LPS into the dorsal column results in an acute, transient expression of iNOS. This NOS isoform produces large amounts of NO, resulting in its rapid summation within a local region. The diffusion of NO away from its cellular source is thought to be more significant than reactions within the NO producing cell itself (Lancaster, 1994). NO is estimated to diffuse in and out of cells thousands of times in a second (Beckman and Koppenol, 1996). Although NO has a multitude of potentially toxic effects, many of these are probably mediated by the oxidation products of NO. One such oxidation product is the highly potent peroxynitrite anion, formed when NO reacts with superoxide. The current study reports that the intraspinal injection of LPS results in an increase in superoxide production, particularly in the acute lesion, as detected by DHE fluorescence. Visualisation of ROS *in vivo* has previously been proven extremely challenging, due to their highly reactive and unstable nature. However, DHE, by virtue of its ability to permeate cell membranes is increasingly being employed to monitor superoxide production (Bindokas et al., 1996; Owusu-Ansah et al., 2008). Initially, DHE was thought to react with superoxide to produce ethidium, which intercalates with DNA resulting in red fluorescence (Rothe and Valet, 1990; Carter et al., 1994). However, recent studies suggest the DHE and superoxide in fact react to produce 2-hydroxyethidium (Zhao et al., 2003; Zhao et al., 2005). Similar to ethidium, 2-hydroxyethidium also intercalates with DNA resulting in a red fluorescence that is

distinctly different from the fluorescence of ethidium (Zhao et al., 2003; Zhao et al., 2005). Thus, if the correct excitation wavelengths are employed, DHE can be used as an *in vivo* probe for the detection of superoxide production. During inflammation, excessive superoxide may be produced enzymatically by NADPH oxidases, which are located on the cell surface of polymorphonuclear cells and macrophages (Babior, 2000; Babior et al., 2002; Vignais, 2002), and non-enzymatically by dysfunctional mitochondria. However, superoxide is relatively unstable, and therefore spontaneously dismutates to form oxygen and hydrogen peroxide (Fridovich, 1978). When NO levels are elevated, superoxide reacts with NO in a diffusion-limited manner (Huie and Padmaja, 1993) such that almost every collision results in the irreversible formation of peroxynitrite (Beckman and Koppenol, 1996). Peroxynitrite is a highly reactive free radical, with a very short half-life, and therefore interacts with proteins near the site of generation. 3-Nitrotyrosine is a putative footprint of tyrosine residues that have been nitrated by peroxynitrite, and is considered a useful measure of NO-mediated damage. Labelling for 3-nitrotyrosine is evident in the dorsal column following the intraspinal injection of LPS, and corresponds precisely with the pattern of iNOS expression. This finding strengthens the argument that NO and superoxide are present in the acute lesion, and lead to the formation of peroxynitrite. Nitrotyrosine residues are also a feature of acute, but not chronic MS lesions (Liu et al., 2001). The nitration of tyrosine residues in proteins results in the inhibition of phosphorylation, which is crucial to cellular regulation and signal transduction (Martin et al., 1990). However, the transient presence of 3-nitrotyrosine suggests that some kind of repair/removal mechanism exists to take care of damaged proteins, and potentially limit the propagation of damage. The fate of nitrated proteins currently remains unclear. Protein nitration is typically viewed as a cumulative, destructive process, however, evidence suggests that nitrated proteins are

either degraded (Souza et al., 2000) or subjected to enzymatic ‘denitration’ (Gow et al., 1996; Kamisaki et al., 1998), the latter of which implies that protein nitration is a dynamic process which is reversible (Aulak et al., 2004).

3.4.3.0 Hypoxia, NO and superoxide can coalesce to promote ‘hypoxia-like’ demyelination

The demyelination consequent to the intraspinal injection of LPS has been described as ‘hypoxia-like‘, and so it resembles the human MS Pattern III lesion that has previously been attributed to mitochondrial dysfunction as a result of exposure to NO (Aboul-Enein et al., 2003). Although NO probably plays a key role, it may not be sufficient to cause damage alone. Indeed, treatment with dexamethasone, despite reducing the inflammation and suppressing iNOS expression, does not reduce the extent of demyelination following the intraspinal injection of LPS (Felts et al., 2005). In the LPS dorsal column lesion, the demyelination occurs primarily at the base of the dorsal column, but there is no tendency for iNOS positive cells to accumulate in this area. Instead, clusters of iNOS positive cells are seen in the adjacent grey matter, cradling the base of the dorsal column. This adjacent grey matter also labels intensely for hypoxia, and excessive superoxide production. Moreover, labelling for this ‘toxic trio’ is greatest at 1 day post LPS injection, 2 days prior to oligodendrocyte loss within the lesion (Schonberg et al., 2007). Thus, the results suggest that perhaps hypoxia, NO and superoxide may work synergistically to induce damage in vulnerable cells such as oligodendrocytes, thereby promoting ‘hypoxia-like’ demyelination. Indeed, the spatio-temporal nature of the hypoxia, NO and superoxide in LPS-injected animals, appears to determine the exact topographical location of the demyelinated lesion two weeks later,

suggesting that these toxic mediators may work together to mediate the structural damage.

Although hypoxia, NO and superoxide are all independently capable of inducing mitochondrial damage (Bolanos et al., 1994; 1995; 1997; Brorson et al., 1999; Heales et al., 1999; Weinberg et al., 2000), collectively they become a formidable force. NO increases the apparent Km of respiration for oxygen (Brown and Cooper, 1994; Mander et al., 2005), i.e. the amount of oxygen required for cellular respiration, thus sensitising the brain and/or spinal cord to hypoxia (Mander and Brown, 2004). Furthermore, prolonged exposure to NO leads to a persistent, non-competitive inhibition of complex I and other respiratory enzymes by S-nitrosylation (Clementi et al., 1998; Beltran et al., 2000), and this has been found to be enhanced by hypoxia (Frost et al., 2005). The presence and aberrant production of superoxide increases the potential for damage, firstly by elevating free iron levels (Flint and Emptage, 1990; Liochev and Fridovich, 1994; Keyer and Imlay, 1996), thereby increasing the rate of DNA damage, and secondly by promoting the formation of peroxynitrite. Excessive peroxynitrite leads to the nitration of proteins, inhibition of mitochondrial proteins, depletion of cellular energy, DNA damage, and eventually cell death (Virag et al., 2003; Korhonen et al., 2005). Oligodendrocytes have a limited capacity to scavenge ROS and they contain enormous intracellular stores of iron (Thorburne and Juurlink, 1996; Cheepsunthorn et al., 1998), rendering them particularly vulnerable to such an insult.

On one hand, the presence of hypoxia in addition to elevated NO is counterintuitive. One would expect an increase in oxygen concentration, or hyperoxia, to result from mitochondrial inhibition by NO. However, molecular oxygen is an essential substrate required for the production of NO (Stuehr and Nathan, 1989; Leone et al., 1991), and previous studies have reported that after 24 hours of macrophage

activation *in vitro*, all the oxygen consumed by these cells is non-mitochondrial, and that 90% of this is due to iNOS activity (Garedew and Moncada, 2008). Indeed, NOS requires 2 oxygen molecules for every NO molecule produced. Given that the half-life of NO *in vivo* is approximately 1 s, then 170 nmol of oxygen/min would be required per gram of tissue to maintain a steady concentration of 1 µM NO (Beckman and Koppenol, 1996). Tissue dysoxia, a characteristic feature of septic shock, has been attributed to the overproduction of NO, which induces a mitochondrial defect and leads to a decrease in oxygen extraction by tissues (Rees et al., 1998; Garedew and Moncada, 2008). Indeed, copious amounts of NO are produced during chronic inflammatory and degenerative disorders such as MS; therefore, a similar mechanism to that of septic shock may exist in such conditions (Moncada and Erusalimsky, 2002) perpetuating the hypoxic environment. By virtue of its ability to inhibit cytochrome oxidase, NO shifts the electron transport chain to a more reduced state, which is known to enhance superoxide formation (Boveris and Chance, 1973). Studies utilising isolated mitochondria have shown that exogenous NO can also generate superoxide anions (Poderoso et al., 1996). Paradoxically hypoxia-induced ROS production has been shown to occur in a number of different tissues, *in vitro* (Chandel et al., 1998; Guzy et al., 2006). This mechanism of superoxide generation, which occurs at the level of complex III, is thought to involve the stabilisation of HIF-1α (Chandel et al., 2000), thus mediating the response to hypoxia. In this mechanism, the mitochondrial respiratory chain acts as an oxygen sensor, by the concomitant release of hydrogen peroxide with superoxide, the former of which decreases the activity of PHD thereby stabilising HIF-1α (Chandel et al., 1998; Guzy and Schumacker, 2006). Furthermore, this stabilisation can be blocked with mitochondrial-targeted antioxidants (Chandel et al., 1998; Guzy and Schumacker, 2006). Besides its ability to induce mitochondrial ROS formation, hypoxia can also

enhance iNOS expression. The promoter region of iNOS contains a hypoxic response element (HRE), and its expression can therefore be regulated by HIF-1α (Melillo et al., 1995; Palmer et al., 1998). Furthermore, hypoxia-induced iNOS expression has been demonstrated *in vivo* (You and Kaur, 2000; Kaur et al., 2006a). It is of interest that hypoxia, NO and superoxide, are all associated with one another, such that NO can promote both hypoxia (Rees et al., 1998; Garedew and Moncada, 2008) and superoxide (Poderoso et al., 1996), whilst hypoxia can promote the formation of NO (Melillo et al., 1995; Palmer et al., 1998; You and Kaur, 2000; Kaur et al., 2006) and superoxide production (Chandel et al., 1998; Chandel et al., 2000; Guzy and Schumacker, 2006). Thus this 'toxic trio' may not only lead to cell damage, but may also potentiate the toxicity via interacting with one another. The toxic effects of the hypoxia, NO and superoxide presumably spread to neighbouring tissue, potentially explaining why the lesion forms where it does.

Collectively, the current findings suggest that hypoxia, NO and superoxide may work in concert to induce an energy deficit in vulnerable cells such as oligodendrocytes in the LPS dorsal column lesion. Oligodendrocytes, by virtue of their dependence on oxidative metabolism, large surface area, and high polyunsaturated fatty acid content, are presumably highly susceptible to such an insult. Indeed, oligodendrocytes are vulnerable to hypoxia (Husain and Juurlink, 1995; Back et al., 2002), in addition to NO (Mitrovic et al., 1994), and NO mediated damage. In an environment that is simultaneously governed by all three toxic mediators, one might suspect that oligodendrocytic mitochondria may become dysfunctional. This in part, is probably due to enhanced production of superoxide anion, and thereby peroxynitrite formation. Hypoxia has been found to increase the inhibitory effect of NO on mitochondria (Frost et al., 2005), and increase the formation of ROS, potentiating the extent of

mitochondrial dysfunction (Li and Jackson, 2002; Dada et al., 2003; Schumacker, 2003). In the LPS dorsal column model, the oligodendrocytes reside in an actively inflammed environment, with large populations of iNOS positive cells. Therefore, there is increased potential for the formation of ROS/RNS, and hence, a scope for mitochondrial dysfunction. The ensuing mitochondrial damage would impinge on the ability of mitochondrial to produce ATP (Murphy, 2009), thereby leading to an energy deficit in affected oligodendrocytes, and demyelination. Despite these findings, however, a recent study has found that oligodendrocytes can survive without functional mitochondrial complex IV, and do so by increasing their glycolytic capacity (Fünfschilling et al., 2012). Although this novel finding has important implications for CNS metabolism, the study was carried out in normal animals, in which there would presumably be a continuous supply of nutrients required to sustain an increased glycolytic rate in oligodendrocytes. During neuroinflammation, however, the metabolic demand of the tissue may outweigh the supply of nutrients such as glucose that is essential for glycolysis. Thus, perhaps during pathological conditions, such as neuroinflammation, this mechanism of increasing the glycolytic capacity in oligodendrocytes to ensure survival would fail.

3.4.4.0 Conclusion

Demyelination in this proven model of the hypoxia-like, Pattern III MS lesion is preceded by labelling for hypoxia, NO and superoxide, all of which can compromise energy production. These toxic mediators can independently impair mitochondrial function, but they can also act synergistically to suppress ATP production further, eventually causing cell death. The findings suggest that within the inflamed CNS,

oligodendrocytes are particularly vulnerable to an energy crisis that is mediated by this 'toxic trio', resulting in 'hypoxia-like' demyelination. Furthermore, the pathophysiological alterations observed in some astrocytes, namely labelling for hypoxia, may be indicative of a role for dysfunctional astrocytes in the development of a demyelinating lesion.

Clearly, the findings of this study warrant further research. Identifying the cause of hypoxia in these lesions, and the mechanisms through which it causes damage, may provide further insight into the sequence of events that lead to demyelination in MS. Thus therapeutic strategies targeted to increase oxygen delivery, inhibit iNOS and scavenge ROS, may prove beneficial in limiting the extent of structural damage.

CHAPTER FOUR

VULNERABILITY OF THE CNS TO HYPOXIA

4.1.0.0 INTRODUCTION

The brain is a metabolically expensive organ, consuming 20% and 10% of the total oxygen (Afifi and Bergman, 2005) and glucose (McKenna et al., 2006), consumed by the body, respectively. Despite this, due to the toxicity of oxygen (Acker, 2005), many mechanisms exist not only to maintain low oxygen conditions in the brain during 'rest', but also to increase oxygenation during periods of activity (Allison et al., 2000). Thus, the oxygen tension of the brain is spatially and temporally heterogeneous. It seems reasonable to presume that due to the vascular architecture, limited glycogen stores, and other intrinsic characteristics, the brain is inherently susceptible to hypoxic insults. Indeed, cortical atrophy has been found in Everest climbers (8848m), and subcortical lesions in inexperienced climbers (Fayed et al., 2006). In addition to such regional vulnerabilities, selective cellular vulnerabilities also exist. Neurons (Goldberg and Choi, 1993) and oligodendrocytes (Husain and Juurlink, 1995; Lyons and Kettenmann, 1998) are particularly vulnerable to perturbations of oxygen concentration, compared with microglia and astrocytes, in culture (Lyons and Kettenmann, 1998). This selective vulnerability is thought to be due to differences in their metabolic make-up (Belanger et al., 2011), and susceptibility to oxidative stress, essentially due to cellular differences in the capacity to scavenge free radicals effectively (Juurlink et al., 1997).

Although hypoxia is an important signal that regulates a wide range of physiological responses, it is also a feature of a number of pathological conditions,

including inflammation. However, the role hypoxia plays in such conditions is unclear. Hypoxia essentially results in the depletion of cellular ATP stores and a subsequent switch to anaerobic glycolysis, which requires a continuous supply of glucose. Given that vascular disruption and nutrient supply are frequently associated with inflammation, one can imagine that hypoxia may potentiate the inflammatory response, even in the CNS. Indeed, severe hypoxia is increasingly being recognised as a neuroinflammagen (Ock et al., 2005), with hypoxia-induced microglial activation suggested to contribute to neuronal damage in stroke as well as in neurodegeneration (Gonzalez-Scarano and Baltuch, 1999). Despite this, little is known about the effects of acute, moderate hypoxia on the naïve spinal cord. MS lesions, characterised by chronic neuroinflammation, show a predilection for the spinal cord. The current study therefore aims to investigate the histopathological correlates of acute hypoxia in the rat spinal cord, to gain an insight into how it may contribute to neuropathology.

4.1.1.0 Aims

1. Identify regions of vulnerability to hypoxia, in the rat spinal cord.
2. Identify cellular vulnerabilities to hypoxia.
3. Determine histopathological changes in response to acute hypoxia.

4.1.2.0 Hypothesis

Regional and cellular vulnerabilities to hypoxia exist in the rat spinal cord.

4.2.0.0 MATERIALS AND METHODS

4.2.1.0 Animals

Female Dark Agouti (DA) rats (163.7g ±7.8, mean ± standard deviation; SD) were exposed to normobaric hypoxia by substituting oxygen with nitrogen using a ProOx 110 controller (Biospherix Ltd, Salem, NY) in a closed hypoxia chamber (Biospherix Ltd). The hypoxic environment was gradually introduced by decreasing the oxygen from 21 to 10% over 20 minutes, prior to continuous exposure to 10% oxygen for 6 hours (h) (n =3), 24 h (n = 6), 48 h (n = 6) and 72 h (n = 6). Control animals were kept in the same chamber, on different days, but exposed to room air (21% oxygen) (n = 6). Food and water were available *ad libitum*.

4.2.2.0 Tissue Processing

A pimonidazole (HPI Inc, Burlington, MA) dose of 180 mg/kg body weight was administered intravenously into the saphenous vein of all animals, under light, brief anaesthesia, with 2% isoflurane, 4 hours prior to perfusion. All animals were terminally anaesthetised with isoflurane, and trans-cardially perfused with phosphate-buffered saline, and then 4% paraformaldehyde (PFA) for fixation. To visualise the spinal cord vasculature, animals exposed to 6 hours of 10% oxygen were additionally perfused with the fluorescent carbocyanine lipophilic dye, DiI (Molecular Probes, Eugene, OR) prior to PFA perfusion, as previously described (Li et al., 2008). The spinal cords were harvested and post-fixed in 4% PFA overnight, prior to cryoprotection in 30% sucrose. The spinal cords were then segmented into 1cm pieces, and frozen by immersion in isopentane pre-cooled in liquid nitrogen, and samples stored at -80^0C until cut. Twelve

micron thick transverse sections (or 20 µm-thick sections for the study of the vasculature) were cut with a cryostat (Leica Microsystems, Germany) at -20^{0}C, and thaw-mounted onto glass slides. The sections were stored frozen at -20^{0}C until use.

4.2.3.0 Histology

4.2.3.1 IHC/IF

Cyrosections (12µm thick) were air dried and examined immunohistochemically or immunofluorescently for a range of markers (Table 4.2.3.1), as described previously (section 2.2.3.1).

4.2.3.2 Double label IHC

Double label IHC with anti-pimonidazole and anti-RECA1 antibodies was performed on tissue from animals exposed for 6 hours to 10% oxygen and perfused with DiI, to identify areas of vulnerability to hypoxia. Double label IHC with anti-pimonidazole and OX-6 antibodies, was also performed on tissue from animals exposed to 24, 48 and 72 hours 10% oxygen, to determine whether there was a tendency for cells capable of antigen presenting to become activated in hypoxia-susceptible areas of the cord.

Sections of spinal cord containing vasculature labelled with the lipophillic dye DiI (Invitrogen, UK), were imaged using a LSM 5 Pascal confocal microscope (Zeiss), prior to proceeding with the IHC protocol. The sections were then processed as above (section 2.2.3.1) with mouse monoclonal antibody against pimonidazole. After developing with DAB, the sections were rinsed in running tap water before incubating in 3% H_2O_2 in PBS for 20 minutes. Next, the sections were incubated with avidin for 15 minutes, briefly rinsed in PBS, and then incubated with biotin for 15 minutes

(Avidin/Biotin Blocking kit; Vector Laboratories Ltd). PBST (0.1% BSA in PBS containing 0.2% Triton-X 100) washes were performed between each step. Sections were incubated with blocker (10% horse serum in PBS containing 0.1% Triton X-100) for at least 30 minutes before incubating with either mouse anti-RECA1 or mouse OX-6 primary antibodies, overnight at 4^{o}C. The following day, the sections were processed as normal by incubating with biotinylated horse anti-mouse secondary antibody followed by incubation with ABC. Finally, RECA-1 and/or OX-6 immunoreactivity was developed using DAB-Ni (Vector Labs), which yields a black colour, followed by dehydration and mounting, as described above.

Table 4.2.3.1: Antibody details for IHC/IF

Antibody	Target	Isotype	Pre-Treatment	Blocker	Dilution	Supplier
Mouse Hypoxyprobe-1-Mab Anti-pimonidazole	Pimonidazole adducts	Mouse IgG_1	$NaBH_4$	0.25% casein (VWR International, UK), in PBS containing 0.1% Triton X-100	1:500	HPI Inc
Mouse Anti-Ox-6	MHC-II Ia	Mouse IgG_1	N/A	5% horse serum (Sigma) in PBS containing 0.1% Triton X-100 10% horse serum for double label IHC	1:600	Abcam
Mouse Anti-RECA-1	Rat Endothelial Cells	Mouse IgG_1	N/A	5% horse serum (Sigma) in PBS containing 0.1% Triton X-100 10% horse serum for double label IHC	1:200	Abcam
Mouse Anti-rat ED1	Activated Macrophages /Microglia (phagocytes)	Mouse IgG_1	N/A	5% horse serum (Sigma) in PBS containing 0.1% Triton X-100	1:200	Serotec
Mouse Anti-GFAP	Astrocytes	Mouse IgG_1	N/A	5% horse serum (Sigma) in PBS containing 0.1% Triton X-100	1:200	Sigma
Rabbit Anti-pimonidazole	Pimonidazole adducts	Rabbit IgG	$NaBH_4$	5% goat serum (Sigma) in PBS containing 0.1% Triton X-100	1:200	HPI Inc
Rabbit Anti-TLR4	Toll-like receptor 4	IgG	Target retrieval solution, pH6.1 (DAKO) at 40^{o}C for 40 minutes	5% goat serum (Sigma) in PBS containing 0.1% Triton X-100	1:200	Abcam

Rabbit Anti-inducible nitric oxide synthase (iNOS)	iNOS (activated macrophages/ microglia)	Rabbit IgG	N/A	5% goat serum (Sigma) in PBS containing 0.1% Triton X-100	1:200	BD Transductions
Rabbit Anti-GFAP	Astrocytes	Rabbit IgG	N/A	5% goat serum (Sigma) in PBS containing 0.1% Triton X-100	1:500	DAKO
Rabbit Anti-carbonic anhydrase 2 (CA2)	Oligodendrocytes	Rabbit IgG	$NaBH_4$	5% goat serum mixed in PBS containing 0.1% Triton X-100	1/200	Kindly provided by N. Gregson
Rabbit Anti-NG2	Chondroitin sulphate proteoglycan (oligodendrocyte precursor cells)	IgG	Target retrieval solution, pH6.1 (DAKO) at 40°C for 40 minutes	5% goat serum (Sigma) in PBS containing 0.1% Triton X-100	1:500	Millipore
Goat Anti-P-Selectin	P-Selectin	IgG	Target retrieval solution, pH6.1 (DAKO) at 40°C for 40 minutes	5% goat serum (Sigma) in PBS containing 0.1% Triton X-100	1:50	Santa Cruz
Rabbit Anti-IBA	Macrophages /Microglia	Rabbit IgG	N/A	5% goat serum (Sigma) in PBS containing 0.1% Triton X-100	1:500 (IHC) 1:200 (IF)	WAKO

4.2.4.0 3D Reconstruction

In order to determine the distribution of pimonidazole labelling in relation to the vasculature, a 3D reconstruction was performed on serial sections that were double labelled with anti-pimonidazole and anti-RECA1 antibodies using a software programme known as Reconstruct (Fiala, 2005). Briefly, micrographs of the serial sections, of a region of interest, were loaded into the software (Figure: 4.2.4.0 A), prior to manual alignment of individual sections. Next, areas of pimonidazole labelling and the vasculature were manually delineated in each section (Figure: 4.2.4.0 B-C), and linked to one another, so that one vessel or pimonidazole region in one section was recognised in an adjacent section. DiI confocal images were then overlaid onto their respective DAB-labelled sections to confirm whether all the delineated vessels were, in fact vessels. Subsequently, the sections were reconstructed into a 3D scene, using the software, and the distances between individual vessels and pimonidazole labelled regions were calculated.

A

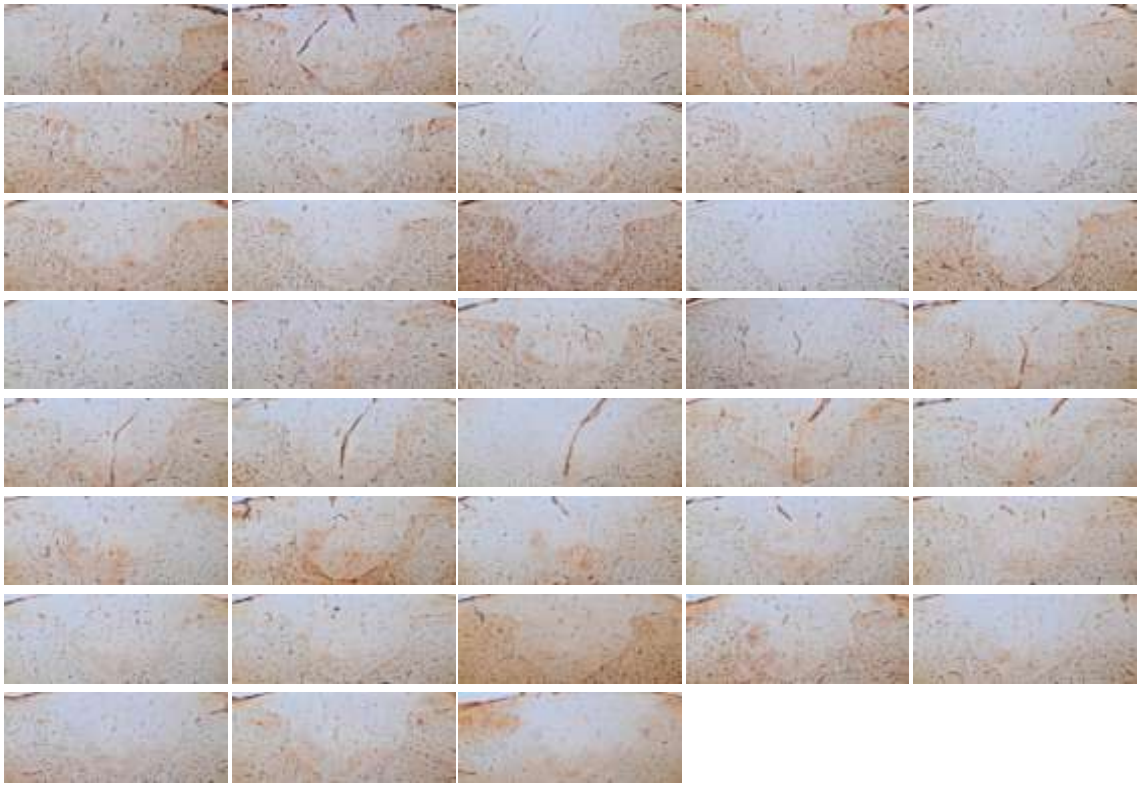

B

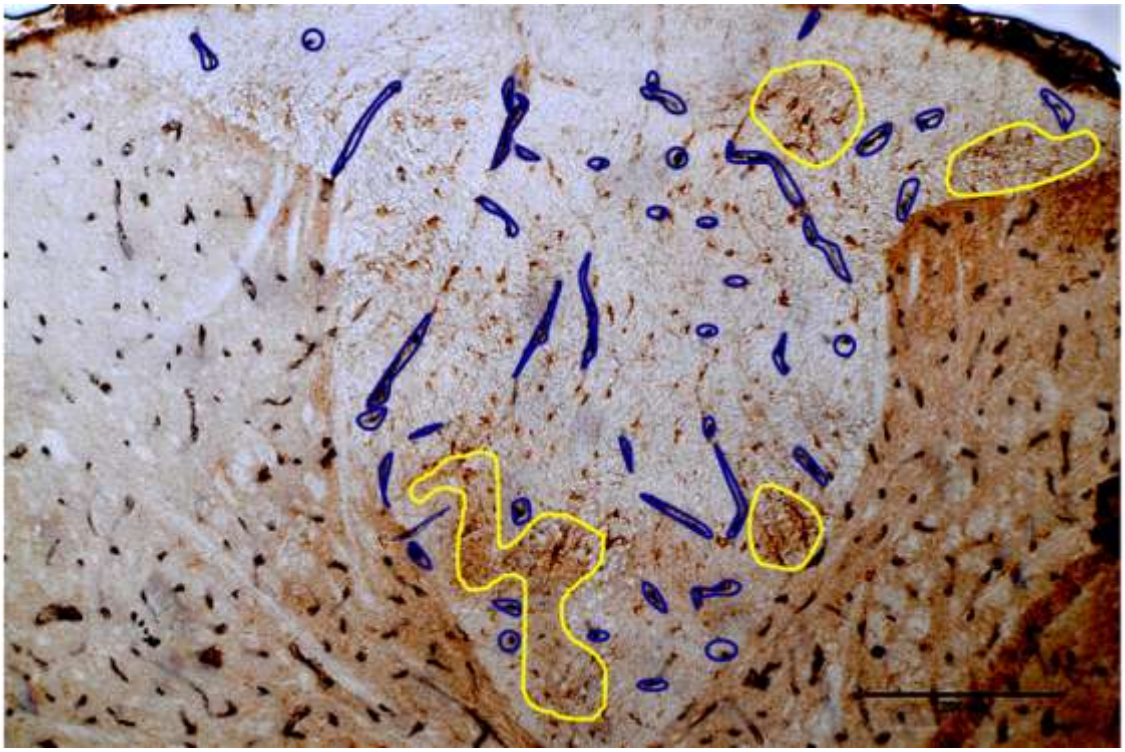

C

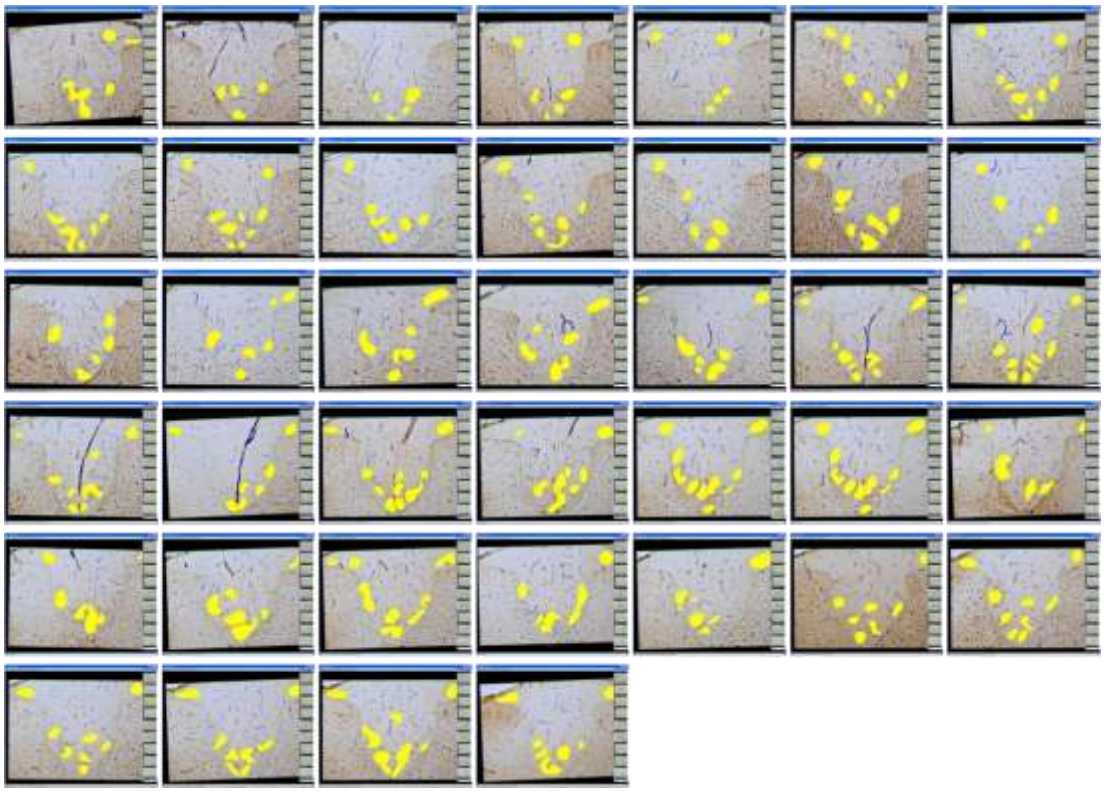

Figure 4.2.4.0: 3D reconstruction of serial histological sections

(A) Serially immunolabelled sections (pimonidazole: brown, RECA-1: black) were photographed and imported into the software. (B) Sections were manually aligned, and pimonidazole positive regions (yellow), and RECA-1^{+} vessels (blue), delineated. (C) This was repeated for every section to enable accurate reconstruction.

4.2.5.0 Microscopy

4.2.5.1 Light Microscopy and Quantification

Tissue stained with DAB was viewed using an Axiophot light microscope (Zeiss, Germany) and pictures taken with a Nikon D300 camera (Nikon, USA). The illumination was kept constant throughout image acquisition. Analysis of the intensity of the labelling with pimonidazole was carried out by tracing around the spinal cord sections (white and grey matter, and grey matter alone), and measuring the pixel intensity using Image J (National institute of health, USA). Quantification of OX-6 positive cells, and phenotype, was carried out manually, at different levels of the cord using Image J. Quantification of all other markers was carried out using the 'analyse particles' tool, on thresholded images, to determine the number, and occasionally the size, of positively labelled cells. The same criteria were used for each image, and area measurements were carried out concurrently.

4.2.5.2 Confocal Laser Microscopy

Confocal fluorescent images were obtained using a Zeiss LSM5 Pascal confocal microscope, with a 40x objective. Excitation wavelengths of 488 nm and 543 nm were provided by argon and helium-neon gas lasers, respectively. Emission filters BP505-530 and LP560 were used for obtaining the images.

4.2.6.0 Statistical Analysis

All data were tested for normality using either the Kolmogorov-Smirnov or the Shapiro-Wilk test, and the stability of variances assessed using the Levene's test. Data that were not normally distributed were evaluated using non-parametric statistics as indicated. P-values of $p<0.05$ (*), $p<0.01$ (**) and $p<0.001$ (***), were considered as statistically significant. All statistical analyses were carried out using SPSS version 14.0 (USA).

4.2.6.1 Statistical Analysis of Pimonidazole Intensity

The pixel intensity of the pimonidazole labelling was normally distributed in all spinal cord sections examined. Therefore, the percentage of pixels labelled with an intensity greater than the control mean plus one standard deviation were counted and compared to the appropriate vertebral segment-matched control using a two-way ANOVA; the room air treatment group and saline-injected group served as controls in each of the respective experiments.

4.2.6.2 Statistical Analysis of Other Labels

The data obtained from sections labelled with RECA-1 followed a normal distribution, therefore, the independent t-test was used to compare the RECA-1 cell density, at each spinal cord segment, between the four groups (24h 10%, 48h 10%, 72h 10% and 21% oxygen) in the acute hypoxia study. The data obtained from sections labelled with OX-6 did not follow a normal distribution, and were therefore analysed using the Mann-Whitney U test. A repeated measures ANOVA was used to compare the cumulative RECA-1 and OX-6 cell densities, between 10% and 21% oxygen. Regression analysis

followed by a Mann-Whitney U test (pairwise comparison) was used to compare the mean cell density of IBA, TLR4 and NG2 data between the two experimental groups. Pearson's Correlation was used to determine if there was any correlation between the intensity of pimonidazole labelling and RECA cell density.

4.3.0.0 RESULTS

4.3.1.0 Exposure to mild hypoxia induces weight loss in DA rats

Exposure of DA rats to 10% oxygen for 24, 48 or 72 hours induced loss of body weight (Figure: 4.3.1.0). The weight loss, recorded as a percentage of the initial body weight, increased with the duration of exposure to 10% oxygen. Following 24 hours of sustained 10% oxygen exposure, an average of 5% of the initial body weight was lost, increasing to 7% and 9% following 48 and 72 hours of 10% oxygen, respectively. No weight loss was observed in the animals exposed to 21% oxygen; in fact they gained 1% of their initial body weight.

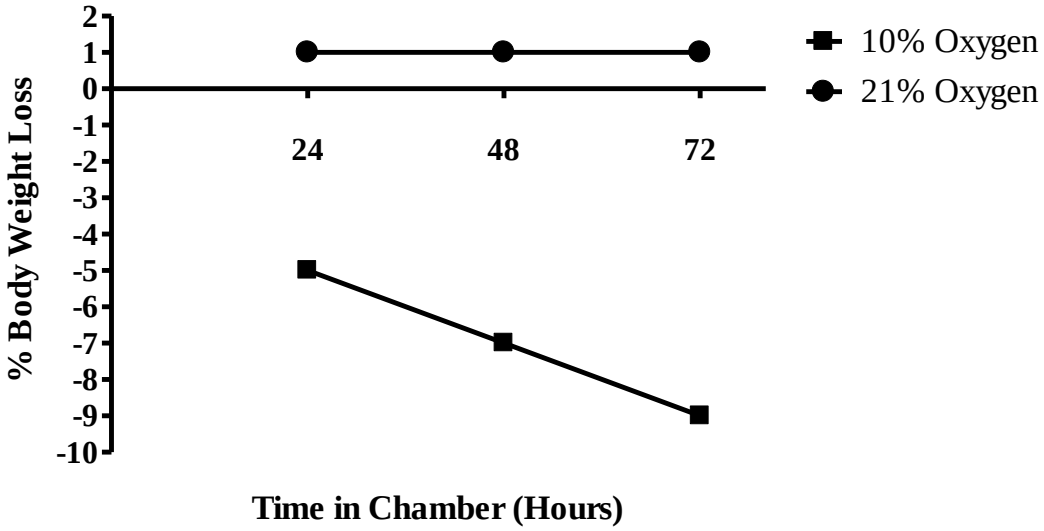

Figure 4.3.1.0: Effect of hypoxia on body weight
A graph showing the percentage loss in body weight in the experimental groups. Values are means. N = 6 per group.

4.3.2.0 Pimonidazole labelling is increased in animals exposed to 10% oxygen

Reducing the inspired oxygen to 10% revealed regions of clear pimonidazole labelling, and thus regions seemingly vulnerable to hypoxia in the rat spinal cord. The white matter of the spinal cord was found to be particularly vulnerable to decreases in inspired oxygen, with the base of the dorsal column, the 'wing' tips, the areas just below the dorsal horns, and a 'halo' of white matter surrounding the grey matter (Figure: 4.3.2.0 A) labelling most strongly for pimonidazole. Such labelling was frequently, if not always, present in all animals exposed to 10% oxygen for 6 hours (Figure: 4.3.2.0 B). At the base of the dorsal column, these areas of pimonidazole labelling were approximately 225-900 μm in length longitudinally, whereas, in the 'wing' tips, the areas of intense labelling were approximately 225-300 μm in length longitudinally. Areas of intense pimonidazole labelling were not observed in the white matter of animals kept at 21% oxygen (Figure: 4.3.2.0 B).

To determine the spatial distribution of labelling for pimonidazole in relation to the location of vessels, double labelled IHC was carried out on serial spinal cord sections from animals exposed to 10% oxygen for 6 hours. 3D reconstruction of a 1 mm length of dorsal column spinal cord tissue, labelled for pimonidazole, RECA1 and DiI, the latter administered transcardially during perfusion, revealed that these pockets of pimonidazole labelling actually occur in between vessels (Figure: 4.3.2.0 C), and particularly in areas where the vessel density is low, such as the 'wing-tip' areas and the base of the dorsal columns.

A

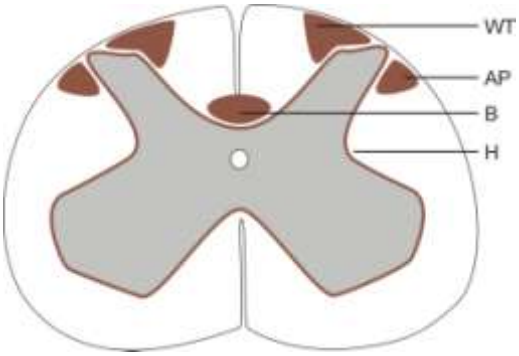

B

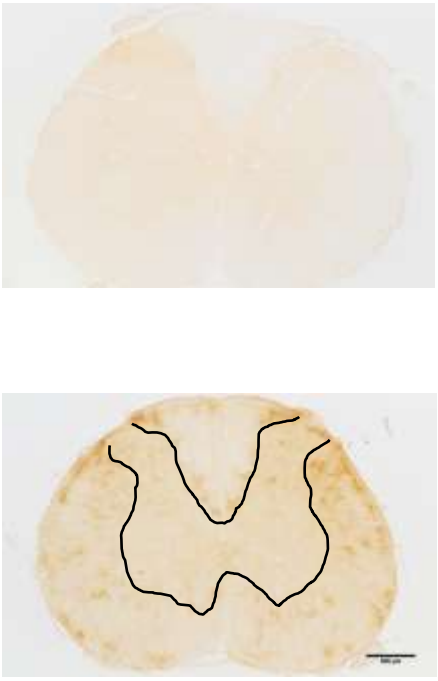

C

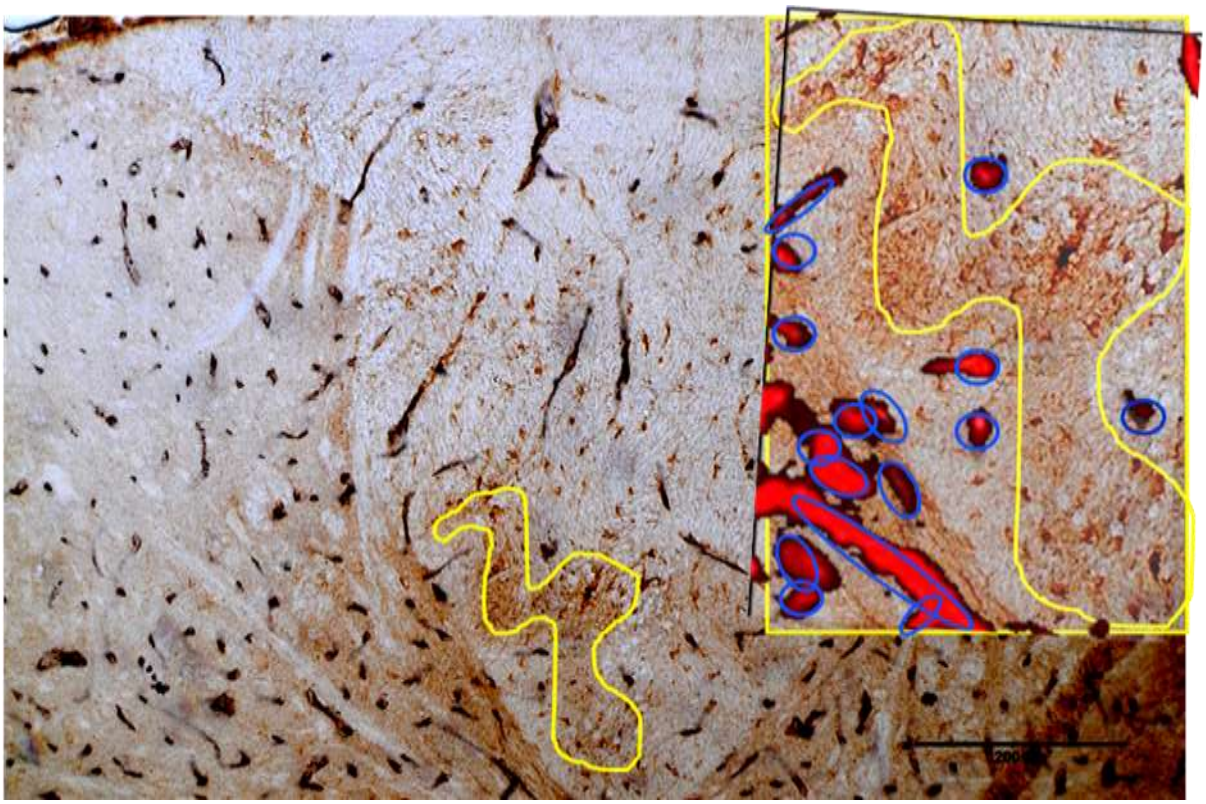

D

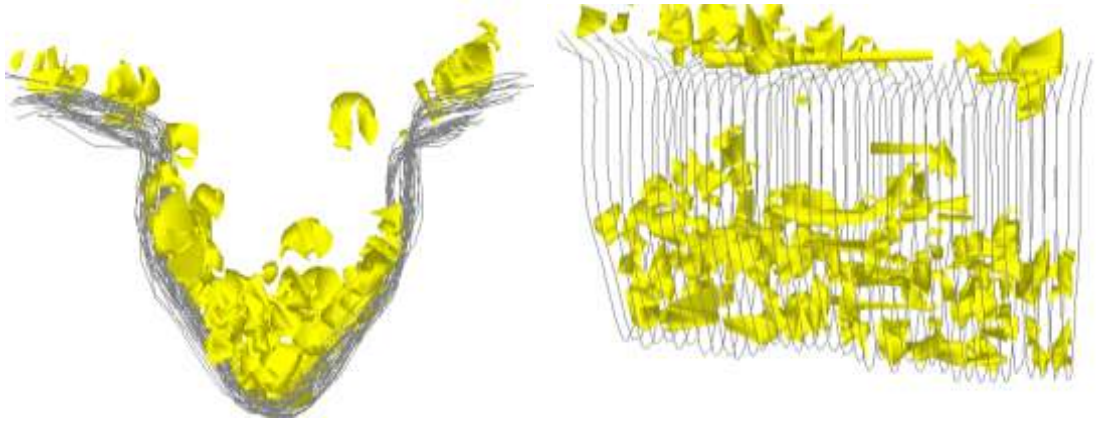

Figure 4.3.2.0: Pimonidazole labelling following 6h 10% oxygen

(A) Schematic showing areas of the spinal cord that frequently label with pimonidazole following exposure to 10% oxygen delineated in brown (WT: 'wing-tip' regions of the dorsal column; B: base of the dorsal column; AP: white matter directly below the superficial dorsal horns; H: a 'halo' of white matter surrounding the grey matter. (B) Spinal cord sections from animals exposed to 10% or 21% oxygen, labelled with pimonidazole, showing positive labelling for pimonidazole in the animal exposed to 10% oxygen, and negative labelling in the animal exposed to 21% oxygen. Scale bar 500µm. (Ci) Sections of spinal cord from an animal exposed to 10% oxygen, and labelled with pimonidazole (brown) and RECA-1 (black), showing that areas of intense pimonidazole labelling at the base if the dorsal column, occur between vessels. Bar 200 µm. Inset shows of an area of pimonidazole labelling (yellow outline), superimposed on an image with DiI labelled vessels (red fluorescence), showing that areas of pimonidazole labelling appear to occur in-between vessels (blue circles/ red fluorescence). Image taken from the base of the dorsal column. (D) 3D reconstruction of the dorsal column from an animal exposed to 10% oxygen, showing the location of areas of intense pimonidazole labelling (yellow), and thus the increased vulnerability of the base of the dorsal column to hypoxia. The illustration on the left shows the dorsal column as viewed from the head to the tail, while the illustration on the right shows the dorsal column as viewed from the side. Micrographs are representative.

4.3.3.0 Acute hypoxia and the spinal cord

4.3.3.1 Pimonidazole labelling occurs in a spatio-temporal manner in animals exposed to 10% oxygen

To identify areas of vulnerability to hypoxia in animals exposed to 24, 48 and 72 hours of 10% oxygen, pimonidazole IHC was carried out on spinal cord sections at different vertebral levels. As described in section 4.3.2.0, both grey and white matter labelling for pimonidazole was observed (Figure: 4.3.3.1 A). Specifically, two patterns of white matter labelling emerged, namely cell-specific labelling (see section 4.3.3.2) and foci of pimonidazole labelling (see section 4.3.3.3) (Figure: 4.3.3.1 A). No such labelling was observed in animals exposed to 21% oxygen (Figure: 4.3.3.1 A). The mean differences in the intensity of the pimonidazole labelling of the total cord (grey matter and white matter combined), and the white matter alone, in animals exposed to 10% or 21% oxygen were statistically significant ($p = 0.04$, $p = 0.01$, respectively). However, there was not a statistically significant difference in the intensity of pimonidazole labelling of the grey matter ($p= 0.088$), between the two groups. The length of exposure to 10% or 21% oxygen did not affect the extent of pimonidazole labelling (total: $p = 0.998$; white matter: $p = 0.891$; grey matter: $p = 0.915$). In all animals exposed to 10% oxygen, there appeared to be a rostro-caudal gradient of pimonidazole labelling, regardless of the duration of exposure (Figure: 4.3.3.1 B-D). When taking into account the labelling of the white matter and grey matter combined, the intensity of pimonidazole labelling increased in the thoracic and cervical spinal cord (Figure: 4.3.3.1 B). A similar pattern was found when just measuring the intensity of the white matter, however, the increased labelling within these two areas of the spinal cord was more prominent (Figure: 4.3.3.1 C). The labelling for pimonidazole in the grey matter, however, showed a noticeable

decrease in the thoracic spinal cord (Figure: 4.3.3.1 D). Interestingly, the different spinal cord levels examined showed a different response to 10% oxygen. The lumbar spinal cord was most affected by 72 hours of 10% oxygen, whereas the upper thoracic spinal cord was most affected by 24 hours of 10% oxygen (Figure: 4.3.3.1 B-D).

A

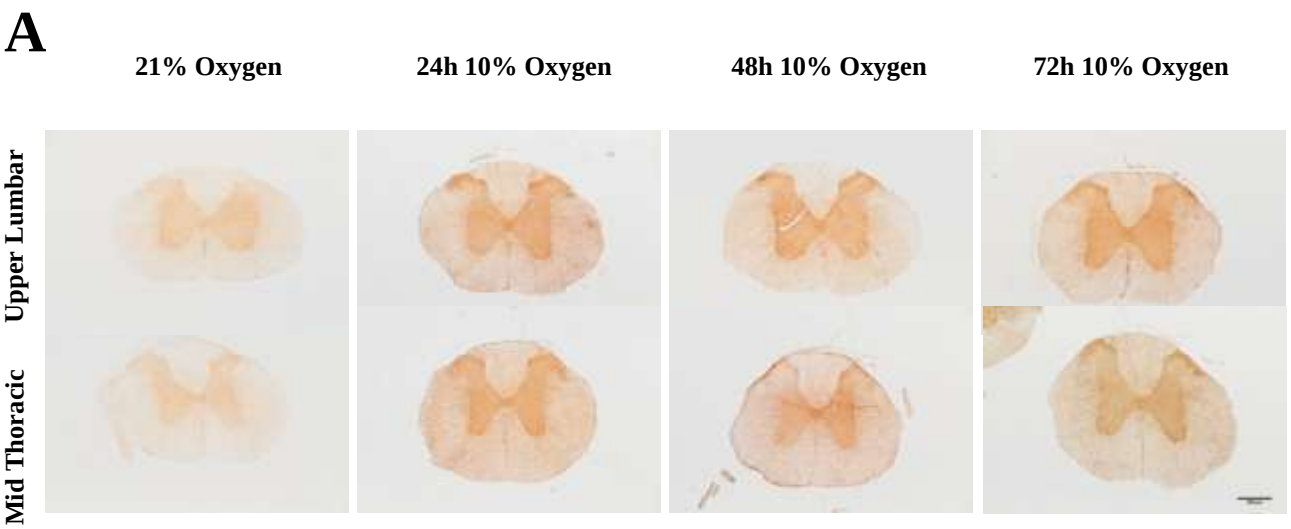
21% Oxygen
24h 10% Oxygen
48h 10% Oxygen
72h 10% Oxygen
Upper Lumbar
Mid Thoracic

B

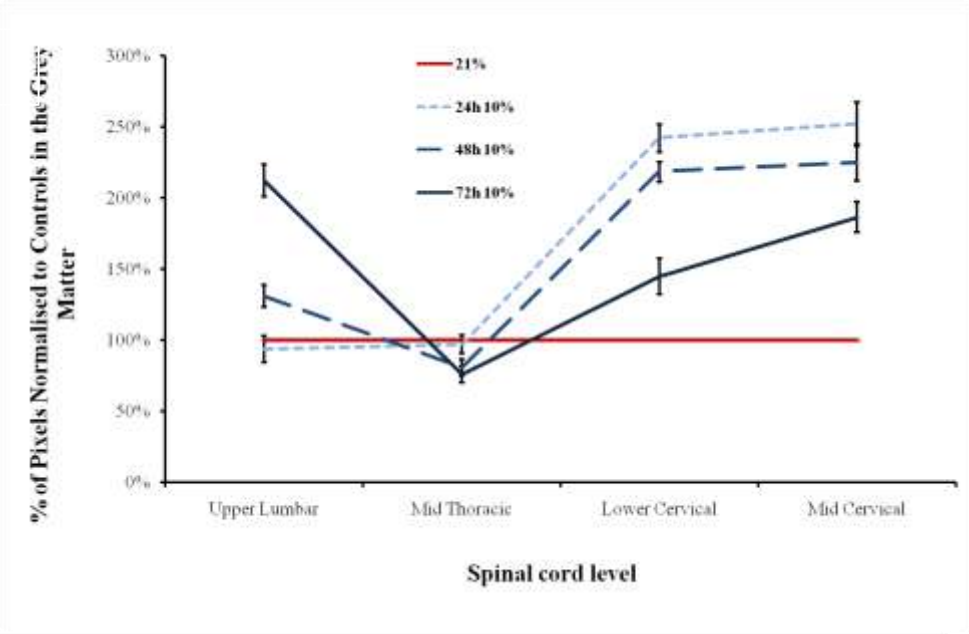
% of Pixels Normalised to Controls in the Grey Matter
300%
250%
200%
150%
100%
50%
0%
21%
24h 10%
48h 10%
72h 10%
Upper Lumbar
Mid Thoracic
Lower Cervical
Mid Cervical
Spinal cord level

C

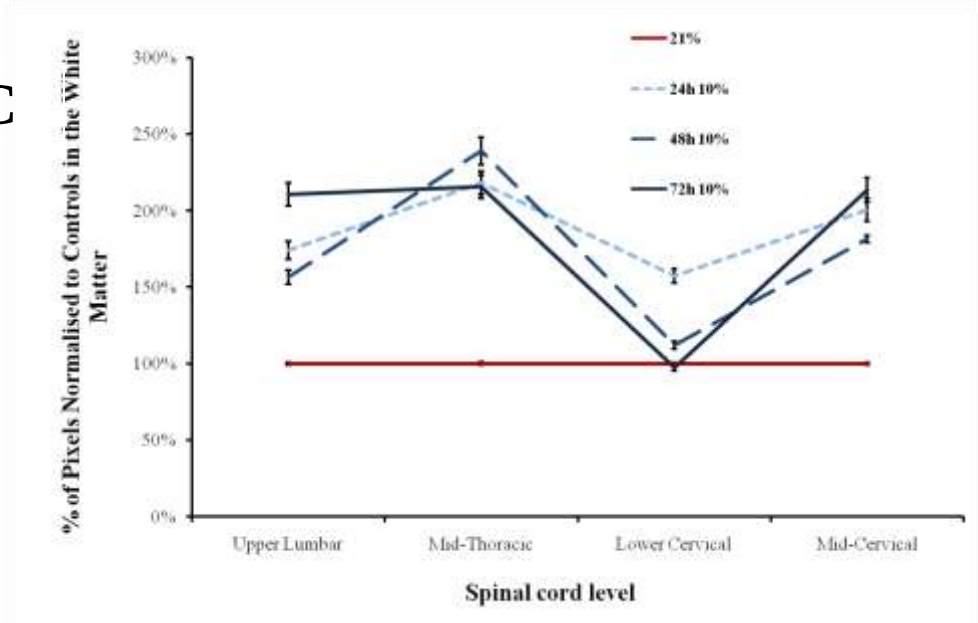
% of Pixels Normalised to Controls in the White Matter
300%
250%
200%
150%
100%
50%
0%
21%
24h 10%
48h 10%
72h 10%
Upper Lumbar
Mid-Thoracic
Lower Cervical
Mid-Cervical
Spinal cord level

Figure 4.3.3.1: Pimonidazole labelling following exposure to 10% oxygen

(A) Micrographs of sections of spinal cord from the upper lumbar and mid-thoracic levels from animals exposed to either lifetime 21%, 24h 10%, 48h 10% or 72h 10%, oxygen, labelled with pimonidazole. Pimonidazole labelling is increased following exposure to 10% oxygen, in both the white and grey matter. Scale bar 500 µm. (B-C) The intensity of pimonidazole labelling varies rostro-caudally in animals exposed to 10% oxygen. The intensity of pimonidazole labelling in the grey matter is increased in the upper lumbar, lower thoracic and mid-cervical cord, but is considerably decreased in the mid-thoracic region, compared with 21% control. (B). There is also a shift from increased labelling in the caudal portions of the cord in animals exposed to 10% oxygen for longer periods, to increased labelling in the rostral portions of cord in animals exposed to 10% oxygen for shorter periods. (C) Labelling in the white matter, is increased in the upper lumbar, mid-thoracic and mid-cervical cord, but decreases in the lower cervical cord. Values are means ± S.D. N=6 per group.

4.3.3.2 Cell-specific labelling with pimonidazole, following acute hypoxia

Besides the grey matter labelling for pimonidazole, a number of cells within the spinal white matter also labelled for pimonidazole (Figure: 4.3.3.2 A), following exposure to acute hypoxia. The positive cells, morphologically, had the appearance of glia, and endothelial cells, therefore double label immunofluorescence was performed to determine their identity.

Arrays of cells labelled positive for pimonidazole in longitudinal sections following exposure to 10%, oxygen at all time points, but co-localisation with GFAP was not observed suggesting that the labelled cells were not astrocytes (Figure: 4.3.3.2 B). Similarly, microglia did not co-localise with pimonidazole at any time point following exposure to 10% oxygen (Figure: 4.3.3.2 C). However, the microglia were found to be closely associated with the pimonidazole-positive cells, often adjacent to, or in between, the array of positively labelled cells (Figure: 4.3.3.2 C). Further double label immunofluorescence with an antibody directed against oligodendrocytes confirmed that these pimonidazole-positive cells were oligodendrocytes (Figure: 4.3.3.2 D). Beautiful arrays of pimonidazole and CA2 positive cells were observed, at all time points following exposure to 10% oxygen. Most, if not all, oligodendrocytes were found to co-label for pimonidazole. Some endothelial cells also co-labelled with pimonidazole in animals exposed to 10% oxygen, at all time points examined (Figure: 4.3.3.2 E).

A

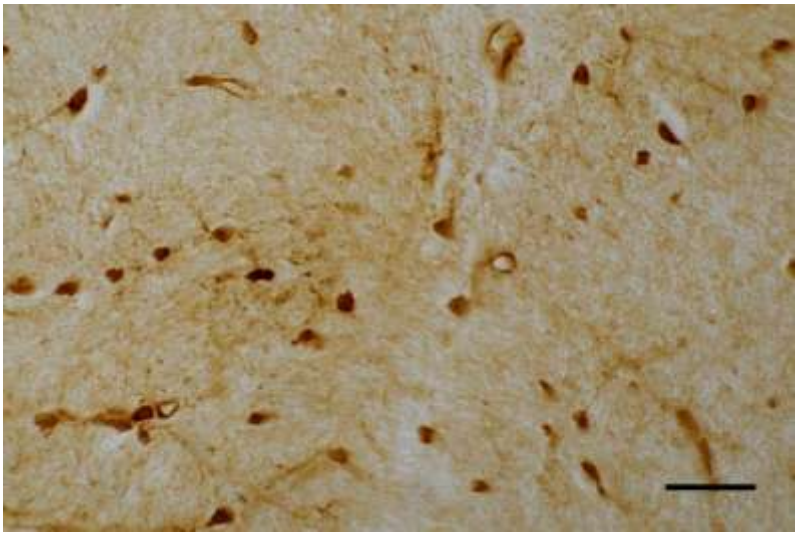

B

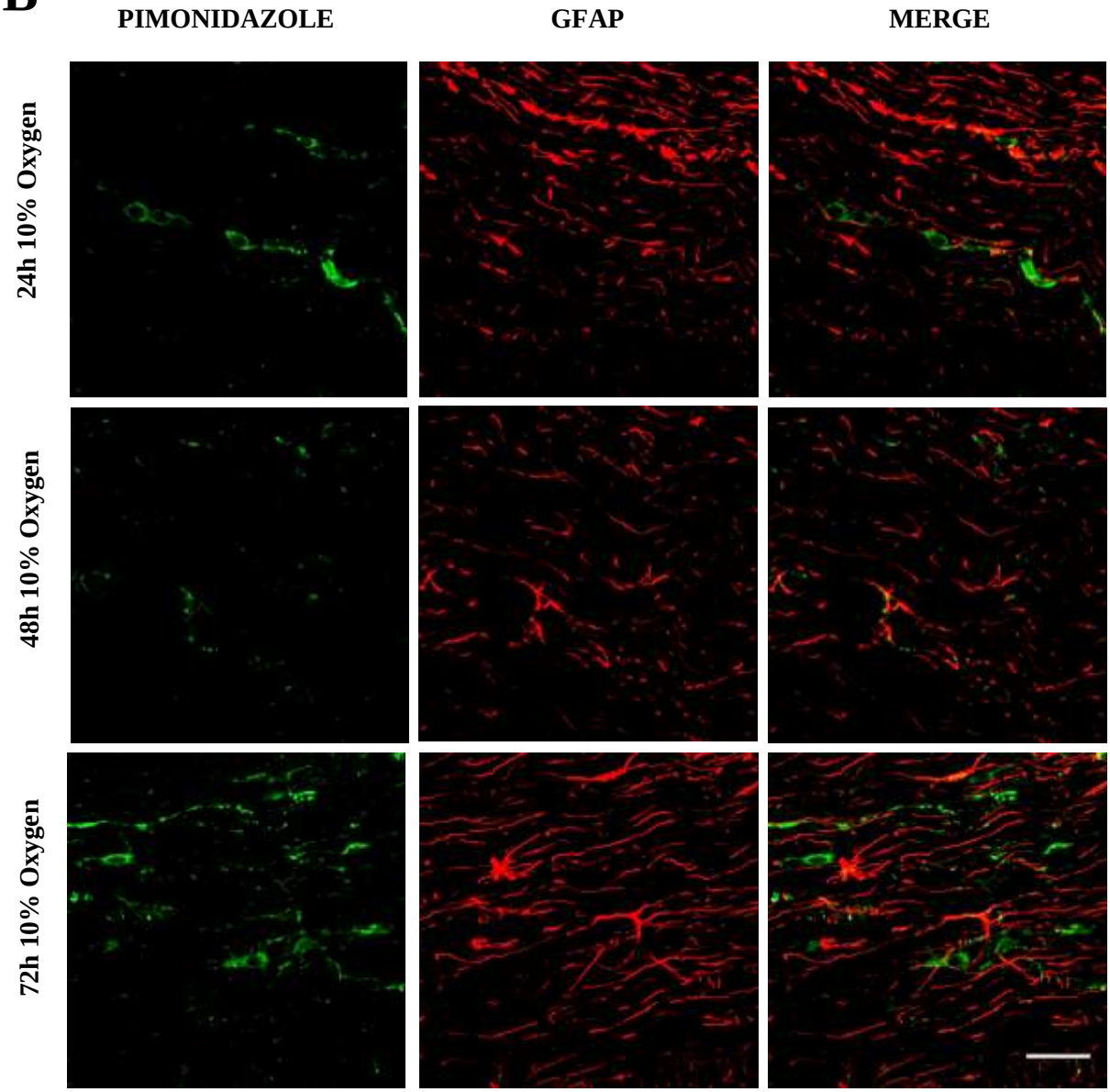
PIMONIDAZOLE
GFAP
MERGE
24h 10% Oxygen
48h 10% Oxygen
72h 10% Oxygen

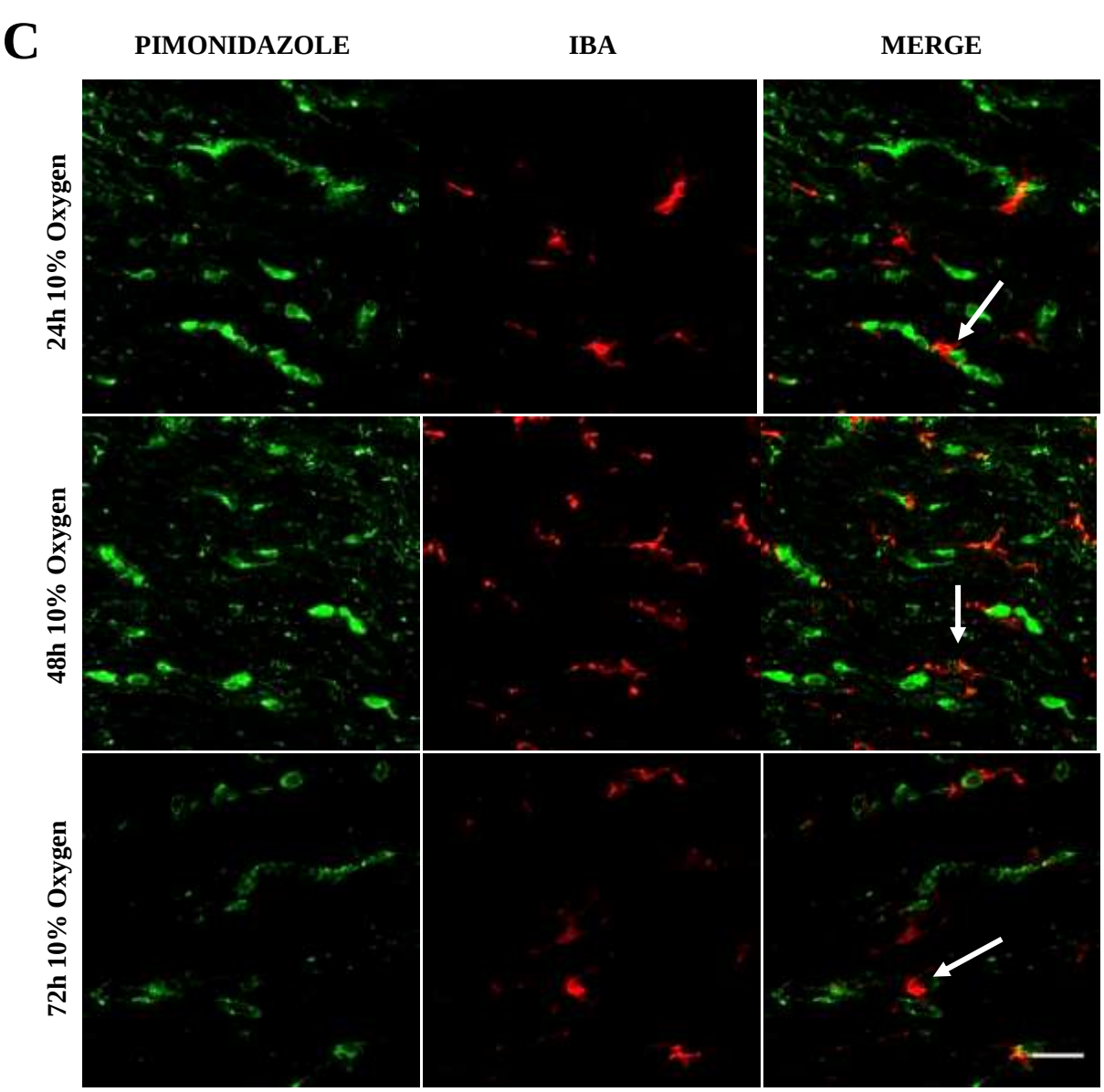
C
PIMONIDAZOLE
IBA
MERGE
24h 10% Oxygen
48h 10% Oxygen
72h 10% Oxygen

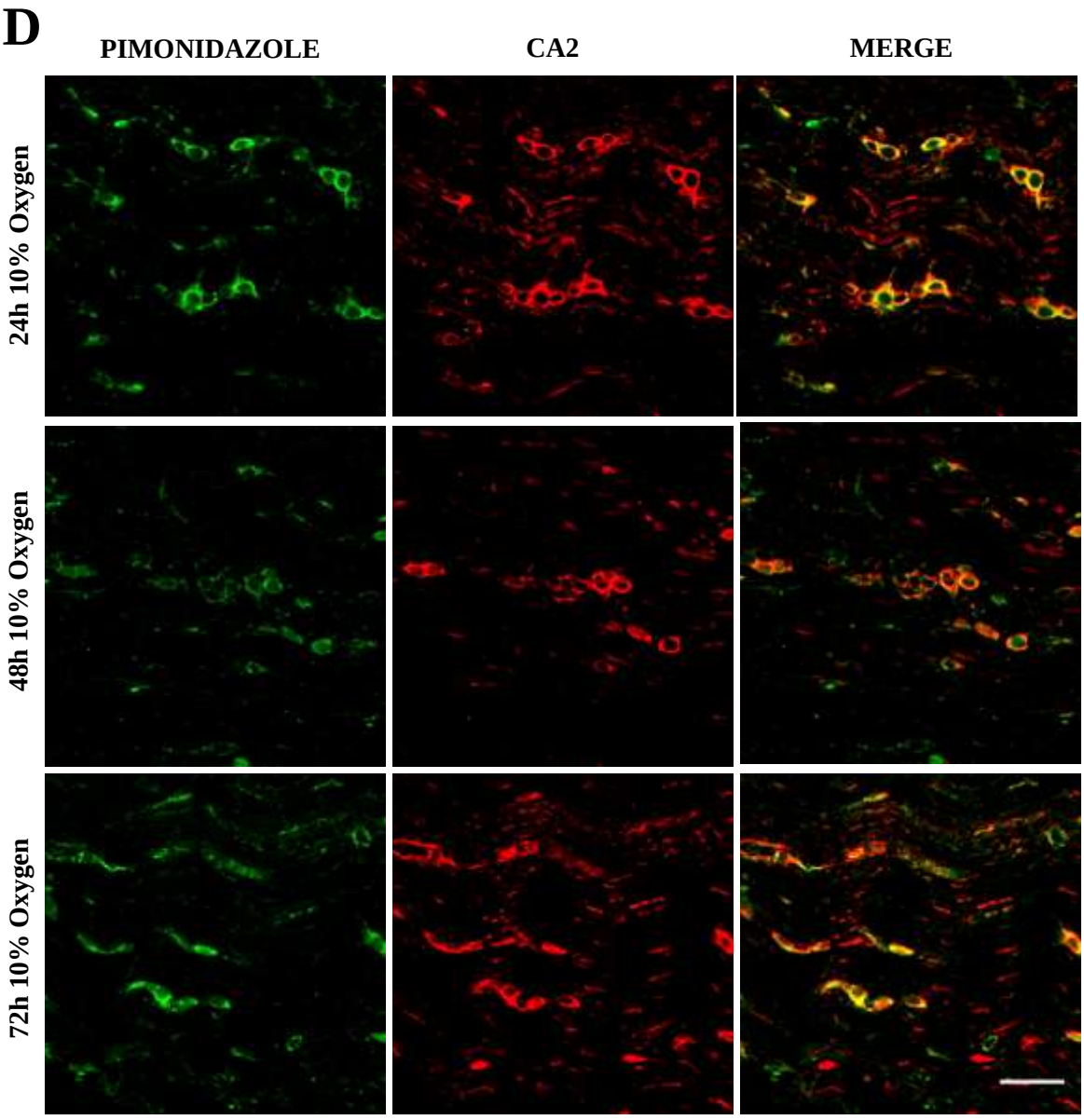
D
PIMONIDAZOLE
CA2
MERGE
24h 10% Oxygen
48h 10% Oxygen
72h 10% Oxygen

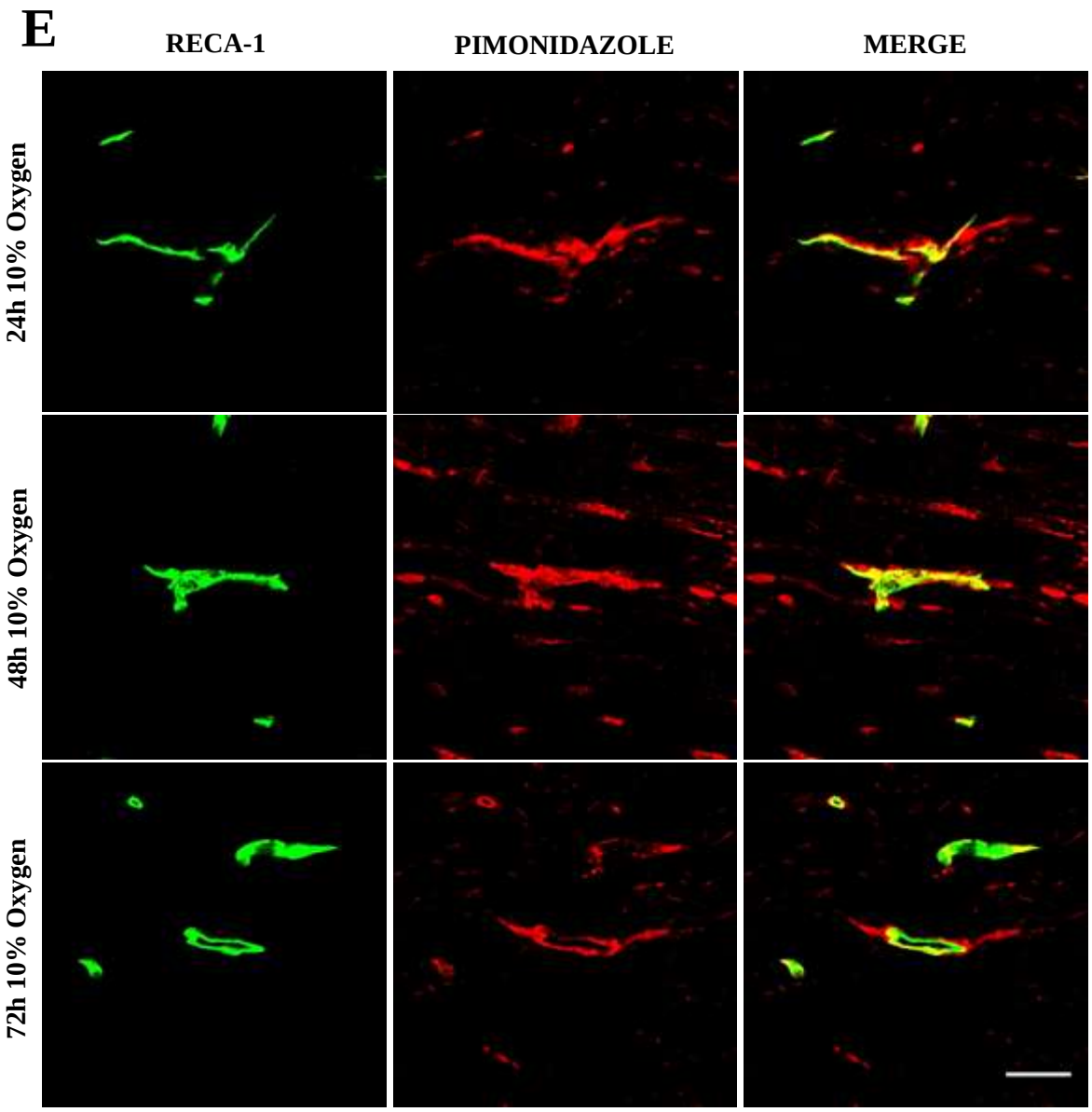

Figure 4.3.3.2: Cell types that label with pimonidazole in the white matter

(A) Transverse spinal cord section from an animal exposed to 10% oxygen, labelled with pimonidazole. The micrograph shows intense cellular labelling in the dorsal column white matter at high magnification. Scale bar 25µm. (B-E) Confocal laser images of spinal cord sections double-labelled to determine the cellular identity of the cells that label for pimonidazole in the dorsal columns. (B) Double label immunofluorescence with anti-pimonidazole (green) and anti-GFAP (red) revealed that astrocytes do not tend to label for pimonidazole following exposure to 10% oxygen, at any of the time points examined. (C) Similarly, microglia (red) also do not label with pimonidazole (green). Rather, the microglia are found in very close proximity to pimonidazole positive cells (arrows). (D) Double label immunofluorescence with anti-pimonidazole (green) and anti-CA2 (red), revealed that most, if not all, oligodendrocytes label intensely for pimonidazole, following exposure to 10% oxygen, at all time points examined. (E) Some endothelial cells (green) were also found to label with pimonidazole (red). Scale bar 100µm. All micrographs are representative.

4.3.3.3 What cells label in intense pimonidazole white matter foci?

In addition to the cell-specific labelling with pimonidazole (section 4.3.3.2), foci of pimonidazole labelling were also evident within the white matter, as described in section 4.3.2.0, following exposure to 10% oxygen. Microscopically, these foci comprised of a number of intensely labelled cells, surrounded by a 'halo' of intensely labelled tissue (Figure: 4.3.3.3 A). Morphologically, the positively labelled cells, within the foci of pimonidazole labelling, had the appearance of oligodendrocytes and microglia. Thus, double label immunofluorescence was performed, to identify these cells.

Some minimal overlap of labelling was observed with GFAP, primarily with astrocytic processes (Figure: 4.3.3.3 B-top), however, no clear co-localisation was observed with either microglia or oligodendrocytes (Figure: 4.3.3.3 B-middle, bottom). Rather, a decrease in cellular labelling for oligodendrocytes was observed in these foci. Further double label fluorescence studies performed with NG2, an antibody directed against oligodendrocyte precursor cells (OPCs), revealed that the cells that label so intensely for pimonidazole in the white matter foci were generally NG2 positive cells (Figure: 4.3.3.3 C). Morphologically, these cells resemble resting microglia, with long, slender processes. Despite the punctuate cellular co-localisation in the centre of the white matter foci, a loss of NG2 immunoreactivity, immediately adjacent to, and surrounding, the NG2/pimonidazole positive cells, was often frequently observed (Figure: 4.3.3.3 D).

A

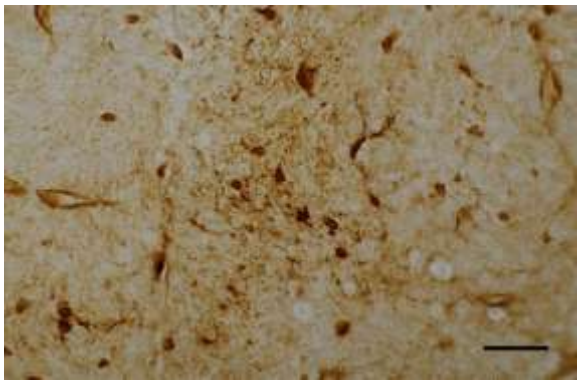

B

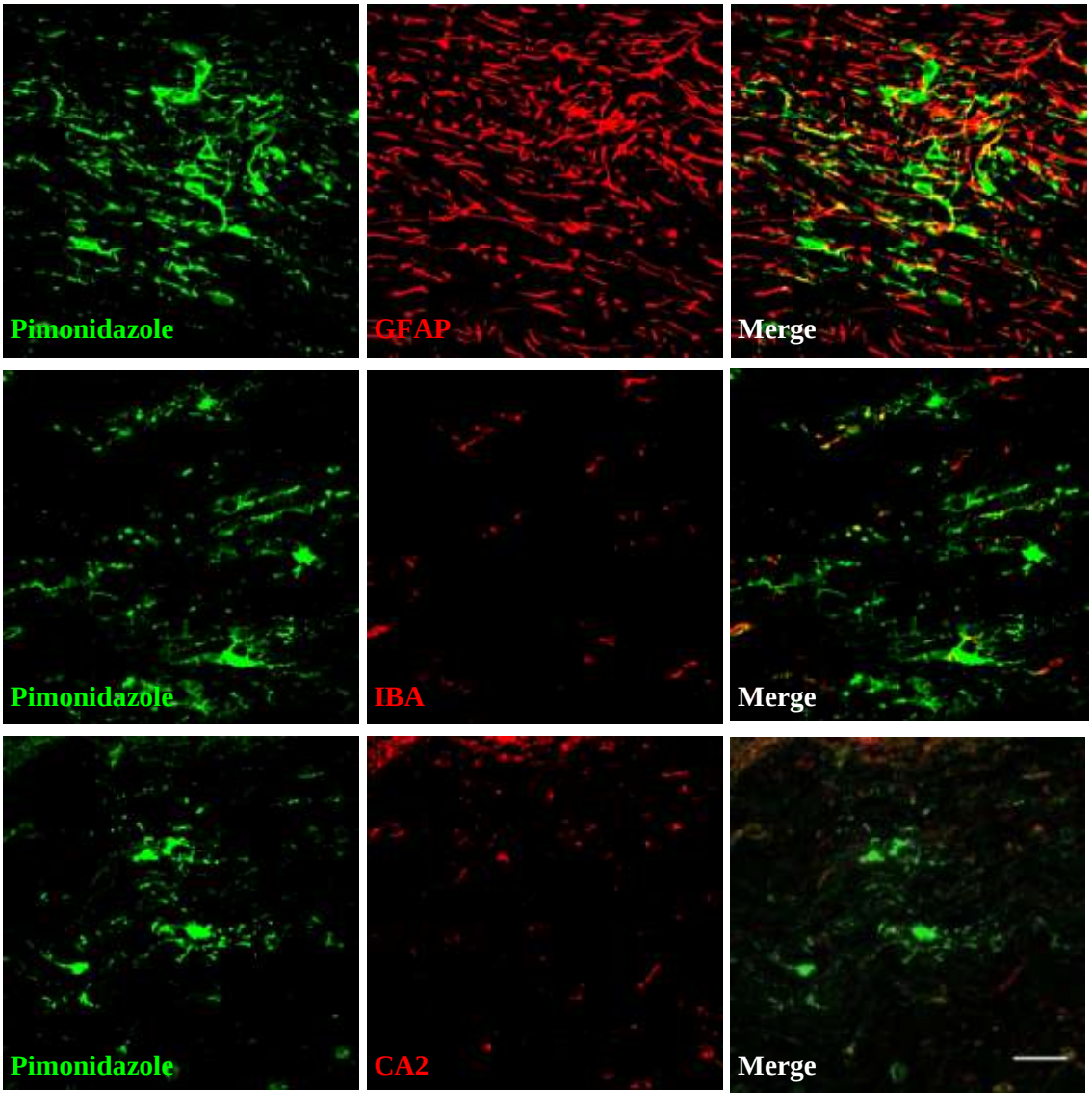
Pimonidazole
GFAP
Merge
Pimonidazole
IBA
Merge
Pimonidazole
CA2
Merge

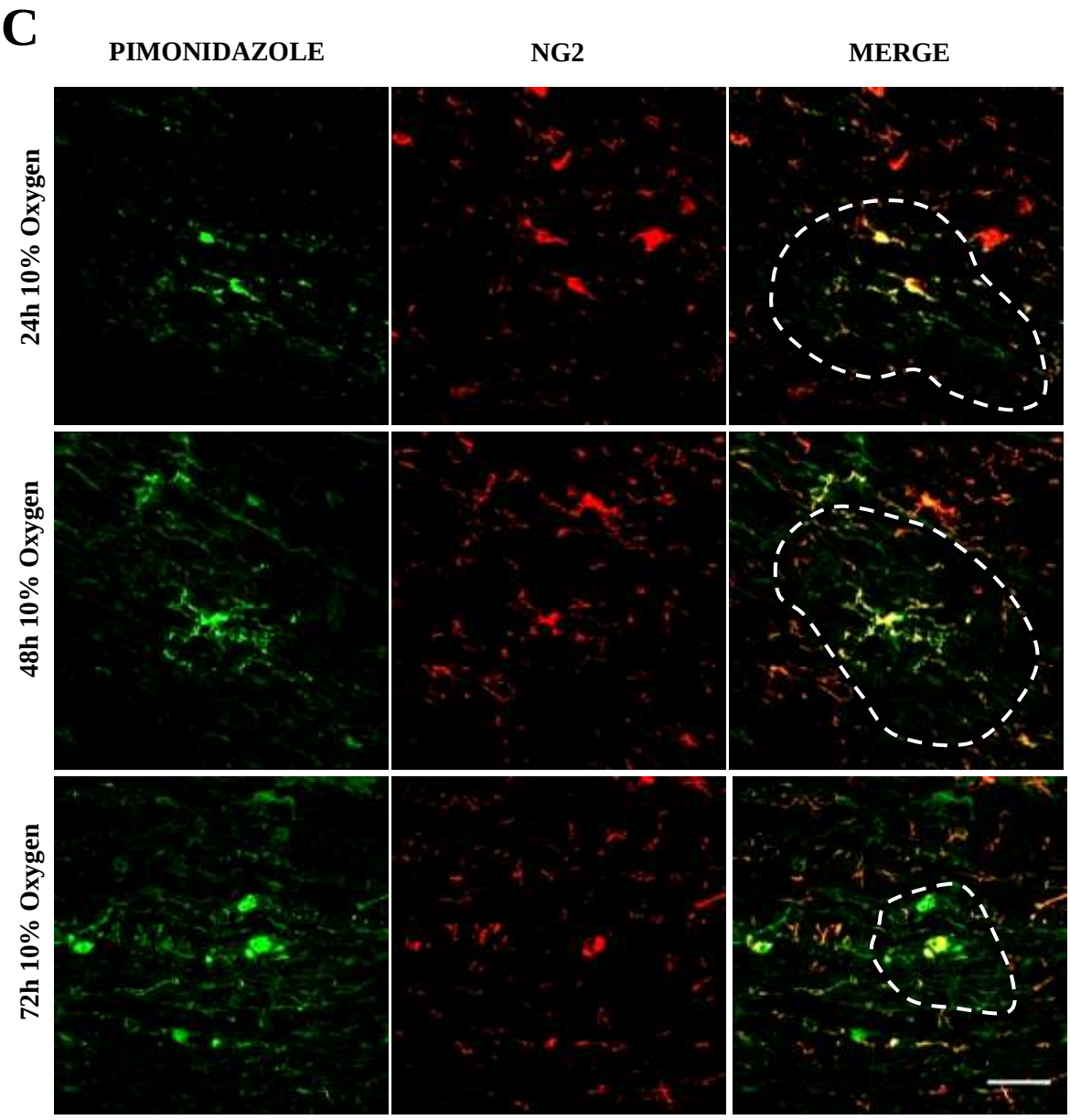

Figure 4.3.3.3: Cell types that label in intense pimonidazole white matter foci
(A) Transverse spinal cord section from an animal exposed to 10% oxygen. The micrograph shows an area of intense pimonidazole labelling in the dorsal column white matter, at high magnification. Scale bar 25 μm. (B) Double label immunofluorescence with markers for astrocytes (GFAP; red), microglia (IBA; red) and oligodendrocytes (CA2; red), revealed that none of these cell types co-labelled with pimonidazole in these intense foci. (C) Co-labelling with an anti-NG2 antibody (red), revealed that oligdendrocyte precursor cells label for pimonidazole in intense pimonidazole white matter foci. Moreover, there is a loss of NG2 immunoreactivity in the vicinity immediately surrounding the NG2-pimonidazole co-labelled cell (white dashed line), at all time points examined. Scale bar 100μm. All micrographs are representative.

4.3.4.0 The effects of acute hypoxia on neurons

In 21% control animals, neurons did not label with pimonidazole, however, following exposure to 10% oxygen, intense neuronal labelling with pimonidazole was observed (Figure: 4.3.4.0). The intensity of labelling was not dependent on the duration of exposure to 10% oxygen, but rather on the decrease in oxygen availability alone. The labelling was mainly localised to the cytoplasm of neurons, but labelling of the surrounding extracellular matrix was also observed.

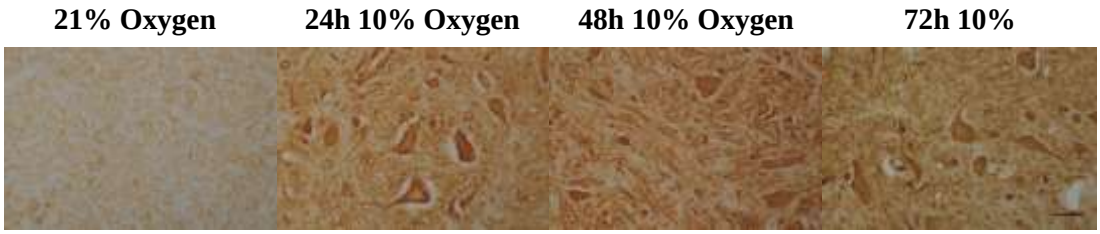

Figure 4.3.4.0: Pimonidazole labelling of neurons following acute hypoxia.
Transverse spinal cord sections from animals exposed to 21% oxygen, and 24h, 48h and 72h 10% oxygen, labelled with pimonidazole. The micrographs show the ventral horn grey matter at high magnification. There is no apparent neuronal labelling in the grey matter of the 21% oxygen control, however there is a considerable amount of labelling within the neurons and the surrounding parenchyma of animals exposed to 10% oxygen. Scale bar 25 μm. All micrographs are representative.

4.3.5.0 Microglial changes in response to acute hypoxia

4.3.5.1 Exposure to acute hypoxia causes an increase in microglial number

The microglial cell density, as indicated by IBA immunoreactivity, was elevated following exposure to 10% oxygen (Figure: 4.3.5.1). This initial increase was evident within the first 24h of exposure to 10% oxygen ($p< 0.001$). Subsequently, following exposure to 48h ($p = 0.012$) and 72h ($p<0.001$) 10% oxygen, the number of microglial cells did not increase further, but remained somewhat stable. A range of different morphological phenotypes was observed following exposure to 10% oxygen, ranging from ramified cells to amoeboid cells.

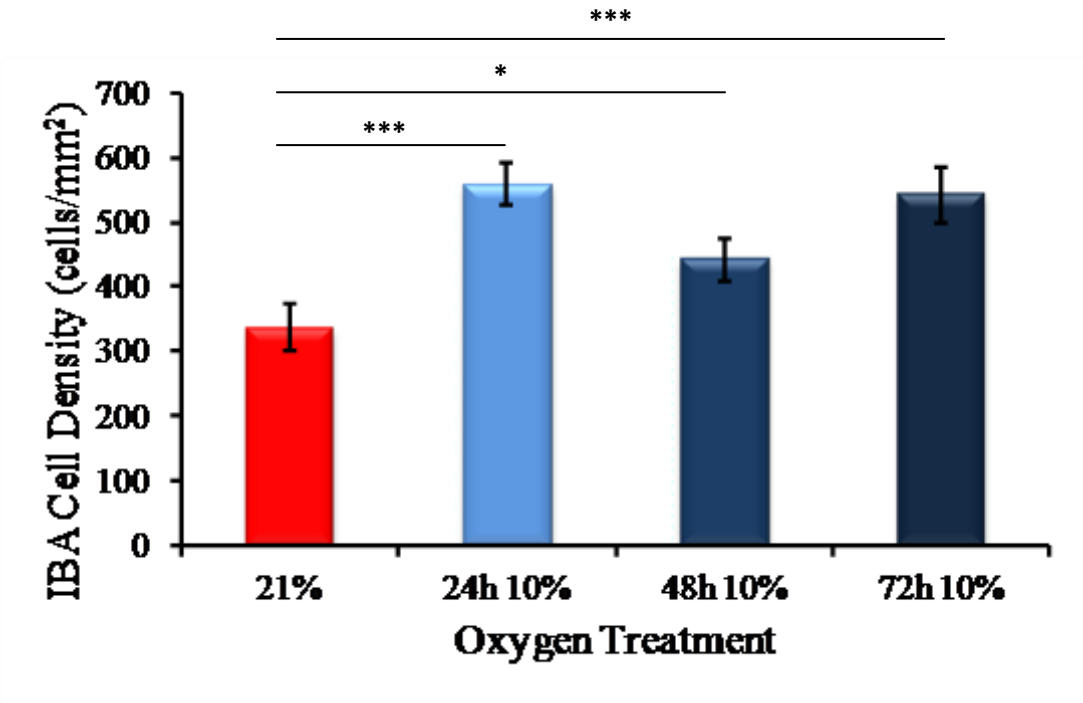

Figure 4.3.5.1: IBA labelling in animals exposed to acute hypoxia

Graph showing the average IBA cell densities in animals exposed to either room air or 10% oxygen, for different durations. Acute hypoxia increases the density of IBA-positive cells, compared with 21% control animals. Values are mean ± S.E.M. Statistical significance was determined by a Mann-Whitney U test, * $p<0.05$, *** $p<0.001$. N=6 per group

4.3.5.2 Exposure to 10% oxygen causes an increase in the number of MHC-II expressing cells

To identify whether modulating the oxygen concentration of inspired gas to 10% can initiate an inflammatory response, we looked for evidence of microglial activation. Immunohistochemistry with an anti-MHC class II antibody (OX-6) revealed that these molecules are constitutively expressed in the spinal cord of all animals, i.e. those exposed to 10%, or 21% oxygen (Figure: 4.3.5.2 A-C). However exposure to 10% oxygen significantly increased the number of cells expressing MHC class II (Figure: 4.3.5.2 A-C). In all the different spinal levels examined, there was a significant increase in the number of cells that labelled positively for MHC class II in animals exposed to 24h of 10% oxygen (upper-lumbar: $p = 0.014$; mid-thoracic: $p = 0.014$; lower-cervical: $p = 0.011$; mid-cervical: $p = 0.011$), 48h of 10% oxygen (upper-lumbar: $p = 0.033$; mid-thoracic $p = 0.011$; lower-cervical: $p = 0.014$; mid-cervical: $p = 0.011$), and 72h of 10% oxygen (upper-lumbar: $p = 0.019$; mid-thoracic: $p = 0.011$; lower-cervical: $p = 0.027$; mid-cervical: $p = 0.014$) compared with 21% oxygen control animals (Figure:. 4.3.5.2 C). These MHC class II expressing cells were primarily located in white matter, predominantly that of the dorsal and ventral columns, with a fewer number of cells in the lateral columns (Figure: 4.3.5.2 A). However a few MHC class II-expressing cells were also found in the grey matter, with some adjacent to motor neurons in the ventral horns (Figure: 4.3.5.2 Aii). Although the number of MHC class II-expressing cells was found to decrease with the duration of exposure to 10% oxygen, their morphology appeared to change with longer exposures. Following 24 hours of 10% oxygen exposure, ramified MHC class II expressing cells with long, slender processes were observed, in addition to very faint labelling of what appeared to be cellular processes (Figure:. 4.3.5.2 Di; Type I). As the duration of exposure to 10% oxygen was increased,

there was also a progressive increase in the proportion of MHC class II positive cells displaying a more ‘activated’ phenotype: a ramified morphology with no apparent cell body labelling (Figure: 4.3.5.2 Dii; Type II), a ramified morphology with labelling of the cell body (Figure: 4.3.5.2 Diii; Type III), rod-like cells with elongated cell bodies and bushy processes (Figure: 4.3.5.2 Div; Type IV), or rounder, amoeboid-like cell bodies with thick retracted processes (Figure: 4.3.5.2 Dv; Type V, Figure: 4.3.5.2 E). This array of microglial phenotypes was observed primarily in the white matter. Double label immunofluorescence confirmed that the MHC class II-expressing cells were microglia (Figure: 4.3.5.2 F). Occasionally, MHC class II positive cells were evident in regions that labelled for hypoxia (Figure: 4.3.5.2 G), although this was fairly rare.

A

i

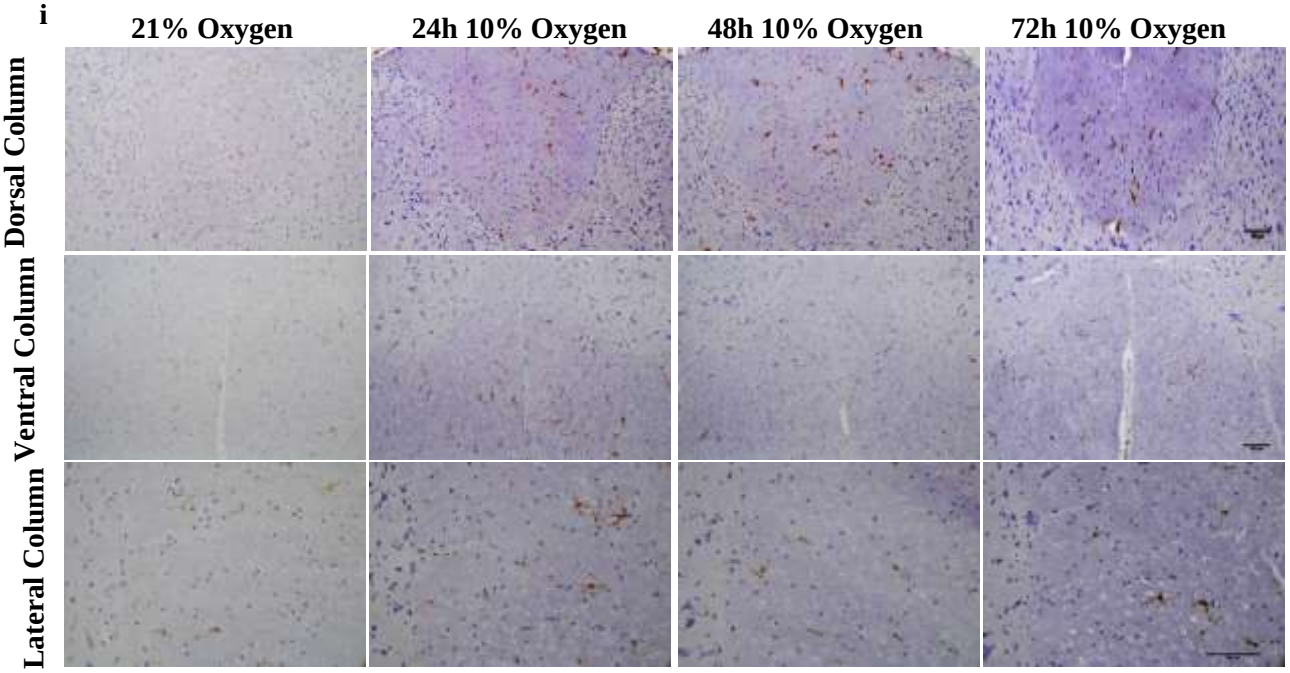
21% Oxygen
24h 10% Oxygen
48h 10% Oxygen
72h 10% Oxygen
Dorsal Column
Ventral Column
Lateral Column

ii

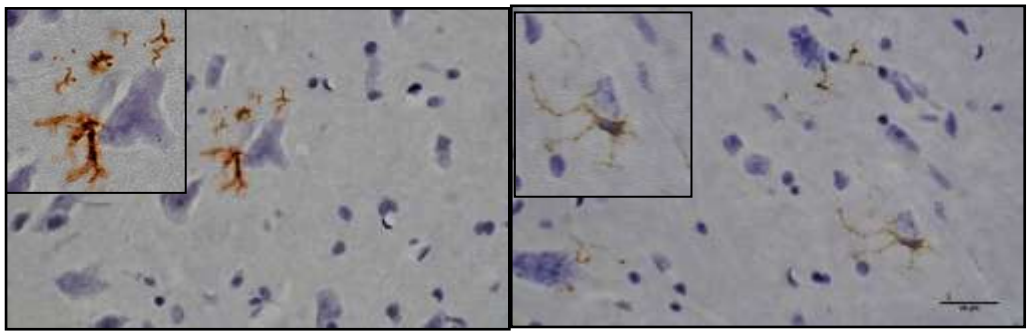

B

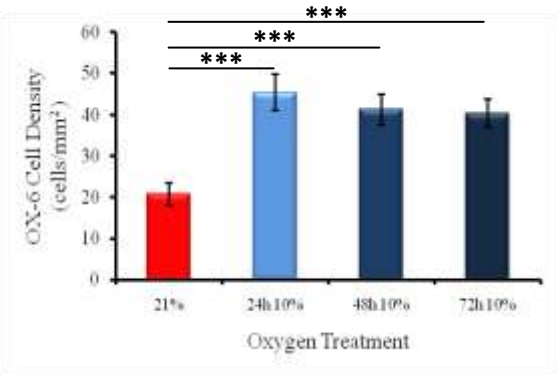
***
***
***
OX-6 Cell Density (cells/mm²)
60
50
40
30
20
10
0
21%
24h10%
48h10%
72h10%
Oxygen Treatment

C

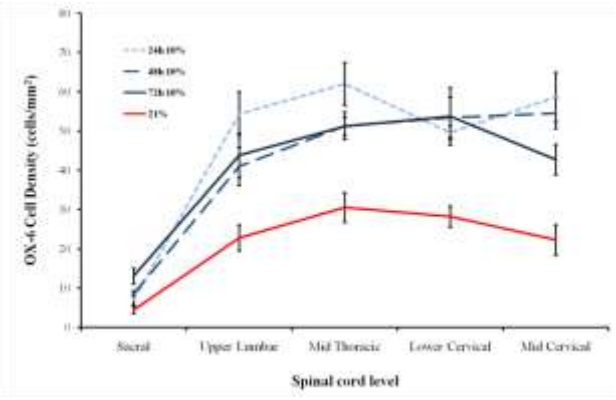
OX-6 Cell Density (cells/mm²)
Sacral
Upper Lumbar
Mid Thoracic
Lower Cervical
Mid Cervical
Spinal cord level

D

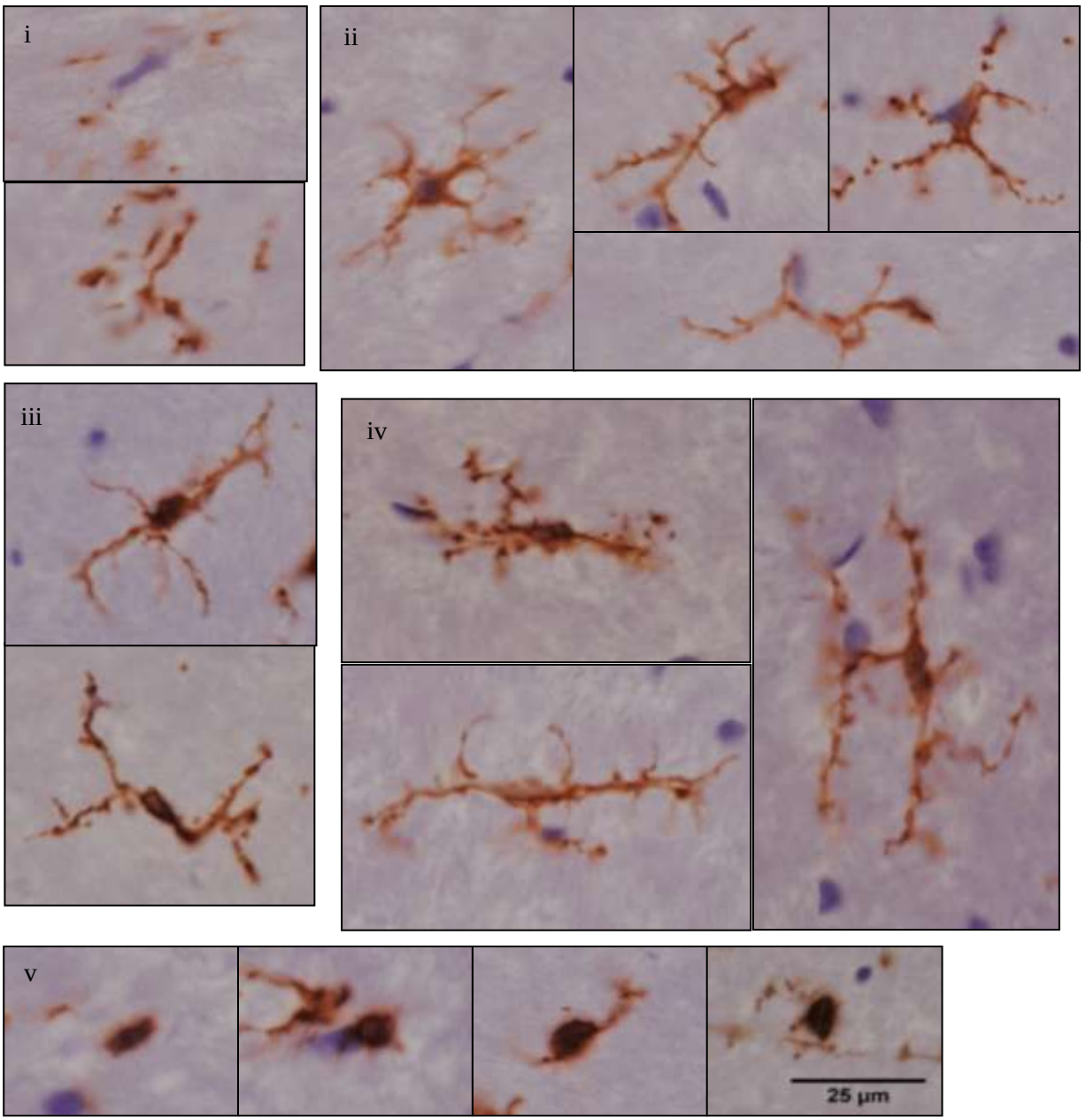
i
ii
iii
iv
v
25 µm

E

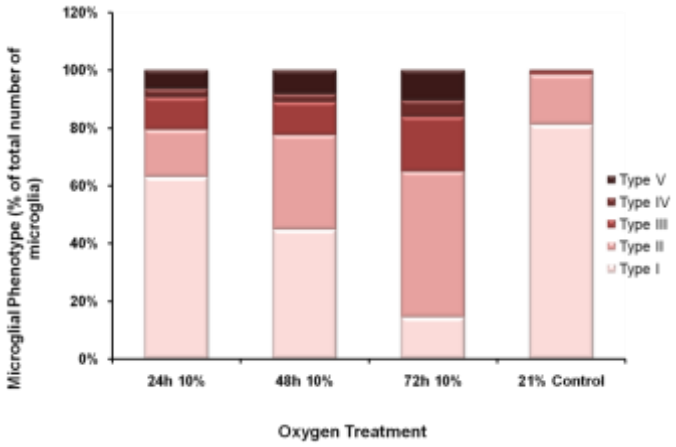
120%
100%
80%
60%
40%
20%
0%
Microglial Phenotype (% of total number of microglia)
24h 10%
48h 10%
72h 10%
21% Control
Oxygen Treatment
Type V
Type IV
Type III
Type II
Type I

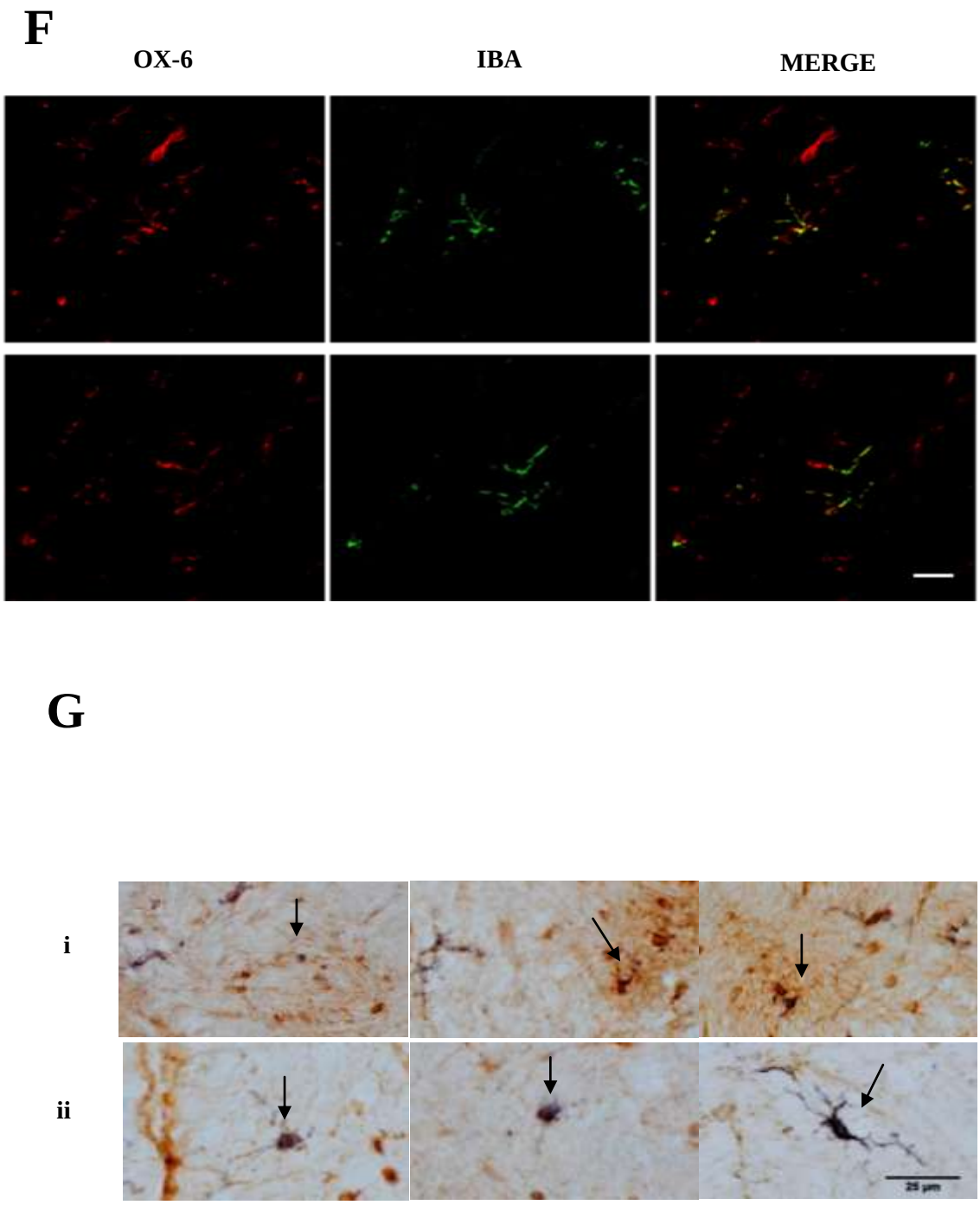

Figure 4.3.5.2: MHC class II expression following exposure to acute hypoxia
(Ai) Micrographs of spinal cord sections from animals exposed to either 21% oxygen, 24h 10% oxygen, 48h 10% oxygen or 72h 10% oxygen, labelled with OX-6, a marker of MHC class II molecules, and counterstained with haematoxylin. Increased expression of MHC class II molecules can be seen in all animals exposed to 10% oxygen, in the dorsal (scale bar 200 µm), ventral (scale bar 200 µm) and lateral (scale bar 100 µm) columns, compared to 21% controls. (Aii) MHC class II positive cells can also be found adjacent to motor neurons in the grey matter of animals exposed to 10% oxygen (scale bar 25 µm). (B) Graphical representation comparing the MHC class II cell density between animals exposed to 10% oxygen for 24h, 48h,and 72h, and animals exposed to 21% oxygen. Values are means ± SD (n=6 per

group). Statistical differences were determined by a repeated measures ANOVA, *** $p<0.001$. (C) The rostro-caudal distribution of MHC class II positive cells, showing that the largest numbers of MHC class II positive cells are present in the mid-thoracic and lower cervical cord. Values are means ± SEM. (D) Morphological classification of MHC class II positive cells. (Type I; i) Faint OX-6 labelling of cellular processes, (Type II; ii) ramified cells with long, slender processes, but no apparent cell body labelling, (Type III; iii) rounded cell bodies that label with OX-6, cells have long, slender processes, (Type IV; iv) rod-like cells, with elongated cell bodies, and long processes, and (Type V; v) amoeboid-like cell bodies with retracted, thick, or no processes. Scale bar 25µm. (E) Graphical representation of MHC class II cells based on their morphological phenotype. Values are mean percentage. (F) Confocal microscopy of double label immunofluorescence showing co-localisation of OX-6 (green) IBA (red), confirming that the MHC class II positive cells are microglia/macrophages, most probably microglia. Scale bar 200µm. (G) Micrographs of spinal cord sections from animals exposed to 10% oxygen, showing MHC class II positive cells (black) in areas that label intensely for pimonidazole (i: arrows) and areas that do not label for pimonidazole (ii). Scale bar 25 µm. All Micrographs are representative.

4.3.5.3 Microglia in animals exposed to 10% oxygen do not express the phagocytic marker ED1 or iNOS

As microglia in animals exposed to 10% oxygen appeared to express MHC-II at increased levels compared with control animals exposed to 21% oxygen, we sought identify their activation status further. Immunohistochemistry with an antibody against ED1, a marker of phagocytic cells, revealed that microglia in the spinal cord of animals exposed to 10% oxygen for 24, 48 and 72 hours do not express the ED1 antigen, thus there was no difference between animals exposed to 10% oxygen and animals exposed to 21% oxygen with respect to ED1 expression (Figure: 4.3.5.3 A). Similarly, labelling for iNOS, another marker of microglial activation, revealed that exposure to acute hypoxia did not induce the expression of iNOS (Figure: 4.3.5.3 B).

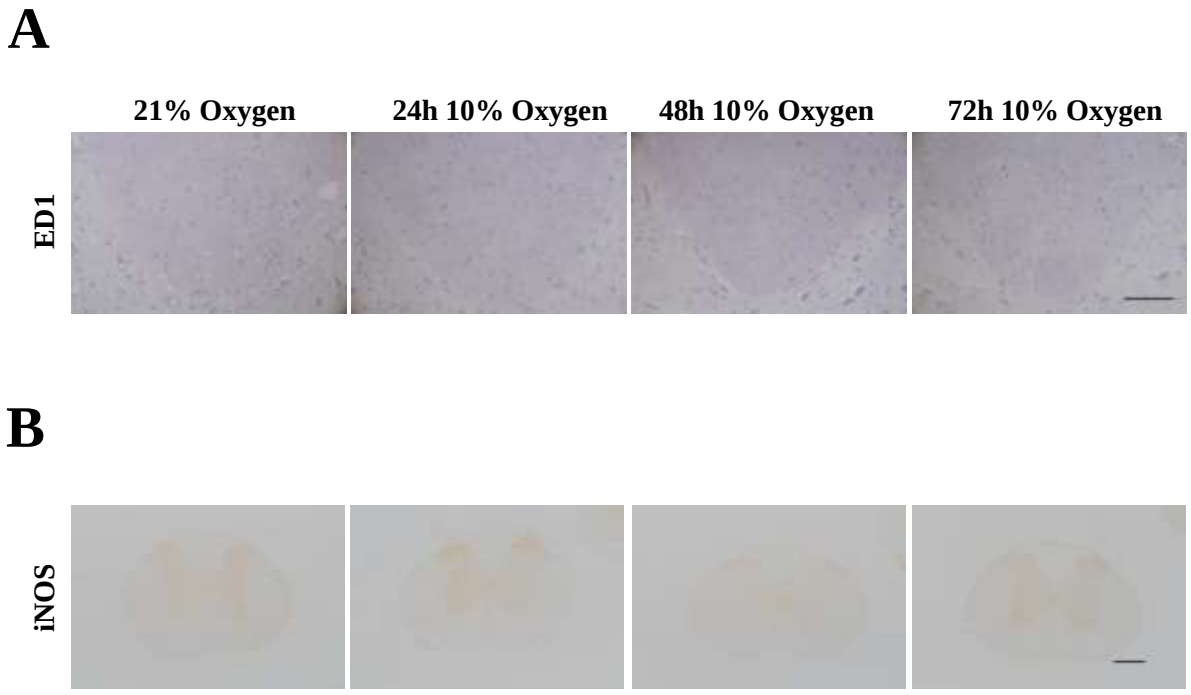

Figure 4.3.5.3: ED1 and iNOS labelling following exposure to 10% hypoxia
(A) Transverse spinal cord sections from animals exposed to 21% or 10% oxygen, labelled with an anti-ED1 antibody, and counterstained with hematoxylin. Micrographs show the dorsal column region of the cord, revealing that exposure to 10% oxygen does not induce ED1 expression. Scale bar 200μm. (B) Labelling with an anti-iNOS antibody also revealed that iNOS expression is not induced following exposure to acute hypoxia. Scale bar 500μm. All micrographs are representative.

4.3.5.4 Acute hypoxia results in an increase in white matter TLR4 expression

Exposure to acute hypoxia resulted in a statistically significant increase in TLR4 expression in the white matter (48 hours 10% oxygen $p = 0.050$; 72 hours 10% oxygen $p<0.001$). Expression was particularly evident microscopically, with the intensity of TLR4 immunoreactivity progressively increasing with the duration of exposure to 10% oxygen (Figure: 4.3.5.4 A). Moreover, the density of TLR4-positive cells increased in a linear manner following exposure to 10% oxygen (Figure: 4.3.5.4 B). TLR-4 positive cells morphologically resembled ramified microglia, with round cell bodies and long slender, arborous processes.

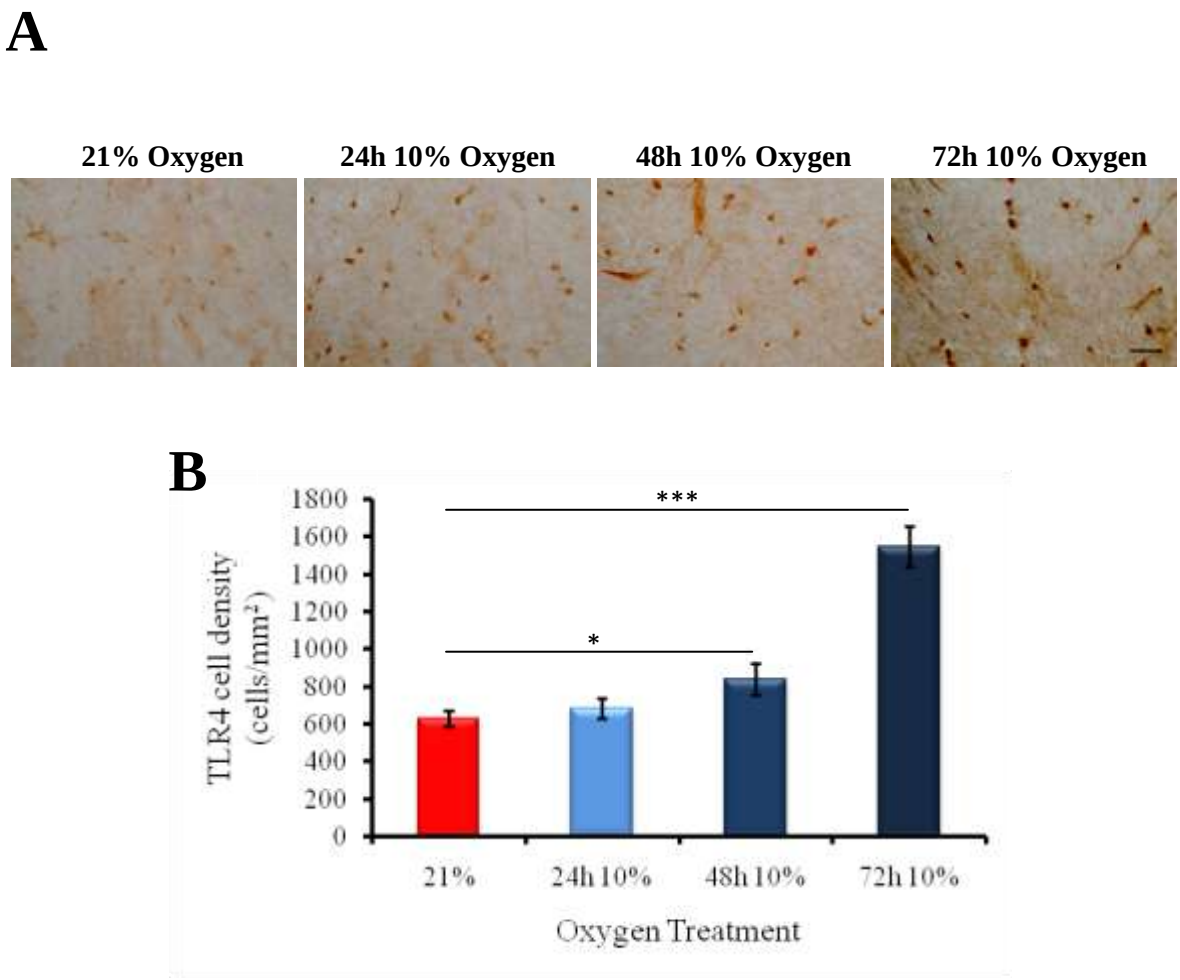

Figure 4.3.5.4: The effects of acute hypoxia on TLR4 expression
(A) Micrographs of spinal cord sections from animals exposed to 21% oxygen, or 24h, 48h or 72h 10% oxygen, labelled with an anti-TLR4 antibody. In 21% oxygen controls, there is some faint labelling of TLR4 positive cells, however, following exposure to 10% oxygen, there is increased expression of TLR4, indicated by the intensity of the labelling. Scale bar 25 μm. (B) Graph showing the TLR4 cell density is most increased following exposure to 72h 10% oxygen. Values are mean ± S.E.M, n=6 per group. Statistical significance was determined by a Mann-Whitney U test, * $p<0.05$, *** $p<0.001$. N=6 per group. All micrographs are representative.

4.3.6.0 Effects of acute hypoxia on oligodendrocyte cell lineage

4.3.6.1 NG2-expressing cells and hypoxia

OPCs were found to label particularly intensely for pimonidazole, therefore their response to acute hypoxia was investigated. In control animals breathing room air (21%), NG2-positive cells were plentiful in number, scattered throughout the spinal parenchyma. Morphologically, they resembled resting microglia, with small cell bodies and ramified, arborous processes (Figure: 4.3.6.1 A). Although exposure to 10% oxygen did not result in a dramatic change in NG2 cell density, except for at 72 hours 10% oxygen (p = 0.016) (Figure: 4.3.6.1 A, B), some NG2 positive cells became progressively hypertrophied as the duration of exposure to 10% increased (p< 0.001) (Figure: 4.3.6.1 A, C). The hypertrophied state was characterised by an enlarged, swollen cell body, with thick retracted processes. Thus, by 72h of exposure to 10% oxygen, the average size of the NG2 cells was more than double that in 21% control animals (Figure: 4.3.6.1 C).

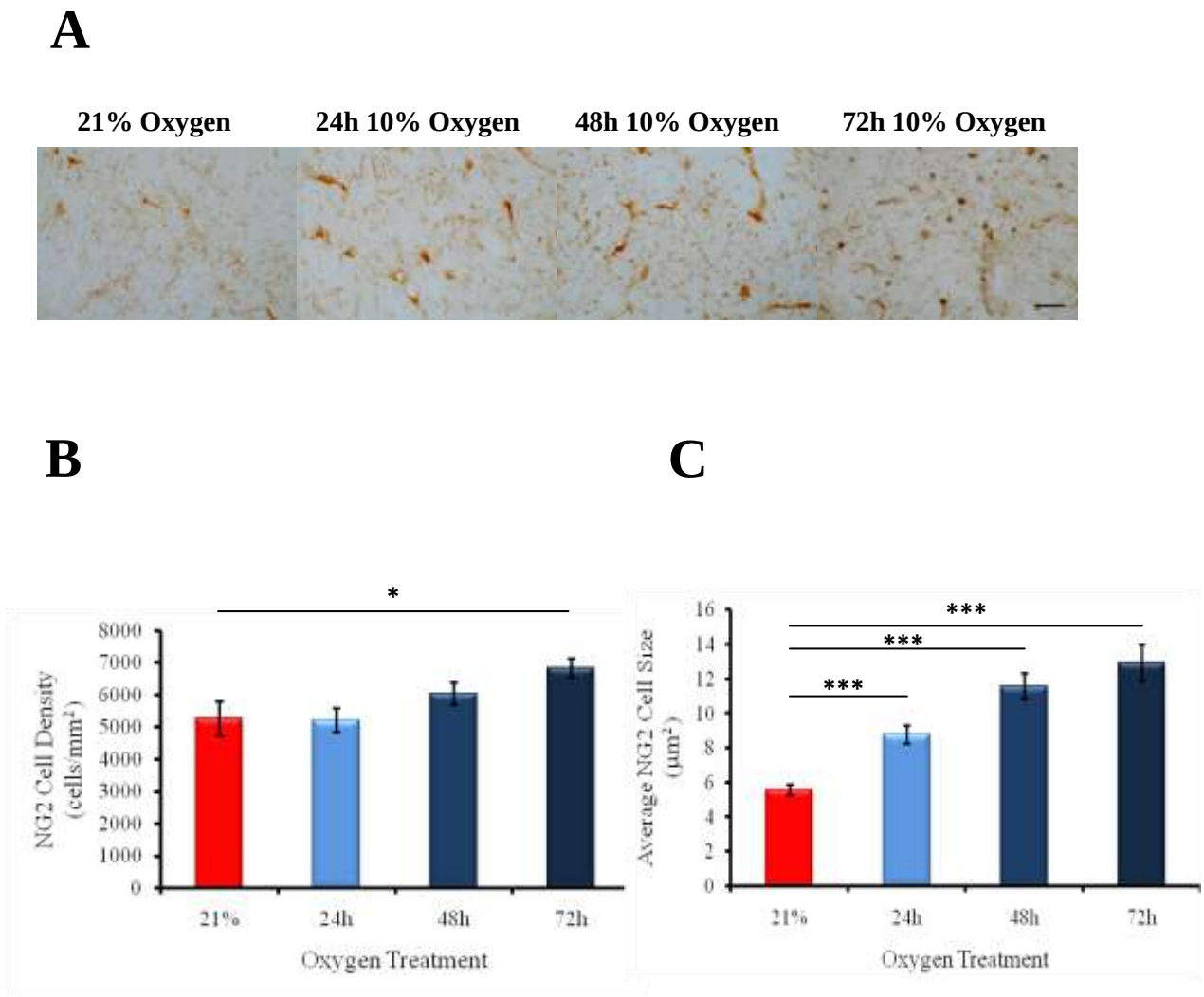

Figure 4.3.6.1: The effects of acute hypoxia on oligodendrocyte precursor cells
(A) Transverse spinal cord sections from animals exposed to 21% oxygen, or 24h, 48h, or 72h 10% oxygen, labelled for NG2. Micrographs show the dorsal column white matter at high magnification. NG2 cell density does not seem to change in response to acute hypoxia; however, the cells seem to become more hypertrophied and amoeboid. Scale bar 25μm. (B) Graph showing there is no substantial change in NG2 cell density following exposure to 10% oxygen at any of the time points examined. Values are means ± S.E.M. (C) Graph of the average NG2 cell size showing a proportional increase in cell size with duration of hypoxia. Values means ± S.E.M. Statistical significance was determined by a Mann-Whitney U test, * $p<0.05$, *** $p<0.001$. N=6 per group. All micrographs are representative.

4.3.6.2 The expression profile of NG2 following acute hypoxia

Besides OPCs, NG2 has also been described to be expressed by microglia and pericytes (Dore-Duffy et al., 2006; Moransard et al., 2011), therefore, double label immunofluorescence was performed to determine whether acute hypoxia had an effect on the expression profile of NG2. In animals breathing room air, NG2 was not found to co-localise with astrocytes (Figure: 4.3.6.2 A), microglia (Figure: 4.3.6.2 B) or endothelial cells (Figure: 4.3.6.2 C). In these animals, some overlap of NG2 and GFAP immunofluorescence was observed (Figure: 4.3.6.2 A), however, this appeared to be a close association of two distinct cell types, rather than co-localisation *per se*. Such an association was also observed in animals exposed to 10% oxygen, in which the hypertrophied NG2-positive cells were often found surrounding astrocytes (Figure: 4.3.6.2 A). As with the 21% control animals, NG2 was not found to co-localise with any of the cell types in animals exposed to 10% oxygen (Figure: 4.6.6.2). However, double label studies with NG2 and RECA-1 (endothelial cells) revealed some interesting findings. In 21% control animals, NG2 positive cells were generally located throughout the parenchyma, with no close association with the vasculature. However, as the duration of exposure to 10% oxygen increased, hypertrophied NG2 cells were found to progressively move closer to the vessels (Figure: 4.3.6.2 C). By 72h of exposure to 10% oxygen, a number of hypertrophied NG2 cells appeared to completely surround and enclose the vessels in the spinal white matter.

A

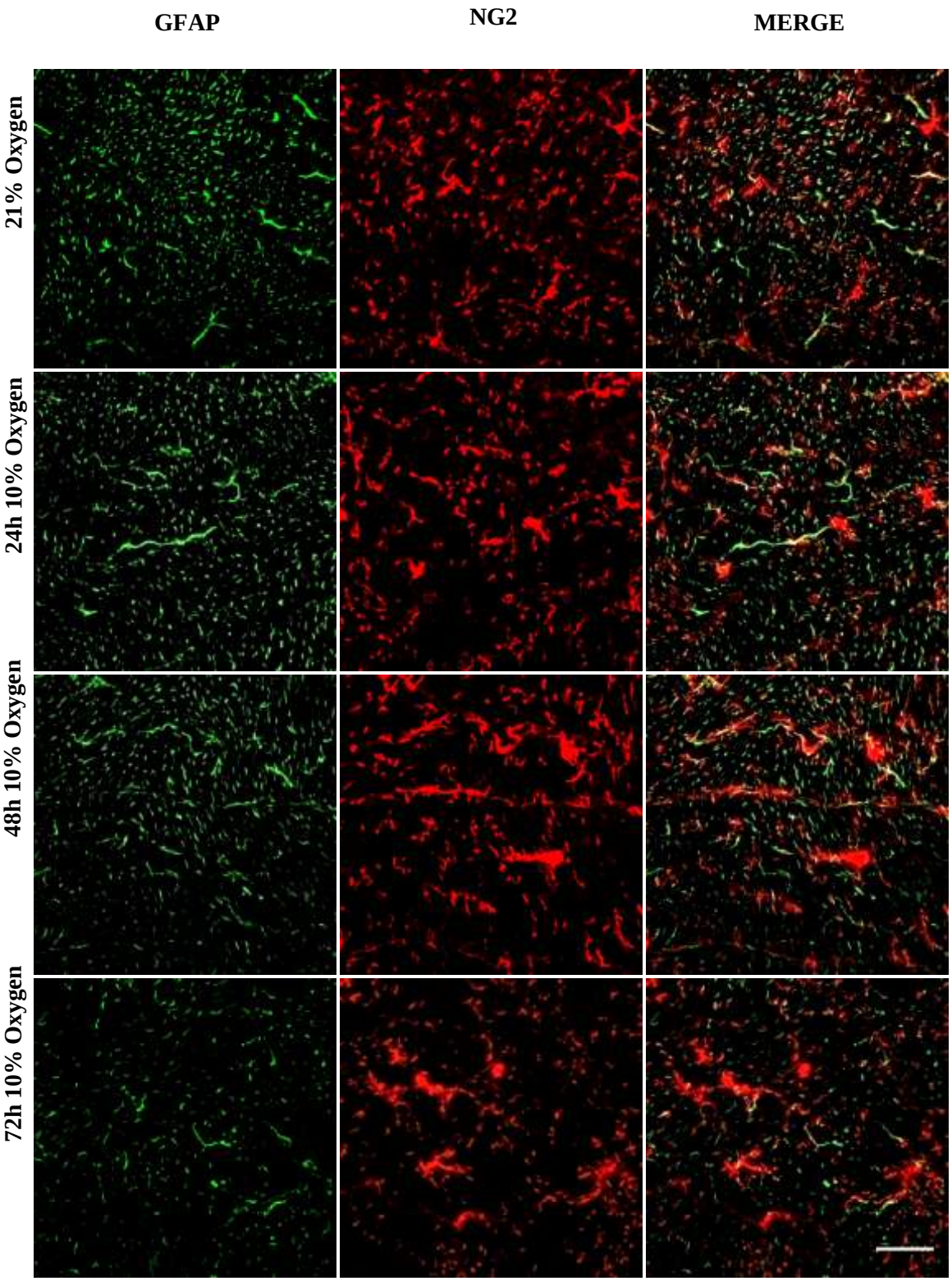
GFAP
NG2
MERGE
21% Oxygen
24h 10% Oxygen
48h 10% Oxygen
72h 10% Oxygen

B

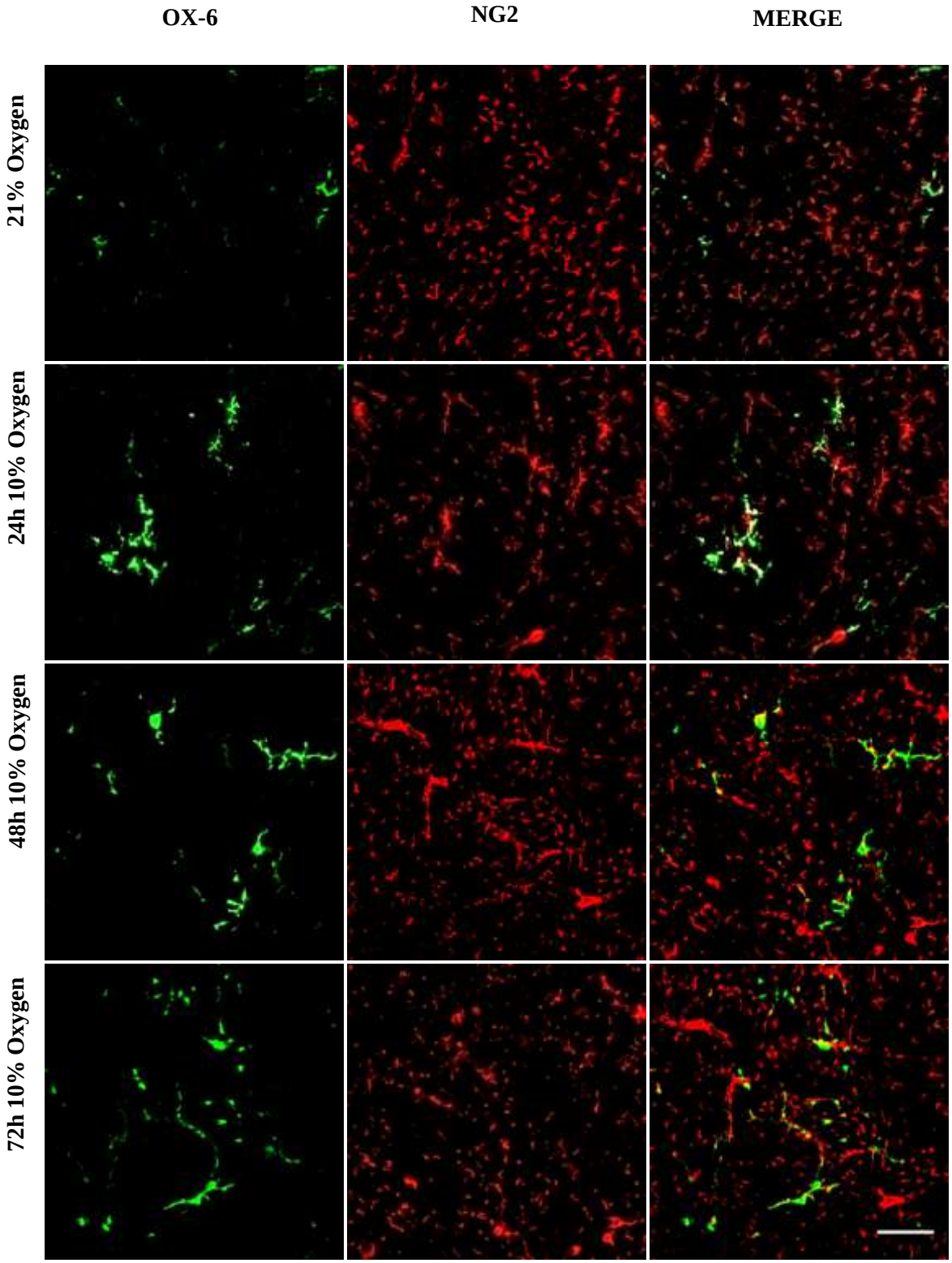
OX-6
NG2
MERGE
21% Oxygen
24h 10% Oxygen
48h 10% Oxygen
72h 10% Oxygen

C

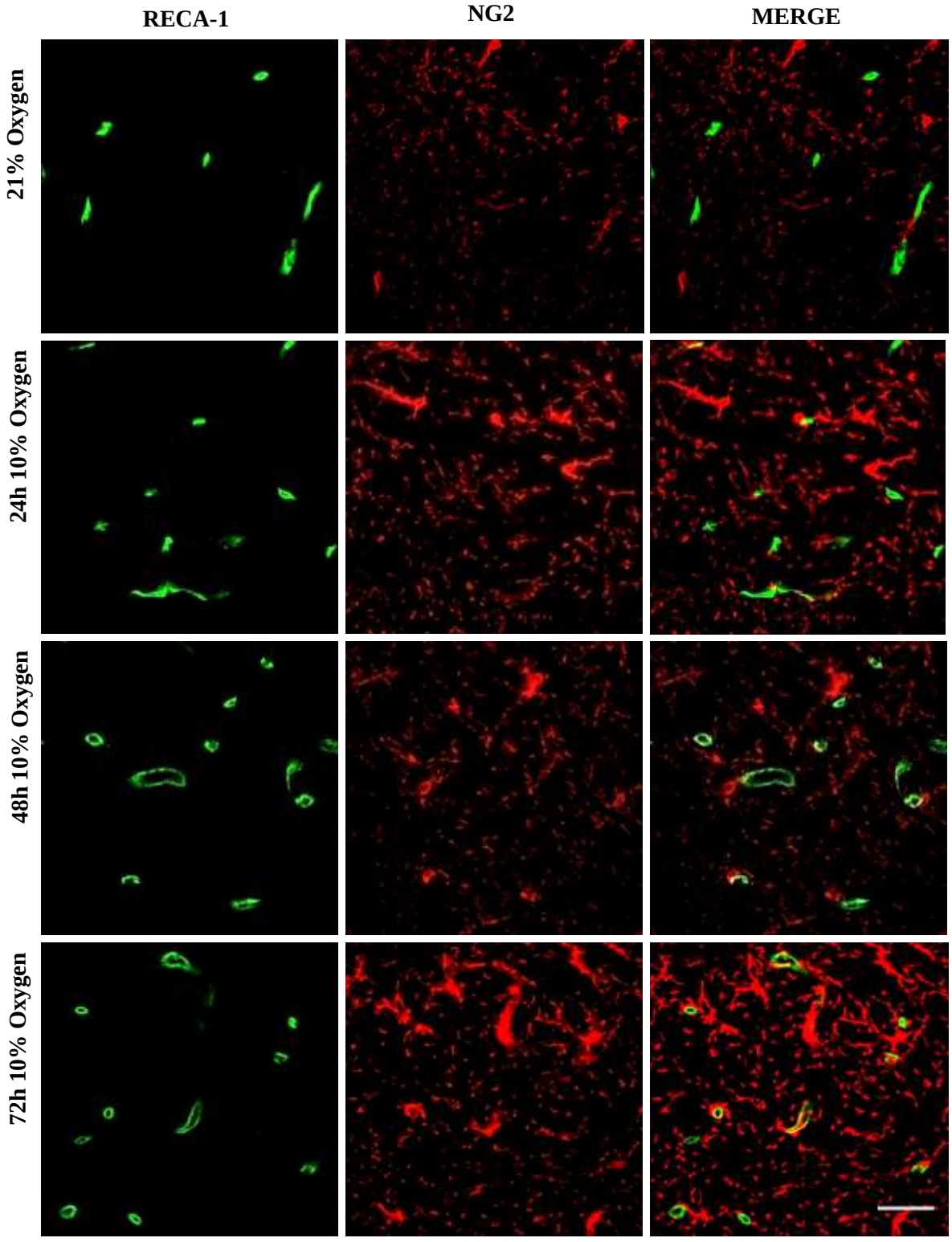
RECA-1
NG2
MERGE
21% Oxygen
24h 10% Oxygen
48h 10% Oxygen
72h 10% Oxygen

Figure 4.3.6.2: NG2 expression profile following exposure to 10% oxygen

(A-C) Confocal laser images from animals exposed to 21% oxygen, or 24h, 48h or 78h 10% double labelled for NG2 (red), and astrocytes (A; green), MHC-II (B; green) and endothelial cells (C; green). (A) Following exposure to 10% oxygen, NG2 does not co-localise with GFAP, however, NG2 positive cells are sometimes closely associated with astrocytes. (B) Similarly, NG2 does not co-localise with MHC-II, following exposure to 10% oxygen. (C) In 21% oxygen controls, NG2 positive cells are found scattered, without any close association with endothelial cells. Following exposure to 24h and 48h 10% oxygen, hypertrophied NG2 positive cells are found in close proximity to endothelial cells. Following 72h 10% oxygen, the number of hypertrophied NG2 positive cells increases, and they are found enclosing the endothelial cells in the vicinity. Scale bar 100μm. All micrographs are representative.

4.3.7.0 The effects of acute hypoxia on endothelial cells

4.3.7.1 Vascular density is not increased in response to acute hypoxia

As expected, acute exposure to 10% oxygen did not affect the vascular density (total: $p = 0.307$; grey matter: $p = 0.427$; white matter: $p = 0.517$; Table 4.3.7.1). However, there was a considerable amount of inter-animal variation (Figure: 4.3.7.1 B) in normal tissue. For example, in the lumbar spinal cord grey matter in animals exposed to 21% oxygen, the vascular density of the grey matter ranged from 774 to 1095 cells/mm^2.

Correlation between the intensity of pimonidazole labelling and the vascular density in the grey and white matter combined (total) was assessed using Pearson's correlation coefficient test. No correlation was found to exist between the intensity of total pimonidazole labelling and the total vascular density ($r = -0.198$, $p = 0.093$), or between the grey matter pimonidazole labelling and the grey matter vascular density ($r = -0.209$, $p = 0.076$). However, a mild negative correlation, which was statistically significant, was found between the intensity of pimonidazole labelling and the vascular density in the white matter ($r = -0.294$, $p = 0.012$), suggesting that in the white matter the intensity of pimonidazole labelling increases as the vascular density decreases.

A

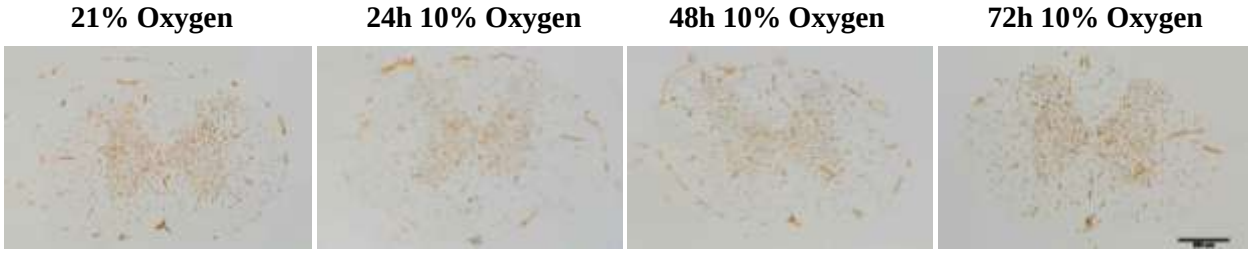

Table 4.3.7.1: Spinal cord vascular density

	Spinal Cord RECA1 Density (cells/mm^2)		
	Total	Grey Matter	White Matter
24h 10% Oxygen	365.28 ± 39.35	795.38 ± 64.20	186.83 ± 29.96
48h 10% Oxygen	370.93 ± 49.73	838.25 ± 81.95	186.63 ± 27.40
72h 10% Oxygen	378.93 ± 66.24	817.24 ± 56.38	196.80 ± 52.83
21% Oxygen	407.22 ± 53.73	868.22 ± 99.22	221.22 ± 35.93

B

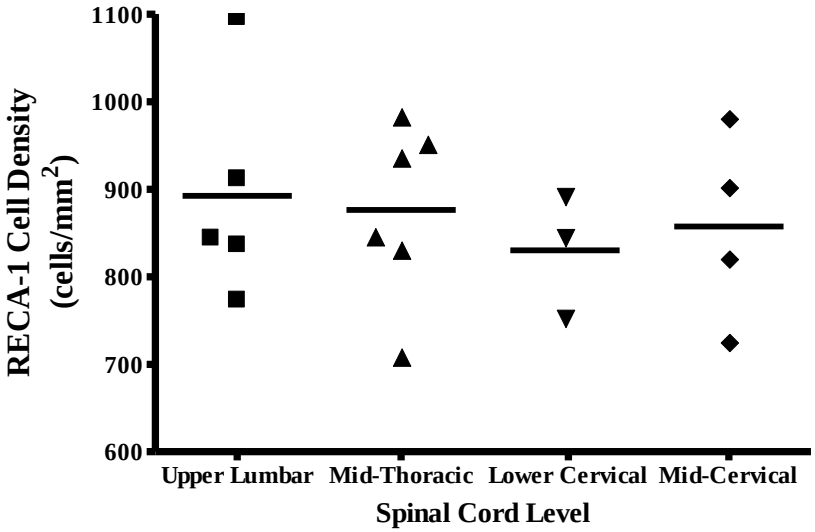

Figure 4.3.7.1: Vascular Density

(A) Spinal cord sections from the upper lumbar region of animals exposed to 21% oxygen, or 24h, 48h or 72h 10% oxygen, labelled with RECA-1.Scale bar 500 µm. Micrographs are representative. (Table 3.1.4) Table showing the cumulative vascular density in the grey and white matter (total), grey matter and white matter. Values are means ± S.D. N=6 per group. (B) A scatter plot of the vascular density in the grey matter of animals exposed to 21% oxygen, showing the inter-animal variation, at different levels of the spinal cords.

4.3.7.2 Exposure to acute moderate hypoxia does not induce IgG leakage

Severe, or prolonged, acute hypoxia is believed to induce vascular leakage in the brain (Schoch et al., 2002), therefore immunohistochemistry with an antibody against IgG was performed. No evidence of IgG immunoreactivity was found in the spinal cords of animals exposed to either 21% (controls) or 10% oxygen, at any of the time points investigated (Figure: 4.3.7.2). Thus, blood-spinal cord barrier integrity appeared to be maintained.

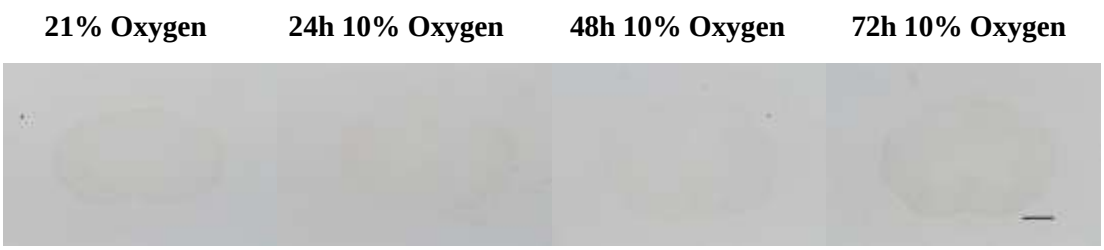

Figure 4.3.7.2: BBB and acute hypoxia
Micrographs of spinal cord sections from animals exposed to 21% oxygen, or 24h, 48h or 72h 10% oxygen labelled for IgG leakage. Exposure to 10% oxygen does not lead to BBB breakdown and IgG leakage. Scale bar 500μm. All micrographs are representative.

4.3.7.3 Exposure to acute hypoxia results in an increase in P-selectin on endothelial cells

P-selectin was expressed at low levels on endothelial cells in the spinal cords of control animals (Figure: 4.3.7.3 A). Following exposure to 10% oxygen, the P-selectin immunoreactivity on endothelial cells increased (Figure: 4.3.7.3 A). The increase was evident within the first 24h of hypoxia, from which point it remained elevated. In some instances, by 72h of exposure to 10% oxygen, intense, prominent P-selectin labelling was also observed on endothelial cells (Figure: 4.3.7.3 B).

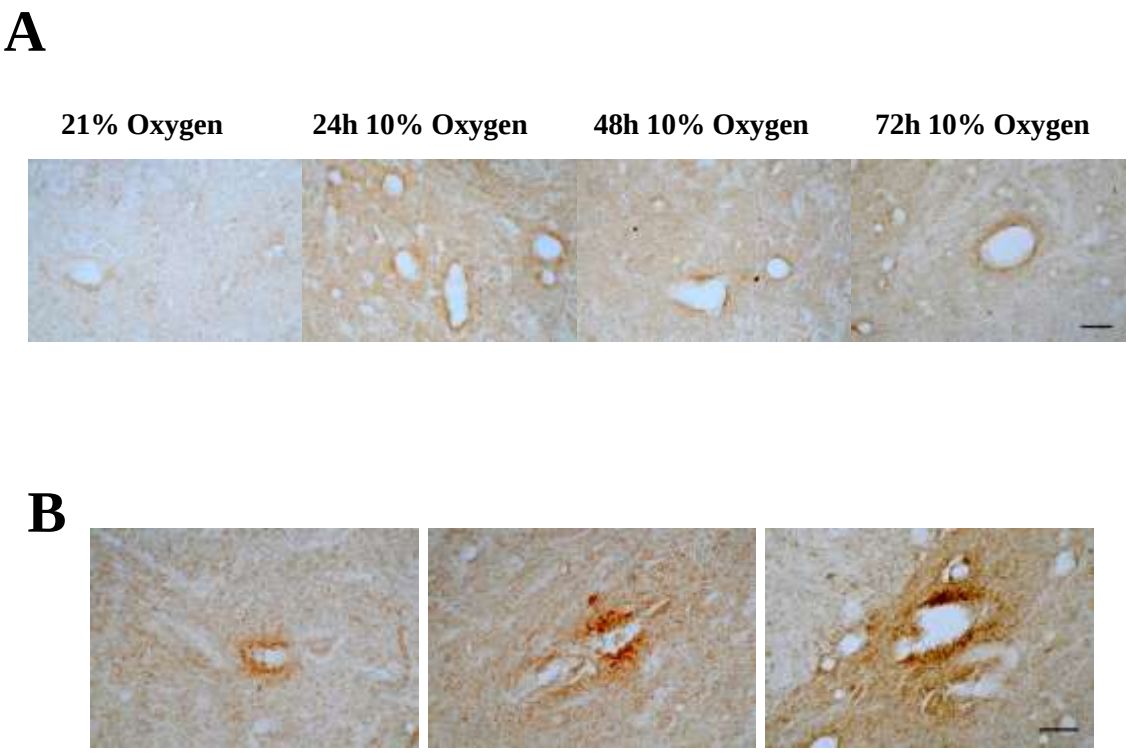

Figure 4.3.7.3: The effects of acute hypoxia on endothelial P-selectin expression
(A-B) Spinal cord sections from animals exposed to 21% oxygen, or 24h, 48h or 72h 10% oxygen, labelled with an anti-P-selectin antibody. (A) Some endothelial P-selectin expression is seen in 21% control animals, however, the expression of endothelial P-selectin is increased in animals exposed to 10% oxygen. (B) Some vessels in animals exposed to 72h 10% oxygen showed substantial P-selectin expression. Scale bar 25 μm. All micrographs are representative.

4.4.0.0 DISCUSSION

The present study provides evidence that reducing the concentration of inspired oxygen can expose regions of increased vulnerability to hypoxia in normal rat spinal cord. Accordingly, both a spatial vulnerability, and a heterogeneous cellular vulnerability, to hypoxia have been revealed. Notably, the results show that acute hypoxia induces microglial activation, suggesting that hypoxia can initiate an inflammatory response. The potential relevance of this finding to understanding MS is discussed.

4.4.1.0 Hypoxia-induced weight loss

The brain and spinal cord rely on a continuous supply of oxygen to meet the metabolic needs of the tissue. It has been suggested that the oxygen supply to the CNS occurs on a 'just sufficient' basis (LaManna et al., 2004), in which the CNS exists in a physiological, but predominantly low-oxygen state (LaManna et al., 2003). The physiological state of relative hypoxia is maintained by structural and functional adaptations, which also respond to changes in supplied oxygen tension (raised or lowered) to compensate for the change and prevent pathology and cell death. Systemic adaptations to prolonged hypoxia are fairly well understood, and include increased ventilation and hematocrit, decreased core temperature, bicarbonate ion excretion and a loss of body mass. The current study shows that exposure of rats to 10% oxygen (balance nitrogen) for 24, 48 and 72 hours results in a linear decrease in body mass (LaManna et al., 1992). Indeed, appetite suppression and decreased food intake are frequently observed due to hypoxia at high altitude (Westerterp et al., 1994; Westerterp

et al., 1999; Shukla et al., 2005). Moreover, some studies have found that hypoxia induces an increase in the levels of circulating leptin, a hormone with a central role in fat metabolism (Chaiban et al., 2008; Ling et al., 2008). Others have also found a direct effect of hypoxia on protein synthesis, with a decrease in whole-body insulin sensitivity and muscle-specific glucose utilisation (Iiyori et al., 2007), and intestinal dysfunction (Boyer and Blume, 1984; Quintero et al., 2010). Nevertheless, the mechanisms of weight loss under hypoxic conditions remain unclear.

4.4.2.0 Spatial and regional vulnerability to hypoxia

Labelling for hypoxia in the current study has revealed 'hypoxia-vulnerable' areas in the spinal white matter of animals exposed to 10% oxygen. Moreover, these pockets of pimonidazole labelling appear to occur *between* vessels, even though the drug is administered via the vasculature. It is easy to understand this finding, namely that regions of white matter that are more remote from vessels may be inherently vulnerable to hypoxia. Indeed, the local capillary tissue oxygen tension decreases from the arterial to the venular end of the vessel (Cater et al., 1961; Nair et al., 1975; Smith et al., 1977) and so it seems reasonable to propose that the pockets of pimonidazole labelling described in the current study may occur between the distal portions of white matter capillaries, although this remains to be investigated. In particular, the regions of hypoxia are likely to occur near veins, as venular blood is the most deoxygenated.

Interestingly, the white matter just below the dorsal horns, the 'wing-tip' regions of the dorsal columns, and the base of the dorsal columns, were shown to have increased susceptibility to hypoxia. The base of the dorsal columns is occupied by the dorsal corticospinal tract that is comprised primarily of small diameter axons. Small

diameter axons, by virtue of their surface to cytoplasmic volume ratio, may both have a relatively high oxygen demand, contributing to hypoxia, and also be predisposed to hypoxic damage. Indeed, axon size is an important determinant of susceptibility to degeneration in MS (Evangelou et al., 2001), with energy deficiency implicated as a key pathogenic mechanism (Stys, 2005; Dutta et al., 2006). Given that hypoxia can deplete metabolic energy vital for maintaining physiological processes, it seems reasonable to suggest that hypoxia may contribute to the selective vulnerability of small diameter axons to degeneration in MS (Evangelou et al., 2001).

Regional differences in the labelling for hypoxia were also found, with the thoracic segment of the spinal cord particularly vulnerable. Indeed, the vascular organisation is such that it creates intrinsic watershed zones at particular levels of the spinal cord (Tveten, 1976), and one of these zones has been reported to be the thoracic spinal cord. Despite this, due to the difference in size of the respective segments, blood flow values at the thoracic level are comparable to those at lumbar and cervical levels (Hayashi et al., 1983). In addition, no significant difference in local tissue oxygen metabolism exists between the various levels (Hayashi et al., 1983). Thus, factors other than differences in vascular density must influence the vulnerability of the thoracic segment to hypoxia, and watershed concepts provide a plausible explanation.

4.4.3.0 Selective cellular vulnerability to hypoxia

4.4.3.1 Oligodendrocyte vulnerability to hypoxia

Oxygen, among other substrates, is a vital requirement of cells, necessary for physiological function and survival. Thus, tight coupling between supply and demand

exists, to ensure effective energy metabolism. Moreover, cells within the CNS have different metabolic profiles, and preferentially utilise different pathways of energy metabolism, enabling them to meet the metabolic demands for specialised physiological function. This diversity, however, renders particular cell types more vulnerable to hypoxic insults. Accordingly, the current study provides evidence that neurons, and cells of oligodendrocyte lineage, in the rat spinal cord, are particularly vulnerable to becoming hypoxic and potentially hypoxia-induced damage. This finding is in agreement with previous studies, *in vitro* (Husain and Juurlink, 1995), and *in vivo* (Back et al., 2002). Indeed, due to their higher energy requirements, neurons rely heavily on a high rate of oxidative metabolism. Despite this, neurons ironically have a limited capacity to defend against oxidative stress (Shih et al., 2003; Belanger et al., 2011). Rather, neurons appear to depend on the high antioxidant potential of astrocytes for their own defence against oxidative stress (Dringen, 2000; Belanger et al., 2011). The metabolic profile of oligodendrocytes, is also specialised, and favours the synthesis of lipids, presumably to make myelin (Sánchez-Abarca et al., 2001). As with neurons, oligodendrocytes also have a limited capacity to defend against oxidative stress. Given that hypoxia can induce ROS production (Chandel et al., 1998; Guzy et al., 2006), it is not surprising that neurons and oligodendrocytes are selectively vulnerable to hypoxia-induced damage. Moreover, oligodendrocytes have a high iron and lipid content, which increases the potential for ROS generation, further increasing the vulnerability of this cell type. However, a recent study (Fünfschilling et al., 2012) contradicts this traditional view of oligodendrocyte vulnerability. Fünfschilling and colleagues appear to show that mature, post-myelinating oligodendrocytes can survive without functional mitochondrial complex IV. The authors propose that mature oligodendrocytes survive

by simply increasing their glycolytic capacity, releasing lactate as an end product, which is rapidly utilised by myelinated axons (Fünfschilling et al., 2012).

In contrast, astrocytes and microglia were found to be relatively resistant to becoming hypoxic, in the current study, as indicated by the lack of pimonidazole labelling. Astrocytes, in particular, exhibit greater metabolic plasticity than neurons (Almeida et al., 2001; Vega et al., 2006), i.e., they are able to adapt their energy metabolism in response to environmental challenges (Belanger et al., 2011), owing to their resistance to hypoxic stresses. For example, following NO-induced mitochondrial inhibition, astrocytes increase glucose metabolism via glycolytic pathways, thereby preventing ATP depletion (Almeida et al., 2001). Similarly, the resistance of microglial cells to hypoxia has been attributed to their ability to easily adapt, and overcome non-physiological conditions (Yun et al., 1997).

4.4.3.2 OPCs display a reactive phenotype following exposure to acute hypoxia

Besides oligodendrocyte vulnerability, $NG2^+$ OPCs in the spinal cord were also affected by exposure to acute hypoxia in the current study. $NG2^+$ OPCs represent a subpopulation of glial cells that are antigenically distinct from other glial cells (Levine et al., 1993; Nishiyama et al., 1997; Reynolds and Hardy, 1997; Keirstead et al., 1998; McTigue et al., 1998; Butt et al., 1999; Ong and Levine, 1999; Dawson et al., 2003), and are found not only during development but are also abundant in the adult rodent brain (Levine et al., 1993; Nishiyama et al., 1996; Reynolds and Hardy, 1997), distributed quite uniformly throughout the white and grey matter. These intriguing cells are inherently plastic, and once activated are able to rapidly proliferate and mature into oligodendrocytes. They display heterogeneity with regard to the different cell types into

which they can develop (Belachew et al., 2003; Alonso, 2005; Cassiani-Ingoni et al., 2006), and function (Bergles et al., 2000; Jabs et al., 2005; Karadottir et al., 2005; Kukley et al., 2007; Ziskin et al., 2007). In the current study, clusters of 'hypoxic' NG2+ cells within foci of intense labelling for hypoxia within the white matter, were often surrounded by a paucity of cells labelling for NG2. Whether this loss represents maturation of NG2+ OPCs, cell death, or migration, remains to be investigated. Indeed, hypoxia has been found to induce premature differentiation of OPCs *in vitro*, and it is thought to contribute to hypomyelination in the developing hypoxic brain (Akundi and Rivkees, 2009). Furthermore, OPCs are particularly vulnerable to hypoxia *in vitro* (Husain and Juurlink, 1995).

The current study also demonstrates that hypoxia induces OPC hypertrophy and clustering around vessels, in a time-dependent manner. It seems reasonable to propose that a morphological change such as hypertrophy may represent a reaction of the $NG2^+$ cells to potentially damaging stimulus. Indeed, this is supported by their perivascular location following 72h of prolonged hypoxia in the present study. Lesions that disrupt the BBB have been shown to induce $NG2^+$ OPC hypertrophy (Rhodes et al., 2006). Although, such a response is not evident following lesions where the BBB remains intact (Rhodes et al., 2006), the present findings suggest that $NG2^+$ cells display surveillance-like functions, allowing them to detect changes within the tissue microenvironment, as has been previously proposed (Dawson et al., 2003; Rhodes et al., 2006).

4.4.4.0 Hypoxia-induced microglial activation

Hypoxia is an important event that regulates a wide range of physiological responses. Microglia represent the first line of immune defence within the CNS, and increasing

evidence suggests that hypoxia-induced microglial activation contributes to neuronal damage in stroke, in addition to the neurodegeneration that results from the direct loss of oxygen and glucose (Gonzalez-Scarano and Baltuch, 1999; Suk, 2005). The present data demonstrate that exposure to acute hypoxia induces mild microglial proliferation and activation, as assessed by the respective density of IBA+ cells and the number of cells expressing MHC class II. Indeed, proliferation and MHC class II expression are a common response of microglia to pathological stimuli. Consistent with the current findings, microglial proliferation (Mander et al., 2005) and activation have previously been described in the brain (Wang and Kaur, 2000) and retina (Kaur et al., 2006b) following hypoxia. An increase in microglial density and number of cells expressing MHC class II may represent a precursor for pathology in an otherwise normal-appearing CNS, or a type of priming or sensitization in the event of a subsequent insult. However, a western blot would confirm whether MHC class II expression is increased in response to hypoxia. Interestingly, activated microglia have been observed in cortical grey matter and normal appearing white matter, remote to areas of active demyelination in MS post-mortem tissue (Allen et al., 2001; De Groot et al., 2001). These preactive lesions are characterised by clusters or nodules of microglial cells expressing the MHC class II antigen. The absence of BBB leakage, leukocyte infiltration and demyelination, in these lesions has led to the suggestion that MS may result from the intrinsic activation of the innate immune system. However, the 'trigger' of this activation remains unknown. The ability of hypoxia to induce similar changes to those seen in preactive lesions is particularly interesting, and will be discussed in further detail later.

Microglia are characterised by their high responsiveness to atypical events, responding robustly to minor pathological challenges to the CNS (Kreutzberg, 1996). They are able to respond in a graded manner to changes in their local environment,

giving rise to an array of phenotypes (Graeber, 2010). Many studies have reported constitutive MHC class II expression in microglia (Lowe et al., 1989; Zhang et al., 2002), however it is thought that this expression is kept to a minimum through contact-dependent inhibition by neurons. Therefore, if neurons reduce this inhibition as a consequence of degeneration or 'distraction' due to hypoxia, the loss of such inhibitory control may represent a potential mechanism through which hypoxia-induced microglial MHC class II could be amplified to cause a wider nidus of inflammation.

A potential avenue of microglial activation is via breakdown of the BBB, and subsequent vascular leakage, and indeed hypoxia is reported to induce such a leakage *in vivo* (Schoch et al., 2002). The consequent exposure of microglia to serum proteins such as fibrinogen would engage CD11b/CD18 integrin heterodimers (Adams et al., 2007), leading to microglial activation. However, arguing against this possibility, no evidence of serum protein leakage was found in the present study.

The current study shows that the morphological phenotype of MHC class II positive microglia varies following hypoxia, such that the percentage of microglia displaying a more activated phenotype increases with the duration of the hypoxia. Microglial activation is a dynamic process, thought to occur in a graded manner (Kreutzberg, 1996). The dynamics of microglial activation have been elegantly shown by time-lapse confocal microscopy *in vitro* (Stence et al., 2001) and *in vivo* (Nimmerjahn et al., 2005). The latter study has drawn attention to the on-going surveillance of brain tissue by the constant 'probing' of their environment with fine processes (Nimmerjahn et al., 2005).

Activated, amoeboid microglia often display phagocytic properties, normally representing one extreme of their capability. The antibody ED1, which recognises an

antigen in lysosomal membranes, is a useful marker of phagocytosis, since the expression of the antigen in macrophages increases with phagocytic activity (Damoiseaux et al., 1994). To determine the activation state of the microglia within the spinal cord following exposure to 10% oxygen, immunohistochemistry with an ED1 antibody was performed, however no evidence of ED1 immunoreactivity was found. It seems that hypoxia causes an activation of microglia (i.e. their density and expression of MHC class II increases) but that activation stops short of the expression of ED1.

Microglia are crucial effector cells of the innate immune system, and following activation they can initiate signalling pathways that can be either protective or destructive. Although the exact mechanisms remain unclear, the cytokine profile and expression of certain proteins in microglia can give an indication of whether the activation is destined to be protective or destructive. The expression of the enzyme iNOS in microglia is usually a good indicator of the activation of a pro-inflammatory signalling pathway. Moreover, the gene responsible for iNOS production has a HRE in its promoter region, and can therefore be induced by hypoxia via HIF-1α (Melillo et al., 1995; Palmer et al., 1998). Although iNOS expression was not evident following exposure to 10% oxygen in the current study, previous research has shown that hypoxia can induce iNOS expression in microglia, *in vitro* (You and Kaur, 2000). This discrepancy may reflect differences in the severity of the hypoxia, and/or the differences between *in vivo* and *in vitro* conditions.

TLRs play a pivotal role in the innate immune response against invading pathogens. To date, more than 10 mammalian TLRs have been identified (Kawai and Akira, 2006), however, microglial TLR4 plays an especially important role in the immune and inflammatory response in the CNS (Jung et al., 2005). The current study demonstrates that TLR4 expression within the spinal cord increases with the duration of

hypoxia, *in vivo*. This is consistent with previous *in vitro* findings in both microglia (Ock et al., 2006) and macrophages (Kim et al., 2010). TLR4 expression is dynamically modulated, and its levels at an infected site are critical for an appropriate inflammatory response: for example, TLR4 deficient mice exhibit a decreased inflammatory response and thereby smaller lesions following brain ischaemia (Caso et al., 2007). Thus, TLR4 is instrumental to inflammatory and pathological responses, and has also been shown to mediate inflammatory neurodegeneration (Lehnardt et al., 2003). The present findings imply that hypoxia may exacerbate inflammatory responses to infections by up-regulating TLR4 expression on microglia, and may therefore have implications for the pathogenesis of neurodegenerative diseases such as MS, a point that I will return to later in the thesis.

4.4.5.0 Regional and inter-animal vascular differences

Adaptive responses are a well-recognised feature during hypoxic insults, and essentially act to minimise the effect of the decreased oxygen availability. One such response is angiogenesis, beginning around day four of mild hypoxic exposure (Xu and LaManna, 2006) and complete by 3 weeks (Pichiule and LaManna, 2002). Consistent with these previous findings, the relatively short duration of exposure to 10% oxygen in the current study did not result in an increase in the vascular density of the spinal cord.

The activated microglia and hypoxia-positive NG2 cells were almost exclusively present in the white matter. It seems likely that this pattern correlates with the much lower vascular density of the white matter (compared with that of the grey matter), which is presumably associated with the decreased metabolic activity of this compartment (Rawe and Perot, 1977; Hayashi et al., 1983b). In addition, the blood

flow in the white matter is significantly lower than the grey matter (Hayashi et al., 1983b). Aside from these considerations, the white matter is primarily served by blood that has initially passed through the grey matter and this anatomical organisation renders the white matter especially vulnerable to hypoxia due to prior oxygen extraction and 'vascular steal' by more proximal spinal tissue.

Besides such a regional and compartmental variation in vascular density, a considerable amount of inter-animal variation in the vascular density was also observed in the current study. This finding suggests that individual animals may have different vulnerabilities to hypoxia as dictated by their vascular anatomy. Indeed, there are regional differences in the vascular density in the hippocampus; the CA1 region, which is particularly vulnerable to degeneration due to mild ischaemia (reviewed in Schmidt-Kastner and Freund, 1991), has a significantly lower vascular density than the CA3 region (Cavaglia et al., 2001), which is more resistant to ischaemic damage than CA1 (reviewed in Schmidt-Kastner and Freund, 1991). Thus, inter-individual variations in vascular density may perhaps explain the predilection for MS lesions to form in specific regions of the CNS. I will return to this point later in the thesis.

4.4.6.0 Hypoxia induces changes in endothelial cells

By virtue of their location, endothelial cells have to cope with alterations in the composition of the blood. One such alteration is hypoxia, and it is thought to have profound effects on endothelial cell function. Hypoxia alone can induce endothelial activation (Dore-Duffy et al., 1999), thereby initiating a cascade of events culminating in neutrophil adherence and recruitment (Milhoan et al., 1992; Arnould et al., 1993; Ginis et al., 1993; Baudry et al., 1998). The current study shows that endothelial cells

become hypoxic following exposure to 10% oxygen, resulting in an increase in the expression of endothelial P-selectin. P-selectin is a cell adhesion molecule expressed on activated endothelial cells and platelets. In unactivated endothelial cells, P-selectin is stored in Weibel-Palade bodies (WPBs) (Bonfanti et al., 1989; Harrison-Lavoie et al., 2006), so that it can be rapidly transported to the endothelium upon activation. Hypoxia has been shown to induce a calcium dependent exocytosis of WPBs (Pinsky et al., 1996), resulting in the overexpression of P-selectin, which then initiates neutrophil binding. Accordingly, hypoxia-induced neutrophil adherence can be blocked using antibodies against P-selectin (Arnould et al., 1993; Rainger et al., 1995). Thus the present findings suggest that hypoxia can facilitate the inflammatory response by modulating the expression of cell adhesion molecules on endothelial cells. This point will be discussed in more detail later in this thesis.

4.4.7.0 Conclusion

The present study provides evidence that the rat spinal cord has selective vulnerabilities to hypoxia expressed at the regional (thoracic segment), compartmental (white matter) and cellular (oligodendrocytes and OPCs) levels. These selective vulnerabilities may be in part dictated by the vascular architecture of the spinal cord, and the intrinsic properties of these levels. Moreover, hypoxia appears to sensitize the spinal cord, firstly by promoting adherence of leukocytes to the endothelium through the upregulation of the CAM P-selectin, and secondly by increasing the responsiveness of microglia, by increasing the number of cells expressing MHC class II and TLR4 molecules. Given that hypoxia is a common feature of inflammation, it seems reasonable to propose that it may perpetuate damage by propagating the immune

response, rather than representing an innocent bystander of the inflammatory milieu. Additionally, the ability of hypoxia to sensitize or prime the resident microglia, may decrease the threshold required for activation of an innate immune response. These findings may have implications for the pathogenesis of number of neurodegenerative diseases, including MS, and the ideas will be brought together later in the thesis to form a hypothesis relevant to this disease.

CHAPTER FIVE

GENERAL DISCUSSION

This thesis demonstrates that true tissue hypoxia, a common, yet underestimated feature of inflammatory lesions, appears to be involved in two of the three of the cardinal features of MS. First, hypoxia is involved in the loss of neurological function observed in MOG-induced EAE, second, and in the development of demyelination in the experimental Pattern III lesion. Finally, this thesis provides evidence that selective regional and cellular vulnerabilities to hypoxia exist in the normal rat spinal cord, and that hypoxia can sensitise resident microglia, thereby decreasing the threshold required to initiate an immune response, or propagating micorglial activation during periods of inflammation . Curiously, despite increasing evidence supporting the notion that the oxygen concentration within active MS and EAE lesions may be low (Simmons et al., 1982; Juhler, 1987; Aboul-Enein et al., 2003; Graumann et al., 2003), the possibility that hypoxia may be a key factor in MS has not been explored until now.

Increasing evidence suggests that an energy failure may represent an important mechanism involved in the pathogenesis of the cardinal features of MS (Aboul-Enein et al., 2003; Mahad et al., 2008; Trapp and Stys, 2009), however, hypoxia, *per se*, is often regarded as an unlikely cause of such a failure because under normal circumstances hypoxia has to be quite profound before it impairs mitochondrial respiration. This is due

to the fact that mitochondrial complex IV has a very low Km for oxygen (<1μM), and so mitochondria are capable of making use of even very low oxygen concentrations for oxidative phosphorylation. However, this advantage fails in inflamed tissue because of the presence of NO. Even very low concentrations of nitric oxide can dramatically raise the mitochondrial Km for oxygen (Brown and Cooper, 1994), meaning that even greater oxygen concentrations than normal may be required to sustain mitochondrial function. Accordingly, even a small change in local oxygen tension may have a large effect on cellular function, when coupled with inflammation involving NO production. Furthermore, elevated levels of ROS, such as superoxide, are also associated with the inflammatory milieu, thereby further increasing the potential for toxicity. Therefore the pathophysiological significance of hypoxia is magnified in neuroinflammatory lesions, such as in MS.

5.1.0.0 Hypoxia and loss of neurological function

This thesis provides chemical, physical and therapeutic evidence that hypoxia, on a background of inflammation, can reversibly induce neurological dysfunction in an animal model of MS, in the absence of demyelination. Traditionally, neurological dysfunction in MS has been attributed to abnormalities in axonal conduction, such as those arising from demyelination (McDonald, 1986). However, more recently, studies have emphasised the potential role of inflammation (Youl et al., 1991; Moreau et al., 1996, and Bitsch et al., 1999), but the exact mechanisms responsible have remained unclear. A role for NO has been invoked (Redford et al., 1997; Shrager et al., 1998), due to the prominence of NO production in some MS lesions (Bo et al., 1994; Bagasra et al., 1995; Johnson et al., 1995), and findings that NO can block axonal conduction in

normal and demyelinated axons. We believe that NO may well be involved, but that its potency may require the concurrent presence of hypoxia.

There are several mechanism(s) by which hypoxia may compromise neurological function. For example, neurons of different brain regions have been shown to exhibit depolarizing and/or hyperpolarising responses following short periods of hypoxia (Fujiwara et al., 1987; Leblond and Kmjevic, 1989). These typical responses are a consequence of a marked decline in intracellular ATP levels (Fujiwara et al., 1987; Nieber et al. 1995), and thereby an energy insufficiency that is mediated by hypoxia. The depolarisation has been attributed to the failure of the Na+/K+ ATPase pump (Fujiwara et al. 1987; Nieber et al. 1995), whereas the hyperpolarisation is thought to be mediated by the opening of ATP-dependent K+ channels (K_{ATP}) (Zhang and Krnjevic, 1993; Fujimura et al. 1997; Finta et al., 1993; Nieber et al. 1995). Changes in membrane potential such as these essentially result in a reversible loss of function, as seen in rMOG EAE. Furthermore, hypoxia has been found to inhibit myelin phosphorylation in oligodendrocytes (Qi and Dawson, 1993), thus disturbing myelination, which could also result in abnormal conduction, although this seems less likely as a leading mechanism of loss of function in view of the prompt restoration of function by breathing oxygen.

Although most neurological deficits in MS are probably due to demyelination and degeneration, this research shows that hypoxia can also cause loss of function, and so it provides a possible explanation for brief relapses that cannot easily be explained by demyelination and degeneration. This realisation opens the door to understand that some more persisting deficits are not necessarily caused only by the demyelination and degeneration to which they are currently attributed. So the current findings introduce hypoxia as a new additonal mechanism for loss of function in MS. At present, the extent to which hypoxia plays a role in causing loss of function in MS remains unclear.

Hypoxia may be a key mechanism responsible for loss of function early in a relapse, before the same symptoms become consolidated by demyelination and degeneration.

5.2.0.0 'Hypoxia-like' demyelination

Neuropathological studies on the human Pattern III MS lesion have led to the suggestion that 'hypoxia-like' demyelination is a consequence of an energy insufficiency, attributed to mitochondrial dysfunction mediated by NO (Aboul-Enein et al., 2005). However, this thesis demonstrates that tissue hypoxia, in association with NO and superoxide, not only precedes demyelination in experimental 'hypoxia-like' Pattern III lesions, but may actually be causally involved in inducing the formation of such lesions. Thus the spatio-temporal nature of the hypoxia, NO and superoxide, appears to determine the exact location of the demyelinated lesion that formed approximately a week later. Notably, the lesion forms at the base of the dorsal column, a region that our results show is particularly vulnerable to hypoxia. This finding is particularly interesting given that the demyelination in both the human Pattern III and experimental lesion has been described to occur via a mechanism that is 'hypoxia-like' (Aboul-Enein et al., 2003). Presumably, the increased vulnerability of the base of the dorsal column to hypoxia reduces the threshold of toxicity required to induce damage. Accordingly, vulnerable cell types, such as oligodendrocytes, shown in this thesis to be particularly hypoxic, succumb to a profound energy deficit due to the combined effects of hypoxia, NO and superoxide, leading to 'hypoxia-like' demyelination. This observation may perhaps help to explain lesion topography in MS. Indeed, some regions of the CNS are vulnerable to to disturbances in vascular perfusion, and hypoxia-mediated damage. These so-called watershed regions are located between two major arterial supplies, and one such area is the periventricular region of the brain where MS lesions are commonly

found. These regions will presumably have a reduced threshold for toxicity and so may not withstand the barrage of toxic mediators during periods of acute and chronic inflammation, resulting in preferential structural damage.

5.3.0.0 Hypoxia and degeneration

Axonal damage can be a major cause of irreversible neurological deficit in patients with MS (Trapp et al., 1998; Bjartmar and Trapp, 2003; Dutta and Trapp, 2007). Although axonal injury is evident in acute MS lesions (Ferguson et al., 1997; Trapp et al., 1998), at this stage the damage may remain clinically silent. However, there is a concomitant on-going, chronic 'slow-burning' of axons that can persist for years (Lassmann, 2007; Trapp and Nave, 2008; Dutta and Trapp, 2011), and is thought to be responsible for the transition to progressive disease. Due to several lines of evidence suggesting a state of impaired mitochondrial energy production (Smith and Lassmann, 2002; Bechtold and Smith, 2005; Dutta et al., 2006; Mahad et al., 2008), in addition to increased energy demand consequent to the greater expression of leaky sodium channels along the denuded axolemma (Craner et al., 2004), demyelinated axons have been suggested to be subjected to a chronic state of 'virtual hypoxia' (Stys, 2004). It is easy to appreciate that this prolonged state of energy insufficiency can promote chronic necrosis and degeneration of axons in the MS brain. Perhaps more important is the fact that a chronic energy insufficiency will render the axons more vulnerable to the wide range of insults that will occur over the years, but it may also directly cause degeneration. For example, the lack of energy substrates disrupts the ionic gradient across the axolemma, resulting in the intracellular accumulation of sodium and calcium, and the loss of potassium (Stys and LoPachin, 1996), resulting in the initiation of calcium-mediated cell death signalling pathways. Indeed, such a mechanism is well established in hypoxic/ischemic

models, hence the term ‘virtual hypoxia’. However, in the light of the current findings, it seems reasonable to hypothesise that demyelinated axons may be in fact rendered to a state of actual tissue hypoxia, rather than ‘virtual hypoxia’. Given that none of the current therapies reduce the ‘slow-burning’ destruction of axons, the current finding that actual tissue hypoxia may be involved in the pathogenesis of MS may provide a better understanding of why chronically demyelinated axons degenerate, and possibly introduce the opportunity to develop novel therapeutic strategies. Nevertheless, the role of hypoxia in axonal degeneration is yet to be elucidated.

5.4.0.0 Hypoxia and the normal spinal cord-implications for MS?

Despite the considerable progress in MS research over the years, the aetiology of the disease remains elusive, although evidence suggests that a complex interplay of genetic and environmental factors is involved (Noseworthy, 1999). It has been traditionally assumed that a dysregulation of the adaptive immune repertoire against one or more CNS antigens may represent the primary trigger of MS (McFarland and Martin, 2007), and this view has long been upheld by the EAE model of MS that mimics the disease. However, increasing evidence suggests that the disease may in fact result from the activation of the innate immune system (Allen and McKeown, 1979; De Groot et al., 2001; Barnett and Prineas, 2004; Marik et al., 2007; van Horssen et al., 2012). Despite these findings, it is not clear how the innate immune system would become activated, in the absence of BBB breakdown, leukocyte infiltration and demyelination (De Groot et al., 2001). In this regard it is interesting to consider the current findings that the spinal cord exhibits regional and cellular vulnerabilities to hypoxia. Furthermore, hypoxia can activate cells of the innate immune system, namely microglia, but also induce the expression of P-selectin on endothelial cells, thereby facilitating leukocyte

transmigration into the CNS. Needless to say, such a microglial response may reflect a protective strategy rather than a phenotypic change that is deleterious. Indeed the lack of induction of iNOS and ED1 expression are suggestive of a response that is not damaging. However, the nature of microglial activation following hypoxia, either protective or deleterious, requires further investigation.

It seems clear that hypoxia can make the innate immune system more receptive to the induction of inflammation, e.g. by responding to an ongoing viral or bacterial infection, but it is less clear whether hypoxia can itself induce inflammation of a sufficient magnitude to result in the formation of an MS lesion. The former mechanism is particularly interesting given that the human herpes Epstein-Barr virus (EBV) is hypothesised to play a role in the aetiology of MS (Ascherio et al., 2001; Thorley-Lawson, 2001; Haahr and Höllsberg, 2006; Pohl et al., 2006; Thacker et al., 2006; Ascherio and Munger, 2007a). Acute infection with EBV is followed by a life-long presence of the latent virus (Golden et al., 1973), which can be reactivated to lytic replication. EBV infection has been described in MS post mortem brain tissue, with the majority of the cells harbouring the latent virus (Serafini et al., 2007; Tzartos et al., 2012). In addition to EBV infection, smoking is also considered a risk factor for MS (Ascherio and Munger, 2007b). Conflicting studies investigating the combined effects of high anti-EBVNA (EBV nuclear antigen) titres and smoking on MS risk, with some studies describing a strong association (Simon et al., 2010) and others describing no association (Sundqvist et al., 2012). Considering that smoking can lead to acute periods of tissue hypoxia (Sagone et al., 1973; Jensen et al., 1991) and hypoxia can reactivate latent EBV *in vitro* (Jiang et al., 2006), it seems reasonable that hypoxia-mediated reactivation of latent EBV in smokers may represent a pathogenetic mechanism of MS, particularly given that EBV infection can elicit an inflammatory response (Tzartos et al.,

2012). Alternatively, the sensitisation of microglia by hypoxia may make the CNS more 'receptive' to invading pathogens that may otherwise not elicit an immune response. It seems reasonable that the magnitude of the hypoxia would be increased in individuals who smoke, thereby reducing the threshold required for the activation of the innate immune system. However, this remains to be investigated.

The current observation that there is considerable inter-individual variation in vascular density may also have implications for MS. It seems reasonable to assume that an individual with a decreased vascular density would be more vulnerable to becoming hypoxic than, say, an individual with a greater vascular density. Such a variation in vascular density may explain why MS is such a heterogeneous disease. Interestingly, a decreased vascular density of the hippocampal CA1 region has been associated with its increased vulnerability to hypoxia/ischaemia, in comparison with other hippocampal regions (Cavaglia et al., 2001), supporting such a theory.

5.5.0.0 Future directions

This thesis demonstrates that acute neuroinflammatory lesions are hypoxic, and that the severity of the hypoxia is sufficient to cause functional and structural consequences, in diseases such as MS. Furthermore, this thesis provides evidence that hypoxia may represent a potential cause of the disease itself. However, these findings give rise to a number of questions that should form the basis of future projects.

1) Despite the observation that hypoxia is a feature of acute neuroinflammation, the exact cause of the hypoxia itself remains unclear. Hypoxia ensues when the demand of oxygen outweighs its supply, so it is important to determine the contribution of individual factors involved in this balance to deduce the cause of the hypoxia during

neuroinflammation. There are a number of likely causes for an impaired oxygen supply including, but not restricted to a) obstruction of venous drainage due to perivascular cuffing by inflammatory cells; b) thrombotic occlusion of the microvasculature; c) reduction in CBV; and d) alterations in CBF. The most likely causes of increased oxygen demand include a) increased cellular load due to the massive infiltration of inflammatory cells; b) increased oxygen consumption for the formation of NO and superoxide, including during respiratory burst activity via NADPH oxidase; and perhaps c) increased metabolic demand to fuel ATP production. All these issues can be addressed experimentally *in vivo*, and would lead to a deeper understanding of the mechanisms involved.

2) The therapeutic benefit of normobaric oxygen was touched on in the current thesis, however, the optimal treatment regime still needs refining. The length, duration, and frequency of exposure are all important factors to consider. Alternative treatments aimed at increasing oxygenation may also prove beneficial, and may warrant investigating. One example is the use of perfluorocarbons (PFC) (reviewed in Spahn, 1999). PFCs are chemically inert synthetic molecules that have the ability to dissolve significant amounts of oxygen. PFCs, by virtue of their small size (<0.2 μm in diameter), are able to perfuse even the smallest of capillaries (4-5 μm in diameter), where blood may not flow under certain conditions. All the oxygen carried by PFCs is in the dissolved state, therefore increasing the partial pressure of oxygen in the microcirculation and augmenting the oxygen diffusion into the tissue. Such an application would presumably have a considerable affect in EAE, given that the maximal tissue oxygenation possible with normobaric oxygen alone is somewhat

limited. Additionally, the safety of prolonged normobaric oxygen exposure requires particular attention as there is a danger of promoting oxidative damage.

3) Finally, the hypothesis that hypoxia may play a role in inducing MS requires further research. Currently, the data are very preliminary. Examining the long-term effects of acute hypoxia is expected to reveal interesting findings. Additionally, identifying whether acute hypoxia can sensitise the CNS to subsequent systemic infections, using agents such as LPS, will be of particular interest.

5.6.0.0 Concluding remarks

This thesis provides novel observations that hypoxia may be a hitherto-unrecognised, yet potentially important factor in two of the three cardinal features of MS, namely inflammation-mediated neurological dysfunction and demyelination. The data are consistent with the notion that neurological dysfunction and structural damage occur due to an energy insufficiency in vulnerable cell types, and suggest that this energy deficit is at least partly mediated by hypoxia. Furthermore, this thesis provides evidence that selective regional and cellular vulnerabilities to hypoxia exist in the normal spinal cord, which may help explain why some cell types are preferentially affected in MS. The findings have implications for our understanding of MS, leading to a deeper understanding of the mechanisms involved and novel potential strategies for therapy.

BIBLIOGRAPHY

Abeles, M., 1991. Corticonics: neural circuits of the cerebral cortex. Cambridge University Press.

Aboul-Enein, F., Lassmann, H., 2005. Mitochondrial damage and histotoxic hypoxia: a pathway of tissue injury in inflammatory brain disease? Acta Neuropathol 109, 49–55.

Aboul-Enein, F., Rauschka, H., Kornek, B., Stadelmann, C., Stefferl, A., Brück, W., Lucchinetti, C., Schmidbauer, M., Jellinger, K., Lassmann, H., 2003. Preferential loss of myelin-associated glycoprotein reflects hypoxia-like white matter damage in stroke and inflammatory brain diseases. J. Neuropathol. Exp. Neurol 62, 25–33.

Acker, H., 2005. The oxygen sensing signal cascade under the influence of reactive oxygen species. Phil. Trans. R. Soc. B 360, 2201–2210.

Adams, R.A., Schachtrup, C., Davalos, D., Tsigelny, I., Akassoglou, K., 2007. Fibrinogen Signal Transduction as a Mediator and Therapeutic Target in Inflammation:Lessons from Multiple Sclerosis. Current Medicinal Chemistry 14, 2925–2936.

Adhya, S., Johnson, G., Herbert, J., Jaggi, H., Babb, J.S., Grossman, R.I., Inglese, M., 2006. Pattern of hemodynamic impairment in multiple sclerosis: dynamic susceptibility contrast perfusion MR imaging at 3.0 T. Neuroimage 33, 1029–1035.

Afifi, A.K., Bergman, R.A., 2005. Functional neuroanatomy: text and atlas, 2nd ed. McGraw-Hill Professional.

Ahmed, N., Kansara, M., Berridge, M.V., 1997. Acute regulation of glucose transport in a monocyte-macrophage cell line: Glut-3 affinity for glucose is enhanced during the respiratory burst. Biochem J 327, 369–375.

Aiello, L.C., Wheeler, P., 1995. The Expensive-Tissue Hypothesis: The Brain and the Digestive System in Human and Primate Evolution. Current Anthropology 36, 199–221.

Airley, R.E., Loncaster, J., Raleigh, J.A., Harris, A.L., Davidson, S.E., Hunter, R.D., West, C.M.L., Stratford, I.J., 2003. GLUT-1 and CAIX as intrinsic markers of hypoxia in carcinoma of the cervix: relationship to pimonidazole binding. Int. J. Cancer 104, 85–91.

Akundi, R.S., Rivkees, S.A., 2009. Hypoxia Alters Cell Cycle Regulatory Protein Expression and Induces Premature Maturation of Oligodendrocyte Precursor Cells. PLoS ONE 4.

Allen, I.V., McKeown, S.R., 1979. A histological, histochemical and biochemical study of the macroscopically normal white matter in multiple sclerosis. Journal of the Neurological Sciences 41, 81–91.

Allison, J.D., Meador, K.J., Loring, D.W., Figueroa, R.E., Wright, J.C., 2000. Functional MRI cerebral activation and deactivation during finger movement. Neurology 54, 135–142.

Almeida, A., Almeida, J., Bolaños, J.P., Moncada, S., 2001. Different responses of astrocytes and neurons to nitric oxide: The role of glycolytically generated ATP in astrocyte protection. PNAS 98, 15294–15299.

Al-Omari, M.H., Rousan, L.A., 2010. Internal jugular vein morphology and hemodynamics in patients with multiple sclerosis. Int Angiol 29, 115–120.

Ames, A., 3rd, 2000. CNS energy metabolism as related to function. Brain Res. Brain Res. Rev. 34, 42–68.

Amor, S., Groome, N., Linington, C., Morris, M.M., Dornmair, K., Gardinier, M.V., Matthieu, J.M., Baker, D., 1994. Identification of epitopes of myelin oligodendrocyte glycoprotein for the induction of experimental allergic encephalomyelitis in SJL and Biozzi AB/H mice. J. Immunol. 153, 4349–4356.

Ances, B.M., Greenberg, J.H., Detre, J.A., 1999. Laser doppler imaging of activation-flow coupling in the rat somatosensory cortex. Neuroimage 10, 716–723.

Andersson, P.-B., Perry, V.H., Gordon†, S., 1992. The acute inflammatory response to lipopolysaccharide in cns parenchyma differs from that in other body tissues. Neuroscience 48, 169–186.

Antulov, R., Carone, D.A., Bruce, J., Yella, V., Dwyer, M.G., Tjoa, C.W., Benedict, R.H.B., Zivadinov, R., 2011. Regionally distinct white matter lesions do not contribute to regional gray matter atrophy in patients with multiple sclerosis. J Neuroimaging 21, 210–218.

Argaw, A.T., Asp, L., Zhang, J., Navrazhina, K., Pham, T., Mariani, J.N., Mahase, S., Dutta, D.J., Seto, J., Kramer, E.G., Ferrara, N., Sofroniew, M.V., John, G.R., 2012. Astrocyte-derived VEGF-A drives blood-brain barrier disruption in CNS inflammatory disease. J. Clin. Invest. 122, 2454–2468.

Arnould, T., Michiels, C., Remacle, J., 1993. Increased PMN adherence on endothelial cells after hypoxia: involvement of PAF, CD18/CD11b, and ICAM-1. Am. J. Physiol. 264, C1102–1110.

Arteel, G.E., Thurman, R.G., Raleigh, J.A., 1998. Reductive metabolism of the hypoxia marker pimonidazole is regulated by oxygen tension independent of the pyridine nucleotide redox state. Eur. J. Biochem 253, 743–750.

Arteel, G.E., Thurman, R.G., Yates, J.M., Raleigh, J.A., 1995. Evidence that hypoxia markers detect oxygen gradients in liver: pimonidazole and retrograde perfusion of rat liver. Br. J. Cancer 72, 889–895.

Ascherio, A., Munger, K.L., 2007a. Environmental risk factors for multiple sclerosis. Part I: the role of infection. Ann. Neurol. 61, 288–299.

Ascherio, A., Munger, K.L., 2007b. Environmental risk factors for multiple sclerosis. Part II: Noninfectious factors. Ann. Neurol. 61, 504–513.

Attwell, D., Laughlin, S.B., 2001. An energy budget for signaling in the grey matter of the brain. J. Cereb. Blood Flow Metab. 21, 1133–1145.

Aulak, K.S., Miyagi, M., Yan, L., West, K.A., Massillon, D., Crabb, J.W., Stuehr, D.J., 2001. Proteomic method identifies proteins nitrated in vivo during inflammatory challenge. Proc. Natl. Acad. Sci. U.S.A. 98, 12056–12061.

Babior, B.M., 1984. The respiratory burst of phagocytes. J. Clin. Invest 73, 599–601.

Babior, B.M., 1999. NADPH Oxidase: An Update. Blood 93, 1464–1476.

Babior, B.M., 2000. The NADPH oxidase of endothelial cells. IUBMB Life 50, 267–269.

Babior, B.M., Lambeth, J.D., Nauseef, W., 2002. The neutrophil NADPH oxidase. Arch. Biochem. Biophys. 397, 342–344.

Back, S.A., Han, B.H., Luo, N.L., Chricton, C.A., Xanthoudakis, S., Tam, J., Arvin, K.L., Holtzman, D.M., 2002. Selective Vulnerability of Late Oligodendrocyte Progenitors to Hypoxia–Ischemia. J. Neurosci. 22, 455–463.

Baddeley, R., Abbott, L.F., Booth, M.C., Sengpiel, F., Freeman, T., Wakeman, E.A., Rolls, E.T., 1997. Responses of neurons in primary and inferior temporal visual cortices to natural scenes. Proc. Biol. Sci 264, 1775–1783.

Bagasra, O., Michaels, F.H., Zheng, Y.M., Bobroski, L.E., Spitsin, S.V., Fu, Z.F., Tawadros, R., Koprowski, H., 1995. Activation of the inducible form of nitric oxide synthase in the brains of patients with multiple sclerosis. Proc. Natl. Acad. Sci. U.S.A. 92, 12041–12045.

Bakshi, R., Shaikh, Z.A., Miletich, R.S., Czarnecki, D., Dmochowski, J., Henschel, K., Janardhan, V., Dubey, N., Kinkel, P.R., 2000. Fatigue in multiple sclerosis and its relationship to depression and neurologic disability. Mult. Scler. 6, 181–185.

Balasubramanian, V., Kimber, D., Berry, M.J., 2nd, 2001. Metabolically efficient information processing. Neural Comput 13, 799–815.

Baracchini, C., Perini, P., Calabrese, M., Causin, F., Rinaldi, F., Gallo, P., 2011. No evidence of chronic cerebrospinal venous insufficiency at multiple sclerosis onset. Ann. Neurol. 69, 90–99.

Barnett, M.H., Parratt, J.D.E., Pollard, J.D., Prineas, J.W., 2009. MS: is it one disease? Int MS J 16, 57–65.

Barnett, M.H., Prineas, J.W., 2004. Relapsing and remitting multiple sclerosis: pathology of the newly forming lesion. Ann. Neurol 55, 458–468.

Baudry, N., Danialou, G., Boczkowski, J., Vicaut, E., 1998. In vivo study of the effect of systemic hypoxia on leukocyte-endothelium interactions. Am. J. Respir. Crit. Care Med. 158, 477–483.

Becanovic, K., Jagodic, M., Sheng, J.R., Dahlman, I., Aboul-Enein, F., Wallstrom, E., Olofsson, P., Holmdahl, R., Lassmann, H., Olsson, T., 2006. Advanced intercross line mapping of Eae5 reveals Ncf-1 and CLDN4 as candidate genes for experimental autoimmune encephalomyelitis. J. Immunol. 176, 6055–6064.

Bechtold, D.A., Smith, K.J., 2005. Sodium-mediated axonal degeneration in inflammatory demyelinating disease. J. Neurol. Sci. 233, 27–35.

Beckman, J.S., Koppenol, W.H., 1996. Nitric oxide, superoxide, and peroxynitrite: the good, the bad, and ugly. Am. J. Physiol. 271, C1424–1437.

Begg, A.C., 2003. Is HIF-1alpha a good marker for tumor hypoxia? Int. J. Radiat. Oncol. Biol. Phys. 56, 917–919.

Belachew, S., Chittajallu, R., Aguirre, A.A., Yuan, X., Kirby, M., Anderson, S., Gallo, V., 2003. Postnatal NG2 proteoglycan-expressing progenitor cells are intrinsically multipotent and generate functional neurons. J. Cell Biol. 161, 169–186.

Bélanger, M., Allaman, I., Magistretti, P.J., 2011. Brain energy metabolism: focus on astrocyte-neuron metabolic cooperation. Cell Metab. 14, 724–738.

Bell, M.D., Perry, V.H., 1995. Adhesion molecule expression on murine cerebral endothelium following the injection of a proinflammagen or during acute neuronal degeneration. J Neurocytol 24, 695–710.

Beltrán, B., Mathur, A., Duchen, M.R., Erusalimsky, J.D., Moncada, S., 2000. The effect of nitric oxide on cell respiration: A key to understanding its role in cell survival or death. Proceedings of the National Academy of Sciences 97, 14602 –14607.

Benita, Y., Kikuchi, H., Smith, A.D., Zhang, M.Q., Chung, D.C., Xavier, R.J., 2009. An integrative genomics approach identifies Hypoxia Inducible Factor-1 (HIF-1)-target genes that form the core response to hypoxia. Nucleic Acids Res 37, 4587–4602.

Bennett, M., Heard, R., 2010. Hyperbaric oxygen therapy for multiple sclerosis. CNS Neurosci Ther 16, 115–124.

Ben-Nun, A., Wekerle, H., Cohen, I.R., 1981. The rapid isolation of clonable antigen-specific T lymphocyte lines capable of mediating autoimmune encephalomyelitis. Eur. J. Immunol. 11, 195–199.

Berger, T., Weerth, S., Kojima, K., Linington, C., Wekerle, H., Lassmann, H., 1997. Experimental autoimmune encephalomyelitis: the antigen specificity of T lymphocytes determines the topography of lesions in the central and peripheral nervous system. Lab. Invest. 76, 355–364.

Bergles, D.E., Roberts, J.D., Somogyi, P., Jahr, C.E., 2000. Glutamatergic synapses on oligodendrocyte precursor cells in the hippocampus. Nature 405, 187–191.

Bettelli, E., 2007. Building different mouse models for human MS. Ann. N. Y. Acad. Sci. 1103, 11–18.

Beynon, C., Kiening, K.L., Orakcioglu, B., Unterberg, A.W., Sakowitz, O.W., 2012. Brain tissue oxygen monitoring and hyperoxic treatment in patients with traumatic brain injury. J. Neurotrauma 29, 2109–2123.

Bindokas, V.P., Jordán, J., Lee, C.C., Miller, R.J., 1996. Superoxide production in rat hippocampal neurons: selective imaging with hydroethidine. J. Neurosci. 16, 1324–1336.

Bitsch, A., Wegener, C., Da Costa, C., Bunkowski, S., Reimers, C.D., Prange, H.W., Brück, W., 1999. Lesion development in Marburg's type of acute multiple sclerosis: from inflammation to demyelination. Mult. Scler. 5, 138–146.

Bjartmar, C., Trapp, B.D., 2003. Axonal degeneration and progressive neurologic disability in multiple sclerosis. Neurotox Res 5, 157–164.

Bö, L., Dawson, T.M., Wesselingh, S., Mörk, S., Choi, S., Kong, P.A., Hanley, D., Trapp, B.D., 1994. Induction of nitric oxide synthase in demyelinating regions of multiple sclerosis brains. Ann. Neurol. 36, 778–786.

Bø, L., Vedeler, C.A., Nyland, H.I., Trapp, B.D., Mørk, S.J., 2003. Subpial demyelination in the cerebral cortex of multiple sclerosis patients. J. Neuropathol. Exp. Neurol. 62, 723–732.

Bø, L, Vedeler, C A, Nyland, H., Trapp, B D, Mørk, S J, 2003. Intracortical multiple sclerosis lesions are not associated with increased lymphocyte infiltration. Mult. Scler. 9, 323–331.

Bö, L, Geurts, J.J.G., van der Valk, P., Polman, C., Barkhof, F., 2007. Lack of correlation between cortical demyelination and white matter pathologic changes in multiple sclerosis. Arch. Neurol. 64, 76–80

Boado, R.J., Pardridge, W.M., 2002. Glucose deprivation and hypoxia increase the expression of the GLUT1 glucose transporter via a specific mRNA cis-acting regulatory element. J. Neurochem. 80, 552–554.

Bolaños, J.P., Almeida, A., Stewart, V., Peuchen, S., Land, J.M., Clark, J.B., Heales, S.J., 1997. Nitric oxide-mediated mitochondrial damage in the brain: mechanisms and implications for neurodegenerative diseases. J. Neurochem. 68, 2227–2240.

Bolaños, J.P., Heales, S.J., Land, J.M., Clark, J.B., 1995. Effect of peroxynitrite on the mitochondrial respiratory chain: differential susceptibility of neurones and astrocytes in primary culture. J. Neurochem. 64, 1965–1972.

Bolaños, J.P., Heales, S.J.R., Peuchen, S., Barker, J.E., Land, J.M., Clark, J.B., 1996. Nitric oxide-mediated mitochondrial damage: A potential neuroprotective role for glutathione. Free Radical Biology and Medicine 21, 995–1001.

Bolaños, J.P., Peuchen, S., Heales, S.J., Land, J.M., Clark, J.B., 1994. Nitric oxide-mediated inhibition of the mitochondrial respiratory chain in cultured astrocytes. J. Neurochem. 63, 910–916.

Bonfanti, R., Furie, B.C., Furie, B., Wagner, D.D., 1989. PADGEM (GMP140) is a component of Weibel-Palade bodies of human endothelial cells. Blood 73, 1109–1112.

Borregaard, N., Herlin, T., 1982. Energy metabolism of human neutrophils during phagocytosis. J. Clin. Invest. 70, 550–557.

Boumezbeur, F., Mason, G.F., De Graaf, R.A., Behar, K.L., Cline, G.W., Shulman, G.I., Rothman, D.L., Petersen, K.F., 2010. Altered brain mitochondrial metabolism in healthy aging as assessed by in vivo magnetic resonance spectroscopy. J. Cereb. Blood Flow Metab. 30, 211–221.

Bouzier, A.K., Thiaudiere, E., Biran, M., Rouland, R., Canioni, P., Merle, M., 2000. The metabolism of [3-(13)C]lactate in the rat brain is specific of a pyruvate carboxylase-deprived compartment. J. Neurochem. 75, 480–486.

Bouzier-Sore, A.-K., Voisin, P., Bouchaud, V., Bezancon, E., Franconi, J.-M., Pellerin, L., 2006. Competition between glucose and lactate as oxidative energy substrates in both neurons and astrocytes: a comparative NMR study. Eur. J. Neurosci. 24, 1687–1694.

Boveris, A., Chance, B., 1973. The mitochondrial generation of hydrogen peroxide. General properties and effect of hyperbaric oxygen. Biochem J 134, 707–716.

Boyer, S.J., Blume, F.D., 1984. Weight loss and changes in body composition at high altitude. J Appl Physiol 57, 1580–1585.

Bradl, M., Lassmann, H., 2010. Oligodendrocytes: biology and pathology. Acta Neuropathol 119, 37–53.

Braitenberg, V., Schüz, A., 1998. Cortex: statistics and geometry of neuronal connectivity. Springer.

Bramow, S., Frischer, J.M., Lassmann, H., Koch-Henriksen, N., Lucchinetti, C.F., Sørensen, P.S., Laursen, H., 2010. Demyelination versus remyelination in progressive multiple sclerosis. Brain 133, 2983–2998.

Braughler, J.M., Duncan, L.A., Chase, R.L., 1986. The involvement of iron in lipid peroxidation. Importance of ferric to ferrous ratios in initiation. J. Biol. Chem. 261, 10282–10289.

Bredt, D.S., 1999. Endogenous nitric oxide synthesis: biological functions and pathophysiology. Free Radic. Res. 31, 577–596.

Brenner, T., Brocke, S., Szafer, F., Sobel, R.A., Parkinson, J.F., Perez, D.H., Steinman, L., 1997. Inhibition of nitric oxide synthase for treatment of experimental autoimmune encephalomyelitis. J. Immunol. 158, 2940–2946.

Brickner, R.M., 1958. Pharmacological reduction of abnormality in multiple sclerosis within minutes: a statistical study. J. Nerv. Ment. Dis. 127, 308–322.

Brickner, R.M., 1955. Phenomenon of relief by flush in multiple sclerosis: Its use as a foundation for therapy. Arch NeurPsych 73, 232–240.

Brink, B.P., Veerhuis, R., Breij, E.C.W., van der Valk, P., Dijkstra, C.D., Bö, Lars, 2005. The pathology of multiple sclerosis is location-dependent: no significant complement activation is detected in purely cortical lesions. J. Neuropathol. Exp. Neurol. 64, 147–155.

Brooks, D.J., Leenders, K.L., Head, G., Marshall, J., Legg, N.J., Jones, T., 1984. Studies on regional cerebral oxygen utilisation and cognitive function in multiple sclerosis. J. Neurol. Neurosurg. Psychiatr. 47, 1182–1191.

Brorson, J.R., Schumacker, P.T., Zhang, H., 1999. Nitric oxide acutely inhibits neuronal energy production. The Committees on Neurobiology and Cell Physiology. J. Neurosci. 19, 147–158.

Brown, A.M., Tekkök, S.B., Ransom, B.R., 2003. Glycogen regulation and functional role in mouse white matter. The Journal of Physiology 549, 501 –512.

Brown, G.C., Bolaños, J.P., Heales, S.J., Clark, J.B., 1995. Nitric oxide produced by activated astrocytes rapidly and reversibly inhibits cellular respiration. Neurosci. Lett. 193, 201–204.

Brown, G.C., Cooper, C.E., 1994. Nanomolar concentrations of nitric oxide reversibly inhibit synaptosomal respiration by competing with oxygen at cytochrome oxidase. FEBS Lett 356, 295–298.

Brück, W., Porada, P., Poser, S., Rieckmann, P., Hanefeld, F., Kretzschmar, H.A., Lassmann, H., 1995. Monocyte/macrophage differentiation in early multiple sclerosis lesions. Ann. Neurol. 38, 788–796.

Bruick, R.K., McKnight, S.L., 2001. A conserved family of prolyl-4-hydroxylases that modify HIF. Science 294, 1337–1340.

Brunelle, J.K., Bell, E.L., Quesada, N.M., Vercauteren, K., Tiranti, V., Zeviani, M., Scarpulla, R.C., Chandel, N.S., 2005. Oxygen sensing requires mitochondrial ROS but not oxidative phosphorylation. Cell Metab 1, 409–414.

Bullock, R. 1997. Injury and Cell function. In: Reilly, P., Bullock, R. Head Injury: Pathophysiology and Management of Severe Closed Injury. Chapman and Hall, London, pp. 121-141.

Butt, A.M., Duncan, A., Hornby, M.F., Kirvell, S.L., Hunter, A., Levine, J.M., Berry, M., 1999. Cells expressing the NG2 antigen contact nodes of Ranvier in adult CNS white matter. Glia 26, 84–91.

Calabrese, M., Rocca, M.A., Atzori, M., Mattisi, I., Favaretto, A., Perini, P., Gallo, P., Filippi, Massimo, 2010. A 3-year magnetic resonance imaging study of cortical lesions in relapse-onset multiple sclerosis. Ann. Neurol. 67, 376–383.

Carmeliet, P., Jain, R.K., 2000. Angiogenesis in cancer and other diseases. Nature 407, 249–257.

Carter, W.O., Narayanan, P.K., Robinson, J.P., 1994. Intracellular hydrogen peroxide and superoxide anion detection in endothelial cells. J. Leukoc. Biol. 55, 253–258.

Caso, J.R., Pradillo, J.M., Hurtado, O., Lorenzo, P., Moro, M.A., Lizasoain, I., 2007. Toll-like receptor 4 is involved in brain damage and inflammation after experimental stroke. Circulation 115, 1599–1608.

Cassiani-Ingoni, R., Coksaygan, T., Xue, H., Reichert-Scrivner, S.A., Wiendl, H., Rao, M.S., Magnus, T., 2006. Cytoplasmic translocation of Olig2 in adult glial progenitors marks the generation of reactive astrocytes following autoimmune inflammation. Exp. Neurol. 201, 349–358.

Cataldo, A.M., Broadwell, R.D., 1986. Cytochemical identification of cerebral glycogen and glucose-6-phosphatase activity under normal and experimental conditions. II. Choroid plexus and ependymal epithelia, endothelia and pericytes. J. Neurocytol 15, 511–524.

Cater, D.B., Garattini, S., Marina, F., Silver, I.A., 1961. Changes of Oxygen Tension in Brain and Somatic Tissues Induced by Vasodilator and Vasoconstrictor Drugs. Proceedings of the Royal Society of London. Series B, Biological Sciences 155, 136–158.

Cavaglia, M., Dombrowski, S.M., Drazba, J., Vasanji, A., Bokesch, P.M., Janigro, D., 2001. Regional variation in brain capillary density and vascular response to ischemia. Brain Res. 910, 81–93.

Chaiban, J.T., Bitar, F.F., Azar, S.T., 2008. Effect of chronic hypoxia on leptin, insulin, adiponectin, and ghrelin. Metab. Clin. Exp 57, 1019–1022.

Chance, B., Oshimo, N., Sugamo, T., & Mayersky, A. 1973. Basic principles of tissue oxygen determination from mitochondrial signals. In: Bruley, DF. Oxygen Transport to Tissue. Plenum Publishing, New York, pp. 277-292.

Chandel, N.S., Maltepe, E., Goldwasser, E., Mathieu, C.E., Simon, M.C., Schumacker, P.T., 1998. Mitochondrial reactive oxygen species trigger hypoxia-induced transcription. Proc. Natl. Acad. Sci. U.S.A. 95, 11715–11720.

Chandel, N.S., McClintock, D.S., Feliciano, C.E., Wood, T.M., Melendez, J.A., Rodriguez, A.M., Schumacker, P.T., 2000. Reactive oxygen species generated at mitochondrial complex III stabilize hypoxia-inducible factor-1alpha during hypoxia: a mechanism of O2 sensing. J. Biol. Chem. 275, 25130–25138.

Chang, A., Tourtellotte, W.W., Rudick, R., Trapp, B.D., 2002. Premyelinating oligodendrocytes in chronic lesions of multiple sclerosis. N. Engl. J. Med. 346, 165–173.

Cheepsunthorn, P., Palmer, C., Connor, J.R., 1998. Cellular distribution of ferritin subunits in postnatal rat brain. J. Comp. Neurol. 400, 73–86.

Chen, Y., Swanson, R.A., 2003. Astrocytes and brain injury. J. Cereb. Blood Flow Metab. 23, 137–149.

Choi, I.-Y., Seaquist, E.R., Gruetter, R., 2003. Effect of Hypoglycemia on Brain Glycogen Metabolism In Vivo. J Neurosci Res 72, 25–32.

Cifelli, Alberto, Arridge, M., Jezzard, P., Esiri, M.M., Palace, J., Matthews, Paul M, 2002. Thalamic neurodegeneration in multiple sclerosis. Ann. Neurol. 52, 650–653.

Clarke DD, Sokoloff L. 1999. Circulation and energy metabolism. In: SiegelGJ, Agranoff BW, Albers RW, Fisher SK, Uhler MD. Basic neurochemistry: Molecular, cellular, and clinical aspects, 6th ed. New York: Raven Press. pp 637–669.

Clark J. 2008. Oxygen toxicity. In: TS Neuman and SR Thom. Physiology and Medicine of Hyperbaric Oxygen Therapy. Philadelphia, PA: Saunders, p. 527–563.

Clementi, E., Brown, G.C., Feelisch, M., Moncada, S., 1998. Persistent inhibition of cell respiration by nitric oxide: crucial role of S-nitrosylation of mitochondrial complex I and protective action of glutathione. Proc. Natl. Acad. Sci. U.S.A 95, 7631–7636.

Cobb, L.M., Hacker, T., Nolan, J., 1990. NAD(P)H nitroblue tetrazolium reductase levels in apparently normoxic tissues: a histochemical study correlating enzyme activity with binding of radiolabelled misonidazole. Br J Cancer 61, 524–529.

Coleman, M.L., Ratcliffe, P.J., 2007. Oxygen sensing and hypoxia-induced responses. Essays Biochem 43, 1–15.

Compston, A., 1997. Genetic epidemiology of multiple sclerosis. J Neurol Neurosurg Psychiatry 62, 553–561.

Compston, A., Coles, A., 2008. Multiple sclerosis. The Lancet 372, 1502–1517.

Connor, J.R., Menzies, S.L., 1996. Relationship of iron to oligodendrocytes and myelination. Glia 17, 83–93.

Cook, S.D., Rohowsky-Kochan, C., Bansil, S., Dowling, P.C., 1995. Evidence for multiple sclerosis as an infectious disease. Acta Neurol. Scand., Suppl.c 161, 34–42.

Cramer, T., Yamanishi, Y., Clausen, B.E., Förster, I., Pawlinski, R., Mackman, N., Haase, V.H., Jaenisch, R., Corr, M., Nizet, V., Firestein, G.S., Gerber, H.P., Ferrara, N., Johnson, R.S., 2003. HIF-1alpha is essential for myeloid cell-mediated inflammation. Cell 112, 645–657.

Craner, M.J., Newcombe, J., Black, J.A., Hartle, C., Cuzner, M.L., Waxman, S.G., 2004. Molecular changes in neurons in multiple sclerosis: Altered axonal expression of Nav1.2 and Nav1.6 sodium channels and Na+/Ca2+ exchanger. Proc Natl Acad Sci U S A 101, 8168–8173.

Croll, S.D., Ransohoff, R.M., Cai, N., Zhang, Q., Martin, F.J., Wei, T., Kasselman, L.J., Kintner, J., Murphy, A.J., Yancopoulos, G.D., Wiegand, S.J., 2004. VEGF-mediated inflammation precedes angiogenesis in adult brain. Exp. Neurol. 187, 388–402.

Cross, A.H., Manning, P.T., Keeling, R.M., Schmidt, R.E., Misko, T.P., 1998. Peroxynitrite formation within the central nervous system in active multiple sclerosis. J. Neuroimmunol. 88, 45–56.

Cross, A.H., Manning, P.T., Stern, M.K., Misko, T.P., 1997. Evidence for the production of peroxynitrite in inflammatory CNS demyelination. J. Neuroimmunol. 80, 121–130.

Cross, A.H., Misko, T.P., Lin, R.F., Hickey, W.F., Trotter, J.L., Tilton, R.G., 1994. Aminoguanidine, an inhibitor of inducible nitric oxide synthase, ameliorates experimental autoimmune encephalomyelitis in SJL mice. J. Clin. Invest. 93, 2684–2690.

D'haeseleer, M., Cambron, M., Vanopdenbosch, L., De Keyser, J., 2011. Vascular aspects of multiple sclerosis. Lancet Neurol 10, 657–666.

Dada, L.A., Chandel, N.S., Ridge, K.M., Pedemonte, C., Bertorello, A.M., Sznajder, J.I., 2003. Hypoxia-induced endocytosis of Na,K-ATPase in alveolar epithelial cells is mediated by mitochondrial reactive oxygen species and PKC-zeta. J. Clin. Invest 111, 1057–1064.

Damoiseaux, J.G., Döpp, E.A., Calame, W., Chao, D., MacPherson, G.G., Dijkstra, C.D., 1994. Rat macrophage lysosomal membrane antigen recognized by monoclonal antibody ED1. Immunology 83, 140–147.

Dawson, M.R.L., Polito, A., Levine, J.M., Reynolds, R., 2003. NG2-expressing glial progenitor cells: an abundant and widespread population of cycling cells in the adult rat CNS. Mol. Cell. Neurosci. 24, 476–488.

De Groot, C.J., Bergers, E., Kamphorst, W., Ravid, R., Polman, C.H., Barkhof, F., Van der Valk, P., 2001. Post-mortem MRI-guided sampling of multiple sclerosis brain lesions: increased yield of active demyelinating and (p)reactive lesions. Brain 124, 1635–1645.

De Girolami, U., Zivin, J.A., 1982. Neuropathology of experimental spinal cord ischemia in the rabbit. J. Neuropathol. Exp. Neurol. 41, 129–149.

De Stefano, N., Matthews, P. M., Filippi, M., Agosta, F., Luca, M.D., Bartolozzi, M.L., Guidi, L., Ghezzi, A., Montanari, E., Cifelli, A., Federico, A., Smith, S.M., 2003. Evidence of early cortical atrophy in MS Relevance to white matter changes and disability. Neurology 60, 1157–1162.

Deloire, M.S.A., Ruet, A., Hamel, D., Bonnet, M., Dousset, V., Brochet, B., 2011. MRI predictors of cognitive outcome in early multiple sclerosis. Neurology 76, 1161–1167.

Di Paola, M., Paola, M.D., Bozzali, M., Fadda, L., Musicco, M., Sabatini, U., Caltagirone, C., 2008. Reduced oxygen due to high-altitude exposure relates to atrophy in motor-function brain areas. Eur. J. Neurol. 15, 1050–1057.

Dobrogowska, D.H., Lossinsky, A.S., Tarnawski, M., Vorbrodt, A.W., 1998. Increased blood-brain barrier permeability and endothelial abnormalities induced by vascular endothelial growth factor. J. Neurocytol. 27, 163–173.

Dore-Duffy, P., Balabanov, R., Beaumont, T., Hritz, M.A., Harik, S.I., LaManna, J.C., 1999. Endothelial activation following prolonged hypobaric hypoxia. Microvasc. Res 57, 75–85.

Dore-Duffy, P., Katychev, A., Wang, X., Buren, E.V., 2006. CNS microvascular pericytes exhibit multipotential stem cell activity. Journal of Cerebral Blood Flow & Metabolism 26, 613–624.

Dringen, R., 2000. Metabolism and functions of glutathione in brain. Prog. Neurobiol. 62, 649–671.

Dutta, R., McDonough, J., Yin, X., Peterson, J., Chang, A., Torres, T., Gudz, T., Macklin, W.B., Lewis, D.A., Fox, R.J., Rudick, R., Mirnics, K., Trapp, B.D., 2006.
Mitochondrial dysfunction as a cause of axonal degeneration in multiple sclerosis patients. Annals of Neurology 59, 478–489.

Dutta, R., Trapp, B.D., 2011. Mechanisms of neuronal dysfunction and degeneration in multiple sclerosis. Progress in Neurobiology 93, 1–12.

Edvinsson L, Mackenzie ET, McCulloch J. 1993. Energy generation in the central nervous system. In: Cerebral Blood Flow and Metabolism, Raven Press, New York, pp. 153-158

Eftekharpour, E., Holmgren, A., Juurlink, B.H., 2000. Thioredoxin reductase and glutathione synthesis is upregulated by t-butylhydroquinone in cortical astrocytes but not in cortical neurons. Glia 31, 241–248.

Ellmerich, S., Mycko, M., Takacs, K., Waldner, H., Wahid, F.N., Boyton, R.J., King, R.H.M., Smith, P.A., Amor, S., Herlihy, A.H., Hewitt, R.E., Jutton, M., Price, D.A., Hafler, D.A., Kuchroo, V.K., Altmann, D.M., 2005. High incidence of spontaneous disease in an HLA-DR15 and TCR transgenic multiple sclerosis model. J. Immunol. 174, 1938–1946.

Elvidge, G.P., Glenny, L., Appelhoff, R.J., Ratcliffe, P.J., Ragoussis, J., Gleadle, J.M., 2006. Concordant regulation of gene expression by hypoxia and 2-oxoglutarate-dependent dioxygenase inhibition: the role of HIF-1alpha, HIF-2alpha, and other pathways. J. Biol. Chem 281, 15215–15226.

Eng, L.F., Reier, P.J., Houle, J.D., 1987. Astrocyte activation and fibrous gliosis: glial fibrillary acidic protein immunostaining of astrocytes following intraspinal cord grafting of fetal CNS tissue. Prog. Brain Res. 71, 439–455.

Erecińska, M., Nelson, D., Vanderkooi, J.M., 1995. Effects of NO-generating compounds on synaptosomal energy metabolism. J. Neurochem. 65, 2699–2705.

Evangelou, N., Konz, D., Esiri, M.M., Smith, S., Palace, J., Matthews, P.M., 2000. Regional axonal loss in the corpus callosum correlates with cerebral white matter lesion volume and distribution in multiple sclerosis. Brain 123 (Pt 9), 1845–1849.

Evangelou, N., Konz, D., Esiri, M.M., Smith, S., Palace, J., Matthews, P.M., 2001. Size-selective neuronal changes in the anterior optic pathways suggest a differential susceptibility to injury in multiple sclerosis. Brain 124, 1813–1820.

Fayed, N., Modrego, P.J., Morales, H., 2006. Evidence of brain damage after high-altitude climbing by means of magnetic resonance imaging. Am. J. Med 119, 168.e1–6.

Felts, P.A., Woolston, A.-M., Fernando, H.B., Asquith, S., Gregson, N.A., Mizzi, O.J., Smith, K.J., 2005. Inflammation and primary demyelination induced by the intraspinal injection of lipopolysaccharide. Brain 128, 1649–1666.

Ferguson, B., Matyszak, M.K., Esiri, M.M., Perry, V.H., 1997. Axonal damage in acute multiple sclerosis lesions. Brain 120 (Pt 3), 393–399.

Fiala, J.C., 2005. Reconstruct: a free editor for serial section microscopy. J Microsc 218, 52–61.

Figley, C.R., Stroman, P.W., 2011. The role(s) of astrocytes and astrocyte activity in neurometabolism, neurovascular coupling, and the production of functional neuroimaging signals. Eur. J. Neurosci. 33, 577–588.

Finta, E.P., Harms, L., Sevcik, J., Fischer, H.D., Illes, P., 1993. Effects of potassium channel openers and their antagonists on rat locus coeruleus neurones. Br. J. Pharmacol. 109, 308–315.

Fiorentino, D.F., Zlotnik, A., Mosmann, T.R., Howard, M., O'Garra, A., 1991. IL-10 inhibits cytokine production by activated macrophages. J Immunol 147, 3815–3822.

Fischer, M.T., Sharma, R., Lim, J.L., Haider, L., Frischer, J.M., Drexhage, J., Mahad, D., Bradl, M., Van Horssen, J., Lassmann, H., 2012. NADPH oxidase expression in active multiple sclerosis lesions in relation to oxidative tissue damage and mitochondrial injury. Brain 135, 886–899.

Fisher, E., Lee, J.-C., Nakamura, K., Rudick, R.A., 2008. Gray matter atrophy in multiple sclerosis: a longitudinal study. Ann. Neurol. 64, 255–265.

Fisniku, L.K., Chard, D.T., Jackson, J.S., Anderson, V.M., Altmann, D.R., Miszkiel, K.A., Thompson, A.J., Miller, D.H., 2008. Gray matter atrophy is related to long-term disability in multiple sclerosis. Ann. Neurol. 64, 247–254.

Flint DH, Emptage MH. In: Biosynthesis of Branched Chain Amino Acids. Barak Z, Chipman D, Schloss JV. Borch & Balaban, Philadelphia: Deerfield; 1990. pp. 285–314.

Fox, C.J., Hammerman, P.S., Thompson, C.B., 2005. Fuel feeds function: energy metabolism and the T-cell response. Nat. Rev. Immunol. 5, 844–852.

Fox, P.T., Raichle, M.E., 1986. Focal physiological uncoupling of cerebral blood flow and oxidative metabolism during somatosensory stimulation in human subjects. Proc. Natl. Acad. Sci. U.S.A. 83, 1140–1144.

Fox, P.T., Raichle, M.E., Mintun, M.A., Dence, C., 1988. Nonoxidative glucose consumption during focal physiologic neural activity. Science 241, 462–464.

Freal, J.E., Kraft, G.H., Coryell, J.K., 1984. Symptomatic fatigue in multiple sclerosis. Arch Phys Med Rehabil 65, 135–138.

Freund, J., Stern, E.R., Pisanti, T.M., 1947. Isoallergic encephalomyelitis and radiculitis in guinea pigs after one injection of brain and Mycobacteria in water-in-oil emulsion. J. Immunol. 57, 179–194.

Fridovich, I., 1978. The biology of oxygen radicals. Science 201, 875 –880.

Friese, M.A., Montalban, X., Willcox, N., Bell, J.I., Martin, R., Fugger, L., 2006. The value of animal models for drug development in multiple sclerosis. Brain 129, 1940–1952.

Frost, M.T., Wang, Q., Moncada, S., Singer, M., 2005. Hypoxia accelerates nitric oxide-dependent inhibition of mitochondrial complex I in activated macrophages. American Journal of Physiology - Regulatory, Integrative and Comparative Physiology 288, R394 –R400.

Fünfschilling, U., Supplie, L.M., Mahad, D., Boretius, S., Saab, A.S., Edgar, J., Brinkmann, B.G., Kassmann, C.M., Tzvetanova, I.D., Möbius, W., Diaz, F., Meijer, D., Suter, U., Hamprecht, B., Sereda, M.W., Moraes, C.T., Frahm, J., Goebbels, S., Nave, K.-A., 2012. Glycolytic oligodendrocytes maintain myelin and long-term axonal integrity. Nature 485, 517–521.

Fujimura, N., Tanaka, E., Yamamoto, S., Shigemori, M., Higashi, H., 1997. Contribution of ATP-sensitive potassium channels to hypoxic hyperpolarization in rat hippocampal CA1 neurons *in vitro*. J. Neurophysiol. 77, 378–385.

Fujiwara, N., Higashi, H., Shimoji, K., Yoshimura, M., 1987. Effects of hypoxia on rat hippocampal neurones *in vitro*. J Physiol 384, 131–151.

Fukuda, K., Okada, Y., Yoshida, H., Aoyama, R., Nakamura, M., Chiba, K., Toyama, Y., 2006. Ischemia-induced disturbance of neuronal network function in the rat spinal cord analyzed by voltage-imaging. Neuroscience 140, 1453–1465.

Gabig, T.G., Bearman, S.I., Babior, B.M., 1979. Effects of oxygen tension and pH on the respiratory burst of human neutrophils. Blood 53, 1133–1139.

Gallagher, C.N., Carpenter, K.L.H., Grice, P., Howe, D.J., Mason, A., Timofeev, I., Menon, D.K., Kirkpatrick, P.J., Pickard, J.D., Sutherland, G.R., Hutchinson, P.J., 2009. The human brain utilizes lactate via the tricarboxylic acid cycle: a 13C-labelled microdialysis and high-resolution nuclear magnetic resonance study. Brain 132, 2839–2849.

Garedew, A., Moncada, S., 2008. Mitochondrial dysfunction and HIF1alpha stabilization in inflammation. J. Cell. Sci 121, 3468–3475.

Geurts, J.J.G., Barkhof, F., 2008. Grey matter pathology in multiple sclerosis. Lancet Neurol 7, 841–851.

Ghandour, M.S., Langley, O.K., Vincendon, G., Gombos, G., Filippi, D., Limozin, N., Dalmasso, C., Laurent, G., 1980. Immunochemical and immunohistochemical study of carbonic anhydrase II in adult rat cerebellum: A marker for oligodendrocytes. Neuroscience 5, 559–571.

Giffard, R.G., Papadopoulos, M.C., Van Hooft, J.A., Xu, L., Giuffrida, R., Monyer, H., 2000. The electrogenic sodium bicarbonate cotransporter: developmental expression in rat brain and possible role in acid vulnerability. J. Neurosci. 20, 1001–1008.

Gilgun-Sherki, Y., Melamed, E., Offen, D., 2004. The role of oxidative stress in the pathogenesis of multiple sclerosis: the need for effective antioxidant therapy. J. Neurol. 251, 261–268.

Ginis, I., Mentzer, S.J., Faller, D.V., 1993. Oxygen tension regulates neutrophil adhesion to human endothelial cells via an LFA-1-dependent mechanism. J. Cell. Physiol. 157, 569–578.

Giovannoni, G., 1998. Cerebrospinal fluid and serum nitric oxide metabolites in patients with multiple sclerosis. Mult. Scler. 4, 27–30.

Goethals, L., Debucquoy, A., Perneel, C., Geboes, K., Ectors, N., De Schutter, H., Penninckx, F., McBride, W.H., Begg, A.C., Haustermans, K.M., 2006. Hypoxia in human colorectal adenocarcinoma: comparison between extrinsic and potential intrinsic hypoxia markers. Int. J. Radiat. Oncol. Biol. Phys. 65, 246–254.

Gold, R., Linington, C., Lassmann, H., 2006. Understanding pathogenesis and therapy of multiple sclerosis via animal models: 70 years of merits and culprits in experimental autoimmune encephalomyelitis research. Brain 129, 1953–1971.

Golden, H.D., Chang, R.S., Prescott, W., Simpson, E., Cooper, T.Y., 1973. Leukocyte-transforming agent: prolonged excretion by patients with mononucleosis and excretion by normal individuals. J. Infect. Dis. 127, 471–473.

González-Scarano, F., Baltuch, G., 1999. Microglia as mediators of inflammatory and degenerative diseases. Annu. Rev. Neurosci. 22, 219–240.

Goodwin, J.L., Uemura, E., Cunnick, J.E., 1995. Microglial release of nitric oxide by the synergistic action of beta-amyloid and IFN-gamma. Brain Res. 692, 207–214.

Goureau, O., Amiot, F., Dautry, F., Courtois, Y., 1997. Control of nitric oxide production by endogenous TNF-alpha in mouse retinal pigmented epithelial and Muller glial cells. Biochem. Biophys. Res. Commun. 240, 132–135.

Gow, A.J., Duran, D., Malcolm, S., Ischiropoulos, H., 1996. Effects of peroxynitrite-induced protein modifications on tyrosine phosphorylation and degradation. FEBS Lett. 385, 63–66.

Graeber, M.B., 2010. Changing face of microglia. Science 330, 783–788.

Greiner, E.F., Guppy, M., Brand, K., 1994. Glucose is essential for proliferation and the glycolytic enzyme induction that provokes a transition to glycolytic energy production. J. Biol. Chem. 269, 31484–31490.

Grossman, M.L., Basbaum, A.I., Fields, H.L., 1982. Afferent and efferent connections of the rat tail flick reflex (a model used to analyze pain control mechanisms). J. Comp. Neurol. 206, 9–16.

Guttmann, C.R., Ahn, S.S., Hsu, L., Kikinis, R., Jolesz, F.A., 1995. The evolution of multiple sclerosis lesions on serial MR. AJNR Am J Neuroradiol 16, 1481–1491.

Guzman, N.J., Fang, M.Z., Tang, S.S., Ingelfinger, J.R., Garg, L.C., 1995. Autocrine inhibition of Na+/K(+)-ATPase by nitric oxide in mouse proximal tubule epithelial cells. J Clin Invest 95, 2083–2088.

Guzy, R.D., Hoyos, B., Robin, E., Chen, H., Liu, L., Mansfield, K.D., Simon, M.C., Hammerling, U., Schumacker, P.T., 2005. Mitochondrial complex III is required for hypoxia-induced ROS production and cellular oxygen sensing. Cell Metab 1, 401–408.

Guzy, R.D., Schumacker, P.T., 2006. Oxygen sensing by mitochondria at complex III: the paradox of increased reactive oxygen species during hypoxia. Experimental Physiology 91, 807–819.

Haahr, S., Höllsberg, P., 2006. Multiple sclerosis is linked to Epstein-Barr virus infection. Rev. Med. Virol. 16, 297–310.

Haider, L., Fischer, M.T., Frischer, J.M., Bauer, J., Höftberger, R., Botond, G., Esterbauer, H., Binder, C.J., Witztum, J.L., Lassmann, H., 2011. Oxidative damage in multiple sclerosis lesions. Brain 134, 1914–1924.

Halliwell B. 1981. In: Sohal, RS. Age Pigments. Elsevier, Amsterdam, pp 1-62.

Halliwell, B., Gutteridge, J.M.C., 1985. Oxygen radicals and the nervous system. Trends in Neurosciences 8, 22–26.

Hansen, A.J., 1985. Effect of anoxia on ion distribution in the brain. Physiol. Rev 65, 101–148.

Harik, S.I., Behmand, R.A., LaManna, J.C., 1994. Hypoxia increases glucose transport at blood-brain barrier in rats. J. Appl. Physiol 77, 896–901.

Harrison-Lavoie, K.J., Michaux, G., Hewlett, L., Kaur, J., Hannah, M.J., Lui-Roberts, W.W.Y., Norman, K.E., Cutler, D.F., 2006. P-selectin and CD63 use different mechanisms for delivery to Weibel-Palade bodies. Traffic 7, 647–662.

Haselhorst, R., Kappos, L., Bilecen, D., Scheffler, K., Möri, D., Radü, E.W., Seelig, J., 2000. Dynamic susceptibility contrast MR imaging of plaque development in multiple sclerosis: application of an extended blood-brain barrier leakage correction. J Magn Reson Imaging 11, 495–505.

Hashimoto, T., Hussien, R., Cho, H.-S., Kaufer, D., Brooks, G.A., 2008. Evidence for the mitochondrial lactate oxidation complex in rat neurons: demonstration of an essential component of brain lactate shuttles. PLoS ONE 3, e2915.

Hauser, S.L., Oksenberg, J.R., 2006. The neurobiology of multiple sclerosis: genes, inflammation, and neurodegeneration. Neuron 52, 61–76.

Hayashi, N., Green, B.A., Gonzalez-Carvajal, M., Mora, J., Veraa, R.P., 1983a. Local blood flow, oxygen tension, and oxygen consumption in the rat spinal cord. Part 2: Relation to segmental level. J. Neurosurg 58, 526–530.

Hayashi, N., Green, B.A., Gonzalez-Carvajal, M., Mora, J., Veraa, R.P., 1983b. Local blood flow, oxygen tension, and oxygen consumption in the rat spinal cord. Journal of Neurosurgery 58, 516–525.

Heales, S.J., Bolaños, J.P., Stewart, V.C., Brookes, P.S., Land, J.M., Clark, J.B., 1999. Nitric oxide, mitochondria and neurological disease. Biochim. Biophys. Acta 1410, 215–228.

Helenius, J., Perkiö, J., Soinne, L., Østergaard, L., Carano, R.A.D., Salonen, O., Savolainen, S., Kaste, M., Aronen, H.J., Tatlisumak, T., 2003. Cerebral hemodynamics in a healthy population measured by dynamic susceptibility contrast MR imaging. Acta Radiol 44, 538–546.

Henderson, A.P.D., Barnett, M.H., Parratt, J.D.E., Prineas, J.W., 2009. Multiple sclerosis: distribution of inflammatory cells in newly forming lesions. Ann. Neurol 66, 739–753.

Herndon, R.M., 1996. Herpesviruses in multiple sclerosis. Arch. Neurol. 53, 123–124.

Hertz, L., Dringen, R., Schousboe, A., Robinson, S.R., 1999. Astrocytes: glutamate producers for neurons. J. Neurosci. Res. 57, 417–428.

Herz, J., Zipp, F., Siffrin, V., 2010. Neurodegeneration in autoimmune CNS inflammation. Exp. Neurol. 225, 9–17.

Hochmeister, S., Grundtner, R., Bauer, J., Engelhardt, B., Lyck, R., Gordon, G., Korosec, T., Kutzelnigg, A., Berger, J.J., Bradl, M., Bittner, R.E., Lassmann, H., 2006. Dysferlin is a new marker for leaky brain blood vessels in multiple sclerosis. J. Neuropathol. Exp. Neurol. 65, 855–865.

Hohlfeld, R., Wekerle, H., 2001. Immunological update on multiple sclerosis. Curr. Opin. Neurol. 14, 299–304.

Holley, J.E., Gveric, D., Newcombe, J., Cuzner, M.L., Gutowski, N.J., 2003. Astrocyte characterization in the multiple sclerosis glial scar. Neuropathol. Appl. Neurobiol. 29, 434–444.

Holley, J.E., Newcombe, J., Whatmore, J.L., Gutowski, N.J., 2010. Increased blood vessel density and endothelial cell proliferation in multiple sclerosis cerebral white matter. Neurosci. Lett. 470, 65–70.

Hölscher, C., 1997. Nitric oxide, the enigmatic neuronal messenger: its role in synaptic plasticity. Trends Neurosci. 20, 298–303.

Hooper, D.C., Ohnishi, S.T., Kean, R., Numagami, Y., Dietzschold, B., Koprowski, H., 1995. Local nitric oxide production in viral and autoimmune diseases of the central nervous system. Proc. Natl. Acad. Sci. U.S.A. 92, 5312–5316.

Hoshino, K., Takeuchi, O., Kawai, T., Sanjo, H., Ogawa, T., Takeda, Y., Takeda, K., Akira, S., 1999. Cutting edge: Toll-like receptor 4 (TLR4)-deficient mice are hyporesponsive to lipopolysaccharide: evidence for TLR4 as the Lps gene product. J. Immunol. 162, 3749–3752.

Hoskin, P.J., Sibtain, A., Daley, F.M., Wilson, G.D., 2003. GLUT1 and CAIX as intrinsic markers of hypoxia in bladder cancer: relationship with vascularity and proliferation as predictors of outcome of ARCON. Br. J. Cancer 89, 1290–1297.

Howell, O.W., Reeves, C.A., Nicholas, R., Carassiti, D., Radotra, B., Gentleman, S.M., Serafini, B., Aloisi, F., Roncaroli, F., Magliozzi, R., Reynolds, R., 2011. Meningeal inflammation is widespread and linked to cortical pathology in multiple sclerosis. Brain 134, 2755–2771.

Hu, S., Sheng, W.S., Peterson, P.K., Chao, C.C., 1995. Differential regulation by cytokines of human astrocyte nitric oxide production. Glia 15, 491–494.

Huie, R.E., Padmaja, S., 1993. The reaction of no with superoxide. Free Radic. Res. Commun. 18, 195–199.

Huseby, E.S., Liggitt, D., Brabb, T., Schnabel, B., Öhlén, C., Goverman, J., 2001. A Pathogenic Role for Myelin-Specific Cd8+ T Cells in a Model for Multiple Sclerosis. J Exp Med 194, 669–676.

Hutchison, G.J., Valentine, H.R., Loncaster, J.A., Davidson, S.E., Hunter, R.D., Roberts, S.A., Harris, A.L., Stratford, I.J., Price, P.M., West, C.M.L., 2004. Hypoxia-inducible factor 1alpha expression as an intrinsic marker of hypoxia: correlation with tumor oxygen, pimonidazole measurements, and outcome in locally advanced carcinoma of the cervix. Clin. Cancer Res 10, 8405–8412.

Iiyori, N., Alonso, L.C., Li, J., Sanders, M.H., Garcia-Ocana, A., O'Doherty, R.M., Polotsky, V.Y., O'Donnell, C.P., 2007. Intermittent hypoxia causes insulin resistance in lean mice independent of autonomic activity. Am. J. Respir. Crit. Care Med 175, 851–857.

Imam, S.A., Guyton, M.K., Haque, A., Vandenbark, A., Tyor, W.R., Ray, S.K., Banik, N.L., 2007. Increased Calpain Correlates with Th1 Cytokine Profile in PBMCs from MS Patients. J Neuroimmunol 190, 139–145.

Itoh, Y., Esaki, T., Shimoji, K., Cook, M., Law, M.J., Kaufman, E., Sokoloff, L., 2003. Dichloroacetate effects on glucose and lactate oxidation by neurons and astroglia in vitro and on glucose utilization by brain in vivo. Proc. Natl. Acad. Sci. U.S.A. 100, 4879–4884.

Ivan, M., Kondo, K., Yang, H., Kim, W., Valiando, J., Ohh, M., Salic, A., Asara, J.M., Lane, W.S., Kaelin Jr., W.G., 2001. HIFα Targeted for VHL-Mediated Destruction by Proline Hydroxylation: Implications for O2 Sensing. Science 292, 464 –468.

Jaakkola, P., Mole, D.R., Tian, Y.M., Wilson, M.I., Gielbert, J., Gaskell, S.J., Von Kriegsheim, A., Hebestreit, H.F., Mukherji, M., Schofield, C.J., Maxwell, P.H., Pugh, C.W., Ratcliffe, P.J., 2001. Targeting of HIF-alpha to the von Hippel-Lindau ubiquitylation complex by O2-regulated prolyl hydroxylation. Science 292, 468–472.

Jabs, R., Pivneva, T., Hüttmann, K., Wyczynski, A., Nolte, C., Kettenmann, H., Steinhäuser, C., 2005. Synaptic transmission onto hippocampal glial cells with hGFAP promoter activity. J. Cell. Sci. 118, 3791–3803.

Janssen, H.L.K., Haustermans, K.M.G., Sprong, D., Blommestijn, G., Hofland, I., Hoebers, F.J., Blijweert, E., Raleigh, J.A., Semenza, G.L., Varia, M.A., Balm, A.J., Van Velthuysen, M.L.F., Delaere, P., Sciot, R., Begg, A.C., 2002. HIF-1A, pimonidazole, and iododeoxyuridine to estimate hypoxia and perfusion in human head-and-neck tumors. Int. J. Radiat. Oncol. Biol. Phys 54, 1537–1549.

Jensen J, G.W., 1991. CIgarette smoking decreases tissue oxygen. Arch Surg 126, 1131–1134. Jiang, J.-H., Wang, N., Li, A., Liao, W.-T., Pan, Z.-G., Mai, S.-J., Li, D.-J., Zeng, M.-S., Wen, J., Zeng, Y.-X., 2006. Hypoxia can contribute to the induction of the Epstein-Barr virus (EBV) lytic cycle. Journal of Clinical Virology 37, 98–103.

Johns, T.G., Kerlero de Rosbo, N., Menon, K.K., Abo, S., Gonzales, M.F., Bernard, C.C., 1995. Myelin oligodendrocyte glycoprotein induces a demyelinating encephalomyelitis resembling multiple sclerosis. J. Immunol. 154, 5536–5541.

Johnson, A.W., Land, J.M., Thompson, E.J., Bolaños, J.P., Clark, J.B., Heales, S.J., 1995. Evidence for increased nitric oxide production in multiple sclerosis. J. Neurol. Neurosurg. Psychiatr. 58, 107. Johnson, T.A.,

Jirik, F.R., Fournier, S., 2010. Exploring the roles of CD8(+) T lymphocytes in the pathogenesis of autoimmune demyelination. Semin Immunopathol 32, 197–209.

Jones, M.V., Nguyen, T.T., Deboy, C.A., Griffin, J.W., Whartenby, K.A., Kerr, D.A., Calabresi, P.A., 2008. Behavioral and pathological outcomes in MOG 35-55 experimental autoimmune encephalomyelitis. J. Neuroimmunol. 199, 83–93.

Juhler, M., 1987. Simultaneous determination of regional cerebral blood flow, glucose metabolism, and pH in acute experimental allergic encephalomyelitis. J. Cereb. Blood Flow Metab. 7, 578–584.

Julien-Dolbec, C., Tropres, I., Montigon, O., Reutenauer, H., Ziegler, A., Decorps, M., Payen, J.F., 2002. Regional response of cerebral blood volume to graded hypoxic hypoxia in rat brain. Br J Anaesth 89, 287–293.

Jung, D.Y., Lee, H., Jung, B.-Y., Ock, J., Lee, M.-S., Lee, W.-H., Suk, K., 2005. TLR4, but not TLR2, signals autoregulatory apoptosis of cultured microglia: a critical role of IFN-beta as a decision maker. J. Immunol. 174, 6467–6476.

Juurlink, B.H., 1997. Response of glial cells to ischemia: roles of reactive oxygen species and glutathione. Neurosci Biobehav Rev 21, 151–166.

Kabat, H., Anderson, J.P., 1943. Acute arrest of cerebral circulation in man: LIEUTENANT RALPH ROSSEN (MC), U.S.N.R. Arch Neurol Psychiatry 50, 510–528.

Kamisaki, Y., Wada, K., Bian, K., Balabanli, B., Davis, K., Martin, E., Behbod, F., Lee, Y.C., Murad, F., 1998. An activity in rat tissues that modifies nitrotyrosine-containing proteins. Proc. Natl. Acad. Sci. U.S.A. 95, 11584–11589.

Kara, P., Friedlander, M.J., 1998. Dynamic modulation of cerebral cortex synaptic function by nitric oxide. Prog. Brain Res. 118, 183–198.

Káradóttir, R., Cavelier, P., Bergersen, L.H., Attwell, D., 2005. NMDA receptors are expressed in oligodendrocytes and activated in ischaemia. Nature 438, 1162–1166.

Karhausen, J., Haase, V.H., Colgan, S.P., 2005. Inflammatory hypoxia: role of hypoxia-inducible factor. Cell Cycle 4, 256–258.

Kasuno, K., Takabuchi, S., Fukuda, K., Kizaka-Kondoh, S., Yodoi, J., Adachi, T., Semenza, G.L., Hirota, K., 2004. Nitric oxide induces hypoxia-inducible factor 1 activation that is dependent on MAPK and phosphatidylinositol 3-kinase signaling. J. Biol. Chem 279, 2550–2558.

Kaur, C., Sivakumar, V., Foulds, W.S., 2006. Early Response of Neurons and Glial Cells to Hypoxia in the Retina. IOVS 47, 1126–1141.

Kautsky, H., 1939. Quenching of luminescence by oxygen. Trans. Faraday Soc. 35, 216–219.

Kawai, T., Akira, S., 2006. TLR signaling. Cell Death Differ. 13, 816–825.

Keirstead, H.S., Levine, J.M., Blakemore, W.F., 1998. Response of the oligodendrocyte progenitor cell population (defined by NG2 labelling) to demyelination of the adult spinal cord. Glia 22, 161–170.

Kennedy, M.K., Torrance, D.S., Picha, K.S., Mohler, K.M., 1992. Analysis of cytokine mRNA expression in the central nervous system of mice with experimental autoimmune encephalomyelitis reveals that IL-10 mRNA expression correlates with recovery. J Immunol 149, 2496–2505.

Kety, S.S., Schmidt, C.F., 1948. The effects of altered arterial tensions of carbon dioxide and oxygen on cerebral blood flow and cerebral oxygen consumption of normal young men. J. Clin. Invest 27, 484–492.

Keyer, K., Imlay, J.A., 1996. Superoxide accelerates DNA damage by elevating free-iron levels. Proc. Natl. Acad. Sci. U.S.A. 93, 13635–13640.

Kilbinger, H., 1996. Modulation of acetylcholine release by nitric oxide. Prog. Brain Res. 109, 219–224.

Kim, S.Y., Choi, Y.J., Joung, S.M., Lee, B.H., Jung, Y.-S., Lee, J.Y., 2010. Hypoxic stress up-regulates the expression of Toll-like receptor 4 in macrophages via hypoxia-inducible factor. Immunology 129, 516–524.

Kirk, S., Frank, J.A., Karlik, S., 2004. Angiogenesis in multiple sclerosis: is it good, bad or an epiphenomenon? Journal of the Neurological Sciences 217, 125–130.

Kiyotaki, C., Peisach, J., Bloom, B.R., 1984. Oxygen metabolism in cloned macrophage cell lines: glucose dependence of superoxide production, metabolic and spectral analysis. J. Immunol. 132, 857–866.

Klimant, I., Meyer, V., KüHl, M., 1995. Fiber-optic oxygen microsensors, a new tool in aquatic biology. Limnology and Oceanography 40, 1159–1165.

Klimova, T., Chandel, N.S., 2008. Mitochondrial complex III regulates hypoxic activation of HIF. Cell Death Differ 15, 660–666.

Kokura, S., Yoshida, N., Yoshikawa, T., 2002. Anoxia/reoxygenation-induced leukocyte-endothelial cell interactions. Free Radic. Biol. Med. 33, 427–432.

Kominsky, D.J., Campbell, E.L., Colgan, S.P., 2010. Metabolic shifts in immunity and inflammation. J. Immunol. 184, 4062–4068.

Kong, T., Eltzschig, H.K., Karhausen, J., Colgan, S.P., Shelley, C.S., 2004. Leukocyte adhesion during hypoxia is mediated by HIF-1-dependent induction of beta2 integrin gene expression. Proc. Natl. Acad. Sci. U.S.A. 101, 10440–10445.

Kong, T., Scully, M., Shelley, C.S., Colgan, S.P., 2007. Identification of Pur alpha as a new hypoxia response factor responsible for coordinated induction of the beta 2 integrin family. J. Immunol. 179, 1934–1941.

König, F.B., Wildemann, B., Nessler, S., Zhou, D., Hemmer, B., Metz, I., Hartung, H.-P., Kieseier, B.C., Brück, W., 2008. Persistence of immunopathological and radiological traits in multiple sclerosis. Arch. Neurol. 65, 1527–1532.

Korhonen, R., Lahti, A., Kankaanranta, H., Moilanen, E., 2005. Nitric oxide production and signaling in inflammation. Curr Drug Targets Inflamm Allergy 4, 471–479.

Koritschoner RS, Schweinburg F. 1925. Induktion von Paralyse und Ruckenmarksentzundung durch Immunisierung von Kaninchen mit menschlichem Ruckenmarksgewebe. Z Immunitatsf Exp Therapie, vol. 42, pp. 217-283.

Kornek, B., Storch, M.K., Weissert, R., Wallstroem, E., Stefferl, A., Olsson, T., Linington, C., Schmidbauer, M., Lassmann, H., 2000. Multiple sclerosis and chronic autoimmune encephalomyelitis: a comparative quantitative study of axonal injury in active, inactive, and remyelinated lesions. Am. J. Pathol. 157, 267–276.

Koulakov, A.A., Chklovskii, D.B., 2001. Orientation preference patterns in mammalian visual cortex: a wire length minimization approach. Neuron 29, 519–527.

Kreutzberg, G.W., 1996. Microglia: a sensor for pathological events in the CNS. Trends Neurosci 19, 312–318.

Krogh, A., 1919. The number and distribution of capillaries in muscles with calculations of the oxygen pressure head necessary for supplying the tissue. J. Physiol. (Lond.) 52, 409–415.

Krupp, L.B., Alvarez, L.A., LaRocca, N.G., Scheinberg, L.C., 1988. Fatigue in multiple sclerosis. Arch. Neurol. 45, 435–437.

Kukley, M., Capetillo-Zarate, E., Dietrich, D., 2007. Vesicular glutamate release from axons in white matter. Nat. Neurosci. 10, 311–320.

Kurenny, D.E., Moroz, L.L., Turner, R.W., Sharkey, K.A., Barnes, S., 1994. Modulation of ion channels in rod photoreceptors by nitric oxide. Neuron 13, 315–324.

Kutzelnigg, A., Lucchinetti, C.F., Stadelmann, C., Brück, Wolfgang, Rauschka, H., Bergmann, Markus, Schmidbauer, M., Parisi, J.E., Lassmann, H., 2005. Cortical demyelination and diffuse white matter injury in multiple sclerosis. Brain 128, 2705–2712.

LaManna, J.C., 2007. Hypoxia in the central nervous system. Essays Biochem 43, 139–151.

LaManna, J.C., Chavez, J.C., Pichiule, P., 2004. Structural and functional adaptation to hypoxia in the rat brain. J. Exp. Biol 207, 3163–3169.

LaManna, J.C., Neal, M., Xu, K., Haxhiu, M.A., 2003. Differential expression of intracellular acidosis in rat brainstem regions in response to hypercapnic ventilation. Adv. Exp. Med. Biol 536, 407–413.

LaManna, J.C., Vendel, L.M., Farrell, R.M., 1992. Brain adaptation to chronic hypobaric hypoxia in rats. J Appl Physiol 72, 2238–2243.

Lassmann, H., 2003. Hypoxia-like tissue injury as a component of multiple sclerosis lesions. J. Neurol. Sci 206, 187–191.

Lassmann, H., 2007. New concepts on progressive multiple sclerosis. Curr Neurol Neurosci Rep 7, 239–244.

Lassmann, H., 2011. Review: the architecture of inflammatory demyelinating lesions: implications for studies on pathogenesis. Neuropathol. Appl. Neurobiol. 37, 698–710.

Lassmann, H., Brück, W., Lucchinetti, C., 2001. Heterogeneity of multiple sclerosis pathogenesis: implications for diagnosis and therapy. Trends Mol Med 7, 115–121.

Lassmann, H., Van Horssen, J., 2011. The molecular basis of neurodegeneration in multiple sclerosis. FEBS Lett. 585, 3715–3723.

Lauro, K.L., LaManna, J.C., 1997. Adequacy of cerebral vascular remodeling following three weeks of hypobaric hypoxia. Examined by an integrated composite analytical model. Adv. Exp. Med. Biol 411, 369–376.

Law, M., Saindane, A.M., Ge, Y., Babb, J.S., Johnson, G., Mannon, L.J., Herbert, J., Grossman, R.I., 2004. Microvascular abnormality in relapsing-remitting multiple sclerosis: perfusion MR imaging findings in normal-appearing white matter. Radiology 231, 645–652.

Leary SM, Thompson AJ. 2003. Treatment for patients with primary progressive multiple sclerosis. In: Cohen JA, Rudick R. Multiple Sclerosis Therapeutics. London: Martin Dunitz; pp. 589-598.

Leblond, J., Krnjevic, K., 1989. Hypoxic changes in hippocampal neurons. J. Neurophysiol. 62, 1–14. Lee, Y., Morrison, B.M., Li, Y., Lengacher, S., Farah, M.H., Hoffman, P.N., Liu, Y., Tsingalia, A., Jin, L., Zhang, P.-W., Pellerin, L., Magistretti, P.J., Rothstein, J.D., 2012. Oligodendroglia metabolically support axons and contribute to neurodegeneration. Nature 62(1), 1-14.

Leenders, K.L., Perani, D., Lammertsma, A.A., Heather, J.D., Buckingham, P., Jones, T., Healy, M.J.R., Gibbs, J.M., Wise, R.J.S., Hatazawa, J., Herold, S., Beaney, R.P., Brooks, D.J., Spinks, T., Rhodes, C., Frackowiak, R.S.J., 1990. Cerebral Blood Flow, Blood Volume and Oxygen Utilization Normal Values and Effect of Age. Brain 113, 27–47.

Lehnardt, S., Massillon, L., Follett, P., Jensen, F.E., Ratan, R., Rosenberg, P.A., Volpe, J.J., Vartanian, T., 2003. Activation of innate immunity in the CNS triggers

neurodegeneration through a Toll-like receptor 4-dependent pathway. Proc Natl Acad Sci U S A 100, 8514–8519.

Leonard, M.O., Cottell, D.C., Godson, C., Brady, H.R., Taylor, C.T., 2003. The Role of HIF-1α in Transcriptional Regulation of the Proximal Tubular Epithelial Cell Response to Hypoxia. Journal of Biological Chemistry 278, 40296 –40304.

Leone, A.M., Palmer, R.M., Knowles, R.G., Francis, P.L., Ashton, D.S., Moncada, S., 1991. Constitutive and inducible nitric oxide synthases incorporate molecular oxygen into both nitric oxide and citrulline. J. Biol. Chem 266, 23790–23795.

Levine, J.M., Stincone, F., Lee, Y.-S., 1993. Development and differentiation of glial precursor cells in the rat cerebellum. Glia 7, 307–321.

Levy, W.B., Baxter, R.A., 1996. Energy efficient neural codes. Neural Comput 8, 531–543.

Li, C., Jackson, R.M., 2002. Reactive species mechanisms of cellular hypoxia-reoxygenation injury. Am. J. Physiol., Cell Physiol 282, C227–241.

Li, X.G., Florence, S.L., Kaas, J.H., 1990. Areal distributions of cortical neurons projecting to different levels of the caudal brain stem and spinal cord in rats. Somatosens Mot Res 7, 315–335.

Li, Y., Song, Y., Zhao, L., Gaidosh, G., Laties, A.M., Wen, R., 2008. Direct labeling and visualization of blood vessels with lipophilic carbocyanine dye DiI. Nat. Protocols 3, 1703–1708.

Li, Z., Chapleau, M.W., Bates, J.N., Bielefeldt, K., Lee, H.C., Abboud, F.M., 1998. Nitric oxide as an autocrine regulator of sodium currents in baroreceptor neurons. Neuron 20, 1039–1049.

Licinio, J., Prolo, P., McCann, S.M., Wong, M.-L., 1999. Brain iNOS: current understanding and clinical implications. Molecular Medicine Today 5, 225–232.

Lin, R.F., Lin, T.S., Tilton, R.G., Cross, A.H., 1993. Nitric oxide localized to spinal cords of mice with experimental allergic encephalomyelitis: an electron paramagnetic resonance study. J. Exp. Med. 178, 643–648.

Ling, Q., Sailan, W., Ran, J., Zhi, S., Cen, L., Yang, X., Xiaoqun, Q., 2008. The effect of intermittent hypoxia on bodyweight, serum glucose and cholesterol in obesity mice. Pak. J. Biol. Sci 11, 869–875.

Linington, C., Lassmann, H., 1987. Antibody responses in chronic relapsing experimental allergic encephalomyelitis: correlation of serum demyelinating activity with antibody titre to the myelin/oligodendrocyte glycoprotein (MOG). J. Neuroimmunol. 17, 61–69.

Linington, C., Bradl, M., Lassmann, H., Brunner, C., Vass, K., 1988. Augmentation of demyelination in rat acute allergic encephalomyelitis by circulating mouse monoclonal antibodies directed against a myelin/oligodendrocyte glycoprotein. Am. J. Pathol. 130, 443–454.

Liochev, S.I., Fridovich, I., 1994. The role of O2.- in the production of HO.: in vitro and in vivo. Free Radic. Biol. Med. 16, 29–33.

Litch, J.A., Bishop, R.A., 2000. High-altitude global amnesia. Wilderness Environ Med 11, 25–28. Liu, J.S., Zhao, M.L., Brosnan, C.F., Lee, S.C., 2001. Expression of inducible nitric oxide synthase and nitrotyrosine in multiple sclerosis lesions. Am. J. Pathol. 158, 2057–2066.

Lowe, J., MacLennan, K.A., Powe, D.G., Pound, J.D., Palmer, J.B., 1989. Microglial cells in human brain have phenotypic characteristics related to possible function as dendritic antigen presenting cells. J. Pathol 159, 143–149.

Lu, F., Selak, M., O'Connor, J., Croul, S., Lorenzana, C., Butunoi, C., Kalman, B., 2000. Oxidative damage to mitochondrial DNA and activity of mitochondrial enzymes in chronic active lesions of multiple sclerosis. Journal of the Neurological Sciences 177, 95–103.

Lu, H., Patel, S., Luo, F., Li, S.-J., Hillard, C.J., Ward, B.D., Hyde, J.S., 2004. Spatial correlations of laminar BOLD and CBV responses to rat whisker stimulation with neuronal activity localized by Fos expression. Magnetic Resonance in Medicine 52, 1060–1068.

Lucchinetti, C., Brück, W., Parisi, J., Scheithauer, B., Rodriguez, M., Lassmann, H., 1999. A quantitative analysis of oligodendrocytes in multiple sclerosis lesions. A study of 113 cases. Brain 122 (Pt 12), 2279–2295.

Lucchinetti, C., Brück, W., Parisi, J., Scheithauer, B., Rodriguez, M., Lassmann, H., 2000. Heterogeneity of multiple sclerosis lesions: implications for the pathogenesis of demyelination. Ann. Neurol 47, 707–717.

Lucchinetti, C., Popescu, B.F.G., Bunyan, R.F., Moll, N.M., Roemer, S.F., Lassmann, H., Brück, Wolfgang, Parisi, J.E., Scheithauer, B.W., Giannini, C., Weigand, S.D., Mandrekar, J., Ransohoff, R.M., 2011. Inflammatory Cortical Demyelination in Early Multiple Sclerosis. New England Journal of Medicine 365, 2188–2197.

Ludwin, S.K., 1997. The pathobiology of the oligodendrocyte. J. Neuropathol. Exp. Neurol. 56, 111–124. Lycke, J., Wikkelsö, C., Bergh, A.C., Jacobsson, L., Andersen, O., 1993. Regional cerebral blood flow in multiple sclerosis measured by single photon emission tomography with technetium-99m hexamethylpropyleneamine oxime. Eur. Neurol. 33, 163–167.

Magistretti, P.J., Pellerin, L., 1996. Cellular bases of brain energy metabolism and their relevance to functional brain imaging: evidence for a prominent role of astrocytes. Cereb. Cortex 6, 50–61.

Magistretti, P.J., Pellerin, L., 1999. Cellular mechanisms of brain energy metabolism and their relevance to functional brain imaging. Philos. Trans. R. Soc. Lond., B, Biol. Sci. 354, 1155–1163.

Magistretti, P.J., Pellerin, L., Rothman, D.L., Shulman, R.G., 1999. Energy on demand. Science 283, 496–497. Mahad, D., Ziabreva, I., Lassmann, H., Turnbull, D., 2008. Mitochondrial defects in acute multiple sclerosis lesions. Brain 131, 1722–1735.

Magliozzi, R., Howell, O., Vora, A., Serafini, B., Nicholas, R., Puopolo, M., Reynolds, R., Aloisi, F., 2007. Meningeal B-cell follicles in secondary progressive multiple sclerosis associate with early onset of disease and severe cortical pathology. Brain 130, 1089–1104.

Magliozzi, R., Howell, O.W., Reeves, C., Roncaroli, F., Nicholas, R., Serafini, B., Aloisi, F., Reynolds, R., 2010. A Gradient of neuronal loss and meningeal inflammation in multiple sclerosis. Ann. Neurol. 68, 477–493.

Mahad, D.J., Ziabreva, I., Campbell, G., Lax, N., White, K., Hanson, P.S., Lassmann, H., Turnbull, D.M., 2009. Mitochondrial changes within axons in multiple sclerosis. Brain 132, 1161–1174.

Manalo, D.J., Rowan, A., Lavoie, T., Natarajan, L., Kelly, B.D., Ye, S.Q., Garcia, J.G.N., Semenza, G.L., 2005. Transcriptional regulation of vascular endothelial cell responses to hypoxia by HIF-1. Blood 105, 659 –669.

Mander, P., Borutaite, V., Moncada, S., Brown, G.C., 2005. Nitric oxide from inflammatory-activated glia synergizes with hypoxia to induce neuronal death. J. Neurosci. Res. 79, 208–215.

Mander, P., Brown, G.C., 2004a. Nitric oxide, hypoxia and brain inflammation. Biochem. Soc. Trans 32, 1068–1069.

Mander, P., Brown, G.C., 2004b. Nitric oxide, hypoxia and brain inflammation. Biochem. Soc. Trans. 32, 1068–1069. Mansfield, K.D., Guzy, R.D., Pan, Y., Young, R.M., Cash, T.P., Schumacker, P.T., Simon, M.C., 2005. Mitochondrial dysfunction resulting from loss of cytochrome c impairs cellular oxygen sensing and hypoxic HIF-alpha activation. Cell Metab 1, 393–399.

Marik, C., Felts, P.A., Bauer, J., Lassmann, H., Smith, K.J., 2007. Lesion genesis in a subset of patients with multiple sclerosis: a role for innate immunity? Brain 130, 2800–2815. Marti, H.H., Risau, W., 1999. Angiogenesis in ischemic disease. Thromb. Haemost 82 Suppl 1, 44–52.

Martin, B.L., Wu, D., Jakes, S., Graves, D.J., 1990. Chemical influences on the specificity of tyrosine phosphorylation. J. Biol. Chem. 265, 7108–7111.

Masumura, M., Hata, R., Nagai, Y., Sawada, T., 2001. Oligodendroglial cell death with DNA fragmentation in the white matter under chronic cerebral hypoperfusion: comparison between normotensive and spontaneously hypertensive rats. Neurosci. Res 39, 401–412.

Mateo, J., García-Lecea, M., Cadenas, S., Hernández, C., Moncada, S., 2003. Regulation of hypoxia-inducible factor-1alpha by nitric oxide through mitochondria-dependent and -independent pathways. Biochem. J 376, 537–544.

Matsumoto, Y., Ohmori, K., Fujiwara, M., 1992. Microglial and astroglial reactions to inflammatory lesions of experimental autoimmune encephalomyelitis in the rat central nervous system. J. Neuroimmunol. 37, 23–33.

Maxwell, P.H., Wiesener, M.S., Chang, G.W., Clifford, S.C., Vaux, E.C., Cockman, M.E., Wykoff, C.C., Pugh, C.W., Maher, E.R., Ratcliffe, P.J., 1999. The tumour suppressor protein VHL targets hypoxia-inducible factors for oxygen-dependent proteolysis. Nature 399, 271–275.

Mayer, C.A., Pfeilschifter, W., Lorenz, M.W., Nedelmann, M., Bechmann, I., Steinmetz, H., Ziemann, U., 2011. The perfect crime? CCSVI not leaving a trace in MS. J. Neurol. Neurosurg. Psychiatr. 82, 436–440.

McDonald, W.I. 1986. The pathophysiology of multiple sclerosis. In: McDonald, WI., Silberberg, DH. The Diagnosis of Multiple Sclerosis. London: Butterworth, pp. 112-133.

McFarland, H.F., Martin, R., 2007. Multiple sclerosis: a complicated picture of autoimmunity. Nat. Immunol. 8, 913–919.

McKenna MC, Gruetter R, Sonnewald U, Waagepetersen H, Schousboe A. 2006. Energy metabolism of the brain: Molecular, cellular and medical aspects. In: Siegel GJ, Albers RW, Brady ST, Price DL. Basic neurochemistry. San Diego: Academic Press. pp 531–558.

McLaurin, J.A., Yong, V.W., 1995. Oligodendrocytes and myelin. Neurol Clin 13, 23–49. McTigue, D.M., Horner, P.J., Stokes, B.T., Gage, F.H., 1998. Neurotrophin-3 and brain-derived neurotrophic factor induce oligodendrocyte proliferation and myelination of regenerating axons in the contused adult rat spinal cord. J. Neurosci. 18, 5354–5365.

McTigue, D.M., Tripathi, R.B., 2008. The life, death, and replacement of oligodendrocytes in the adult CNS. J. Neurochem. 107, 1–19.

Melillo, G., Musso, T., Sica, A., Taylor, L.S., Cox, G.W., Varesio, L., 1995. A hypoxia-responsive element mediates a novel pathway of activation of the inducible nitric oxide synthase promoter. J. Exp. Med. 182, 1683–1693.

Mews, I., Bergmann, M, Bunkowski, S., Gullotta, F., Brück, W, 1998. Oligodendrocyte and axon pathology in clinically silent multiple sclerosis lesions. Mult. Scler. 4, 55–62.

Milhoan, K.A., Lane, T.A., Bloor, C.M., 1992. Hypoxia induces endothelial cells to increase their adherence for neutrophils: role of PAF. Am J Physiol Heart Circ Physiol 263, H956–H962.

Millan, M.T., Geczy, C., Stuhlmeier, K.M., Goodman, D.J., Ferran, C., Bach, F.H., 1997. Human monocytes activate porcine endothelial cells, resulting in increased E-selectin,

interleukin-8, monocyte chemotactic protein-1, and plasminogen activator inhibitor-type-1 expression. Transplantation 63, 421–429.

Miller, D.H., Barkhof, F., Frank, J.A., Parker, G.J.M., Thompson, A.J., 2002. Measurement of atrophy in multiple sclerosis: pathological basis, methodological aspects and clinical relevance. Brain 125, 1676–1695.

Mitchison, G., 1992. Axonal trees and cortical architecture. Trends Neurosci 15, 122–126.

Mitrovic, B., Ignarro, L.J., Montestruque, S., Smoll, A., Merrill, J.E., 1994. Nitric oxide as a potential pathological mechanism in demyelination: Its differential effects on primary glial cellsin vitro. Neuroscience 61, 575–585.

Molander, C., Grant, G., 1985. Cutaneous projections from the rat hindlimb foot to the substantia gelatinosa of the spinal cord studied by transganglionic transport of WGA-HRP conjugate. The Journal of Comparative Neurology 237, 476–484.

Moncada, S., Erusalimsky, J.D., 2002. Does nitric oxide modulate mitochondrial energy generation and apoptosis? Nat. Rev. Mol. Cell Biol 3, 214–220.

Mong, F.S., 1990. Dendritic distributions of motor neurons innervating fast and slow muscles of the hind limb of rats. J Hirnforsch 31, 259–267.

Moody, D.M., Bell, M.A., Challa, V.R., 1990. Features of the cerebral vascular pattern that predict vulnerability to perfusion or oxygenation deficiency: an anatomic study. AJNR Am J Neuroradiol 11, 431–439.

Moransard, M., Dann, A., Staszewski, O., Fontana, A., Prinz, M., Suter, T., 2011. NG2 expressed by macrophages and oligodendrocyte precursor cells is dispensable in experimental autoimmune encephalomyelitis. Brain 134, 1315–1330.

Moreau, T., Coles, A., Wing, M., Isaacs, J., Hale, G., Waldmann, H., Compston, A., 1996. Transient increase in symptoms associated with cytokine release in patients with multiple sclerosis. Brain 119 (Pt 1), 225–237.

Mortola, J., 1993. Hypoxic Hypometabolism in Mammals. Physiology 8, 79 –82.

Murphy, M.P., 2009. How mitochondria produce reactive oxygen species. Biochem J 417, 1–13. Nair, A., Frederick, T.J., Miller, S.D., 2008. Astrocytes in Multiple Sclerosis: A Product of their Environment. Cell Mol Life Sci 65, 2702–2720.

Nair, P., Whalen, W.J., Buerk, D., 1975. PO2 of cat cerebral cortex: response to breathing N2 and 100 per cent O21. Microvasc. Res 9, 158–165.

Nair, A., Frederick, T.J., Miller, S.D., 2008. Astrocytes in Multiple Sclerosis: A Product of their Environment. Cell Mol Life Sci 65, 2702–2720.

Ndubuizu, O., LaManna, J.C., 2007. Brain tissue oxygen concentration measurements. Antioxid. Redox Signal. 9, 1207–1219.

Nieber, K., Sevcik, J., Illes, P., 1995. Hypoxic changes in rat locus coeruleus neurons in vitro. J Physiol 486, 33–46.

Nikić, I., Merkler, D., Sorbara, C., Brinkoetter, M., Kreutzfeldt, M., Bareyre, F.M., Brück, W., Bishop, D., Misgeld, T., Kerschensteiner, M., 2011. A reversible form of axon damage in experimental autoimmune encephalomyelitis and multiple sclerosis. Nature Medicine 17, 495–499.

Nimmerjahn, A., Kirchhoff, F., Helmchen, F., 2005. Resting microglial cells are highly dynamic surveillants of brain parenchyma in vivo. Science 308, 1314–1318. Nishimura, N., Schaffer, C.B., Friedman, B., Lyden, P.D., Kleinfeld, D., 2007. Penetrating arterioles are a bottleneck in the perfusion of neocortex. Proc Natl Acad Sci U S A 104, 365–370.

Nishiyama, A., Lin, X.H., Giese, N., Heldin, C.H., Stallcup, W.B., 1996. Co-localization of NG2 proteoglycan and PDGF alpha-receptor on O2A progenitor cells in the developing rat brain. J. Neurosci. Res. 43, 299–314.

Nishiyama, A., Yu, M., Drazba, J.A., Tuohy, V.K., 1997. Normal and reactive NG2+ glial cells are distinct from resting and activated microglia. J. Neurosci. Res. 48, 299–312.

Noseworthy, J.H., 1999. Progress in determining the causes and treatment of multiple sclerosis. Nature 399, A40–A47.

Ock, J., Cho, H.-J., Hong, S.H., Kim, I.K. y. e. o. m., Suk, K., 2005. Hypoxia as an Initiator of Neuroinflammation: Microglial Connections. Current Neuropharmacology 3, 183–191. Oda, T., Hirota, K., Nishi, K., Takabuchi, S.,

Oda, S., Yamada, H., Arai, T., Fukuda, K., Kita, T., Adachi, T., Semenza, G.L., Nohara, R., 2006. Activation of hypoxia-inducible factor 1 during macrophage differentiation. Am. J. Physiol., Cell Physiol 291, C104–113.

Okuda, Y., Nakatsuji, Y., Fujimura, H., Esumi, H., Ogura, T., Yanagihara, T., Sakoda, S., 1995. Expression of the inducible isoform of nitric oxide synthase in the central nervous system of mice correlates with the severity of actively induced experimental allergic encephalomyelitis. J. Neuroimmunol. 62, 103–112.

Oleszak, E.L., Zaczynska, E., Bhattacharjee, M., Butunoi, C., Legido, A., Katsetos, C.D., 1998. Inducible nitric oxide synthase and nitrotyrosine are found in monocytes/macrophages and/or astrocytes in acute, but not in chronic, multiple sclerosis. Clin. Diagn. Lab. Immunol. 5, 438–445.

Ong, W.Y., Levine, J.M., 1999. A light and electron microscopic study of NG2 chondroitin sulfate proteoglycan-positive oligodendrocyte precursor cells in the normal and kainate-lesioned rat hippocampus. Neuroscience 92, 83–95.

Owusu-Ansah, E., Yavari, A., Banerjee, U., 2008. A protocol for in vivo detection of reactive oxygen species. Protocol Exchange. Palmer, L.A., Semenza, G.L., Stoler, M.H., Johns, R.A., 1998. Hypoxia induces type II NOS gene expression in pulmonary artery endothelial cells via HIF-1. Am. J. Physiol. 274, L212–219.

Papadopoulos, D., Ewans, L., Pham-Dinh, D., Knott, J., Reynolds, R., 2006a. Upregulation of α-synuclein in neurons and glia in inflammatory demyelinating disease. Molecular and Cellular Neuroscience 31, 597–612.

Papadopoulos, D., Pham-Dinh, D., Reynolds, R., 2006b. Axon loss is responsible for chronic neurological deficit following inflammatory demyelination in the rat. Experimental Neurology 197, 373–385.

Patrikios, P., Stadelmann, C., Kutzelnigg, A., Rauschka, H., Schmidbauer, M., Laursen, H., Sorensen, P.S., Brück, W., Lucchinetti, C., Lassmann, H., 2006. Remyelination is extensive in a subset of multiple sclerosis patients. Brain 129, 3165–3172.

Paxinos, G. 1995, The Rat Nervous System, 2 edn, Academic Press Inc, California.

Peterson, J.W., Bö, L, Mörk, S., Chang, A., Trapp, B D, 2001. Transected neurites, apoptotic neurons, and reduced inflammation in cortical multiple sclerosis lesions. Ann. Neurol. 50, 389–400.

Peyssonnaux, C., Datta, V., Cramer, T., Doedens, A., Theodorakis, E.A., Gallo, R.L., Hurtado-Ziola, N., Nizet, V., Johnson, R.S., 2005. HIF-1α expression regulates the bactericidal capacity of phagocytes. J. Clin. Invest. 115, 1806–1815. Phelps, C.H., 1972. Barbiturate-induced glycogen accumulation in brain. An electron microscopic study. Brain Res 39, 225–234.

Pichiule, P., LaManna, J.C., 2002. Angiopoietin-2 and rat brain capillary remodeling during adaptation and deadaptation to prolonged mild hypoxia. Journal of Applied Physiology 93, 1131 –1139.

Pinsky, D.J., Naka, Y., Liao, H., Oz, M.C., Wagner, D.D., Mayadas, T.N., Johnson, R.C., Hynes, R.O., Heath, M., Lawson, C.A., Stern, D.M., 1996. Hypoxia-induced exocytosis of endothelial cell Weibel-Palade bodies. A mechanism for rapid neutrophil recruitment after cardiac preservation. J Clin Invest 97, 493–500.

Poderoso, J.J., Carreras, M.C., Lisdero, C., Riobó, N., Schöpfer, F., Boveris, A., 1996. Nitric oxide inhibits electron transfer and increases superoxide radical production in rat heart mitochondria and submitochondrial particles. Arch. Biochem. Biophys. 328, 85–92.

Pohl, D., Krone, B., Rostasy, K., Kahler, E., Brunner, E., Lehnert, M., Wagner, H.-J., Gärtner, J., Hanefeld, F., 2006. High seroprevalence of Epstein-Barr virus in children with multiple sclerosis. Neurology 67, 2063–2065.

Pollard, T.D., Borisy, G.G., 2003. Cellular motility driven by assembly and disassembly of actin filaments. Cell 112, 453–465.

Prineas, J.W., Kwon, E.E., Goldenberg, P.Z., Ilyas, A.A., Quarles, R.H., Benjamins, J.A., Sprinkle, T.J., 1989. Multiple sclerosis. Oligodendrocyte proliferation and differentiation in fresh lesions. Lab. Invest. 61, 489–503.

Prineas, J.W., Kwon, E.E., Cho, E.S., Sharer, L.R., Barnett, M.H., Oleszak, E.L., Hoffman, B., Morgan, B.P., 2001. Immunopathology of secondary-progressive multiple sclerosis. Ann. Neurol. 50, 646–657.

Proescholdt, M.A., Heiss, J.D., Walbridge, S., Mühlhauser, J., Capogrossi, M.C., Oldfield, E.H., Merrill, M.J., 1999. Vascular endothelial growth factor (VEGF) modulates vascular permeability and inflammation in rat brain. J. Neuropathol. Exp. Neurol. 58, 613–627.

Proescholdt, M.A., Jacobson, S., Tresser, N., Oldfield, E.H., Merrill, M.J., 2002. Vascular endothelial growth factor is expressed in multiple sclerosis plaques and can induce inflammatory lesions in experimental allergic encephalomyelitis rats. J. Neuropathol. Exp. Neurol. 61, 914–925.

Qi, Y., Dawson, G., 1993. Effects of Hypoxia on Oligodendrocyte Signal Transduction. Journal of Neurochemistry 61, 1097–1104.

Qin, J., Goswami, R., Balabanov, R., Dawson, G., 2007. Oxidized phosphatidylcholine is a marker for neuroinflammation in multiple sclerosis brain. J. Neurosci. Res. 85, 977–984.

Qu, H., Håberg, A., Haraldseth, O., Unsgård, G., Sonnewald, U., 2000. (13)C MR spectroscopy study of lactate as substrate for rat brain. Dev. Neurosci. 22, 429–436.

Quintero, P., Milagro, F.I., Campión, J., Martínez, J.A., 2010. Impact of oxygen availability on body weight management. Med. Hypotheses 74, 901–907.

Raine, C.S., Scheinberg, L., Waltz, J.M., 1981. Multiple sclerosis. Oligodendrocyte survival and proliferation in an active established lesion. Lab. Invest. 45, 534–546.

Rainger, G.E., Fisher, A., Shearman, C., Nash, G.B., 1995. Adhesion of flowing neutrophils to cultured endothelial cells after hypoxia and reoxygenation in vitro. Am J Physiol Heart Circ Physiol 269, H1398–H1406.

Raleigh, J.A., Calkins-Adams, D.P., Rinker, L.H., Ballenger, C.A., Weissler, M.C., Fowler, W.C., Jr, Novotny, D.B., Varia, M.A., 1998. Hypoxia and vascular endothelial growth factor expression in human squamous cell carcinomas using pimonidazole as a hypoxia marker. Cancer Res 58, 3765–3768.

Rawe, S.E., Perot, P.L., Jr, 1977. Autoradiographic metabolic studies in experimentally produced spinal cord trauma. Surg Forum 28, 453–455.

Redford, E.J., Kapoor, R., Smith, K.J., 1997. Nitric oxide donors reversibly block axonal conduction: demyelinated axons are especially susceptible. Brain 120 (Pt 12), 2149–2157.

Rees, D.D., Monkhouse, J.E., Cambridge, D., Moncada, S., 1998. Nitric oxide and the haemodynamic profile of endotoxin shock in the conscious mouse. Br. J. Pharmacol 124, 540–546.

Reier, P.J., Houle, J.D., 1988. The glial scar: its bearing on axonal elongation and transplantation approaches to CNS repair. Adv Neurol 47, 87–138.

Rejdak, K., Eikelenboom, M.J., Petzold, A., Thompson, E.J., Stelmasiak, Z., Lazeron, R.H.C., Barkhof, F., Polman, C.H., Uitdehaag, B.M.J., Giovannoni, G., 2004. CSF nitric oxide metabolites are associated with activity and progression of multiple sclerosis. Neurology 63, 1439–1445.

Reynolds, R., Hardy, R., 1997. Oligodendroglial progenitors labeled with the O4 antibody persist in the adult rat cerebral cortex in vivo. J. Neurosci. Res. 47, 455–470.

Rhodes, K.E., Raivich, G., Fawcett, J.W., 2006. The injury response of oligodendrocyte precursor cells is induced by platelets, macrophages and inflammation-associated cytokines. Neuroscience 140, 87–100.

Rist, R.J., Jones, G.E., Naftalin, R.J., 1991. Effects of macrophage colony-stimulating factor and phorbol myristate acetate on 2-D-deoxyglucose transport and superoxide production in rat peritoneal macrophages. Biochem. J. 278 (Pt 1), 119–128.

Rivero-Melián, C., Grant, G., 1991. Choleragenoid horseradish peroxidase used for studying projections of some hindlimb cutaneous nerves and plantar foot afferents to the dorsal horn and Clarke's column in the rat. Exp Brain Res 84, 125–132.

Rodriguez, M., Scheithauer, B., 1994. Ultrastructure of multiple sclerosis. Ultrastruct Pathol 18, 3–13. Roscoe, W.A., Welsh, M.E., Carter, D.E.,

Karlik, S.J., 2009. VEGF and angiogenesis in acute and chronic MOG((35-55)) peptide induced EAE. J. Neuroimmunol. 209, 6–15.

Rosenstein, J.M., Mani, N., Silverman, W.F., Krum, J.M., 1998. Patterns of brain angiogenesis after vascular endothelial growth factor administration in vitro and in vivo. PNAS 95, 7086–7091.

Rothe, G., Valet, G., 1990. Flow cytometric analysis of respiratory burst activity in phagocytes with hydroethidine and 2',7'-dichlorofluorescin. J Leukoc Biol 47, 440–448.

Rothman, D.L., Behar, K.L., Hyder, F., Shulman, R.G., 2003. In vivo NMR studies of the glutamate neurotransmitter flux and neuroenergetics: implications for brain function. Annu. Rev. Physiol. 65, 401–427.

Ryn, Z., 1988. Psychopathology in mountaineering--mental disturbances under high-altitude stress. Int J Sports Med 9, 163–169.

Saadi, S., Wrenshall, L.E., Platt, J.L., 2002. Regional manifestations and control of the immune system. FASEB J. 16, 849–856.

Sagone, A.L., Lawrence, T., Balcerzak, S.P., 1973. Effect of Smoking on Tissue Oxygen Supply. Blood 41, 845–851.

Sánchez-Abarca, L.I., Tabernero, A., Medina, J.M., 2001. Oligodendrocytes use lactate as a source of energy and as a precursor of lipids. Glia 36, 321–329.

Sawcer, S., Hellenthal, G., Pirinen, M., Spencer, C.C.A., Patsopoulos, N.A., et al., 2011. Genetic risk and a primary role for cell-mediated immune mechanisms in multiple sclerosis. Nature 476, 214–219.

Schievink, W.I., Luyendijk, W., Los, J.A., 1988. Does the artery of Adamkiewicz exist in the albino rat? J. Anat 161, 95–101.

Schmidt-Kastner, R., Freund, T.F., 1991. Selective vulnerability of the hippocampus in brain ischemia. Neuroscience 40, 599–636.

Schoch, H.J., Fischer, S., Marti, H.H., 2002. Hypoxia-induced vascular endothelial growth factor expression causes vascular leakage in the brain. Brain 125, 2549–2557.

Schofield, C.J., Ratcliffe, P.J., 2004. Oxygen sensing by HIF hydroxylases. Nat. Rev. Mol. Cell Biol 5, 343–354.

Schofield, C.J., Zhang, Z., 1999. Structural and mechanistic studies on 2-oxoglutarate-dependent oxygenases and related enzymes. Curr. Opin. Struct. Biol 9, 722–731.

Schonberg, D.L., Popovich, P.G., McTigue, D.M., 2007. Oligodendrocyte generation is differentially influenced by toll-like receptor (TLR) 2 and TLR4-mediated intraspinal macrophage activation. Journal of Neuropathology and Experimental Neurology 66, 1124–1135.

Schumacker, P.T., 2003. Current paradigms in cellular oxygen sensing. Adv. Exp. Med. Biol 543, 57–71.

Schurr, A., Miller, J.J., Payne, R.S., Rigor, B.M., 1999. An increase in lactate output by brain tissue serves to meet the energy needs of glutamate-activated neurons. J. Neurosci. 19, 34–39.

Schurr, A., Payne, R.S., 2007. Lactate, not pyruvate, is neuronal aerobic glycolysis end product: an in vitro electrophysiological study. Neuroscience 147, 613–619.

Schurr, A., Payne, R.S., Miller, J.J., Rigor, B.M., 1997. Brain lactate is an obligatory aerobic energy substrate for functional recovery after hypoxia: further in vitro validation. J. Neurochem. 69, 423–426.

Sciamanna, M.A., Lee, C.P., 1993. Ischemia/reperfusion-induced injury of forebrain mitochondria and protection by ascorbate. Arch. Biochem. Biophys. 305, 215–224.

Seabrook, T.J., Littlewood-Evans, A., Brinkmann, V., Pöllinger, B., Schnell, C., Hiestand, P.C., 2010. Angiogenesis is present in experimental autoimmune encephalomyelitis and pro-angiogenic factors are increased in multiple sclerosis lesions. J Neuroinflammation 7, 95.

Seigel, GJ., Alberts, RW., Brady, ST, Price, DL. 2006. Energy Metabolism. In: Bazan, N. Basic Neurochemistry: Molecular, Cellular and Medical Aspects. 7 ed. Elsevier Academic Press, Canada, pp. 531-547

Semenza, G., 2002. Signal transduction to hypoxia-inducible factor 1. Biochem. Pharmacol 64, 993–998.

Semenza, G.L., 2007. Hypoxia-inducible factor 1 (HIF-1) pathway. Sci. STKE 2007, cm8.

Serafini, B., Rosicarelli, B., Franciotta, D., Magliozzi, R., Reynolds, R., Cinque, P., Andreoni, L., Trivedi, P., Salvetti, M., Faggioni, A., Aloisi, F., 2007. Dysregulated Epstein-Barr virus infection in the multiple sclerosis brain. J Exp Med 204, 2899–2912.

Serres, S., Bezancon, E., Franconi, J.-M., Merle, M., 2005. Ex vivo NMR study of lactate metabolism in rat brain under various depressed states. J. Neurosci. Res. 79, 19–25.

Sharma, R., Fischer, M.-T., Bauer, J., Felts, P.A., Smith, K.J., Misu, T., Fujihara, K., Bradl, M., Lassmann, H., 2010. Inflammation induced by innate immunity in the central nervous system leads to primary astrocyte dysfunction followed by demyelination. Acta Neuropathol 120, 223–236.

Shih, A.Y., Johnson, D.A., Wong, G., Kraft, A.D., Jiang, L., Erb, H., Johnson, J.A., Murphy, T.H., 2003. Coordinate regulation of glutathione biosynthesis and release by Nrf2-expressing glia potently protects neurons from oxidative stress. J. Neurosci. 23, 3394–3406.

Shockley, R.P., LaManna, J.C., 1988. Determination of rat cerebral cortical blood volume changes by capillary mean transit time analysis during hypoxia, hypercapnia and hyperventilation. Brain Res 454, 170–178.

Shrager, P., Custer, A.W., Kazarinova, K., Rasband, M.N., Mattson, D., 1998. Nerve conduction block by nitric oxide that is mediated by the axonal environment. J. Neurophysiol. 79, 529–536.

Shukla, V., Singh, S.N., Vats, P., Singh, V.K., Singh, S.B., Banerjee, P.K., 2005. Ghrelin and leptin levels of sojourners and acclimatized lowlanders at high altitude. Nutr Neurosci 8, 161–165.

Shweiki, D., Itin, A., Soffer, D., Keshet, E., 1992. Vascular endothelial growth factor induced by hypoxia may mediate hypoxia-initiated angiogenesis. Nature 359, 843–845.

Sibson, N.R., Dhankhar, A., Mason, G.F., Rothman, D.L., Behar, K.L., Shulman, R.G., 1998. Stoichiometric coupling of brain glucose metabolism and glutamatergic neuronal activity. Proc. Natl. Acad. Sci. U.S.A. 95, 316–321.

Sick, T.J., Lutz, P.L., LaManna, J.C., Rosenthal, M., 1982. Comparative brain oxygenation and mitochondrial redox activity in turtles and rats. Journal of Applied Physiology 53, 1354 –1359.

Siesjo, B. K. 1978. Brain Energy Metabolism, John Wiley and Sons, Chichester.

Simka, M., Kostecki, J., Zaniewski, M., Majewski, E., Hartel, M., 2010. Extracranial Doppler sonographic criteria of chronic cerebrospinal venous insufficiency in the patients with multiple sclerosis. Int Angiol 29, 109–114.

Simmons, R.D., Bernard, C.C., Singer, G., Carnegie, P.R., 1982. Experimental autoimmune encephalomyelitis. An anatomically-based explanation of clinical progression in rodents. J. Neuroimmunol. 3, 307–318.

Simon, K.C., Van der Mei, I.A.F., Munger, K.L., Ponsonby, A., Dickinson, J., Dwyer, T., Sundström, P., Ascherio, A., 2010. Combined effects of smoking, anti-EBNA antibodies, and HLA-DRB1*1501 on multiple sclerosis risk. Neurology 74, 1365–1371.

Singh, A.V., Zamboni, P., 2009. Anomalous venous blood flow and iron deposition in multiple sclerosis. J. Cereb. Blood Flow Metab. 29, 1867–1878.

Singhal, A.B., Wang, X., Sumii, T., Mori, T., Lo, E.H., 2002. Effects of normobaric hyperoxia in a rat model of focal cerebral ischemia-reperfusion. J. Cereb. Blood Flow Metab. 22, 861–868.

Slavin, A., Ewing, C., Liu, J., Ichikawa, M., Slavin, J., Bernard, C.C., 1998. Induction of a multiple sclerosis-like disease in mice with an immunodominant epitope of myelin oligodendrocyte glycoprotein. Autoimmunity 28, 109–120.

Smith, D., Pernet, A., Hallett, W.A., Bingham, E., Marsden, P.K., Amiel, S.A., 2003. Lactate: a preferred fuel for human brain metabolism in vivo. J. Cereb. Blood Flow Metab. 23, 658–664.

mith, K.J., Kapoor, R., Felts, P.A., 1999. Demyelination: the role of reactive oxygen and nitrogen species. Brain Pathol. 9, 69–92.

Smith, K.J., Kapoor, R., Hall, S.M., Davies, M., 2001. Electrically active axons degenerate when exposed to nitric oxide. Ann. Neurol. 49, 470–476.

Smith, K.J., Lassmann, H., 2002. The role of nitric oxide in multiple sclerosis. The Lancet Neurology 1, 232–241.

Smith, K.J., McDonald, W.I., 1999. The pathophysiology of multiple sclerosis: the mechanisms underlying the production of symptoms and the natural history of the disease. Philos Trans R Soc Lond B Biol Sci 354, 1649–1673.

Smith, R.H., Guilbeau, E.J., Reneau, D.D., 1977. The oxygen tension field within a discrete volume of cerebral cortex. Microvasc. Res 13, 233–240.

Sokoloff, L., 1981. Relationships among local functional activity, energy metabolism, and blood flow in the central nervous system. Fed. Proc. 40, 2311–2316.

Song, S.Y., Asaji, T., Tanizaki, Y., Fujimaki, T., Matsutani, M., Okeda, R., 1986. Cerebral thrombosis at altitude: its pathogenesis and the problems of prevention and treatment. Aviat Space Environ Med 57, 71–76.

Soulika, A.M., Lee, E., McCauley, E., Miers, L., Bannerman, P., Pleasure, D., 2009. Initiation and progression of axonopathy in experimental autoimmune encephalomyelitis. J. Neurosci. 29, 14965–14979.

Souza, J.M., Choi, I., Chen, Q., Weisse, M., Daikhin, E., Yudkoff, M., Obin, M., Ara, J., Horwitz, J., Ischiropoulos, H., 2000. Proteolytic degradation of tyrosine nitrated proteins. Arch. Biochem. Biophys. 380, 360–366.

Stadelmann, C., 2011. Multiple sclerosis as a neurodegenerative disease: pathology, mechanisms and therapeutic implications. Curr. Opin. Neurol. 24, 224–229.

Stadelmann, C., Wegner, C., Brück, W., 2011. Inflammation, demyelination, and degeneration - recent insights from MS pathology. Biochim. Biophys. Acta 1812, 275–282.

Stence, N., Waite, M., Dailey, M.E., 2001. Dynamics of microglial activation: a confocal time-lapse analysis in hippocampal slices. Glia 33, 256–266.

Stern, E.L., Quan, N., Proescholdt, M.G., Herkenham, M., 2000. Spatiotemporal induction patterns of cytokine and related immune signal molecule mRNAs in response to intrastriatal injection of lipopolysaccharide. Journal of Neuroimmunology 109, 245–260.

Storch, M.K., Stefferl, A., Brehm, U., Weissert, R., Wallström, E., Kerschensteiner, M., Olsson, T., Linington, C., Lassmann, H., 1998. Autoimmunity to myelin oligodendrocyte glycoprotein in rats mimics the spectrum of multiple sclerosis pathology. Brain Pathol 8, 681–694.

Stromnes, I.M., Goverman, J.M., 2006. Active induction of experimental allergic encephalomyelitis. Nat Protoc 1, 1810–1819.

Stuehr, D.J., Nathan, C.F., 1989. Nitric oxide. A macrophage product responsible for cytostasis and respiratory inhibition in tumor target cells. J. Exp. Med 169, 1543–1555.
Stys, P.K., 2004. Axonal degeneration in multiple sclerosis: is it time for neuroprotective strategies? Ann. Neurol. 55, 601–603.

Stys, P.K., 2005. General mechanisms of axonal damage and its prevention. J. Neurol. Sci. 233, 3–13.

Stys, P.K., Lopachin, R.M., Jr, 1996. Elemental composition and water content of rat optic nerve myelinated axons during in vitro post-anoxia reoxygenation. Neuroscience 73, 1081–1090.

Stys, P.K., Zamponi, G.W., Van Minnen, J., Geurts, J.J.G., 2012. Will the real multiple sclerosis please stand up? Nat. Rev. Neurosci. 13, 507–514.

Suh, S.W., Bergher, J.P., Anderson, C.M., Treadway, J.L., Fosgerau, K., Swanson, R.A., 2007. Astrocyte Glycogen Sustains Neuronal Activity during Hypoglycemia: Studies with the Glycogen Phosphorylase Inhibitor CP-316,819 ([R-R*,S*]-5-Chloro-N-[2-

hydroxy-3-(methoxymethylamino)-3-oxo-1-(phenylmethyl)propyl]-1H-indole-2-carboxamide). Journal of Pharmacology and Experimental Therapeutics 321, 45 –50.

Sun, X., Tanaka, M., Kondo, S., Okamoto, K., Hirai, S., 1998. Clinical significance of reduced cerebral metabolism in multiple sclerosis: a combined PET and MRI study. Ann Nucl Med 12, 89–94.

Sundqvist, E., Sundström, P., Lindén, M., Hedström, A.K., Aloisi, F., Hillert, J., Kockum, I., Alfredsson, L., Olsson, T., 2012. Lack of replication of interaction between EBNA1 IgG and smoking in risk for multiple sclerosis. Neurology 79, 1363–1368.

Svenningsson, A., Petersson, A.S., Andersen, O., Hansson, G.K., 1999. Nitric oxide metabolites in CSF of patients with MS are related to clinical disease course. Neurology 53, 1880–1882.

Swank, R.L., Roth, J.G., Woody, D.C., Jr, 1983. Cerebral blood flow and red cell delivery in normal subjects and in multiple sclerosis. Neurol. Res. 5, 37–59. Swanson, R.A., 1992. Astrocyte glutamate uptake during chemical hypoxia in vitro. Neurosci. Lett. 147, 143–146.

Swanson, R.A., Farrell, K., Stein, B.A., 1997. Astrocyte energetics, function, and death under conditions of incomplete ischemia: a mechanism of glial death in the penumbra. Glia 21, 142–153.

Swanson, R.A., Sagar, S.M., Sharp, F.R., 1989. Regional brain glycogen stores and metabolism during complete global ischaemia. Neurol. Res 11, 24–28. Swartz, H.M., 2007. On Tissue Oxygen and Hypoxia. Antioxidants & Redox Signaling 9, 1111–1114.

Szabó, C., 1996. DNA strand breakage and activation of poly-ADP ribosyltransferase: a cytotoxic pathway triggered by peroxynitrite. Free Radic. Biol. Med. 21, 855–869.

Szabó, C., 2003. Multiple pathways of peroxynitrite cytotoxicity. Toxicol. Lett. 140-141, 105–112. Taylor, C.T., Colgan, S.P., 2007. Hypoxia and gastrointestinal disease. J. Mol. Med. 85, 1295–1300.

Teixeira, S.A., Varriano, A.A., Bolonheis, S.M., Muscará, M.N., 2005. Experimental autoimmune encephalomyelitis: A heterogeneous group of animal models to study human multiple sclerosis. Drug Discovery Today: Disease Models 2, 127–134.

Thacker, E.L., Mirzaei, F., Ascherio, A., 2006. Infectious mononucleosis and risk for multiple sclerosis: a meta-analysis. Ann. Neurol. 59, 499–503.

Thorburne, S.K., Juurlink, B.H., 1996. Low glutathione and high iron govern the susceptibility of oligodendroglial precursors to oxidative stress. J. Neurochem. 67, 1014–1022.

Thorley-Lawson, D.A., 2001. Epstein-Barr virus: exploiting the immune system. Nat. Rev. Immunol. 1, 75–82.

Trapp, B.D., Nave, K.-A., 2008. Multiple sclerosis: an immune or neurodegenerative disorder? Annu. Rev. Neurosci. 31, 247–269.

Trapp, B.D., Peterson, J., Ransohoff, R.M., Rudick, R., Mörk, S., Bö, L., 1998. Axonal transection in the lesions of multiple sclerosis. N. Engl. J. Med. 338, 278–285.

Trapp, B.D., Quarles, R.H., 1984. Immunocytochemical localization of the myelin-associated glycoprotein Fact or Artifact? Journal of Neuroimmunology 6, 231–249.

Trapp, B.D., Stys, P.K., 2009. Virtual hypoxia and chronic necrosis of demyelinated axons in multiple sclerosis. Lancet Neurol 8, 280–291.

Turrens, J.F., Freeman, B.A., Levitt, J.G., Crapo, J.D., 1982. The effect of hyperoxia on superoxide production by lung submitochondrial particles. Archives of Biochemistry and Biophysics 217, 401–410.

Tveten, L., 1976. Spinal cord vascularity. IV. The spinal cord arteries in the rat. Acta Radiol Diagn (Stockh) 17, 385–398.

Tzartos, J.S., Khan, G., Vossenkamper, A., Cruz-Sadaba, M., Lonardi, S., Sefia, E., Meager, A., Elia, A., Middeldorp, J.M., Clemens, M., Farrell, P.J., Giovannoni, G., Meier, U.-C., 2012. Association of innate immune activation with latent Epstein-Barr virus in active MS lesions. Neurology 78, 15–23.

van Horssen, J., Brink, B.P., de Vries, H.E., van der Valk, P., Bø, Lars, 2007. The Blood-Brain Barrier in Cortical Multiple Sclerosis Lesions. Journal of Neuropathology and Experimental Neurology 66, 321–328.

van Horssen, J., Singh, S., Van der Pol, S., Kipp, M., Lim, J.L., Peferoen, L., Gerritsen, W., Kooi, E.-J., Witte, M.E., Geurts, J.J., De Vries, H.E., Peferoen-Baert, R., Van den Elsen, P.J., Van der Valk, P., Amor, S., 2012. Clusters of activated microglia in normal-appearing white matter show signs of innate immune activation. J Neuroinflammation 9, 156.

van Laarhoven, H.W.M., Kaanders, J.H.A.M., Lok, J., Peeters, W.J.M., Rijken, P.F.J.W., Wiering, B., Ruers, T.J.M., Punt, C.J.A., Heerschap, A., Van der Kogel, A.J., 2006. Hypoxia in relation to vasculature and proliferation in liver metastases in patients with colorectal cancer. Int. J. Radiat. Oncol. Biol. Phys 64, 473–482.

van Noort, J.M., Bsibsi, M., Gerritsen, W.H., Van der Valk, P., Bajramovic, J.J., Steinman, L., Amor, S., 2010. Alphab-crystallin is a target for adaptive immune responses and a trigger of innate responses in preactive multiple sclerosis lesions. J. Neuropathol. Exp. Neurol. 69, 694–703.

van Raam, B.J., Sluiter, W., De Wit, E., Roos, D., Verhoeven, A.J., Kuijpers, T.W., 2008. Mitochondrial membrane potential in human neutrophils is maintained by complex III activity in the absence of supercomplex organisation. PLoS ONE 3, e2013.

Varga, A.W., Johnson, G., Babb, J.S., Herbert, J., Grossman, R.I., Inglese, M., 2009. White matter hemodynamic abnormalities precede sub-cortical gray matter changes in multiple sclerosis. J. Neurol. Sci. 282, 28–33.

Véga, C., R. Sachleben, L., Gozal, D., Gozal, E., 2006. Differential metabolic adaptation to acute and long-term hypoxia in rat primary cortical astrocytes. Journal of Neurochemistry 97, 872–883.

Vibulsreth, S., Hefti, F., Ginsberg, M.D., Dietrich, W.D., Busto, R., 1987. Astrocytes protect cultured neurons from degeneration induced by anoxia. Brain Res. 422, 303–311.

Vignais, P.V., 2002. The superoxide-generating NADPH oxidase: structural aspects and activation mechanism. Cell. Mol. Life Sci. 59, 1428–1459.

Virág, L., Szabó, E., Gergely, P., Szabó, C., 2003. Peroxynitrite-induced cytotoxicity: mechanism and opportunities for intervention. Toxicol. Lett. 140-141, 113–124.

Vladimirova, O., O'Connor, J., Cahill, A., Alder, H., Butunoi, C., Kalman, B., 1998. Oxidative damage to DNA in plaques of MS brains. Mult. Scler. 4, 413–418.

Walmsley, S.R., Cadwallader, K.A., Chilvers, E.R., 2005a. The role of HIF-1alpha in myeloid cell inflammation. Trends Immunol 26, 434–439.

Wallstrom E, Olsson T. 2008, Rat models of EAE. In: P. M. Conn. Sourcebooks of models for biomedical research. Humana Press Inc, New Jersey, pp. 547-557.

Walz, W., Mukerji, S., 1988. Lactate production and release in cultured astrocytes. Neurosci. Lett. 86, 296–300.

Wang, D., Kaur, C., 2001. Choroid plexus epithelial cells in adult rats show structural alteration but not apoptosis following an exposure to hypobaric hypoxia. Neuroscience Letters 297, 77–80.

Wang, G.L., Jiang, B.H., Rue, E.A., Semenza, G.L., 1995. Hypoxia-inducible factor 1 is a basic-helix-loop-helix-PAS heterodimer regulated by cellular O2 tension. Proc Natl Acad Sci U S A 92, 5510–5514.

Waxman, S.G., Craner, M.J., Black, J.A., 2004. Na+ channel expression along axons in multiple sclerosis and its models. Trends Pharmacol. Sci. 25, 584–591.

Weinberg, J.M., Venkatachalam, M.A., Roeser, N.F., Nissim, I., 2000. Mitochondrial dysfunction during hypoxia/reoxygenation and its correction by anaerobic metabolism of citric acid cycle intermediates. PNAS 97, 2826–2831.

Weinshenker, B.G., Bass, B., Rice, G.P., Noseworthy, J., Carriere, W., Baskerville, J., Ebers, G.C., 1989. The natural history of multiple sclerosis: a geographically based study. I. Clinical course and disability. Brain 112 (Pt 1), 133–146.

Westerterp, K.R., Kayser, B., Wouters, L., Le Trong, J.L., Richalet, J.P., 1994. Energy balance at high altitude of 6,542 m. J. Appl. Physiol 77, 862–866.

Westerterp-Plantenga, M.S., Westerterp, K.R., Rubbens, M., Verwegen, C.R., Richelet, J.P., Gardette, B., 1999. Appetite at “high altitude” [Operation Everest III (Comex-’97)]: a simulated ascent of Mount Everest. J. Appl. Physiol 87, 391–399.

Willis, S.N., Stadelmann, C., Rodig, S.J., Caron, T., Gattenloehner, S., Mallozzi, S.S., Roughan, J.E., Almendinger, S.E., Blewett, M.M., Brück, W., Hafler, D.A., O’Connor, K.C., 2009. Epstein–Barr virus infection is not a characteristic feature of multiple sclerosis brain. Brain 132, 3318–3328.

Witte, M.E., Bø, L., Rodenburg, R.J., Belien, J.A., Musters, R., Hazes, T., Wintjes, L.T., Smeitink, J.A., Geurts, J.J.G., De Vries, H.E., Van der Valk, P., Van Horssen, J., 2009. Enhanced number and activity of mitochondria in multiple sclerosis lesions. J. Pathol. 219, 193–204.

Wong-Riley, M., Anderson, B., Liebl, W., Huang, Z., 1998. Neurochemical organization of the macaque striate cortex: Correlation of cytochrome oxidase with Na+K+ATPase, NADPH-diaphorase, nitric oxide synthase, and N-Methyl-d-aspartate receptor subunit 1. Neuroscience 83, 1025–1045.

Wong-Riley, M.T., 1989. Cytochrome oxidase: an endogenous metabolic marker for neuronal activity. Trends Neurosci 12, 94–101.

Wood, S.C., 1991. Interactions between hypoxia and hypothermia. Annu. Rev. Physiol 53, 71–85.

Wood, S.C., Gonzales, R., 1996. Hypothermia in hypoxic animals: mechanisms, mediators, and functional significance. Comp. Biochem. Physiol. B, Biochem. Mol. Biol 113, 37–43.

Woolf, C.J., Fitzgerald, M., 1986. Somatotopic organization of cutaneous afferent terminals and dorsal horn neuronal receptive fields in the superficial and deep laminae of the rat lumbar spinal cord. J. Comp. Neurol. 251, 517–531.

Wuerfel, J., Bellmann-Strobl, J., Brunecker, P., Aktas, O., McFarland, H., Villringer, A., Zipp, F., 2004. Changes in cerebral perfusion precede plaque formation in multiple sclerosis: a longitudinal perfusion MRI study. Brain 127, 111–119.

Wykoff, C.C., Beasley, N.J.P., Watson, P.H., Turner, K.J., Pastorek, J., Sibtain, A., Wilson, G.D., Turley, H., Talks, K.L., Maxwell, P.H., Pugh, C.W., Ratcliffe, P.J., Harris, A.L., 2000. Hypoxia-inducible Expression of Tumor-associated Carbonic Anhydrases. Cancer Research 60, 7075 –7083.

Xia, X., Lemieux, M.E., Li, W., Carroll, J.S., Brown, M., Liu, X.S., Kung, A.L., 2009. Integrative analysis of HIF binding and transactivation reveals its role in maintaining histone methylation homeostasis. Proceedings of the National Academy of Sciences 106, 4260 –4265.

Xu, K., Lamanna, J.C., 2006. Chronic hypoxia and the cerebral circulation. J. Appl. Physiol 100, 725–730. Yamashita, T., Ando, Y., Obayashi, K., Uchino, M., Ando, M., 1997.

Changes in nitrite and nitrate (NO2-/NO3-) levels in cerebrospinal fluid of patients with multiple sclerosis. J. Neurol. Sci. 153, 32–34.

Yarowsky, P.J., Ingvar, D.H., 1981. Symposium summary. Neuronal activity and energy metabolism. Fed. Proc. 40, 2353–2362.

You, Y., Kaur, C., 2000. Expression of induced nitric oxide synthase in amoeboid microglia in postnatal rats following an exposure to hypoxia. Neurosci. Lett. 279, 101–104.

Youl, B.D., Turano, G., Miller, D.H., Towell, A.D., Macmanus, D.G., Moore, S.G., Jones, S.J., Barrett, G., Kendall, B.E., Moseley, I.F., Tofts, P.S., Halliday, A.M., Mcdonald, W.I., 1991. The Pathophysiology of Acute Optic Neuritis an Association of Gadolinium Leakage with Clinical and Electrophysiological Deficits. Brain 114, 2437–2450.

Zamboni, P., Galeotti, R., Menegatti, E., Malagoni, A.M., Tacconi, G., Dall'Ara, S., Bartolomei, I., Salvi, F., 2009. Chronic cerebrospinal venous insufficiency in patients with multiple sclerosis. J Neurol Neurosurg Psychiatry 80, 392–399.

Zeis, T., Graumann, U., Reynolds, R., Schaeren-Wiemers, N., 2008. Normal-appearing white matter in multiple sclerosis is in a subtle balance between inflammation and neuroprotection. Brain 131, 288–303.

Zeis, T., Probst, A., Steck, A.J., Stadelmann, C., Brück, W., Schaeren-Wiemers, N., 2009. Molecular Changes in White Matter Adjacent to an Active Demyelinating Lesion in Early Multiple Sclerosis. Brain Pathology 19, 459–466.

Zhang, G.X., Li, J., Ventura, E., Rostami, A., 2002. Parenchymal microglia of naïve adult C57BL/6J mice express high levels of B7.1, B7.2, and MHC class II. Exp. Mol. Pathol 73, 35–45.

Zhang, L., Krnjević, K., 1993. Whole-cell recording of anoxic effects on hippocampal neurons in slices. J. Neurophysiol. 69, 118–127.

Zhao, H., Joseph, J., Fales, H.M., Sokoloski, E.A., Levine, R.L., Vasquez-Vivar, J., Kalyanaraman, B., 2005. Detection and characterization of the product of hydroethidine and intracellular superoxide by HPLC and limitations of fluorescence. PNAS 102, 5727–5732.

Zhao, H., Kalivendi, S., Zhang, H., Joseph, J., Nithipatikom, K., Vásquez-Vivar, J., Kalyanaraman, B., 2003. Superoxide reacts with hydroethidine but forms a fluorescent product that is distinctly different from ethidium: potential implications in intracellular fluorescence detection of superoxide. Free Radical Biology and Medicine 34, 1359–1368.

Zhao, W., Tilton, R.G., Corbett, J.A., McDaniel, M.L., Misko, T.P., Williamson, J.R., Cross, A.H., Hickey, W.F., 1996. Experimental allergic encephalomyelitis in the rat is inhibited by aminoguanidine, an inhibitor of nitric oxide synthase. J. Neuroimmunol. 64, 123–133.

Zielke, H.R., Zielke, C.L., Baab, P.J., 2009. Direct measurement of oxidative metabolism in the living brain by microdialysis: a review. J. Neurochem. 109 Suppl 1, 24–29.

Ziskin, J.L., Nishiyama, A., Rubio, M., Fukaya, M., Bergles, D.E., 2007. Vesicular release of glutamate from unmyelinated axons in white matter. Nat. Neurosci. 10, 321–330.